AD651403

THE
SHOCK AND VIBRATION
BULLETIN

FEBRUARY 1967

A Publication of
**THE SHOCK AND VIBRATION
INFORMATION CENTER**
Naval Research Laboratory, Washington, D.C.

Office of
The Director of Defense
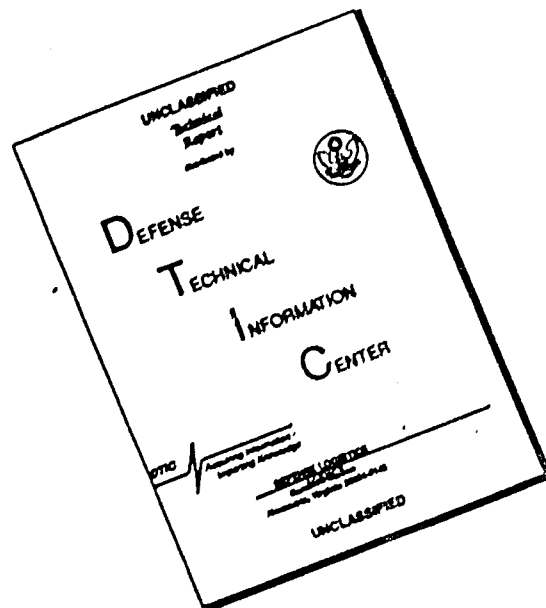Research and Engineering

THE
SHOCK AND VIBRATION
BULLETIN

FEBRUARY 1967

A Publication of
THE SHOCK AND VIBRATION
INFORMATION CENTER
Naval Research Laboratory, Washington, D.C.

Office of
The Director of Defense
Research and Engineering

DISCLAIMER NOTICE

THIS DOCUMENT IS BEST QUALITY AVAILABLE. THE COPY FURNISHED TO DTIC CONTAINED A SIGNIFICANT NUMBER OF PAGES WHICH DO NOT REPRODUCE LEGIBLY.

SYMPOSIUM MANAGEMENT

The Shock and Vibration Information Center

William W. Mutch, Director

Henry C. Pusey, Coordinator

Rudolph H. Volin, Coordinator

Jean B. Goldbecker, Editor

Katherine G. Jahnel, Administrative Secretary

36th Program Committee

William R. Forlifer, NASA Goddard Space Flight Center

Edward H. Schell, Air Force Flight Dynamics Laboratory

George Stathopoulos, Naval Ordnance Laboratory

James M. Taylor, U.S. Army Missile Command

Air Force Liaison

Los Angeles Scientific and Technical Liaison Office, Research and Technology
Division, Air Force Systems Command

Lt. Col. Kenneth W. Cook

Arthur E. Kimberly

Bulletin Production

Graphic Arts Branch, Technical Information Division,
Naval Research Laboratory

CONTENTS

PART 6

Data Analysis and Instrumentation

PAPERS APPEARING IN PART 1
Part 1 - Confidential
(Titles Unclassified)

DYNAMIC DESIGN ANALYSIS METHOD PREDICTION VERSUS TEST MEASUREMENT
OF SHIPBORNE EQUIPMENT RESPONSE
    R. O. Belsheim and A. F. Dick, Naval Research Laboratory, Washington, D.C.

COMPARISON OF SHOCK MOTIONS INDUCED BY AIR BLAST AND UNDERWATER
EXPLOSIONS
    Robert E. Fuss and Kenneth T. Cornelius, David Taylor Model Basin, Washington, D.C.

ANALYSIS OF 21B WEAPONS SKID FOR VERTICAL SHOCK
    John W. McNabb, Northern Ohio University, Ada, Ohio

NERVA NUCLEAR REACTOR VIBRATION ANALYSIS AND TEST PROGRAM WITH
EMPHASIS ON NONLINEAR RESPONSES
    R. D. Burack, D. F. Miller, and A. F. Maguire, Westinghouse Electric Corporation,
    Pittsburgh, Pennsylvania

RECENT SOVIET RESEARCH IN SHOCK, VIBRATION, AND NONLINEAR MECHANICS*
    David B. Singer, Aerospace Corporation, San Bernardino, California

PAPERS APPEARING IN PART 2

Opening Session

THE CHALLENGE OF THE SECOND HALF OF THE DECADE
    R. G. Loewy, University of Rochester, Rochester, New York

SHOCK AND VIBRATION - A PERSPECTIVE
    Alan Powell, David Taylor Model Basin, Washington, D.C.

Shock

YIELDING EFFECTS ON SHOCK SPECTRA
    William R. Mentzer, Jr., Bowles Engineering Corporation, Silver Spring, Maryland,
    and Patrick F. Cunniff, University of Maryland, College Park, Maryland

SHOCK SPECTRA OF PRACTICAL SHAKER SHOCK PULSES
    John R. Fagan and Anthony S. Baran, Radio Corporation of America, Princeton, New Jersey

---

*This manuscript was not available at the time this part of the Bulletin went to press. It is hoped that
the paper will be published at a later date.

AVERAGING FUNDAMENTAL VIBRATION CONTROL SIGNALS: A THEORETICAL STUDY
W. W Shurtleff, Sandia Corporation, Albuquerque, New Mexico

CONTROL TECHNIQUES FOR MULTI-SHAKER VIBRATION SYSTEMS
Richard A. Arone, Wyle Laboratories, Huntsville, Alabama, and Paul A. Brock,
Sine Engineering Company, Granada Hills, California

STRAIN RESPONSE OF SIMPLY SUPPORTED BEAMS TO POINT AND ACOUSTIC LOADING
Tony L. Parrott and Joseph A. Drischler, NASA Langley Research Center,
Langley Station, Hampton, Virginia

PREDICTION OF FLIGHT VIBRATION LEVELS FOR THE SCOUT LAUNCH VEHICLE
Robert B. Bost, LTV Aerospace Corporation, LTV Astronautics Division, Dallas, Texas

RESPONSE OF STRUCTURAL COMPONENTS OF A LAUNCH VEHICLE TO IN-FLIGHT
ACOUSTIC AND AERODYNAMIC ENVIRONMENTS
Khushi L. Chandiramani and Richard H. Lyon, Bolt Beranek and Newman Inc.,
Cambridge, Massachusetts

DYNAMIC VIBRATIONS OF THICK-WALLED ELASTIC ANISOTROPIC CYLINDERS AND
SPHERES WITH INTERNAL DAMPING
Gabriel Cinelli, Argonne National Laboratory, Argonne, Illinois

EFFECT OF ASYMMETRICAL TRAPEZOIDAL PULSE ON SINGLE-DEGREE-OF-FREEDOM
SYSTEMS
H. Saunders, General Electric Company, Philadelphia, Pennsylvania

PAPERS APPEARING IN PART 7

Structural Reliability

ESTIMATE OF EFFECT OF SPACECRAFT VIBRATION QUALIFICATION TESTING
ON RELIABILITY
Clyde V. Stahle, Jr., The Martin Company, Baltimore, Maryland

S-IC RELIABILITY PROGRAM FROM STRUCTURAL LIFE VIEWPOINT
Roy L. Rich and James A. Roberts, The Boeing Company, New Orleans, Louisiana

STRUCTURAL RELIABILITY - PANEL SESSION

Design Data and Methods

DYNAMIC ANALYSIS OF ATS-B SPACECRAFT
Saul M. Kaplan and Victor Terkun, Hughes Aircraft Company, El Segundo, California

SPACECRAFT DESIGN FOR ATLAS TORSIONAL SHOCK TRANSIENT
Sol Davis, Fairchild Hiller, Republic Aviation Division, Farmingdale, Long Island, New York

COMPARISON OF PREDICTED AND MEASURED LAUNCH LOADS FOR SNAP 10A
Everett A. Robb and A. P. Gelman, Atomics International, Canoga Park, California

GROUND-WIND-INDUCED OSCILLATIONS OF GEMINI-TITAN AIR VEHICLE AND ITS ERECTOR
John E. Tomassoni and William H. Lambert, The Martin Company, Baltimore, Maryland

NOISE LEVEL MEASUREMENTS FOR IMPROVED DELTA, ATLAS/AGENA-D, AND TAT/AGENA-D
LAUNCH VEHICLES
Lloyd A. Williams and William B. Tereniak, NASA Goddard Space Flight Center, Greenbelt,
Maryland

THE "VACUUM SPRING"
K. D. Robertson, U.S. Army Materials Research Agency, Watertown, Massachusetts

SELF-ADAPTIVE VIBRATION BALANCING DEVICE FOR HELICOPTERS
W. Euan Hooper, The Boeing Company, Morton, Pennsylvania

SHOCK RESPONSE OF ELECTRONIC EQUIPMENT CABINETS BY NORMAL MODE METHOD
T. K. Hasselman and C. M. Hwang, TRW Systems, Redondo Beach, California

DAMPED VIBRATIONS OF ELASTICALLY SUPPORTED RIGID BODY WITH COUPLING
BETWEEN TRANSLATION AND ROTATION
Francis H. Collopy, ITEK Corporation, Lexington, Massachusetts

MISSILE HANDLING ANALYSIS
C. R. Brown and Alex J. Avis, Westinghouse Electric Corporation, Sunnyvale, California

vii

DATA ANALYSIS AND INSTRUMENTATION

EFFECT OF DIGITIZING DETAIL ON SHOCK AND
FOURIER SPECTRUM COMPUTATION OF FIELD DATA*

M. Gertel and R. Holland
Allied Research Associates, Inc.
Concord, Massachusetts

A preliminary study of the effects on shock and Fourier spectrum dig-
ital computation accuracy due to varying shock record duration and the
degree of analog-to-digital conversion has been conducted. Three com-
plex multi-frequency, long-duration shock records representative of
gunfire shock conditions in armored vehicles were selected for carry-
ing out this study. Shock and Fourier spectra were digitally computed
with a range of analog-to-digital point densities of 900 to 10,000 points/
sec and arbitrarily selected time durations of 15 to 60 msec for the
sample shock records. These results are compared to previously
computed reference shock and Fourier spectra obtained for the sample
shock records defined by 16,500 to 20,000 points/sec and 60 msec du-
ration. The final results of the investigation are presented as spectral
plots of the percent variation relative to the reference. These plots
are called the variation spectra and are useful for estimating the maxi-
mum possible error in shock and Fourier spectra computation due to
lack of detail in digitizing the shock input. It is concluded for the pres-
ent investigation that a digital point density of 10,000 points/sec and a
record duration of 60 msec are minimally adequate for spectral com-
putations between 10 to 2,000 cps.

M. Gertel

INTRODUCTION

The shock acceleration motions which re-
sult from a ballistic projectile impact on ar-
mored steel structures are extremely complex
and cannot be defined by a simple analytic equa-
tion. These shock motions can best be catego-
rized as comprising transient multiple frequency
decaying vibrations of varying intensities. Since
definition of shock environments is mainly for
the purpose of determining system responses
to such motions, it has been found advantageous
in many fields to define a complex shock motion
directly in terms of its response effects on
simple systems with a wide range of natural
frequencies. The shock spectrum accomplishes
this. Shock spectra have been successfully uti-
lized [1-6] to define shock environments for
equipment and structures to withstand earth-
quakes, underwater mine explosions, and air-
craft landing impacts.

Shock and Fourier spectral analyses of
complex shock environments may be performed
by either analog or digital computer techniques.

1

However, when large quantities of field data must be analyzed, high-speed automatic digital computing and plotting methods are preferable since the results become immediately available.

Recursion formulas suitable for efficient digital computation of shock and Fourier spectra for complex mechanical shock transients have been presented by O'Hara [7]. These equations have been used successfully with an IBM 7094 digital computer and General Dynamics SC 4020 Computer Plotter for determinations of shock and Fourier spectra for highly complex shock motions typical of armored vehicles [8,9]. It was shown that the digital computation of shock and Fourier spectra is extremely precise. The accuracy of the result is only limited by the precision with which the original shock record is digitized for input to the computer.

In preparation for the application of digital computer techniques to determine shock and Fourier spectra representative of field environmental conditions in military and space vehicles, it is essential to establish practical precision limits for digitizing the field data. Presented herein is a limited preliminary study of the effect on shock and Fourier spectrum digital computation accuracy due to varying precision in defining the shock input. In particular, this study is concerned with:

1. The effect of varying the incremental time spacing or density of analog-to-digital conversion, i.e., point density; and

2. The effect of arbitrary time or record duration cutoff in a complex shock record.

The study of these effects has been carried out on a comparative basis using three complex long-duration shock records whose shock and Fourier spectra were computed and available from a previous investigation [8]. These previously computed spectra are referred to as the "reference spectra" for the present study and were obtained from the sample records with an analog-to-digital point density of 20,000 points/sec and a record duration of 60 msec.

The study reported herein has been carried out with a range of analog-to-digital point densities of 900 to 10,000 points/sec and arbitrarily selected record durations between 16 and 60 msec. The results of this investigation are presented in the form of spectral plots of the percent variation relative to the reference spectra. These plots are called the variation spectra and are useful for estimating the maximum possible error occurring in shock and

Fourier spectra computations due to lack of detail in digitizing the shock input.

SHOCK AND FOURIER SPECTRAL ANALYSES OF SELECTED SAMPLE SHOCK RECORDS

For purposes of carrying out the present preliminary study of the effects on shock and Fourier spectrum digital computation accuracy due to varying precision in defining the shock input, three complex long-duration shock records which were previously analyzed [8] were selected. The first sample record is an idealized transient acceleration with two decaying sinusoidal frequency components. The second and third sample records are complex multiple-frequency transient accelerations recorded during a drop-hammer type shock test representative of projectile impact conditions in an armored vehicle.

The sample shock records used for this study are described in the following subsections with presentations of their time histories and reference shock and Fourier spectra in the Appendix. The effects on shock and Fourier spectral computations for the sample records due to varying the analog-to-digital time increment or point density and the record duration are presented as variation spectra. The variation at each frequency in the spectrum is expressed as a percentage of the corresponding point in the reference spectrum for the sample record. The variation is computed using the following simple relation:

$$\text{Variation} = 100 \times \frac{|\text{Computed Value - Reference Value}|}{\text{Reference Value}} \%.$$
(1)

The implications to be drawn from the variation spectra developed here are discussed in the final sections of this report.

Analysis of Sample Shock Record No. 1

The time history of the first shock record studied is shown in Fig. A-1 of the Appendix. The equation of this idealized shock motion is indicated on the figure and can be seen to comprise damped 100- and 300-cps frequency components. The shock and Fourier spectra for this record are reproduced from Ref. 8 as Fig. A-2. These are the reference spectra for the ensuing analyses of this shock and, as noted

2

TABLE 1

Sample Comparison of Theoretical and Computer Program Peak Responses for
Two-Component Decaying Sinusoidal Acceleration Shock Input [8]

Frequency (cps)	Peak Response (in.)		Diff. (in.)	Error (%)
	Theoretical Solution	Shock Program		
10	-1.27048	-1.2701	+0.0004	0.0315
30	-0.480569	-0.48040	+0.00017	0.0354
80	-0.278056	-0.27797	+0.00009	0.0323
100	-0.246923	-0.24680	+0.00012	0.0485
120	-0.131544	-0.13153	+0.00001	0.00761
200	-0.0457847	-0.045753	-0.000011	0.024
280	-0.0476972	-0.047644	+0.000053	0.111
300	-0.0497754	-0.049824	-0.000049	0.0988
350	-0.0272114	-0.027138	+0.000073	0.269
1,000	-0.00174328	-0.0017374	+0.0000059	0.339

in Fig. A-2, were computed for a record duration of 60 msec and an analog-to-digital point density of 16,500 points/sec. The extremely high precision in the digital computation of these reference spectra is indicated in Table 1.

For purposes of comparison with the above reference spectrum, undamped maximax shock spectra were computed for sample shock record No. 1 with the duration fixed at 60 msec and digital point densities of 1500, 1200, and 900 points/sec. The results are presented in Fig. A-3 as a spectrum of variations with respect to the reference.

In preparation for studying the effects of arbitrary shock record duration cutoff, the computer program was modified to print out the time of occurrence of the peak response for each spectral frequency. A computer run was then made with the sample record cutoff at 50 msec and the "reference" digital point density of 16,500 points/sec. Figure A-4 presents the results of this run.

Figure A-4 indicates for this shock motion that, except for frequencies below 20 cps and near the 100- and 300-cps components, the majority of peak responses occur early in the record near the first few major input peaks. In general, it may be assumed that the early peak responses will not be affected by cutting off the shock record any time after they occur. Response time histories to the 50-msec sample input were then computed for groups of frequencies below 20 cps and near the 100- and 300-cps components. With these response time histories and the previous data, undamped maximax shock spectra were constructed for shock record duration cutoffs of 15, 20, 30, 40, and 50

msec. The results of this work are presented in Fig. A-5 as a spectrum of variations with respect to the reference data of Fig. A-2.

Analysis of Sample Shock
Record No. 2

The time history of the second shock record studied is shown in Fig. A-6. This record is oscillograph record No. 00906-1 of the U. S. Army Frankford Arsenal Environmental Laboratory. The reference undamped and damped shock and Fourier spectra for this record are reproduced from Ref. 8 as Figs. A-7 and A-8. These reference spectra were computed for the sample shock record digitized with 20,000 points/sec and a duration of 60 msec. The digital point density of the sample record was reduced by a factor of two, for three successive shock spectrum computer runs with and without damping. The results are presented in Figs. A-9 and A-10, respectively, as damped and undamped variation spectra with respect to the reference spectra of Figs. A-7 and A-8.

For purposes of observing the effect of selecting arbitrary record durations for sample record No. 2, undamped and damped shock spectrum computer runs were made with the reference digital point density of 20,000 points/sec and record durations of 43 and 17 msec. These durations respectively cut off the sample record at approximately 10 and 20 percent of the double amplitude or peak-to-peak acceleration of the shock record. The results of these runs are presented as variation spectra in Figs. A-11 and A-12. Also superimposed on these figures are variation spectra plotted from data in Ref. 8 for an 80-msec duration of the

3

reference shock record. This duration corresponds approximately to 2 percent of the peak-to-peak value of the original record, whereas the reference 60-msec duration is approximately 5 percent.

Analysis of Sample Shock Record No. 3

The time history of the third shock record studied is shown in Fig. A-13. This is oscillograph record 00908-2 of the U. S. Army Frankford Arsenal Environmental Laboratory. The reference undamped and damped shock and Fourier spectra for this record are reproduced from Ref. 8 as Figs. A-14 and A-15. As in the previous case, these reference spectra were computed for the sample shock record digitized with 20,000 points/sec and a duration of 60 msec. Undamped and damped variation spectra with respect to the reference are presented in Figs. A-16 and A-17 for digitizing point densities of 2,500 to 10,000 points/sec and duration held constant at 60 msec.

Undamped and damped variation spectra computed for the sample record with arbitrarily selected durations of 45 and 23 msec are presented in Figs. A-18 and A-19. As in the previous case, these durations respectively correspond to cutting off the sample record at approximately 10 and 20 percent of the peak-to-peak value of the original record. The 60-msec reference record corresponds to cutting off the original record at approximately 5 percent of its peak-to-peak value.

Fourier Spectrum Variation for Sample Record No. 3 — To complement the determinations of shock spectrum variations described in the previous sections, a similar study was conducted with the Fourier Magnitude Spectrum for sample shock record No. 3. The reference Fourier spectrum for this work is shown in Fig. A-14 and is identical to the undamped residual shock spectrum as noted in the figure. The Fourier variation spectrum due to reducing the digitizing point density from 20,000 to 10,000 points/sec is presented in Fig. A-20. These data are discussed later at greater length.

DISCUSSION OF RESULTS

The primary emphasis in the present work has been to determine the effects of record digitizing detail on digital computer shock spectrum computations. Only a small amount of consideration has been given to the Fourier

spectral data obtained during the program; however, it is expected that the conclusions reached for shock spectral computations should be equally applicable for Fourier spectra.

Several significant observations and trends can be detected from the shock and Fourier Variation Spectra presented in the Appendix for the three complex sample shock records investigated. These variation spectra clearly confirm the intuitively anticipated result that the accuracy of digital computer spectral computations will decrease with: (a) reductions in the analog-to-digital point density used to define the shock record input to the computer, and (b) arbitrary reductions in the time duration cutoff for a complex long-duration record. In general, the present preliminary data suggest that a digital point density of 10,000 points/sec and a record duration of 60 msec, which corresponds to approximately 5 percent of the maximum peak-to-peak shock amplitude, will provide for a nominal spectrum computation accuracy within 5 percent from 10 to 1,000 cps and within 10 percent up to 2,000 cps. This seems minimally adequate for spectral computations for most field measurement programs. Further, more detailed observations are presented in the following paragraphs.

Effects of Digital Point Density

The number of points used to describe digitally a shock acceleration record time history has a noticeable effect on digital shock spectrum "response" computations at low as well as high frequencies. This is clearly evident in the maximax variation spectrum of Fig. A-3, for the idealized two-frequency-component shock record of Fig. A-1. The low-frequency variation was not anticipated, because for almost any point density we have a large number of points available to define each full cycle of low-frequency oscillation which may be present. It appears that the low-frequency peak response variations are significantly affected because these components are responsive to the velocity content of the shock. Digitizing a shock acceleration curve, in effect, replaces the curve with straight-line segments, introducing an accumulative loss of area of velocity segments for the length of the record. An analysis of the velocity change (or area) and peak acceleration of the idealized record of Fig. A-1 as a function of digital point density is presented in Table 2. It can be seen that the decreases in velocity change as a function of point density of the idealized record compare almost exactly with the low-frequency variation spectra of Fig. A-3. The corresponding variations noted for peak

4

TABLE 2
Effects of Digital Point Density on Velocity Change and
Peak Acceleration of Idealized Shock Record of Fig. A-2

Point Density (points/sec)	Velocity Change (in./sec)	Velocity Variation (%)	Peak Acceleration (g)	Acceleration Variation (%)
∞	79.25	-	130	-
16,500	79.22	0.38	130	0
1,500	75.59	3.73	121	6.92
1,200	73.28	7.53	129	0.77
900	68.23	13.91	123	5.38

acceleration in Table 2 seem to be random in nature.

The increasing trend of high-frequency spectral computation errors indicated by all the variation spectra in the Appendix is to be expected for digital shock spectrum computation. As described in Refs. 8 and 9, the procedure for obtaining the shock spectra involves computing a response time history with the same number of points used to digitize the shock input. For any given digital point density, as the spectrum natural frequency increases, there will be a corresponding decrease in the number of points available to define one complete cycle of the response sinusoids. A maximum error in defining the peak amplitudes of the response sinusoids occurs when the available digitizing points equally "straddle" a peak. The maximum error E due to digitizing the response is as follows [8,9]:

$$E = 100 \left(1 - \cos \frac{\pi}{n}\right) \%, \qquad (2)$$

where n is the number of points per cycle of response sinusoid.

The "digitizing error" defined by Eq. (2) is plotted in Fig. 1 as a function of the number of points n used to digitize one complete cycle of any given sinusoid. Superimposed in Fig. 1 are plotted data points which represent the maximax shock spectrum variations from Fig. A-3 corresponding to the 100- and 300-cps "transient resonance" frequency components. The close agreement between these computed transient resonance variation spectra and the error function defined by Eq. (2) suggest that this function is quite satisfactory for preliminary estimates of digitizing requirements.

It is important to point out here that the amplitude error function of Eq. (2) is applicable for both input and response sinusoidal components. The total error which may result in
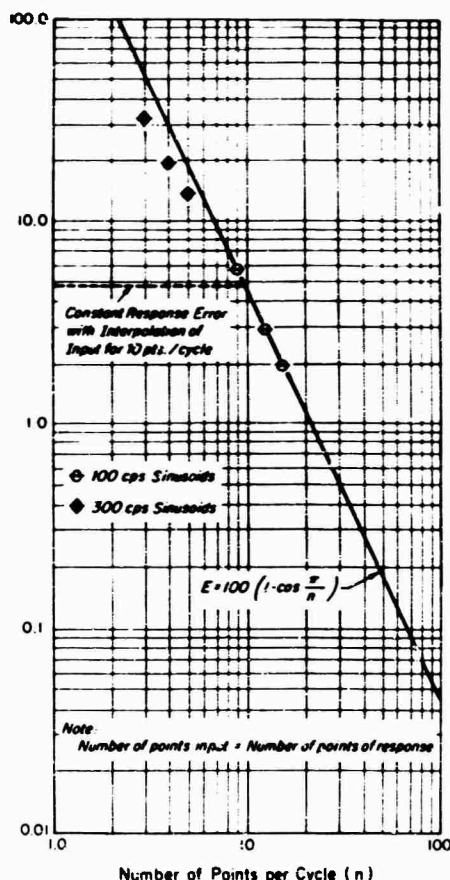
Fig. 1 - Maximum error in peak response amplitude due to number of points defining the response time history

spectral computation is actually due to a combination of errors in defining the amplitudes of both the input and response sinusoids; this is in addition to the "velocity loss" error effect on low-frequency components noted earlier. To prevent a large buildup of response computation errors due to insufficient digitizing detail at

5

high frequencies, the present computer program automatically provides for linear interpolation of the digitized input so that high-frequency response time histories are always defined by at least 10 points/cycle. Thus, even though the input peak amplitude may be considerably in error due to insufficient digitizing, i.e., $n < 10$, the response computation is always accurate to within 5 percent as noted by the dashed horizontal line in Fig. 1. The major error in spectral computations when the input is defined with less than 10 points/cycle is governed primarily by the input.

Due to the highly complex, multiple-frequency nature of sample shock records Nos. 2 and 3 in Figs. A-6 and A-13, a detailed analysis of computation errors due to digitizing was not attempted. Rather, envelopes of the maximax variation spectra as a function of digitizing density with and without damping for both records were prepared and are presented in Figs. 2 and 3. It is immediately evident, as can also be detected from Fig. 1, that the variations in computed spectra increase markedly at high frequencies as the digitizing point density decreases. The variation in the damped maximax shock spectra is considerably less than for the undamped case, and this is presented for

reference purposes in Fig. 3. Based on the envelope of undamped maximax variation spectra in Fig. 2, it may be tentatively concluded that an analog-to-digital point density of 10,000 points/sec will permit spectral computation accuracy of within 5 percent up to 1,000 cps and within 10 percent up to 2,000 cps. Essentially the same conclusions are obtained from the digitizing error function of Eq. (2) plotted in Fig. 1. This is further confirmation that Eq. (2) can be utilized for estimating digitizing requirements as a function of desired accuracy in spectral computation.

Effect of Shock Record Duration Cutoff

Examination of the damped and undamped maximax variation spectra due to varying time duration cutoff in the Appendix indicates that significant deviations in spectral computation accuracy primarily occur in two regions:

1. Low-Frequency Region — For the three sample shock records studied, significant variations occur in the low-frequency region below approximately 20 cps for arbitrary shock durations of approximately 50 msec and below approximately 50 cps (except for Frankford
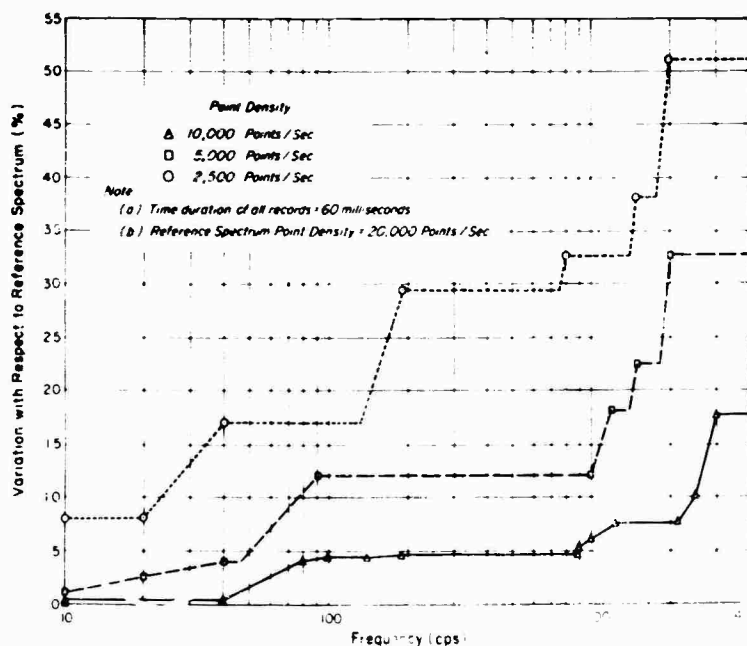
Fig. 2 - Envelope of undamped maximax variation spectra of records 00909-1 and 00908-2 due to decreasing digital point density

6

Fig. 3 - Envelope of 5 percent damped maximax variation
spectra of records 00906-1 and 00908-2 due to decreasing
digital point density

Record 00906-1) for shock durations of approx-
imately 20 msec. It may be noted on comparing
Figs. A-5, A-11, and A-18 that the low-frequency
variations are considerably greater for the ar-
bitrarily short-duration highly complex sample
shock records than for the idealized record.
The observed low-frequency variations may be
partially, but not completely, explained by the
changes in the velocity content of each shock
resulting from duration cutoff. The complete
explanation of the observed low-frequency vari-
ations requires further investigation. However,
based on the present available limited data, it
appears that low-frequency variations can be
expected when the dimensionless frequency
parameter of the shock is $f\tau \leq 1$, where f is
frequency in cps, and τ is shock record dura-
tion in seconds.

2. Resonant Frequency Region — Significant
spectral variations occur at each major fre-
quency component of the input shock. This is
particularly evident from Fig. A-5 for the
idealized shock record. The shock record
duration determines the number of repetition
cycles which may occur at any frequency, and
hence is a major factor in establishing the
severity of a transient undamped resonance
condition. This transient resonance effect is
apparently negligible in the damped variation

spectra which are presented for reference pur-
poses in Figs. A-12 and A-19.

It appears from the present limited data on
effects of varying duration that the reference
shock record length of 60 msec is perhaps the
safest compromise duration for maximum ac-
curacy over the largest range of frequencies.
In Figs. A-11 and A-12, only a small amount of
positive variation is indicated by increasing the
record duration cutoff to 80 msec. Inasmuch
as the 60-msec record duration corresponds
approximately to 5 percent of the peak-to-peak
amplitude of the shock, this can be regarded as
an alternative criterion for selection of record
duration in a complex shock.

Fourier Spectrum

A large high-frequency variation is shown
in Fig. A-20 due to computing the magnitude of
the Fourier spectrum of Record 00908-2 with a
reduced point density of 10,000 points/sec in-
stead of 20,000 points/sec. The greatest vari-
ations in Fig. A-20 occur at the "notches" or
frequency voids which are evident in the refer-
ence Fourier spectrum of Fig. A-14. At these
notches the spectrum curves are very steep;
hence, any minor differences introduced by

7

digitizing point density or time duration will appear as a large variation. Similar large variations were evident during visual examinations of the Fourier spectrum computer printouts for Record 00906-1.

The significance of these Fourier spectra variations cannot be deduced from the present results. It is possible that what presently seems to be very large variations may have little effect on the application of the Fourier spectrum to compute the time history of the input and response at any location in a structure when the steady-state transfer function at that location is known. The inverse transformation of the Fourier spectrum to obtain the time history of the motion involves an integration process; hence, the area under the entire spectrum is just as important as the magnitude of any particular frequency. Probably the best method for evaluating the effect of point density and time duration on the Fourier spectrum would be to attempt to reconstruct the original shock time history record. This was beyond the scope of the present limited investigation.

CONCLUSIONS

The results of the digital computer shock and Fourier spectral analyses presented herein as a function of varying analog-to-digital point densities and shock record durations provide a basis for establishing acceptable limits for these parameters. It is evident that for maximum computation accuracy, the digital point density and shock record duration must be sufficiently large to define the peak acceleration, velocity content, and repetitive frequency components in the shock. Based on the analyses of three complex shock records, typical of gunfire shock conditions which have been investigated here, it is concluded that a digital point density of 10,000 points/sec and a record duration of 60 msec should be adequate for most digital computer spectral analyses of field data. The record duration of 60 msec corresponds approximately with an amplitude which is 5 percent of the maximum peak-to-peak value for the two most complex records studied. The suggested record duration and digitizing density provide, in the present cases, a nominal spectrum computation accuracy of within 5 percent between 10 to 1,000 cps and within 10 percent from 1,000 to 2,000 cps. Improved accuracy over an extended lower and higher frequency range will be achieved by increasing the digital point density and record duration.

REFERENCES

1. M. A. Biot, "A Mechanical Analyzer for the Prediction of Earthquake Stresses," Bull. Seismological Soc. Am., Vol. 31, pp. 143-149, 1941

2. T. Caughey and D. E. Hudson, "A Response Spectrum Analyzer for Transient Loading Studies," Proc. Soc. Experimental Stress Anal., Vol. 13, No. 1, 1955

3. Y. C. Fung, "The Analysis of Dynamic Stresses in Aircraft Structures During Landing as Nonstationary Random Processes," J. Appl. Mech., Vol. 22, No. 4, pp. 449-457, Dec. 1955

4. J. H. Green, "The Response of Missile Components to Water-Entry Shock," Shock and Vibration Bull. No. 26, Part 2, Dec. 1958

5. G. W. Housner, "Behavior of Structures During Earthquakes," J. Eng. Mech. Div.

Proc. ASCE, Paper No. 2220, EM 4, Oct. 1959

6. L. S. Jacobsen and R. S. Ayre, Engineering Vibrations with Applications to Structures and Machinery. McGraw-Hill, New York, 1958

7. G. J. O'Hara, "A Numerical Procedure for Shock and Fourier Analysis," NRL Rept. 5772, June 1962

8. M. Gertel and R. Holland, "Analysis of Shock Records Using a Digital Computer," U. S. Army Frankford Arsenal Rept. R-1763, AD 465410, May 1965

9. M. Gertel and R. Holland, "Definition of Shock Design and Test Criteria Using Shock and Fourier Spectra of Transient Environments," Shock and Vibration Bull. No. 35, Part 6, Jan. 1966

Appendix

SHOCK, FOURIER, AND VARIATION SPECTRAL DATA
FOR SELECTED SAMPLE SHOCK RECORDS
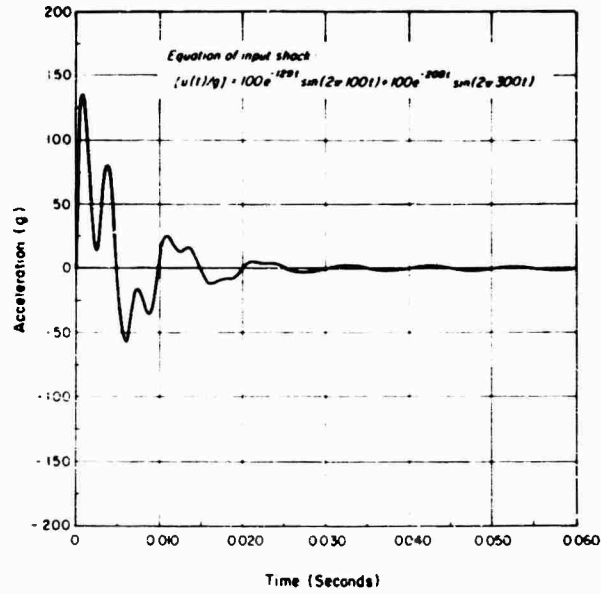
Fig. A-1 - Sample record No. 1: Time history for idealized two-component superimposed decaying sinusoidal acceleration shock record, frequency components 100 and 300 cps [8]
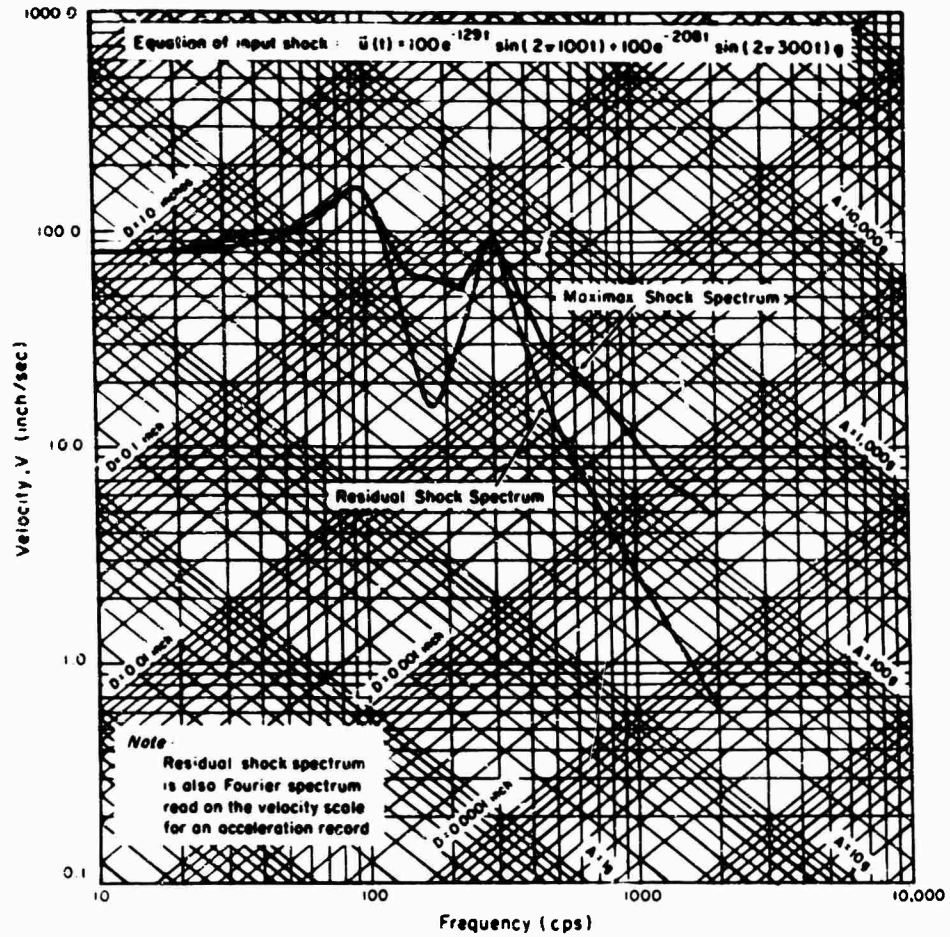
Fig. A-2 - Maximax and residual spectra for the idealized two-component decaying sinusoidal acceleration shock record of Fig. A-1, digitizing point density 16,500 points/sec, duration of record 60 msec [8]
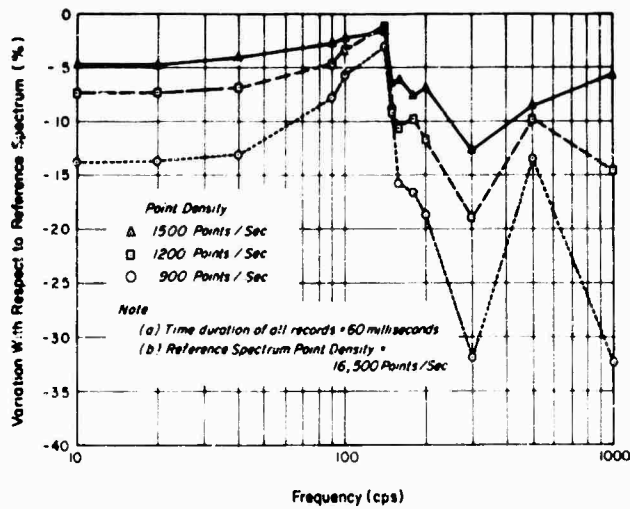
Fig. A-3 - Undamped maximax variation spectra due to decreasing digital point density for the idealized decaying sinusoidal shock record of Fig. A-1

10
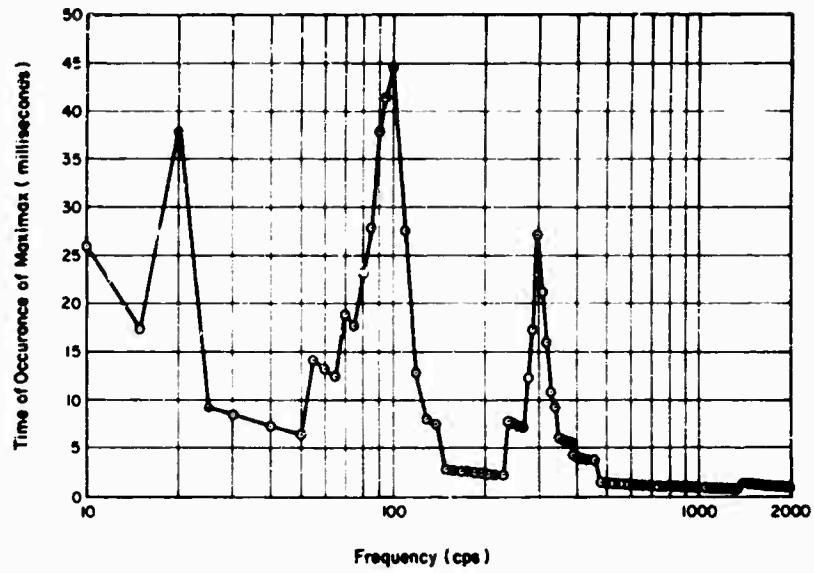
Fig. A-4 - Time of occurrence of maximax response for
the idealized decaying sinusoidal shock record of Fig. A-1
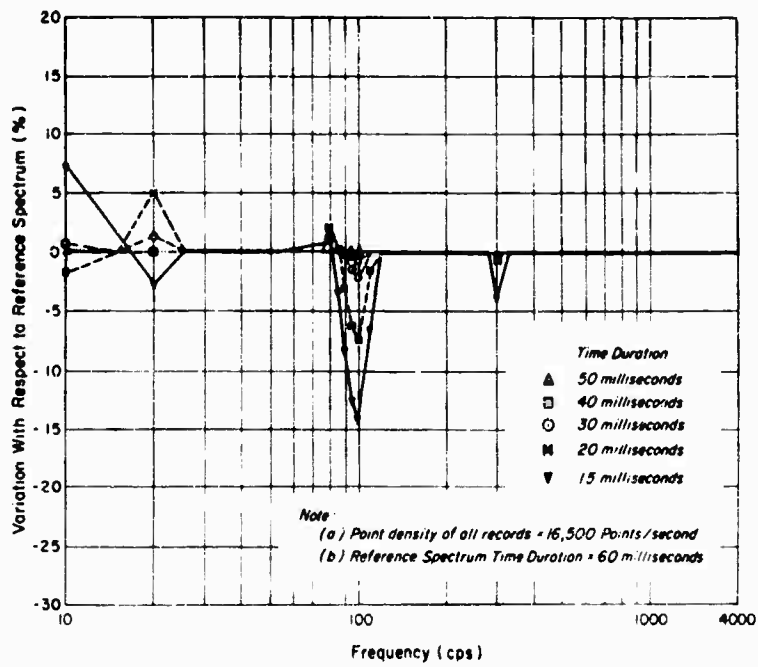
Fig. A-5 - Undamped maximax variation spectra due to
reducing time duration of idealized decaying sinusoidal
shock record of Fig. A-1

11
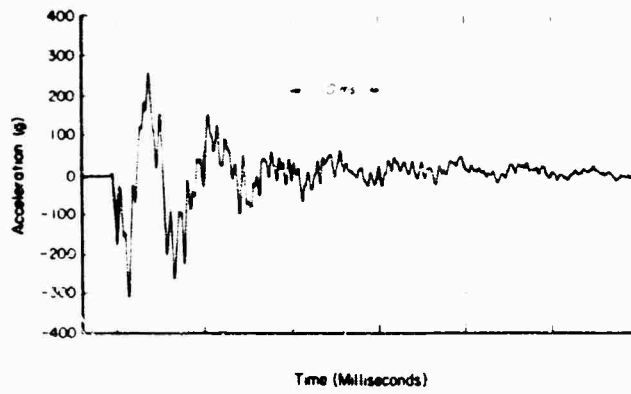
Fig. A-6 - Sample record No. 2: Time history
for Frankford Arsenal shock record 00906-1 [8]
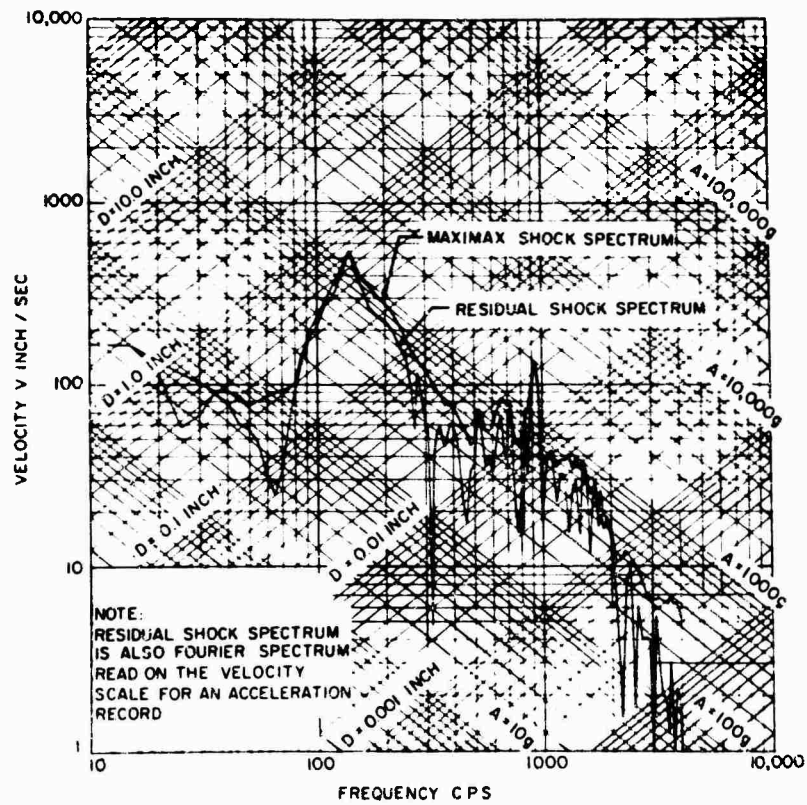
Fig. A-7 - Maximax and residual spectra for record
00906-1: Digitizing point density 20,000 points/sec,
duration of record 60 msec [8]

12

Fig. A-8 - Damped shock spectra for record 00906-1: Digitizing point density 20,000 points/sec, duration of record 60 msec [8]
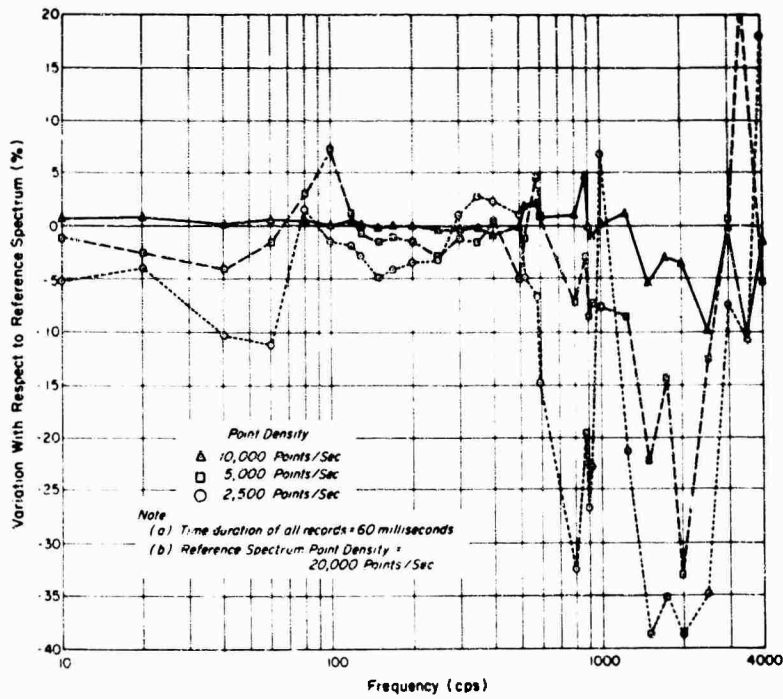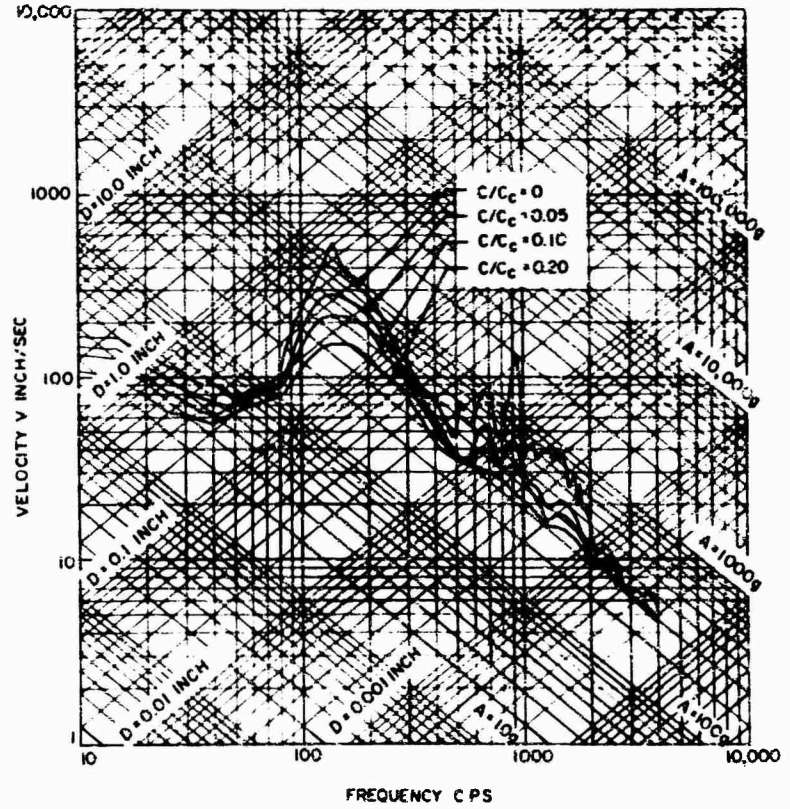
Fig. A-9 - Undamped maximax variation spectra due to decreasing digital point density of record 00906-1

13
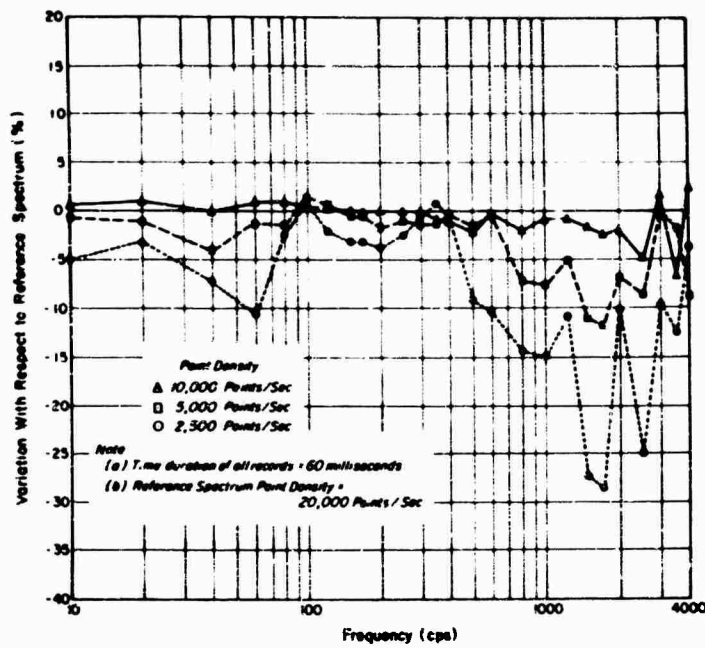
Fig. A-10 - Five percent damped maximax variation
spectra due to decreasing digital point density of
record 00906-1
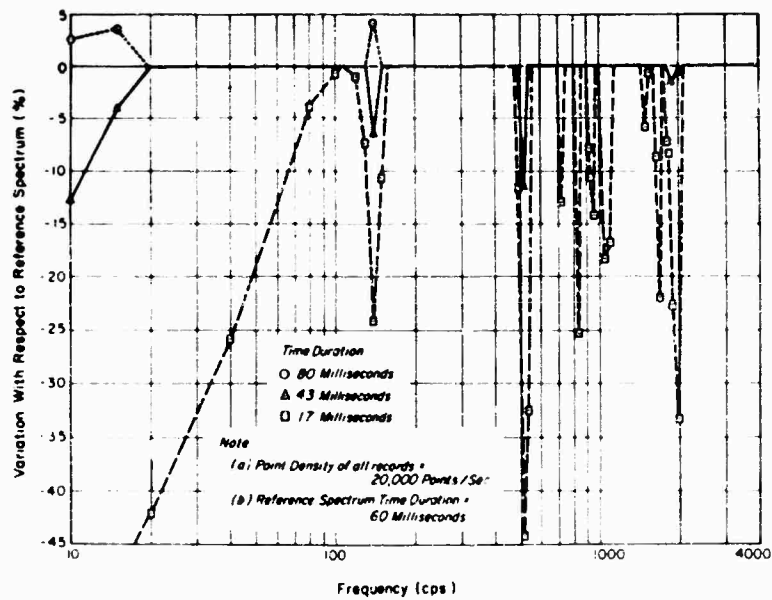
Fig. A-11 - Undamped maximax variation spectra due
to varying time duration cutoff for record 00906-1

14
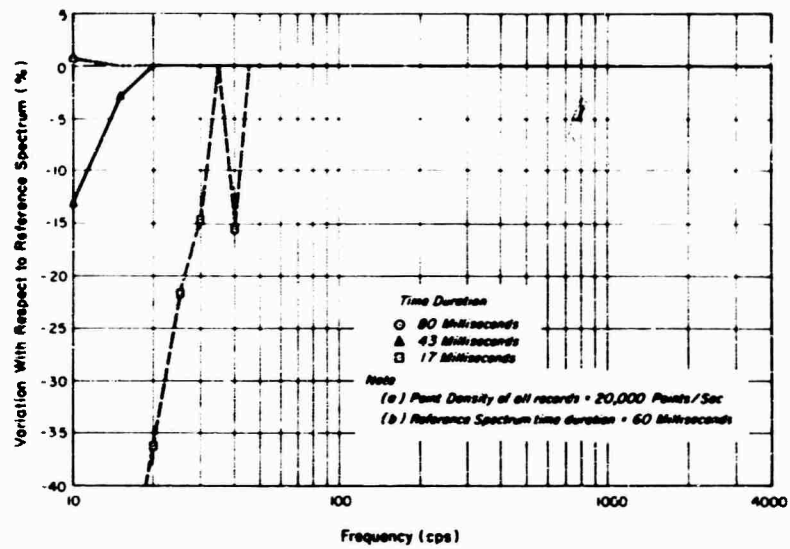
Fig. A-12 - Five percent damped maximax variation spectra
due to varying time duration cutoff for record 00906-1
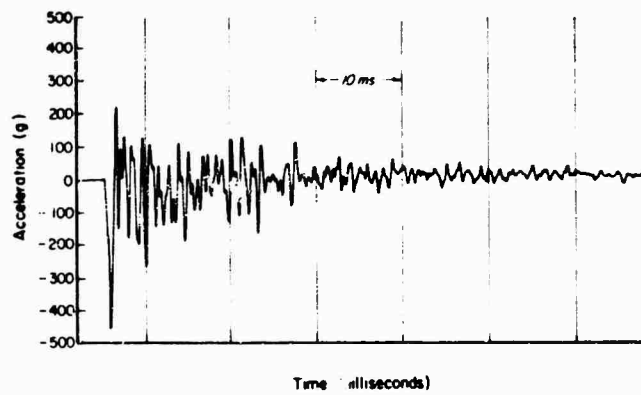
Fig. A-13 - Sample record No. 3: Time history
for Frankford Arsenal shock record 00908-2 [8]

15
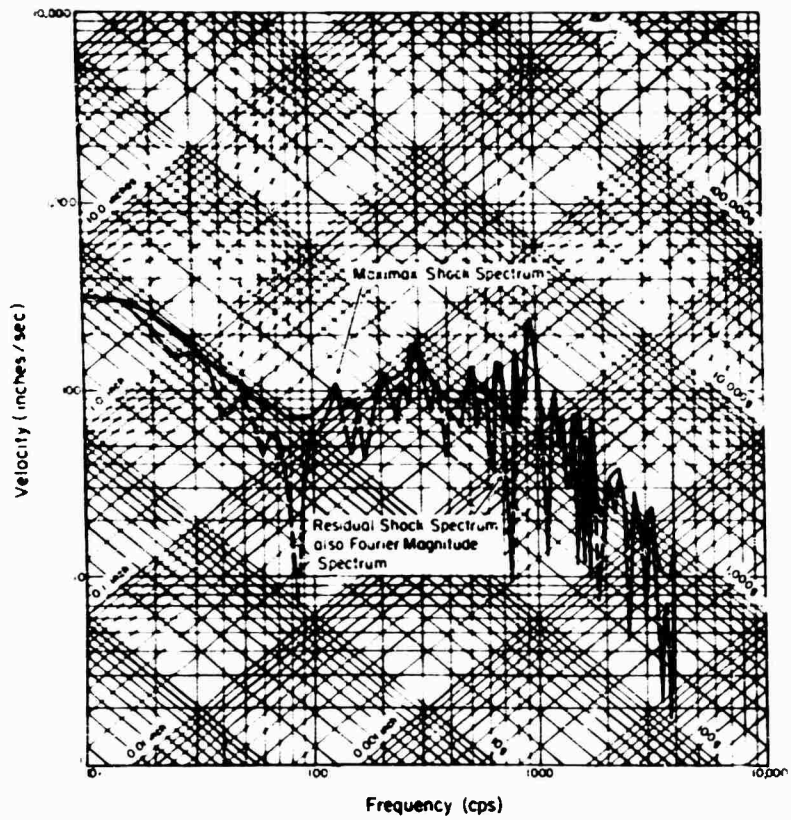
Fig. A-14 - Maximax and residual spectra for record 00908-2: Digitizing point density 20,000 points/sec, duration of record 60 msec [8]

Fig. A-15 - Damped shock spectra for record 00908-2: Digitizing point density 20,000 points/sec, duration of record 60 msec [8]

16
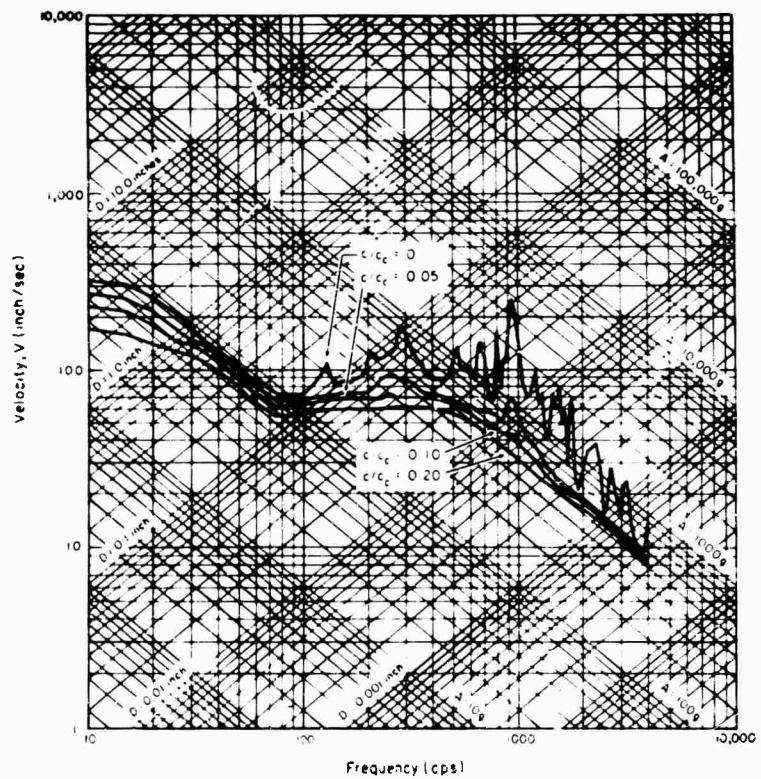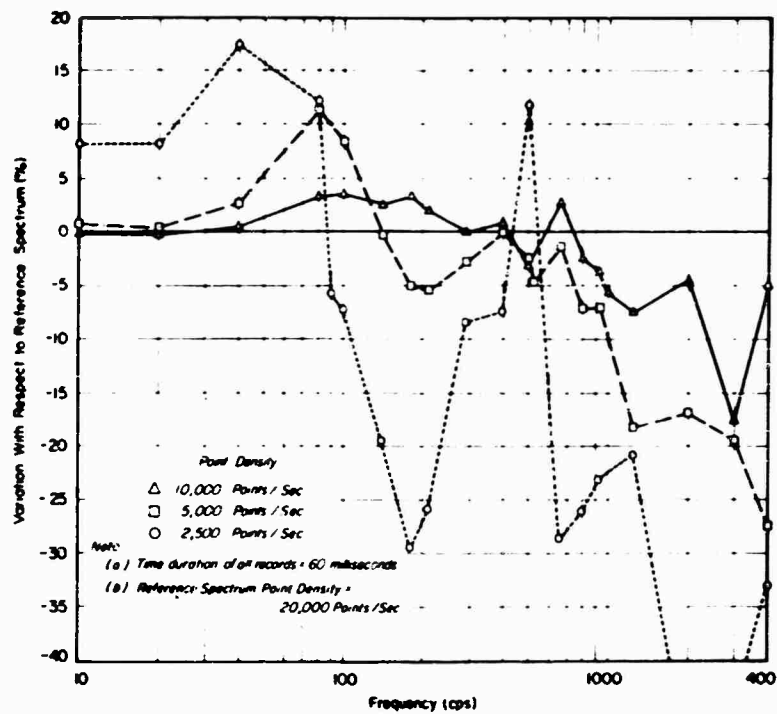
Fig. A-16 - Undamped maximax variation spectra due
to decreasing digital point density of record 00908-2
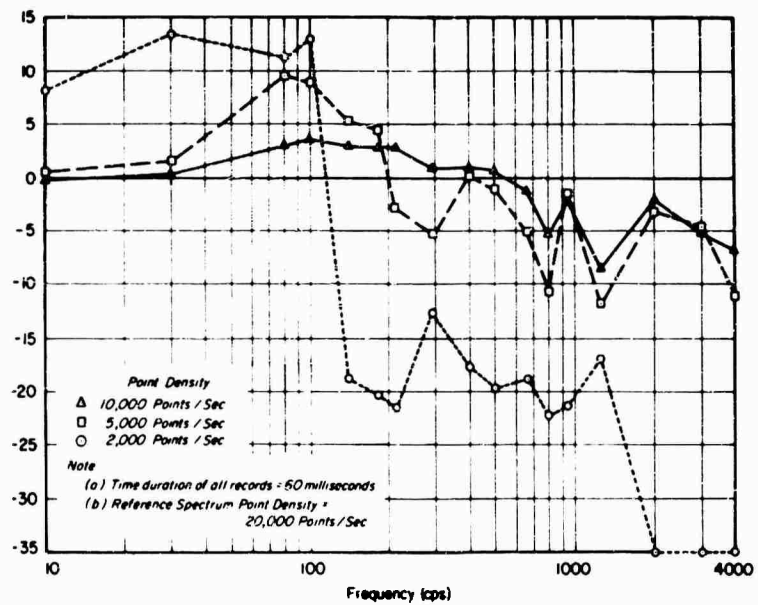
Fig. A-17 - Five percent damped maximax variation
spectra due to decreasing digital point density of
record 00908-2

17
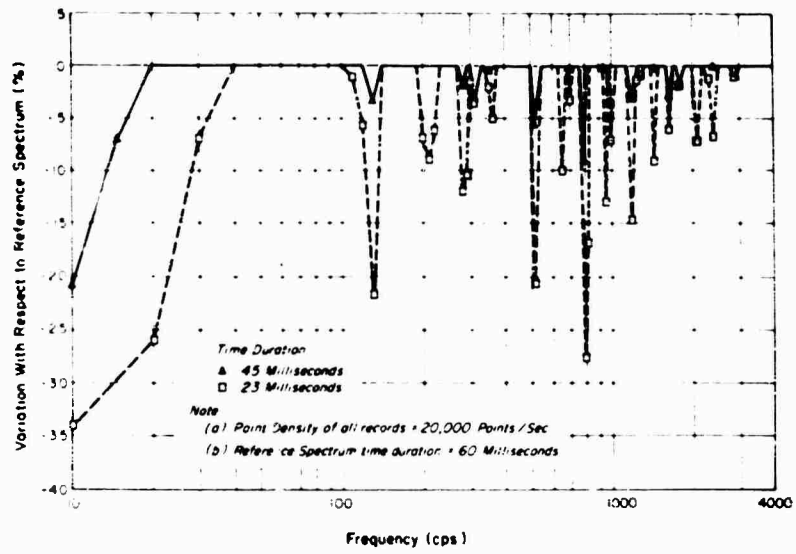
Fig. A-18 - Undamped maximax variation spectra due to
varying time duration cutoff for record 00908-2
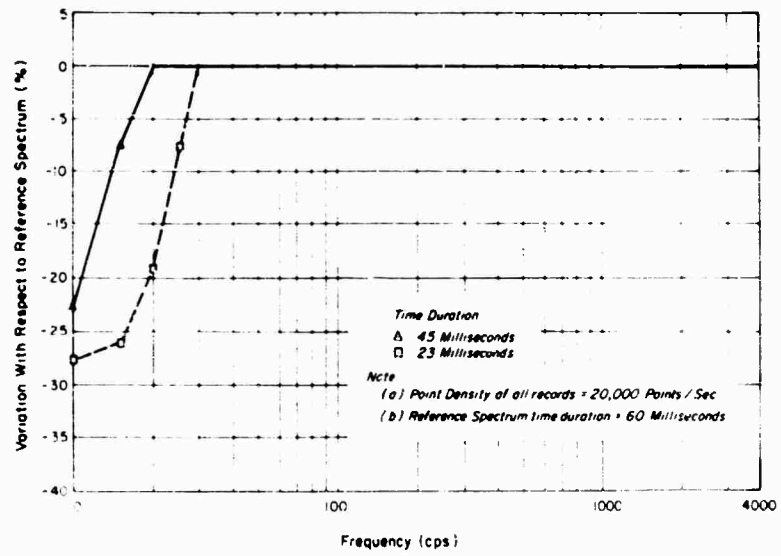
Fig. A-19 - Five percent damped maximax variation spectra
due to varying time duration cutoff for record 009 8-2

18
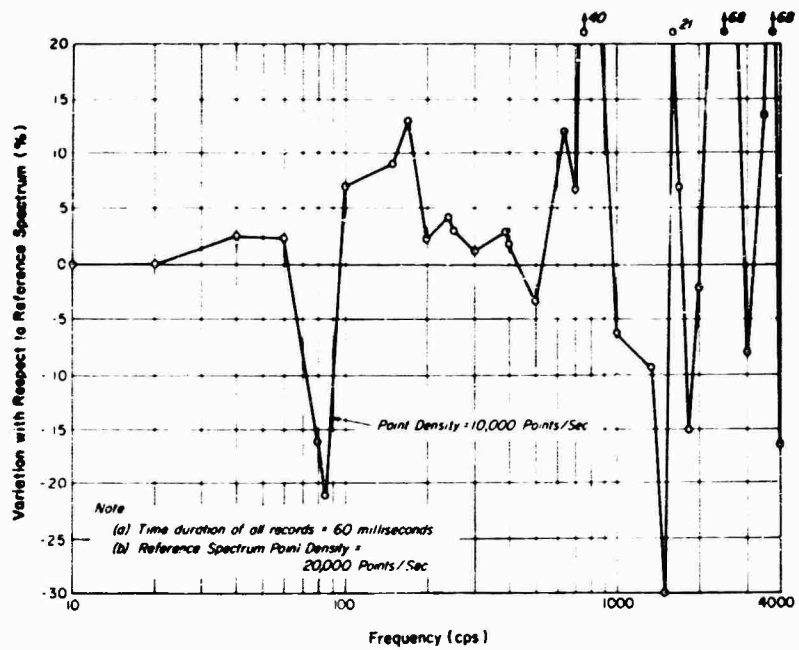
Fig. A-20 - Fourier magnitude variation spectrum due
to decreasing digital point density of record 00908-2

*   *   *

19

AUTOMATED DIGITAL SHOCK DATA
REDUCTION SYSTEM*

Walter B. Murfin
Sandia Corporation
Albuquerque, New Mexico

A method of automatically digitizing, editing, filtering, reducing, comparing, displaying, and storing shock data is described. The desired final display of the shock data is graphical and can be given in two forms: the acceleration-time history and the shock spectrum. Subsidiary operations include automatic editing of data to eliminate spurious or unwanted points, filtering to remove undesired high-frequency components, or computation of Fourier spectra.

The acceleration-time history is often useful for confirming the validity of the data, but gives little insight into possible damaging effects. It is often of dubious value for comparing the severity of dissimilar shock environments. The shock spectrum, on the other hand, may be of value in estimating damaging effects or relative severity of environments and for determining "equivalent" laboratory tests. The spectra are being used as the final form of data presentation in the Sandia Environmental Data Bank.

An educational program is described which has been found useful for acquainting designers with the utility of the approach. Certain types of pulses which do not lend themselves to the shock spectrum treatment are described, and examples are given showing the flow and presentation of data from rough "first look" records through final reduction. The mathematical methods for computing shock and Fourier spectra and for filtering are described in sufficient detail to permit adaption to other data systems.

W. B. Murfin

Shock tests of systems, structures, and components have been increasing in number and complexity at Sandia Corporation for several years. Ground impact tests, blast tests, and transportation tests are conducted almost daily on complete systems. In addition, extensive qualification testing of components is carried out.

The sheer volume of data collected has become bewildering. Improvements in instrumentation and recording techniques have made it possible to collect far more data than in years past. Before the installation of the system described in this report, reduction of this mass of data consisted merely of annotating oscillograms of the shock records, as shown in Fig. 1, which were then delivered to the systems or component designer without comment. Obviously, there is a very significant possibility of human error in such an operation. The designer was not only swamped with a tremendous volume of data but, unless he happened to be a

near-expert in the fields of instrumentation and mechanical shock, was unable to determine what records were valid or how to apply the data to refinements of design. In addition to these errors of omission, the annotator could very easily make errors in calibrate levels, channel identification, etc.
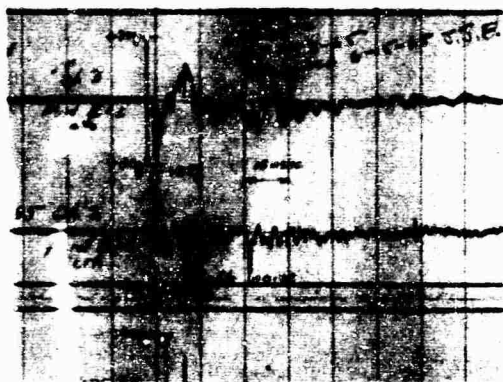
Fig. 1 - Annotated oscillogram

A further defect of the process was the crudity in attempting to redefine a field environment in terms of an achievable laboratory test. Many engineers confronted with such a situation find it expedient simply to tabulate the peaks and durations experienced in field environments, using the maximum value that has been recorded as a laboratory test. Recognizing that oscillatory components of the environment probably have a damaging effect, the engineer might arbitrarily increase the level of the laboratory test in the hope that unknown factors of the field environment would be adequately represented.

In an attempt to regularize the reduction of data, the following desiderata were considered:

1. The final reduction should be graphical and should lend itself to tabulation,

2. Some means of determining the validity of the data is necessary,

3. The data should be readily applicable to design improvements,

4. It should be possible to determine a realizable laboratory test from the data,

5. The data must be in a format acceptable to designers and dynamicists,

6. The data should be readily storable,

7. "Hash" and noise should be removable,

8. The time lag from test to final report should be minimized, and

9. Human error should be minimized.

The shock spectrum technique appeared to satisfy most of these considerations. Shock spectra are discussed extensively by Vigness [1] and Rubin [2] and will not be further explained here.

Shock spectra can be presented graphically, can be easily stored, and are usable for design improvements and laboratory test planning. However, the validity of the data cannot be determined easily from the shock spectrum. It was felt advisable, therefore, to include the acceleration-time history along with the shock spectrum.

Analog data reduction was considered first. A type of analog shock spectrum computer was developed and tested, but was found to have many disadvantages, including the following:

1. Operation of even a simple analog shock spectrum computer requires intervention by a skilled operator,

2. Human error can be a problem even with great care, and

3. The plots turned out were less neat than desired.

Digital reduction was next investigated. This, it was felt, could materially reduce human error. The cost, unfortunately, would be high, but we believed that the advantages of the method would outweigh this disadvantage.

At present, shock records are kept on magnetic tape in analog form. These analog tapes are then digitized by an Astrodata Model 4101 analog-to-digital converter. Only those portions of the analog tape containing actual pulses are digitized. A digitizing rate of at least 15 times the highest frequency of interest is used; normally this is chosen to be at least 15 times the cutoff frequency of any low-pass filter used in conditioning the analog signal

All further operations are now carried out on the digital tape. The analog tape is retained for 90 days in case any portion needs to be redigitized, and is then available for reuse.

22

Before any use is made of the digital tape, a quick-look oscillogram made from the analog tape is scrutinized jointly by a test engineer, a dynamicist, and if desired, the design engineer. Any records showing indications of cable breakage, zero shift, excessive noise, or other glaring defects are automatically discarded. A plot of the acceleration-time history of such records is usually made, but no further reduction is carried out.

The remaining records are now quickly checked to decide which ones will be reduced to shock spectra. In general, records from transducers placed on components are avoided. It is felt that such pulses should be treated as responses rather than inputs. Exceptions to this rule are made in cases where one component is mounted on another, or where a component contains many parts so that the response of the component case can be considered an input to the parts. We are always cautious about reducing data that appear imperfect or invalid. Seldom more than 10 percent of the channels on a systems test will be marked for complete reduction.

The digital tape (which contains all the pulses and calibrations) is now reduced in a CDC 3600 computer. The flow of information is shown in block diagram form in Fig. 2.

Some of the options available include:

1. Low-pass filtering to any desired cutoff frequency;

2. Editing to remove unnecessary points;

3. Plotting of tne acceleration-time history before or after filtering and editing, or both;

4. Removal of spurious or questionable sections; and

5. Computation of the shock spectrum, which can be plotted or printed, or both.

An option not yet present because of lack of demand is the computation of the Fourier spectrum, but it can be included at any time.

Plotting is done on a Stromberg Carlson SC 4020 high-speed plotter. Each plot has any desired identification printed on it, as well as the total velocity change of the pulse. Since all pulses are digitized at a very high frequency, each pulse contains many unnecessary points. Editing reduces the number of points.

All the digital points are scanned in turn. If the omission of any point would result in an
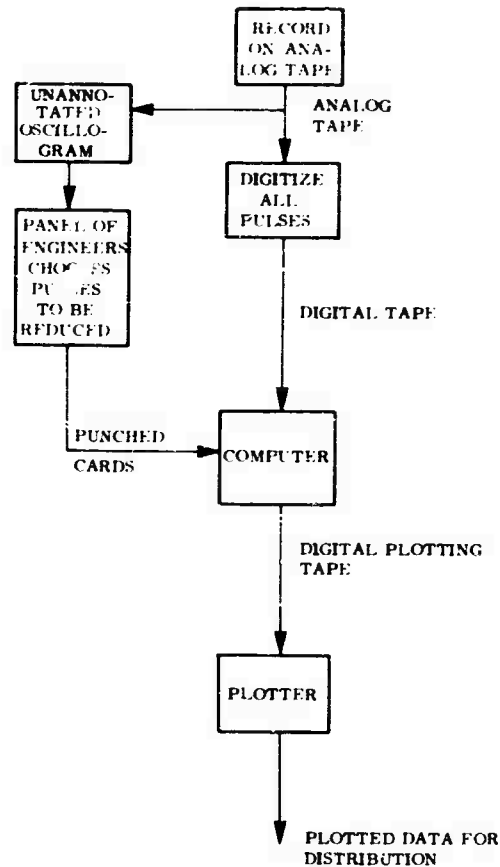
Fig. 2 - Digital shock data reduction

error exceeding some predetermined percentage of full scale, that point is retained. The process is shown diagrammatically in Fig. 3.

Editing removes much of the "hash" and noise, resulting in a cleaner plot. The effects of editing at 1, 2, and 5 percent of the calibrate level are shown in Figs. 4, 5, 6, and 7. The associated shock spectra (Figs. 8, 9, 10, and 11) show that the edits have resulted in only very minor deviations in the shock spectra. A standard edit of 1 percent has been selected; this has been tried on a wide variety of shock pulses and appears to be satisfactory.

Filtering is accomplished by the digital equivalent of an analog filter. The transfer function of the filtering system is shown in Fig. 12. The transfer function of the filter is

$$G(s) \quad \frac{\omega^4}{(s^2 + \sqrt{2}\ \omega s + \omega^2)^2} \cdot \qquad (1)$$

Such a transfer function is given by

23

Fig. 3 - Edit criteria

SECOND PULSE -- 5 KC FILTER
NO EDIT
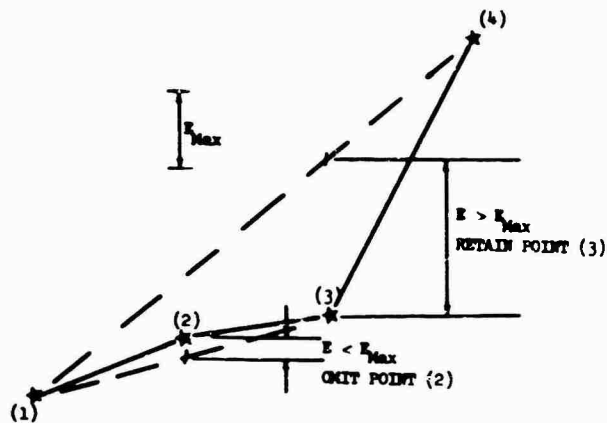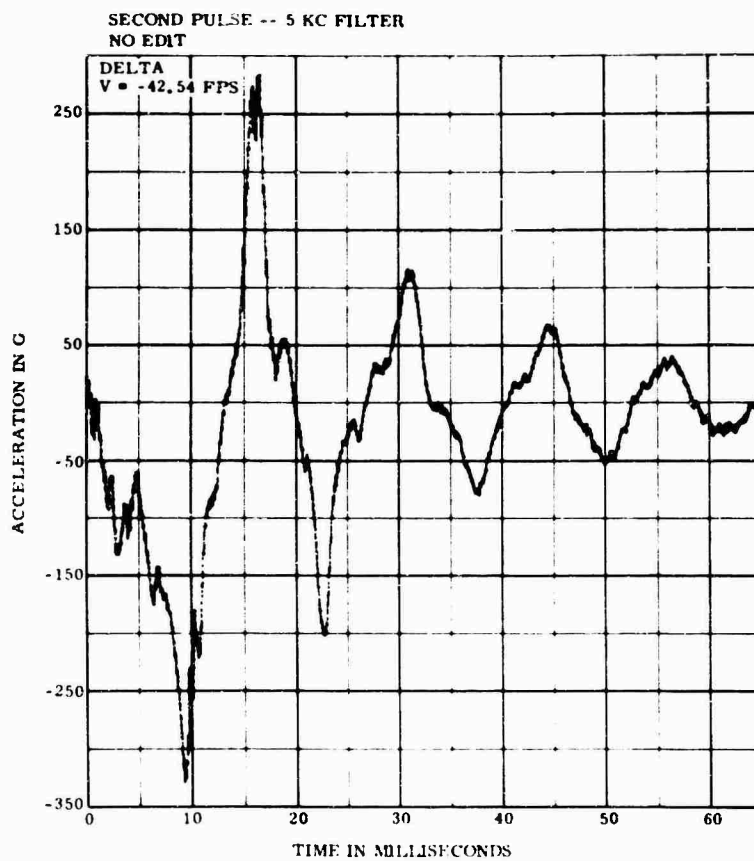
Fig. 4 - Pulse with no edit

$$\frac{d^4 y}{dt^4} + 2\sqrt{2} \quad \frac{d^3 y}{dt^3} + 2 \cdot 2 \frac{d^2 y}{dt^2}$$

$$+ 2\sqrt{2} \quad \frac{3}{dt} \frac{dy}{dt} + \frac{4}{y} + \frac{4}{x} \quad 0 . \qquad (2)$$

where y is the filtered output, x is the unfiltered input, and is the circular cutoff frequency of the filter. The equation is solved using Runge-Kutta integration. The plot of a typical filtered pulse is shown in Fig. 13, which may be compared with the original pulse on Fig. 4.

24
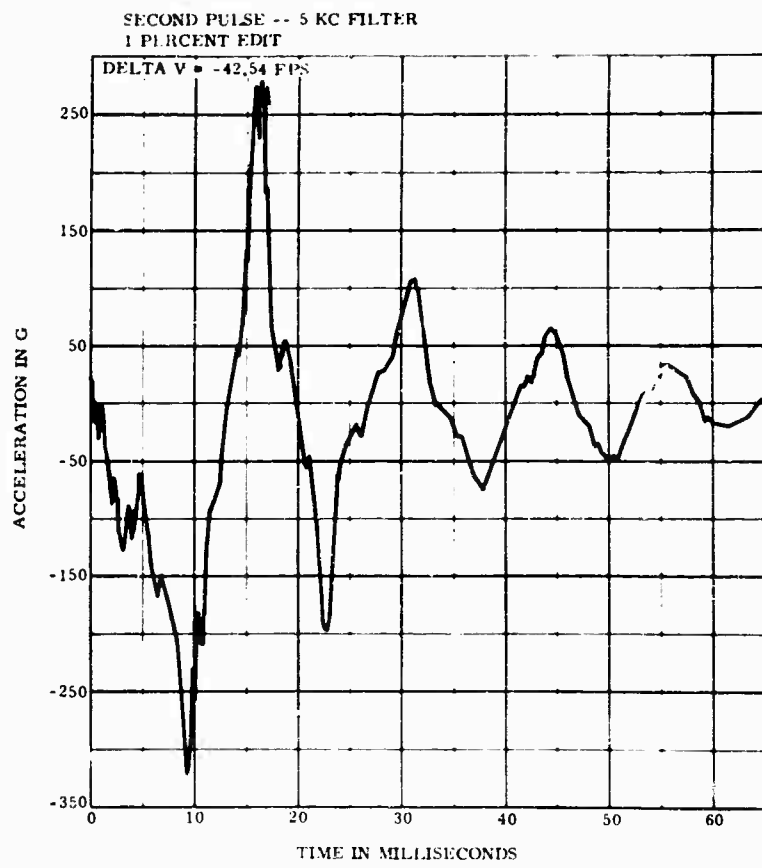
Fig. 5 - Pulse with 1 percent edit

25
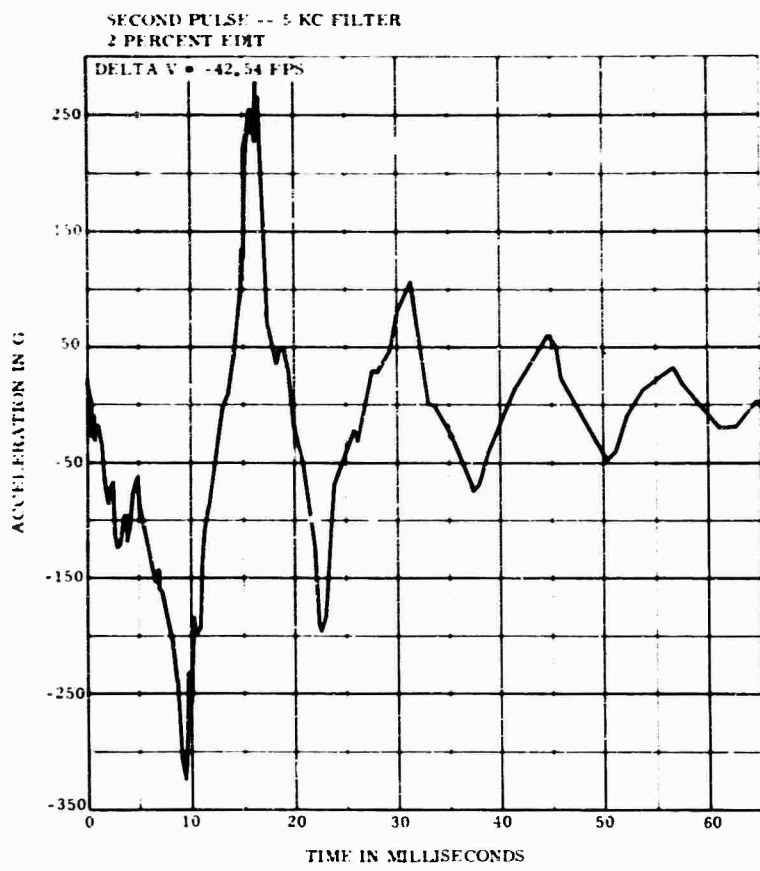
Fig. 6 - Pulse with 2 percent edit
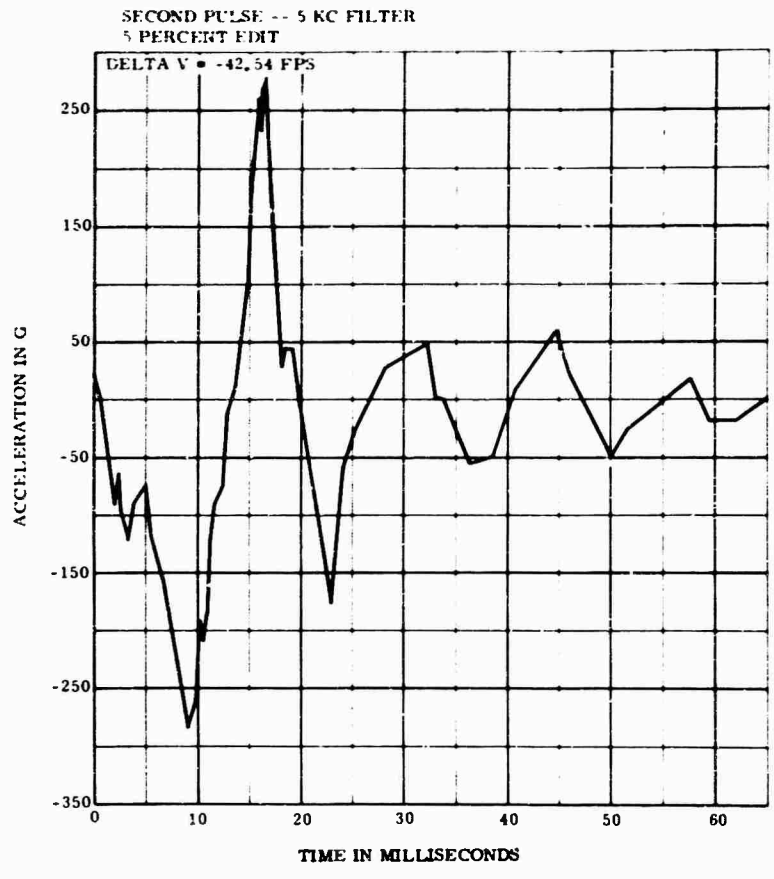
Fig. 7 - Pulse with 5 percent edit

27
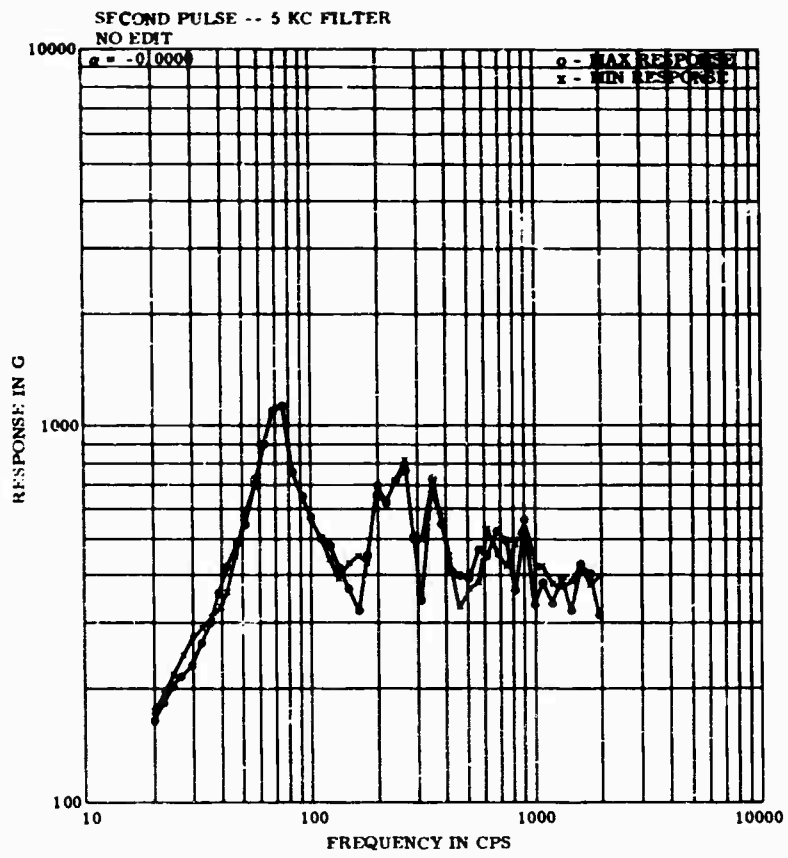
Fig. 8 - Spectrum, no edit

28
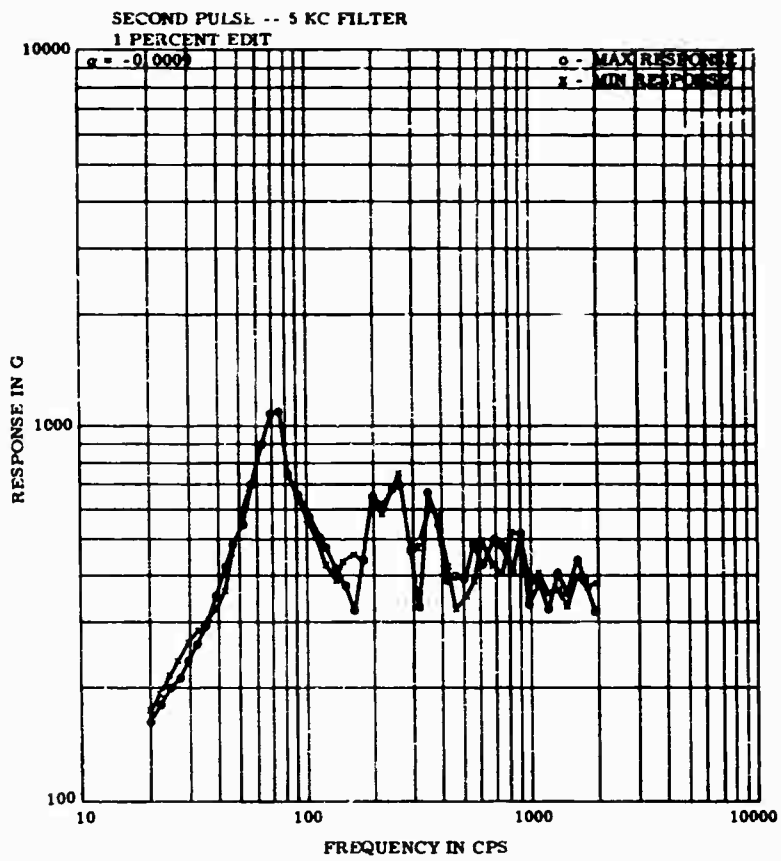
Fig. 9 - Spectrum, 1 percent edit
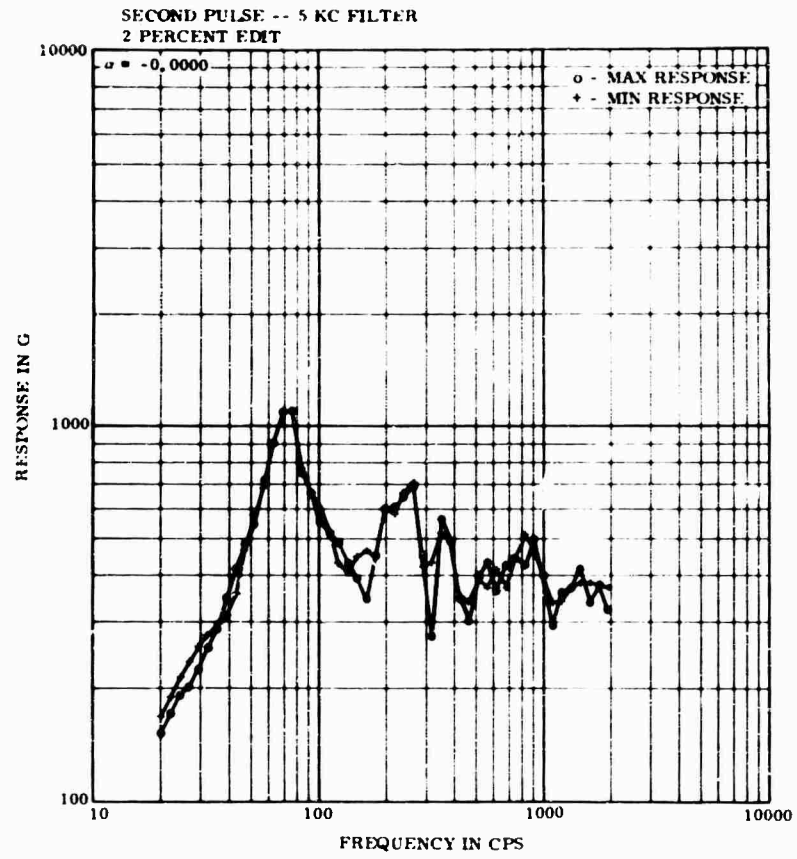
Fig. 10 - Spectrum, 2 percent edit

30
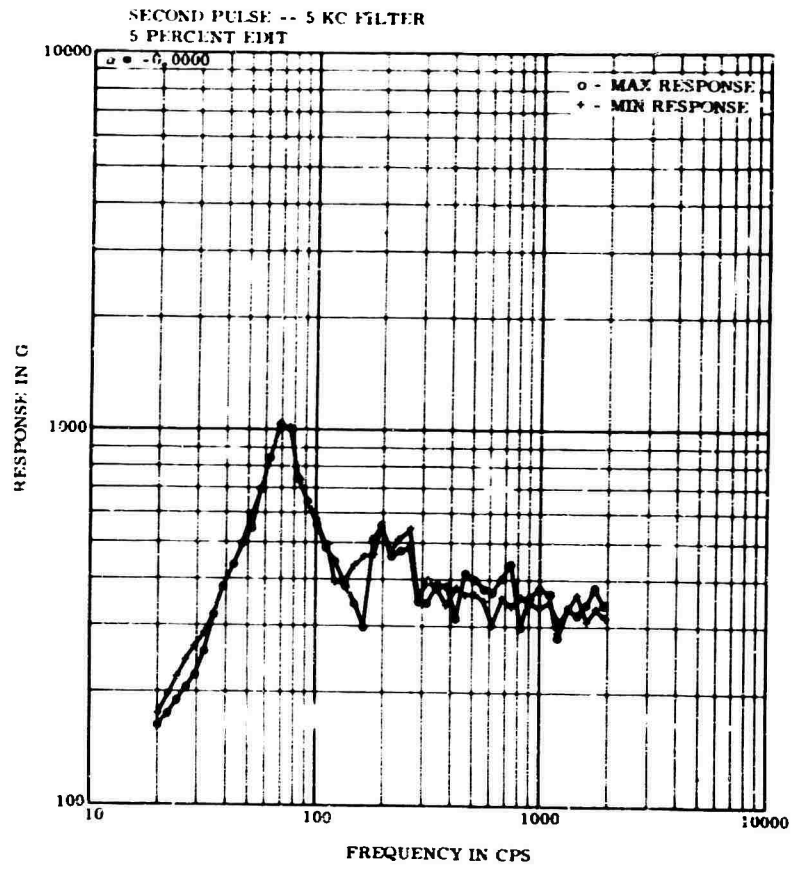
Fig. 11 - Spectrum, 5 percent edit

Fig. 12 - Filter characteristics
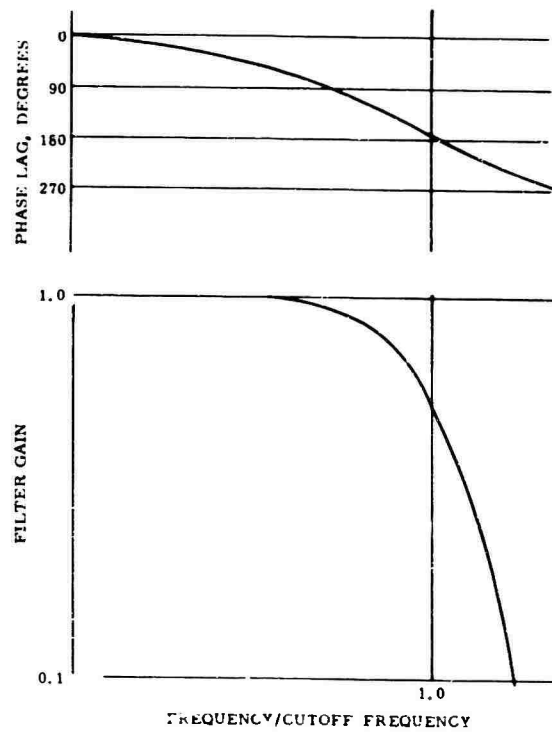
SECOND PULSE -- 500 CPS FILTER
NO EDIT
DELTA V = -42.54 FPS
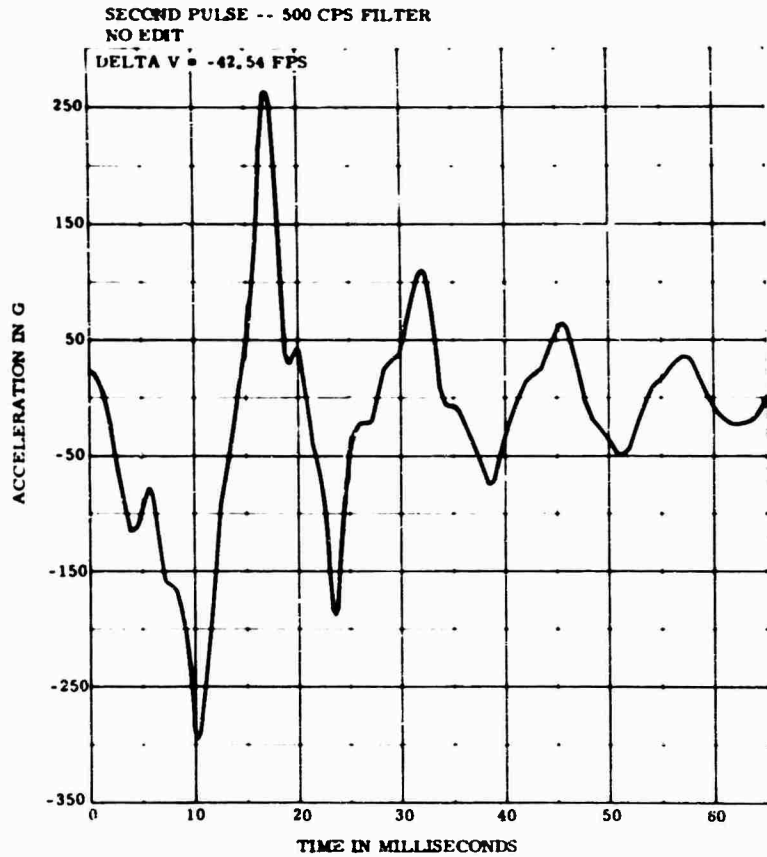
Fig. 13 - Filtered pulse

The computation of shock spectra is relatively simple, but somewhat more time consuming The input is considered to be piecewise linear between the digitized points.

Consider a single-degree-of-freedom system whose base undergoes an acceleration of $A_x(t)$. The equations are developed for an undamped system, because the algebra becomes somewhat involved for a damped system. Damping is indeed included in the actual computer programs. Because the input is piecewise linear, it can be represented by

$$A_x(t) \quad \quad t \quad t_o \quad t \quad t_o + \Delta t . \quad (3)$$

The response y to a displacement input x is given by

$$y + \quad^2 y \quad \quad^2 x . \quad (4a)$$

or, in a more useful form for our purposes,

$$A_y + \quad^2 A_y \quad \quad^2 A_x . \quad (4b)$$

Using the Laplace transform, we have

$$A_y(s) \quad \frac{\quad^2 A_x(s) + A_y(0) + s A_y(0)}{s^2 + \quad^2} . \quad (5)$$

This can be solved to give values of A_y and $\dot{A}_y$ at $t \quad t_o + \Delta t$

$$A_y(t + \Delta t) \quad (\quad + \quad t_o)(1 - \cos \quad \Delta t) + \quad \Delta t$$

$$\frac{\dot{A}_y(t_o)}{\quad} \sin \quad \Delta t + A(t_o) \cos \quad \Delta t$$

$$- \frac{\quad}{\quad} \sin \quad \Delta t . \quad (6)$$

and

$$\dot{A}_y(t + \Delta t) \quad \quad (\quad + \quad t_o) \sin \quad \Delta t + \quad (1 - \cos \quad \Delta t)$$

$$- \quad A_y(t_o) \sin \quad \Delta t + \dot{A}_y(t_o) \cos \quad \Delta t . \quad (7)$$

The time interval Δt is chosen to be $1/20$ of the natural period, or less when required to maintain piecewise linearity over the interval.

32

Maximum (positive) and minimum (negative) response spectra are plotted for 0, 3, and 10 percent of critical damping in Figs. 14, 15, and 16. It is also possible to plot the envelopes of a number of spectra. If desired, the spectrum of the relative displacement between the component and the base can also be plotted.

Any frequency limits can be chosen. Frequency steps are logarithmic, so the density of frequency points is uniform on a log-log scale. We have presently standardized on frequencies increasing by intervals of 10 percent.

Choosing a suitable laboratory test is essentially a hand operation, but requires very little time. Transparent overlays of normalized ideal laboratory pulses (half-sines, triangles, haversines, etc.) have been plotted on all the log-log scales used for spectrum plots. The overlays are shifted on the spectrum plot until the spectrum of the laboratory pulse just envelopes the spectrum of the environmental pulse, as shown in Fig. 15. The spectrum of a 420-g 8.3-msec half-sine envelopes the spectrum of the environmental pulse.

At the beginning of our program, designers were somewhat unwilling to utilize shock spectrum data because of unfamiliarity with the technique. Also, as Fig. 15 indicates, the laboratory test pulse very much exceeds the environmental pulse in both amplitude and velocity change. This must be explained to the designer.

Direct assistance is given to design engineers in applying the method. The advantages and limitations of the technique have been explained in short lectures. As a result, considerable enthusiasm has been generated in design and test organizations.

One of the outgrowths of the automated system has been a reduction in the time lag from test to final report. This is due largely to the elimination of hand annotation of oscillograms. The appearance of reports has also been en- · ced. Another benefit is the ease of storage in the Sandia Environmental Data Bank. Because all records have been scrutinized by a knowledgeable group of engineers and only the most significant are chosen for spectrum reduction, it can be assumed that nearly all the spectra are significant and valid.
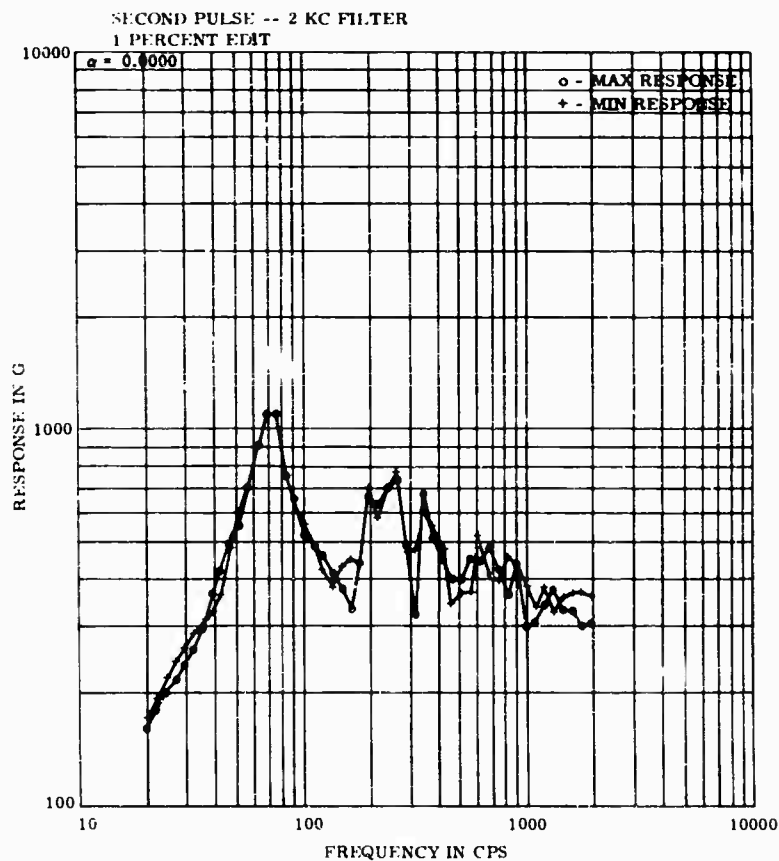
Fig. 14 - Spectrum, no damping

33
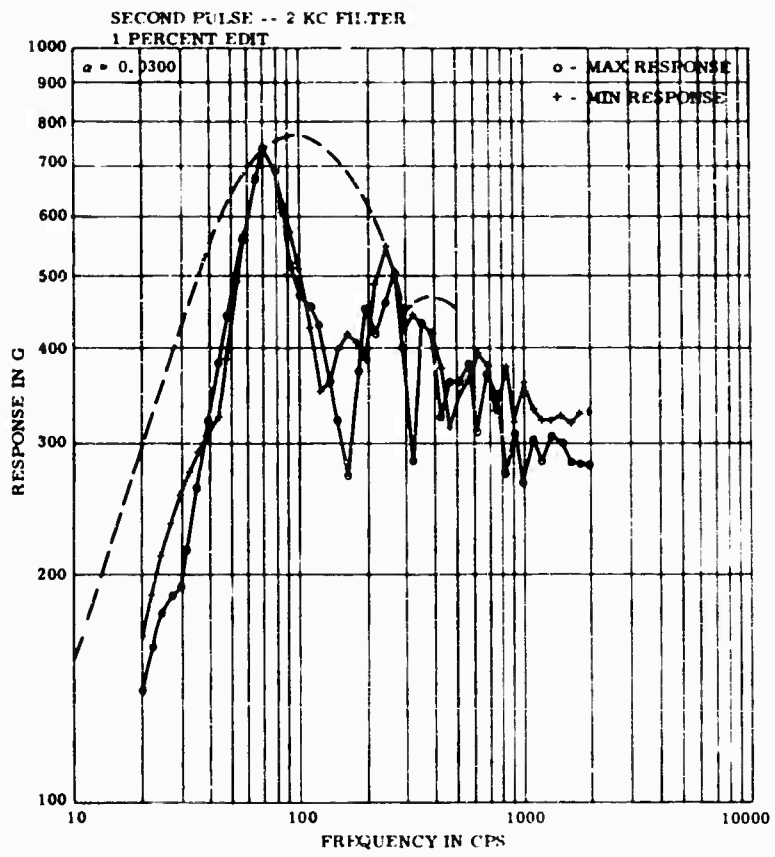
Fig. 15 - Spectrum, 5 percent damping
with test pulse spectrum

34

SECOND PULSE -- 2 KC FILTER
1 PERCENT EDIT

$\alpha = 0.1000$

o - MAX RESPONSE
+ - MIN RESPONSE

RESPONSE IN G

FREQUENCY IN CPS
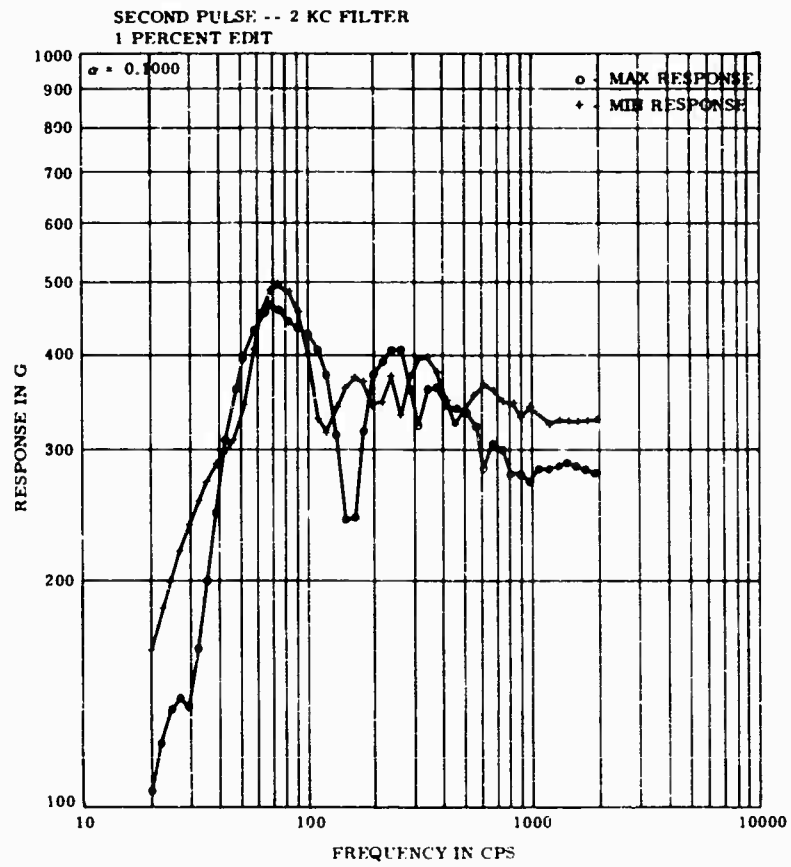
Fig. 16 - Spectrum, 10 percent damping

35

The automated shock data system has not yet been developed into its final format. Changes and improvements are in process at all times. However, the utility of the system has already shown itself in the relatively short time it has been in use. It is expected that eventually all of Sandia's shock data will be reduced by this system, resulting in considerable improvement in the utility of the data.

ACKNOWLEDGMENTS

R. W. Bradshaw developed the data handling programs. A. R. Nord assisted in the shock spectrum program.

REFERENCES

1. I. Vigness, "Elementary Considerations of Shock Spectra," Shock and Vibration Bull. No. 34, Part 3, pp. 211-222, Dec. 1964

2. Sheldon Rubin, "Concepts in Shock Data Analysis," Shock and Vibration Handbook (C. M. Harris and C. E. Crede, ed.), Vol. 2, Chap. 23, pp. 23-1 to 23-37. McGraw-Hill, New York, 1961

DISCUSSION

Mr. Holland (Allied Research Associates): Is the digital response computed at every digital input point?

Mr. Murfin: No, it is independent of the digital input frequency. We use 20 points per cycle, which gives a maximum error of about 1 percent according to Gertel's curve.

*   *   *

AUTOMATED ANALOG METHOD OF SHOCK ANALYSIS

F. X. Prendergast
Bell Telephone Laboratories
Whippany, New Jersey

An automated analog method for determining the frequency response of various second-order systems to shock inputs is described. The method can be used to perform shock spectrum analysis and to study shock response of various types of nonlinear systems.

The unique features of this method are: (a) the analog program is designed to be used with a medium-sized analog computer; (b) automatic frequency stepping is accomplished by the use of multipliers in the analog of the second-order system, instead of potentiometers; and (c) the operating mode of the computer can be slaved to shock pulses, either synthesized within the computer or recorded on magnetic tape.

The paper also describes two methods of plotting frequency response: a simplified technique which results in a bar graph presentation, and a peak detection and sample-hold technique which results in a point-to-point plot. An x-y plotter can be used as a readout device for either of these methods.

Examples are given which demonstrate the use of the method in obtaining shock spectra. A study of a typical nonlinear system's response to shock inputs is also presented.

F. X. Prendergast

INTRODUCTION

The analog computer is an excellent tool for solving linear and many types of nonlinear second-order differential equations. It is particularly suitable for determining system response-time histories and rapidly assessing the effects of various parameter changes on system response. Conversely, using the analog computer to determine frequency response functions requires a great deal of tedious operator time to change parameters, record peak values, and plot results.

It would be helpful if an automated program could be developed to perform these routine functions. Obviously, if an analog facility is large enough and is equipped with servo-set potentiometers, automation is no problem. The purpose of this paper is to describe an automated method for determining the frequency response of various second-order systems to shock inputs, which can be used with the usual assortment of amplifiers, integrators, multipliers, and comparators.

A STEP TOWARD AUTOMATION

The automated analog computer method for determining the frequency response of various systems can be best described by applying it to the linear single-degree-of-freedom system shown in Fig. 1. The maximax response of this system, $\ddot{x}$, to a shock input $\ddot{y}$ applied at the base is the familiar acceleration shock spectrum. The differential equation of motion for this system is
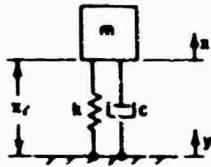
Fig. 1 - Single-degree of-
freedom system

$$\ddot{x} + 2\zeta\omega\dot{x}_r + \omega^2 x_r = 0 . \qquad (1)$$

where ω is the undamped natural frequency of
the system and ζ is the damping ratio. This
can be written in terms of the single variable
x_r by making the substitution

$$x = x_r + y \qquad (2)$$

Equation (1) now becomes

$$\ddot{x}_r + 2\zeta\omega\dot{x}_r + \omega^2 x_r = \ddot{y} . \qquad (3)$$

The usual analog computer program for
Eq. (3) is shown in Fig. 2. The analog symbols
used are from the EAI Handbook [1]. If this
program is used to perform a frequency re-
sponse analysis, the two ω potentiometers must
be adjusted for each new frequency considered.
Obviously, then, the first step toward automat-
ing the system is to replace these potentiome-
ters with devices that will also perform the po-
tentiometer function, but can be controlled
electronically rather than mechanically. The
quarter-square multipliers are used for this
purpose. The analog program for the single-
degree-of-freedom system, using multipliers
instead of potentiometers, is shown in Fig. 3.
As is evident, this program allows the frequency
parameter to be changed quite easily by supply-
ing a voltage ω to the two multipliers. The
program has additional features which are not
immediately obvious. One potentiometer can
now supply a voltage which represents ω, and
also control the abscissa of the x-y plotter.
This dual control allows the frequency to be
changed by any arbitrary amount without the
necessity for reading actual potentiometer val-
ues. No matter what frequency is chosen, the
response will appear in the proper position on
the plotter.
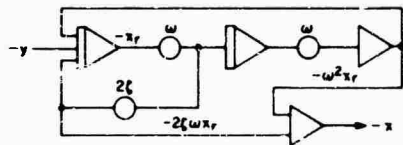
Fig. 2 - Conventional analog
computer program for single-
degree-of-freedom system
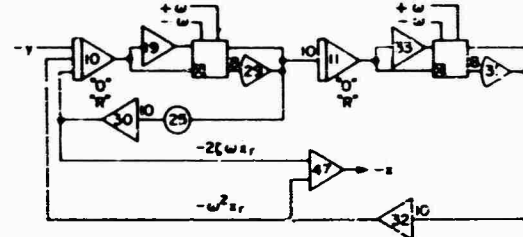
Fig. 3 - Analog program, single-degree-
of-freedom system with multipliers

This first step provides a semiautomatic
program which can be used in cases where the
setup time for a fully automated system is not
justified. Although the need for an operator is
not eliminated, his task is made much less
tedious. This approach is particularly useful
in cases where the frequency response of a
system to only one or two types of pulses is
required.

The "O" and "R" symbols on each of the
integrators in Fig. 3 represent operate and re-
set voltages supplied by the mode control cir-
cuit which will be described below. In the case
of integrators 10 and 11, the "O" voltage is
connected to the operate relays of the integrators
and the "R" voltage is connected to the reset
relays of the integrators.

MODE CONTROL

The next step in automating the analog pro-
gram is the provision of a means of cycling the
operate-reset modes of the computer. Two
methods are presented. The first is to be used
when the shock pulse is internally generated in
the computer. In this method the cycle timing
can be chosen by the operator and even changed
during a run to speed up the program. The only
requirement is that the operate time is long
enough to allow the response to reach its peak.

The second method is used when the input
pulse is stored on a magnetic tape loop. The
cycle time for this case is fixed by the length of
the tape loop. The only freedom that the oper-
ator has in operate time is that he can skip a
cycle if it is necessary to increase the operate
time.

Mode Control — Internally Generated
Pulse

To control the cycle time of the computer,
an asymmetric sawtooth is generated using one
integrator and two comparators as shown in
Fig. 4. The output of integrator 15 in Fig. 4 is

38

the required sawtooth shown in Fig. 5. When the slope of the sawtooth is negative, the comparator terminals are in the positive position, and when the slope of the sawtooth is positive the comparator position is negative. Thus, one pair of these comparator terminals can be used to supply operate and reset voltages to the single-degree-of-freedom system. As integrator 15 operates continuously, the integrators of the single-degree-of-freedom system will alternate between the operate and the reset modes. The three potentiometers 30, 31, and 32 in Fig. 4 are used to control the duration of operate and reset times.

This gate will be discussed later in more detail. The trigger pulse is a rectangular pulse which is recorded on a separate track just before the pulse to be analyzed. The trigger pulse throws the contacts of comparator 38 to the negative side. These contacts are locked in this position until the output of integrator 15, which is put in the operate mode by the comparator, reaches a high enough voltage to reverse the process. The wave produced by integrator 15 is shown in Fig. 7. The operate-reset modes of the single-degree-of-freedom system are slaved to the mode of integrator 15.

Fig. 4 - Mode control program, internally generated pulse
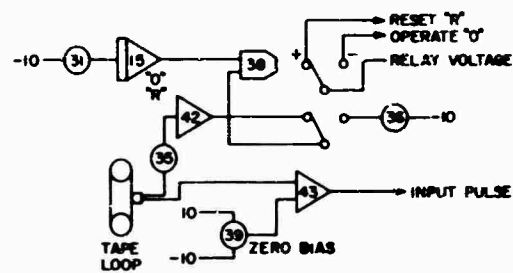
Fig. 6 - Mode control program, tape recorded pulse

Fig. 5 - Mode control cycle waveform, internally generated pulse
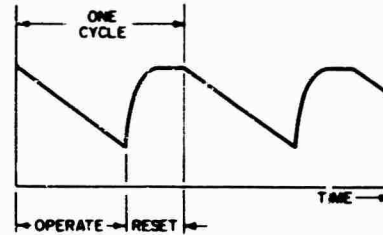
Fig. 7 - Mode control cycle waveform, tape recorded pulse

Mode Control — Magnetic Tape
  Loop Pulse

The objective in this case is to generate a wave similar to that of Fig. 5, but slaved to a signal on a magnetic tape loop. Figure 6 shows the analog program which produces this wave. The pulse to be analyzed and a trigger pulse are fed from the tape loop to the computer. The forcing function is fed into a summing amplifier where any unwanted dc component can be biased out. If the magnetic tape is noisy, following the pulse, the output of amplifier 42 can be fed to a gating device to eliminate the noise.

FREQUENCY STEPPING CIRCUIT

Figure 8 shows the computer program for the frequency stepping circuit. Its function is to provide a voltage which represents frequency in the single-degree-of-freedom system. It must provide a constant voltage when the main system is in the operate mode, and increase (or decrease) this voltage by a prescribed amount when the main system is in its reset mode. This is accomplished by operating integrator 03 during the main system reset cycle and holding integrator 03 during the operate cycle.

Potentiometer 00 controls the rate of change in . This rate is positive as shown in

39
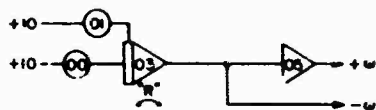
Fig. 8 - Frequency step-
ping program

Fig. 8, but it could be reversed merely by
changing the polarity of the reference voltage
supplied to potentiometer 00. Potentiometer
01 provides a means of starting a run at any
arbitrary initial frequency.

PULSE GATING

As mentioned above, it is sometimes nec-
essary to gate the input pulse when the magnetic
tape loop has excessive noise following the pulse.
It is also necessary to provide a similar type of
gating circuit for computer generated pulses. For
instance, if the pulse to be generated and analyzed
is a half-sine wave, it is produced by starting a
sine wave generator, which can be programmed
on the computer, at the beginning of the operate
cycle. A gate is then used to cut off the sine
wave generator after one-half cycle. Figure 9
shows the computer program for gating the input
pulse. An input function is fed through the relay
contacts as shown. These contacts are opened
when the output of integrator 21 reaches a pre-
set negative voltage. Potentiometer 22 controls
the length of the gate.
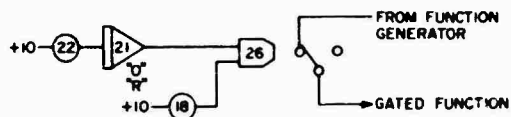
Fig. 9 - Pulse gating program

PLOTTING

In the system under discussion, it is neces-
sary to find the maximax response of the single-
degree-of-freedom system at each frequency,
and plot this value as a function of frequency.
One simple technique is to rectify the output
using the program shown in Fig. 10, and plot
the rectified signal as a vertical line on an x-y
plotter. The horizontal position on the graph
can be controlled by the voltage which repre-
sents x in the second-order system. The pen
of the plotter can be raised and lowered in the
proper sequence by slaving it to the operate-

reset cycle of the second-order system. Fig-
ures 11 and 12 are typical of the type of graphs
produced by this method.
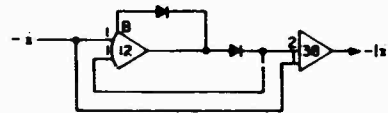
Fig. 10 - Full wave rectifier
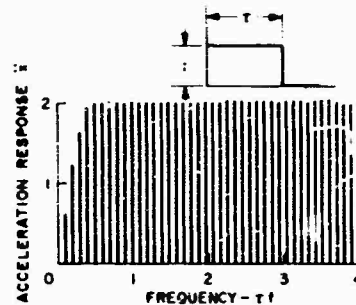
Fig. 11 - Maximax shock
spectrum, unit rectangu-
lar pulse, $\tau = 0$
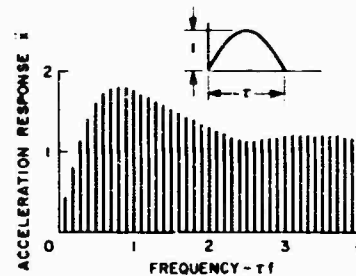
Fig. 12 - Maximax shock
spectrum, unit half-sine
pulse, $\tau = 0$

One disadvantage to this simple plotting
program involving the low-frequency response
capability of the plotter is the possibility of pen
overshoot influencing the peak detection. Be-
cause of this limitation, the programs shown in
Figs. 13 and 14 were added to the system. The
program in Fig. 13 is a peak detection circuit
while that in Fig. 14 is a low-pass sample-hold
circuit. The output of the rectifier is fed through
the peak detection and the sample-hold circuits,
and then to the x-y plotter. Bar graphs similar
to Figs. 11 and 12 can also be drawn with this
setup, but now the real-time frequencies of the
second-order system are not limited by the
pen response.

40
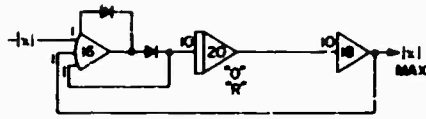
Fig. 13 - Peak detector
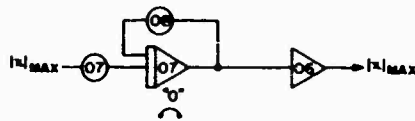
Fig. 14 - Low-pass sample-
hold program

By programming the pen to drop for a
short period of time after the main system has
been reset, a point-to-point plot such as shown
later in Figs. 20, 21 and 25 can be drawn. The
analog program for this circuit is shown in
Fig. 15.
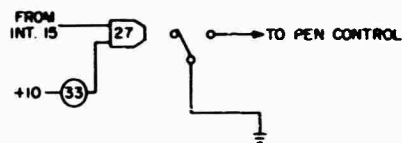
Fig. 15 - Pen control program,
point-to-point plot

OPERATION OF OVERALL
PROGRAM

Figure 16 shows the complete analog com-
puter program for the response of a single-
degree-of-freedom system to a half-sine pulse.
This specific case is used to show the functions
of several of the major elements in the program.

Figure 17 presents a series of graphs which
show the relationships of these major elements
with respect to time. The three complete cycles
shown represent the operation of the system at
three different frequencies. Graph a is the out-
put of integrator 15 which is the principal ele-
ment in the mode control and gating circuits.
Note how the operate and reset modes corre-
spond to the slope of the asymmetric curve.
Graph b represents the gated input pulse which
occurs at the beginning of each operate cycle.
Graph c represents the output $\ddot{x}$ of the single-
degree-of-freedom system. For this example,
the damping of the system was set at zero.

Each of the three cycles shows a different re-
sponse corresponding to the three separate fre-
quencies of the system. Graph d shows the
output of amplifier 38 which is the absolute
value of the response $\ddot{x}$. Graph e is the output
of the peak detection circuit, amplifier 18.
Note that this curve holds the peak of the rec-
tified output until the system has reset. Graph
f shows the output of the sample-hold circuit,
amplifier 06. Note that it samples the peak
value of the response during the operate time
and holds this value during reset time. Graph
g shows which part of the output of the sample-
hold circuit is actually plotted. The short
dashed lines of this graph represent the pen
writing time. Graph h is a plot of the output of
amplifier 05 which represents the frequency
of the system. Note that this maintains a con-
stant value during the system operate time and
increases during the system reset time.

The potentiometer functions in Fig. 16 are
tabulated below:

Potentiometer	Function
No. 00	Frequency increment control.
No. 01	Initial operating frequency.
No. 06	Amplitude of gated forcing function.
No. 07	Low-pass filter response control.
No. 08	Same as 07; same setting if no gain is required.
No. 13	Amplitude of sine-wave forcing function.
No. 18	Length of pulse gate.
No. 22	Same as 18.
No. 25	Damping of responding second-order system.
No. 26	Damping of sinusoidal forcing function.
No. 27	Frequency of forcing function.
No. 28	Same as 27.
No. 30	Amplitude of sawtooth wave-form.
No. 31	Length of operating cycle.
No. 32	Length of reset cycle.
No. 33	Plotter pen writing time.

ACCURACY

Since the purpose of this paper is to discuss
automation of an analog program, and not analog
computer programming itself, only inaccuracies
introduced by automation will be considered.
One such inaccuracy is caused by substituting
multipliers, which are nonlinear devices, to
perform the linear function normally done by
potentiometers. The degree of inaccuracy can

41
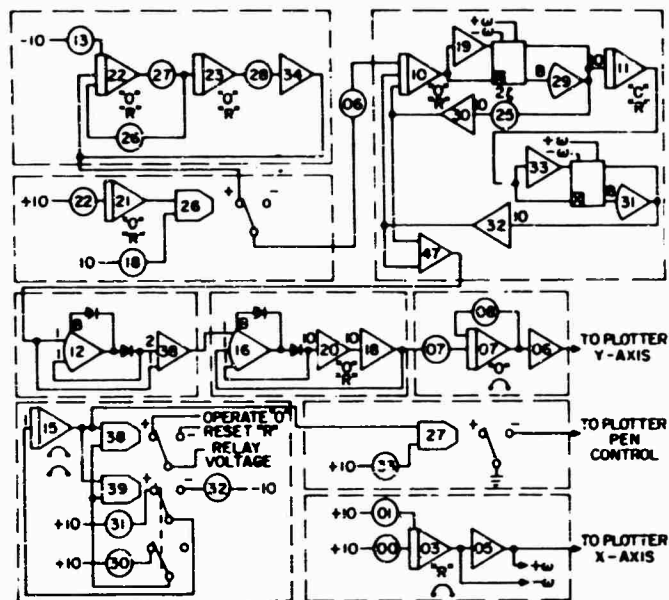
Fig. 16 - Automated analog computer diagram for shock spectrum analysis of half-sine pulse
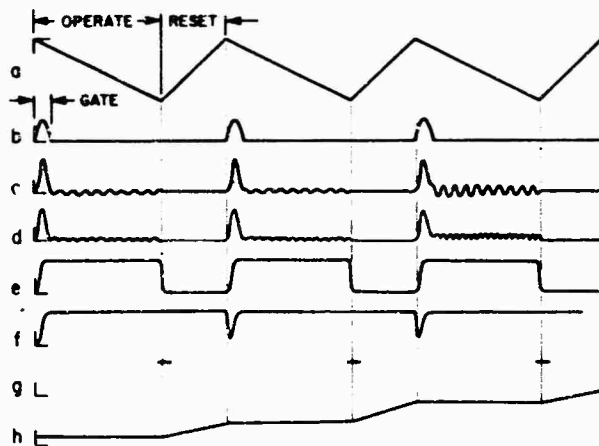
Fig. 17 - Typical readouts of subprograms in automated system

best be seen by examining the shock spectrum of a rectangular pulse as shown in Fig. 11. The analytic solution indicates that the spectrum should have a constant value of two for normalized frequencies higher than 0.5. The graph in Fig. 11 has a slight waviness to it with an error of about 1 or 2 percent. This is due to the non-linearity of the multipliers. This error can be kept to a minimum by properly magnitude scaling the multipliers.

The only other inaccuracy introduced in the automated program is in the leakage of the peak detector circuit. This can be minimized, and almost eliminated, by proper diode selection.

It is felt that the automated program eliminates the chance of human error in reading potentiometer settings. As mentioned previously, the conventional method of frequency analysis involves the tedious job of setting two or three potentiometers for each frequency in the desired spectrum.

42

APPLICATION TO SHOCK
SPECTRUM ANALYSIS

Throughout the description of the automated frequency response system we have been using a maximax shock spectrum as an example. Figures 11 and 12, mentioned above to illustrate a type of plotting, represent maximax shock spectra for the classical rectangular and half-sine shock pulses. Figures 18 and 19 are also shock spectra of classical pulses. Figure 18 is the spectrum of a terminal sawtooth, and Fig. 19 is that of a damped sine wave. Figure 20 is the same spectrum as in Fig. 19, but using the alternate plotting system. Figure 21 is an example of a shock spectrum of a real pulse analyzed by this automated program. This pulse was recorded during a recent missile firing. The shock spectra of the above-mentioned classical pulses agree with those published by Jacobsen and Ayre [2].
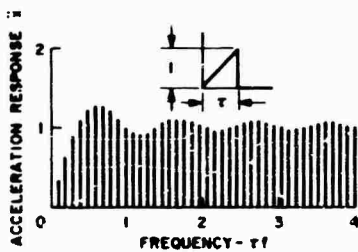
Fig. 18 - Maximax shock spectrum, unit terminal sawtooth, ' = 0
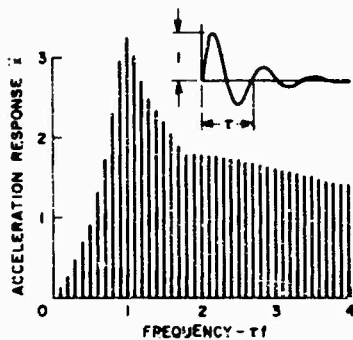
Fig. 19 - Maximax shock spectrum, unit mped s ne pulse, = 0, ba graph presentation

Though each of the examples given are for maximax spectra, it would be a simple matter to plot the residual or even the Fourier spectra
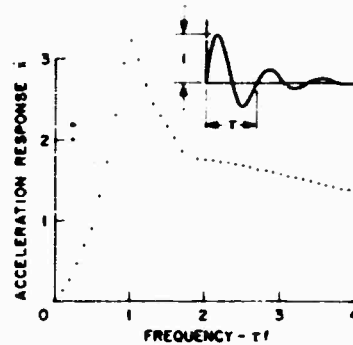
Fig. 20 - Maximax shock spectrum, unit damped sine pulse, ' = 0, point-to-point presentation
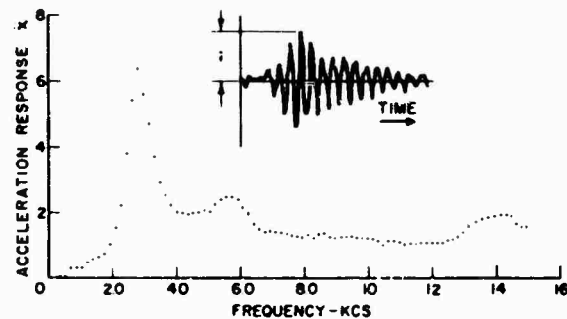
Fig. 21 - Maximax shock spectrum of pulse recorded during recent missile firing, ' = 0.03, recorded pulse time-scaled 1028:1

if desired. If more than one x-y plotter is available, these could be plotted simultaneously.

APPLICATION TO A NONLINEAR
SYSTEM

Up to this point, only the linear single-degree-of-freedom system has been used in conjunction with the automated shock response program. To illustrate its use with nonlinear systems, we will consider the shock response of a bilinear single-degree-of-freedom system. This is a system which has different but constant spring rates, depending on whether the spring is in tension or compression about some reference axis. The mathematical model for this system is shown in Fig. 22.

An undamped system is assumed to facilitate the analytic approach (see Appendix) which will be used as a check on the computer results.

43
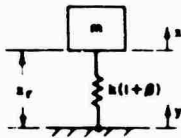
Fig. 22 - Bilinear single-degree-of-freedom system

The addition of damping to the computer program is obviously a simple step but will not be considered in this analysis.

The symbols in Fig. 22 represent the usual vibration parameters and coordinates. The symbol represents the bilinear characteristic of the spring. It has the following properties:

$$-1 \quad \quad \text{when } x \quad 0 ;$$
$$\quad 0 \quad \text{when } x \quad 0 . \tag{4}$$

Figure 23 shows the force-displacement characteristic of the bilinear spring. The equation of motion for the mass in Fig. 22 can be written as

$$m\ddot{x} \cdot k(1 \cdot)x_r \quad 0 . \tag{5}$$
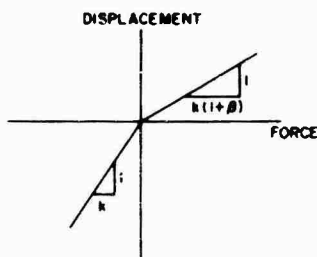
Fig. 23 - Bilinear spring characteristics

This can be normalized by letting $\quad k \; m$ and also reduced to the single variable x_r by making the substitution $\ddot{x} \quad \ddot{x}_r \cdot \ddot{y}$:

$$\ddot{x}_r \cdot (1 \cdot)x_r \quad \ddot{y} . \tag{6}$$

The analog program for Eq. (6) is shown in Fig. 24. It is the same as that of a linear single-degree-of-freedom system except for the half-wave rectifier which represents the function. As shown in Fig. 24, the nonlinear parameter can be set at any value from 0 to 1. To illustrate the effect of the nonlinearity and the use of the automated program, an acceleration response spectrum of the bilinear system to a unit rectangular pulse is given in Fig. 25. For this case, was set equal to one.

An analytic solution for the shock response of the bilinear system to a unit rectangular pulse is given in the Appendix. Note that the curve in Fig. 25 is in complete agreement with Eqs. (A-14) and (A-15).
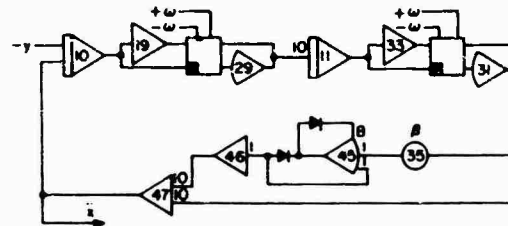
Fig. 24 - Analog program, bilinear single-degree-of-freedom system
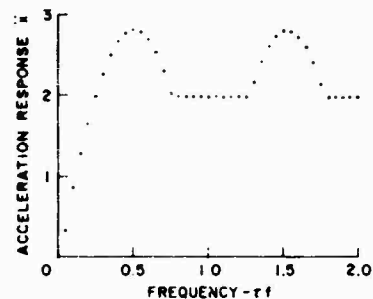
Fig. 25 - Maximax response spectrum of bilinear single-degree-of-freedom system to a unit rectangular pulse, -1, $= 0$

OTHER APPLICATIONS

Shock response curves of many other types of nonlinear systems can be made with this automated analog program. Hard and soft spring systems and systems with Coulomb damping and velocity square damping are just a few of the possibilities. Almost any nonlinear variation of the basic single-degree-of-freedom system can be automated.

The automated program can also be used to study the response of multi-degree-of-freedom systems to shock inputs, although it is doubtful whether it would be worth automating a system which is more complicated than two degrees. With a little variation in the method described above, it can be used in steady-state frequency analysis of both linear and nonlinear systems.

44

In fact, the automation technique discussed in this paper can be used in almost any situation where a repetitive type operation is performed, and one or two parameters are changed incrementally between operations.

SUMMARY

This paper has presented a technique for automating an analog computer program for determining the frequency response of a second-order system to shock inputs. The principal feature of the program, which enables automation using only a medium-sized analog computer, is the substitution of quarter-square multipliers for potentiometers in the second-order system. This permits the frequency parameter of the system to be varied by changing a voltage rather than the mechanical shaft of a potentiometer.

Automated mode control of the computer was described for cases in which the input pulses are synthesized by the computer, and also where they are recorded on magnetic tape.

Two methods of plotting frequency response are also described. The first is a simplified technique which merely plots the rectified output of the second-order system as a vertical line on an x-y plotter. The second involves peak detection and sample-hold circuitry, but enables us to operate at much higher real-time frequencies and to plot either bar or point-to-point graphs.

Examples demonstrating the use of the program in shock spectrum analysis and in the frequency response of nonlinear systems are given. It is also pointed out that this type of automation can be used whenever the conventional programming technique requires many potentiometer settings between operations.

ACKNOWLEDGMENT

The author is indebted to H. R. Buchanan for his assistance in the development of this program and in the preparation of illustrations for this paper.

REFERENCES

1. Alan Carlson and George Hannauer, "Handbook of Analog Computation," Electronics Associates, Inc., 1964

2. Lydik S. Jacobsen and Robert S. Ayre, "A Comparative Study of Pulse and Step-Type Loads on a Simple Vibratory System," ATI-139914, DDC, Jan. 25, 1952

Appendix

ANALYTIC SOLUTION FOR SHOCK RESPONSE OF BILINEAR SYSTEM TO UNIT RECTANGULAR PULSE

Consider the equation of motion of the bilinear system shown in Fig. 22:

$$\ddot{x}_r + \omega^2(1 + \epsilon)x_r = -\ddot{y}. \qquad (A-1)$$

If the forcing function $\ddot{y}$ is a unit rectangular pulse of duration τ, the solution for the relative displacement and absolute acceleration responses of the equivalent linear system ($\epsilon = 0$) are

$$x_r = \frac{1}{\omega^2}(\cos \omega t - 1), \quad 0 < t < \tau; \qquad (A-2)$$

$$x_r = \frac{1}{\omega^2}[(1 - \cos \omega \tau)\cos \omega t + \sin \omega \tau \sin \omega t], \quad \tau < t; \qquad (A-3)$$

$$\ddot{x} = 1 - \cos \omega t. \qquad (A-4)$$

and

$$\ddot{x} = (\cos \omega \tau - 1)\cos \omega t + \sin \omega \tau \sin \omega t, \quad \tau < t. \quad (A-5)$$

The maximum positive and negative responses are functions of $\omega \tau$, or the relation between the length of the pulse and the natural frequency of the system. They can be found by examining Eqs. (A-4) and (A-5). Equation (A-4) has a maximum positive value of

$$\ddot{x}_{max} = \begin{cases} 1 - \cos \omega \tau, & 0 < \omega \tau < \pi \\ 2, & \omega \tau > \pi \end{cases} \qquad (A-6)$$

it is never negative. Equation (A-5) is essentially the equation of free vibration with no damping. Therefore, the maximum positive

45

value will equal the maximum negative value for $t > \tau$. From Eq. (A-5) the maximum is

$$\ddot{x}_{max} = 2 \sin \frac{\tau}{2} \qquad (A-7)$$

The maximax acceleration is the maximum of Eqs. (A-6) and (A-7). This is found to be

$$\ddot{x}_{max} \begin{cases} 2 \sin \frac{\tau}{2}, & \tau < \pi \\ 2, & \tau > \pi \end{cases} \qquad (A-8)$$

Since the bilinear system is piecewise linear for values of x_r, which are either all positive or all negative, the above solution for the linear case ($\beta = 0$) can be used as an aid in finding the response of the bilinear system to the rectangular pulse.

According to Eq. (A-2), the relative displacement is always negative during the pulse time. Thus the effect of nonlinearity can be ignored for this part of the solution. Equation (A-2) is valid for all values of β, the bilinear parameter. To find the response after the pulse, we make use of the fact that the system, although nonlinear, is in free undamped vibration. By using the conditions of relative displacement and relative velocity at the end of the pulse, we can calculate the relative velocity of the system when x_r crosses the zero axis:

$$\dot{x}_r (x_r = 0) = \pm \frac{2}{\tau} \sin \frac{\tau}{2} \qquad (A-9)$$

From this we can calculate the maximum negative and positive relative displacements for $t > \tau$:

$$x_{r_{max}} = -\frac{2}{\tau} \sin \frac{\tau}{2}, \quad x_r < 0. \qquad (A-10)$$

$$x_{r_{max}} = \frac{2}{\tau(1+\beta)^{1/2}} \left| \sin \frac{\tau}{2} \right|, \quad x_r > 0. \qquad (A-11)$$

Comparing the responses during and after the pulse, we find that the overall maximum, independent of sign, is the maximum of

$$x_r = \frac{2}{\tau(1+\beta)^{1/2}} \sin \frac{\tau}{2} \qquad (A-12)$$

and

$$x_r \begin{cases} \frac{2}{\tau} \sin \frac{\tau}{2}, & \tau < \pi \\ 2, & \tau > \pi \end{cases} \qquad (A-13)$$

In terms of acceleration, these can be written as

$$\ddot{x} = 2(1+\beta)^{1/2} \sin \frac{\tau}{2} \qquad (A-14)$$

and

$$\ddot{x} \begin{cases} 2 \sin \frac{\tau}{2}, & \tau < \pi \\ 2, & \tau > \pi \end{cases} \qquad (A-15)$$

Note that for negative values of β, the response spectrum is independent of β and is the same as for the linear case, which is illustrated in Fig. 11.

DISCUSSION

Mr. Fitzgibbon (Mechanics Research, Inc.): What would it cost per plot to use this technique for volume data production, and how would the cost compare with that of a similar job done by digital analysis?

Mr. Prendergast: I did not mean to leave the impression that this is meant for volume work. I think it is more useful in studies of unusual systems, such as nonlinear systems, than as a tool for shock spectrum analysis. Actually we use digital methods for pure shock spectrum analysis, but where anything unusual occurs, for example, for finding the effect of filtering on shock pulses and roll-off of amplifiers, we use this system. It takes about an hour or two to set up and 20 minutes to plot about 40 or 50 frequencies. I do not believe the method is applicable to production work.

* * *

46

VIBRATION DATA REDUCTION TECHNIQUES
AS APPLIED TO SATURN S-II VEHICLE

Joseph D. Weatherstone
North American Aviation
Downey, California

J. D. We_therstone

INTRODUCTION

The Saturn S-II contract has resulted in the largest vibration measurement program in the history of North American Aviation. Long before this contract was awarded to the Space and Information Systems Division in 1961, it was obvious that existing facilities for vibration data reduction were inadequate to handle the quantity of data that would be produced during the testing and development of the vehicle.

The Saturn S-II is the second stage of Saturn V, the vehicle designed to send the Apollo space capsule to the moon. The S-II is 33 ft in diameter, 82 ft long, and will weigh nearly 1,000,000 lb fully loaded. Power is provided by five J-2 liquid-hydrogen-fueled rocket engines with individual thrusts of 200,000 lb. Figure 1 shows a cutaway of the S-II.

VIBRATION DATA REDUCTION FACILITY

NASA funding for the S-II made it possible to employ a complete systems concept in the planning of a new vibration data reduction facility. Usually such a facility starts with odd pieces of equipment that are subsequently added to, the result being something of a hodgepodge. In such cases, a process or a machine is apt to be poorly used because it is inherently incompatible with other pieces of equipment.

S-II vibration data requirements indicated that the number of measurements per test would range from approximately 50 to 100. Test durations would extend from a couple of seconds to 395 sec or more. With such qualifications in mind, system requirements were drawn up to provide the following:

1. High-speed analysis subsystem — This is capable of computing the power spectral density (PSD) or average amplitude of a random data signal for each of 50 consecutive frequency segments over a 3 kHz bandwidth in real time. (Real time data are original or reproduced data concurrent with the test being performed.) The filter bandwidths vary from 10 to 100 Hz in steps compatible with other systems used to reduce Saturn data.

2. Digital conversion subsystem — This is capable of converting data from the high-speed analysis subsystem to a digital format recorded on 1/2-in. magnetic tape suitable for processing on a digital computer.

3. Detail analysis subsystem — This is capable of producing analog plots of PSD, cross-spectral density, and transfer functions.

4. Peripheral equipment — This is capable of reproducing data from the originally recorded format, and is necessary in making the facility self-supporting.

Responsibility for the fabrication, installation and acceptance-testing of the entire system was delegated to the manufacturer. The equipment ultimately designed to accomplish this is shown in Fig. 2. The detail analysis subsystem on the left consists of 2-1/2 channels of a typical heterodyne swept-filter analyzer system. A single switch on the front control panel determines the mode of operation, permitting

47
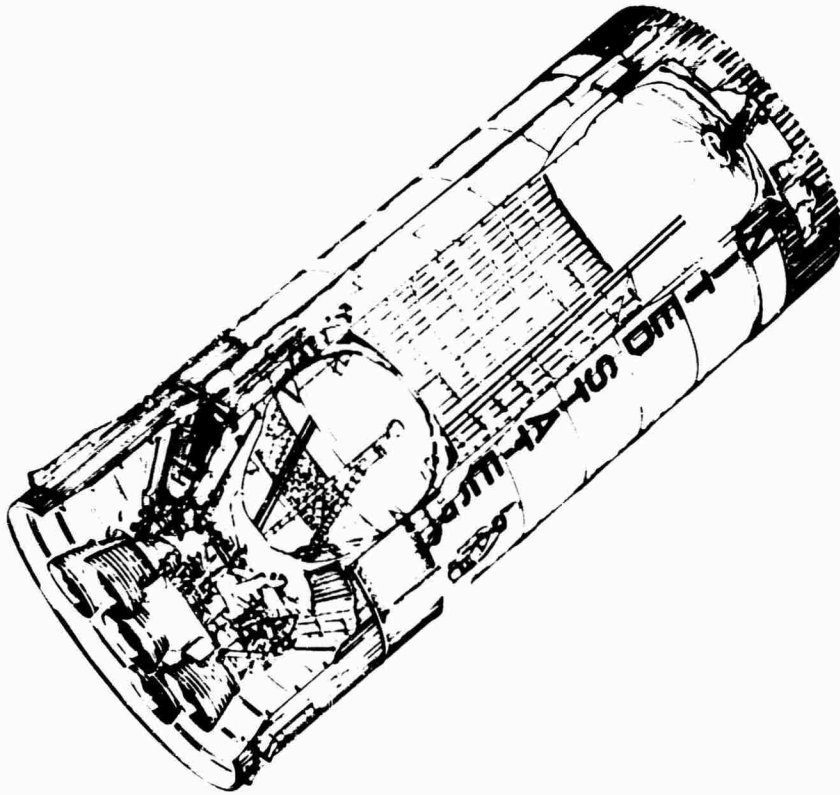
Fig. 1 - Saturn S-II cutaway

Fig. 2 - Vibration analysis and cycle count system

48

either an independent c synchronous operation of the two channels. The system components may also be combined to produce a transmissibility function, coherent and quadrature spectrum, or transfer function. A central monitor point can be switched on to monitor each basic step of the computation in each channel. In this manner, an overall system performance check can be made in a matter of seconds.

The two tape recorders on the left are capable of recording on, or reproducing from, either 1 2- or 1-in. magnetic tapes in FM or direct-record formats. These recorders operate in the reel-to-reel or loop mode with equal ease.

Demodulation equipment contained in the next equipment rack is capable of demodulating IRIG-FM-multiplexed data signals and single-sideband multiplexed signals. The following two racks house oscillograph recorders which use direct-write or processed paper.

Figure 3 shows the high-speed analyzer subsystem (HSAS) in detail. It contains 50 identical circuits, each incorporating a crystal type bandpass filter. These filters provide the system with a much finer frequency resolution than that obtainable with analyzers using magnetostrictive type bandpass filters. Operating modes selected from the front panel make provisions for random or periodic data, power or linear amplitude, and smoothed or integrated output. The period of integration can be varied from one to 99 sec in 1-sec steps. The data

input to the analyzer is in real time. The output of the analyzer is normally routed from a solid-state high-speed multiplexer to an analog-to-digital converter, and on to core storage. The time required to compute a PSD plot can be as short as 1 sec and the time to record the plot information less than 1 10 sec. Operating continuously, the system can put out a PSD plot at the end of each integration time and immediately start in on the next integration. Other options for output presentations are an oscilloscope plot, a tabulated plot from a digital voltmeter (in which case the system cannot operate in the continuous mode), or a continuous oscillograph presentation of the output from each filter.

The remainder of the digital conversion system, the format control buffer (FCB), is shown in Fig. 4. The FCB receives digital data from the high-speed analyzer, stores it in memory until a set amount has been accumulated, and then transfers the entire block of information onto magnetic tape. Also connected to the FCB is an elapsed time-word generator which operates concurrently with the HSAS. The elapsed time word can be multiplexed in with the data for each plot, enabling the plot to be referenced back to any significant event during the test. Data from the analog to digital converter can be accepted at rates up to 24,000 conversions per second. The resulting tape is compatible with IBM 7094 computers used to process the data.

The control console, Fig. 5, ties all the subsystems together, and contains all the
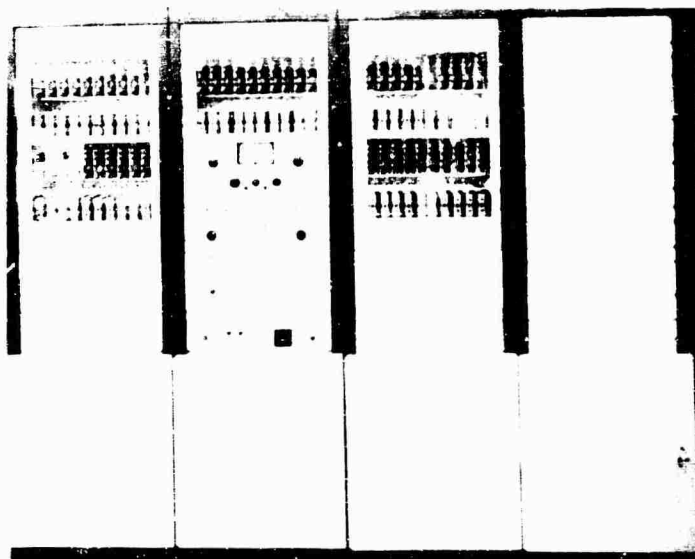
Fig. 3 - High-speed analyzer subsystem (HSAS)
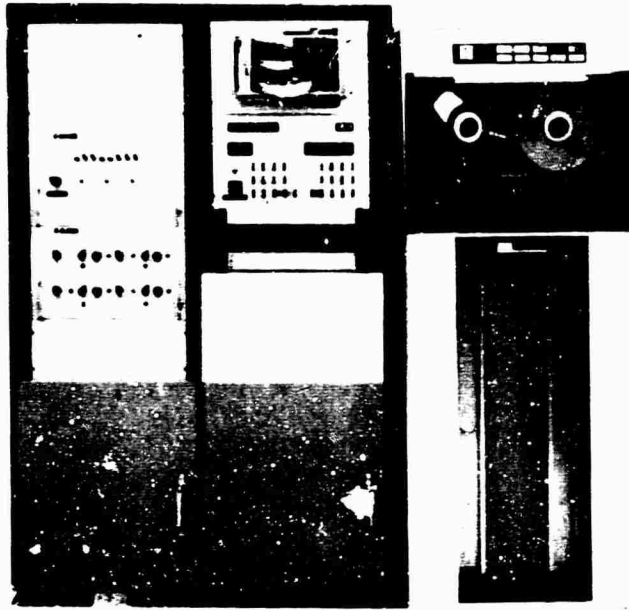
Fig. 4 - Format control buffer

equipment normally required for system setup, monitor and control. An example of the system's space-for-growth requirement can be seen by the patchboard located on the console. (The patch panel is a central point from which test or data signals can be routed to any piece of equipment in the system.) A smaller patchboard could have accommodated the required interconnections, but the larger board provides room for growth. Much of the unused portion of the board, shown here, has been put to use since this picture was made.

All test and monitoring equipment normally used during system calibration and operation is built into the console or equipment racks, with

input or output patching provided at the patchboard. With such equipment ready for immediate use in a specific location, it is difficult to overestimate the hours this convenience has saved. Certainly the systems concept has proven itself in the performance of this system. The convenience of the control panels, monitoring and test equipment, and test points have made the system a pleasure to operate and have more than satisfied the objectives for which it was designed.

VIBRATION ANALYSIS PROGRAM

The vibration analysis system was purchased with a specific data plan in mind—that of
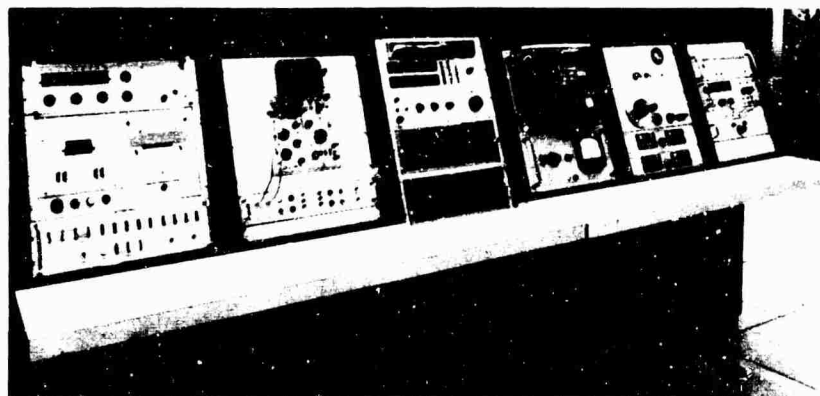
Fig. 5 - Control console

using a high-speed analyzer to perform a quick-look analysis of all vibration data acquired during a test and a digital analyzer to verify the results. The principal form of output is a magnetic tape which can be processed on an IBM 7094 computer. From this, it becomes possible to define special points of interest occurring during certain test measurements. If indicated, a more detailed analysis can be performed by the detail analysis subsystem.

A computer program was prepared to scale the data. This would use the transducer calibration, tabulate the data point by point, and plot the results of each PSD analysis on log paper with a Stromberg-Carlson 4020 plotter. A typical plot is shown in Fig. 6.

Output from the high-speed analysis system was checked many times against the detail analysis system. Differences in results were largely attributed to the bandpass filter characteristics of the two analyzers. In addition, various operator techniques were taken into consideration. However, the results have adequately provided the quick-look analysis originally sought.

Variations in integration time were investigated, and little difference, if any, could be attributed to this factor. Eventually, however, it was determined that ten plots per measurement, per test, were optimum except for very short test durations. Consequently, each test length was divided by ten, and the result was used for the integration time.

This plan worked well on early tests where a large amount of data had not yet been acquired. However, on following tests, more measurements were recorded, and over 500 data plots were obtained. These plots provided a fairly accurate three-dimensional measurement picture, and were especially useful in pinpointing instrumentation failures occurring during a test. Nevertheless, usefulness of the data was restricted by sheer quantity and the limited number of man-hours available to analyze it.

To alleviate the problem, the digital computer program was expanded to summarize all data obtained from a single measurement in a single plot. On such a plot, the maximum, mean, and minimum level PSD are shown. In addition, the standard deviation at each frequency is computed and plotted. In this way, most of the PSD information can be summarized in a single plot, as shown in Fig. 7.

In the future, it is to be hoped that greater use will be made of the digital computer in making such analyses. With various data available within the computer, it will be possible to perform extensive statistical analyses which could result in significant conclusions. For the present, however, no statistical criteria can substitute for the efforts of the data analyst.

CONCLUSIONS

Equipment capable of reducing large amounts of vibration data in a short time has
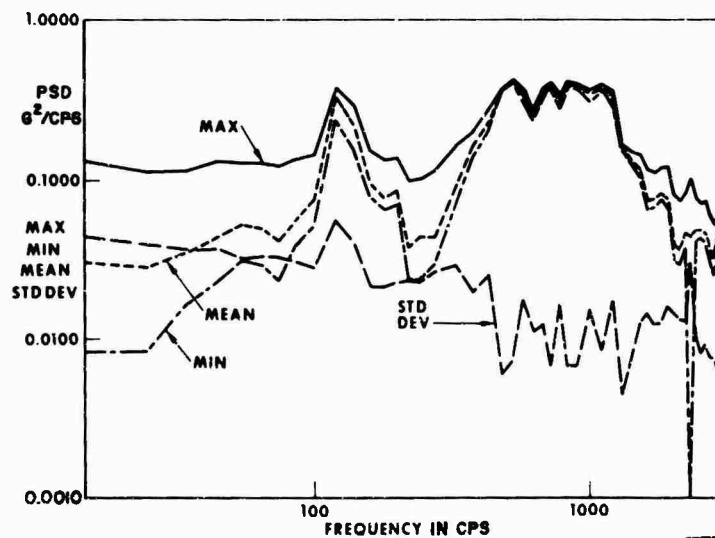
Fig. 6 - Stromberg-Carlson 4020 plot

51
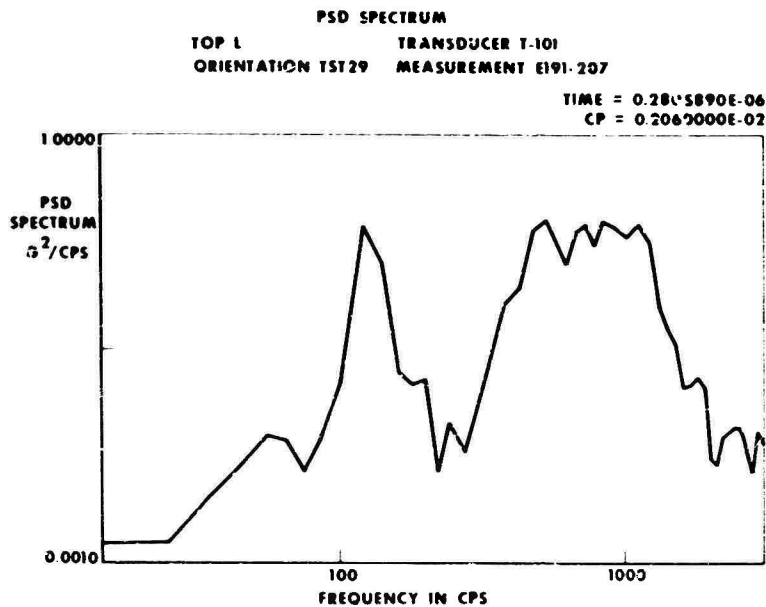
Fig. 7 - Computer output from high-speed analysis system

been repeatedly demonstrated. However, our ability to extract and absorb the most significant information contained in such data does not appear to have kept pace with the hardware developments. One conclusion seems obvious:

with the development of highly efficient vibration data reduction equipment, the time has come to place increased emphasis on new methods for utilizing this source of information.

DISCUSSION

Mr. Hughes (Naval Ordnance Laboratory, White Oak): Did you use a time code generator to mark your tape so it would search for certain records?

Mr. Weatherstone: The test tapes we obtained from all tests have a time code already recorded on them, which we used.

Mr. Hughes: I assume you get a low-density tape from your analog-to-digital converter. Did you convert this to a high-density FORTRAN-compatible tape when some other program language is used?

Mr. Weatherstone: The converter produces a high-density tape which is not immediately FORTRAN compatible, but the program first makes the conversion into FORTRAN. The rest of the program is in FORTRAN.

Mr. Szecsody (Sundstrand Corp.): How many statistical degrees of freedom did you use

in the quick-look data? How did you check your signal-to-noise ratio for the real-time data?

Mr. Weatherstone: I cannot answer your first question. To check noise, we generally measure a recording without any signal and compare it with a recording with a signal.

Mr. Szecsody: What averaging time did you use?

Mr. Weatherstone: The averaging time varies from 2 to 30 sec. Actually it depends on the length of the test. We might have a 360-sec test and divide that by 10, using 36 sec per plot.

Mr. Szecsody: Did you use 1/3-octave channels?

Mr. Weatherstone: No, it is neither a linear nor an octave analysis. We used a group of 10-cps followed by a group of 20-cps and

then a group of 50-cps followed by a group of 100-cps bandpass filters to cover the 3-kc band.

Mr. Szecsody· I ask the question on the signal-to-noise rate because while I was working with NASA, there was almost a fetish in reducing data through machines, with no realization that most of the data had a natural frequency of 60 Hz.

Mr. Weatherstone: We have seen some of that too, but I think we can generally recognize that.

Mr. Gorton (Pratt & Whitney Aircraft): I understand you do not use this method for analyzing very short transients.

Mr. Weatherstone: That is true.

*   *   *

DIGITAL ANALYSIS OF SATURN ENVIRONMENTAL
TEST RESPONSE DATA

Daniel J. Bozich
Wyle Laboratories
Huntsville, Alabama

The immense size of the Saturn space vehicles has resulted in labora-
tory environment simulation test programs of large proportions just to
test structural components. An analysis requirement of unprecedented
magnitude arises from the large number of transducers involved. Con-
ventional analog data acquisition and analysis techniques are too cum-
bersome, time-consuming and expensive for the task of acquiring and
analyzing up to 576 channels of vibration response data from each of
many test runs. Therefore, a three-position coaxial switch presents
192 transducer response signals at one time to 192 signal conditioning
amplifier systems, which, in turn, present these signals to the on-line
192 channel analog-to-digital computer system. This system can ac-
quire random test data from 576 data channels within a 6-min test dura-
tion and sinusoidal sweep test data from 192 channels at a time. These
data can be acquired over a nominal frequency range of 0 to 20,000 Hz.
They can be analyzed to obtain, for example, autocorrelations, cross-
correlations, power spectral densities, cross-power spectral densities,
amplitude probability densities, joint amplitude probability densities,
transfer functions, coherence functions input impedances, transfer im-
pedances, transmissibilities, and amp udes versus frequency. This
paper contains brief technical descriptions of the hybrid analog/digital
computer system, the requirements for converting analog data to digital
form, the methods used to handle large numbers of channels, the anal-
ysis techniques used to reduce the data to engineering terms, and the
accuracies and confidence limits of the results.

Results are included of a special computer program which can numeri-
cally filter the acquired random data into various passbands for more
selective analyses. This technique results in increased resolution and
accuracy in the lower frequency bands where it is needed. Examples
of the results of this program are presented with an analog comparison.

D. J. Bozich

INTRODUCTION

Wyle Laboratories has been engaged in
qualification testing of Saturn space vehicle
structures and structural components to ex-
pected acoustic and vibration environments
since 1963. As a result of the immense sizes
of the Saturn vehicles, the large numbers of re-
sponse measurements required from an in-
creased number of test conditions, and the lim-
ited amount of time available for data review, a
unique high-speed hybrid analog/digital data
acquisition and analysis system was developed.

The computer facility comprises a Control Data Corporation CDC 3300 digital computer, an on-line analog-to-digital conversion subsystem, and a primary data conditioning system. The overall system is capable of acquiring up to 192 data channels at one time and up to 576 data channels during a single test through a three-position coaxial switch before each channel of signal conditioning electronics. This system is being used at present to acquire data from acoustic and vibration environmental tests of specific full-scale structural sections of the second (S-II) stage of the Saturn V space vehicle over response frequency ranges of 5 to 2000 and 5 to 300 Hz, respectively. The system can handle random or sine sweep data over a frequency range of 0 to 20,000 Hz.

Data can be acquired from transducers measuring the structural response to random forces and sine sweep forces. The parameters and methods used to acquire the data are covered in detail in Refs. 1, 2 and 3. The data acquired from a random test can be statistically analyzed to obtain autocorrelations and power spectral densities (PSD), crosscorrelations and cross-power spectral densities, amplitude probability densities, joint amplitude probability densities, transfer functions, coherence functions, and mean, variances, standard deviation, skewness and kurtosis statistical parameters. Likewise, the data obtained from a sinusoidal sweep test can be analyzed with deterministic accuracies to yield amplitudes versus frequency, transmissibilities, input impedances and mobilities, transfer impedances and mobilities, and response mode shapes at resonance frequencies.

A new selective and variable bandwidth random analysis program is described which can effectively analyze random data more efficiently and accurately in about the same time as required for a constant bandwidth analysis. This program uses numerical low-pass filtering to decrease the frequency range of the data successively by octaves. The redundant data points are then "decimated" [4, see also description of decimation process later in paper] and analyzed within each respective octave either by the constant bandwidth technique or with a set of constant percentage bandpass numerical filters. This technique results in increased resolution and accuracy in the lower frequency bands where it is needed. Results of this program are compared to a constant bandwidth PSD obtained from a normal analog analysis.

ANALOG/DIGITAL DATA SYSTEM

The analog-to-digital data system shown in Figs. 1 and 2 is directly on line to a digital computer system which formats and records the data on digital magnetic tape. This system is capable of acquiring in real time sinusoidal and random signals in the frequency range from 0 to 10,000 Hz, nominally, and, with somewhat decreasing accuracy, up to 25,000 Hz.

The analog/digital data system comprises three distinct subsystems: the data acquisition and conditioning system which includes the multiposition coaxial switch network and the conventional analog instrumentation, the analog-to-digital data conversion system, and the digital

Data Acquisition and Conditioning System
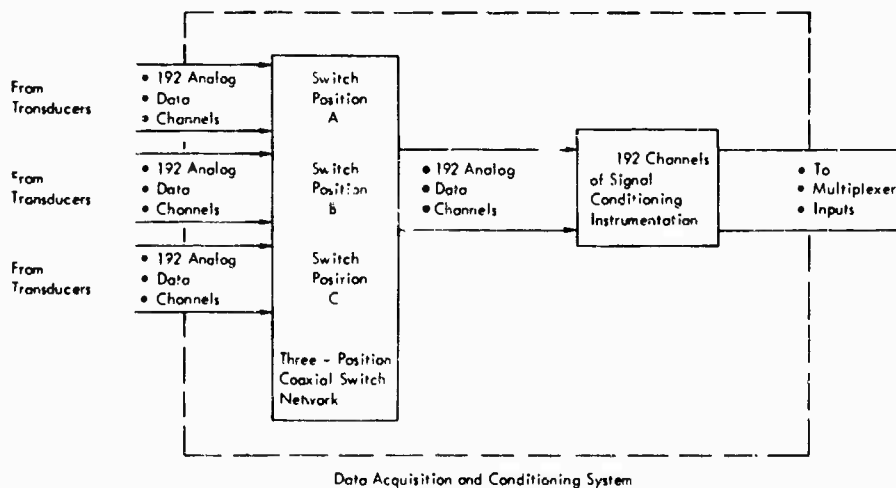
Fig. 1 - Multiple switching between matched sets of transducers to one set of signal conditioning instrumentation
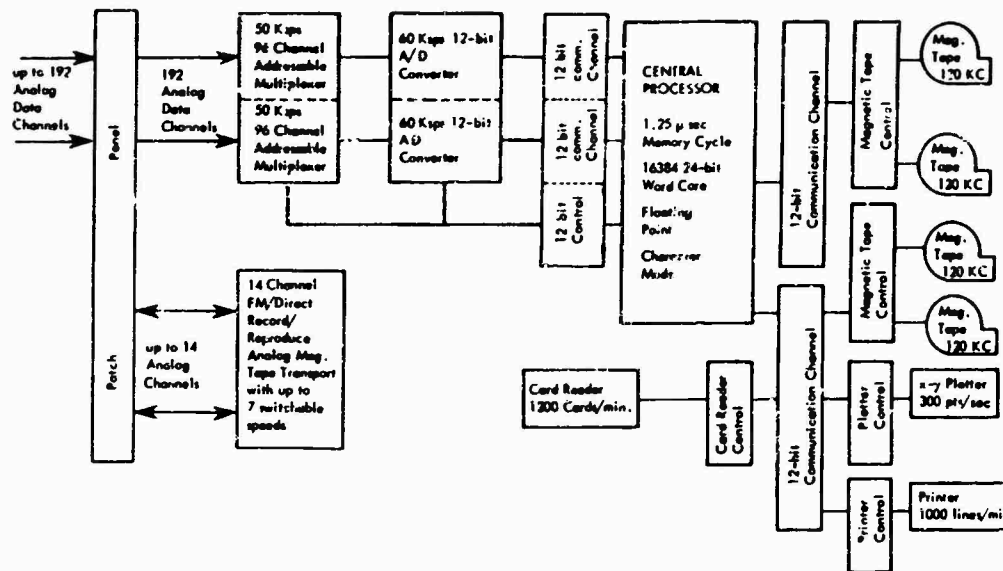
Fig. 2 - Computer facility CDC 3300 computer system
(real-time on-line application)

computer system. These three systems are required for data acquisition; however, only the digital computer system is needed for later data analysis and data presentation (plotting and/or printing).

Data Acquisition and Conditioning
  System

Figure 1 illustrates schematically the main features of the data acquisition and conditioning system. A three-position 192-channel coaxial switching network on the input to the signal conditioning system allows switching between three sets of 192 transducers where the corresponding transducers of each set have been calibrated and matched to the respective signal conditioning channel. Thus, a total of 576 input channels can be acquired during a single test. The outputs from the 192 signal conditioning channels are sent to the data conversion system.

Analog data recorded on 1-in. 14-channel magnetic tape can be played back, in either the FM or direct mode, directly on line to the data conversion system for digital processing. Up to eight switch-selected speeds can be used to reproduce high-frequency data recorded at low speed, at a speed and frequency range which is compatible with both the data conversion system and the applicable computer program. This feature extends the capability of the facility for adapting to special customer requirements.

Data Conversion System

The analog/digital system presently installed at Wyle Laboratories is shown schematically in Fig. 2. The data conversion system is used on line to convert analog signals received during a test from 2 channels at a time to two 12-bit binary words which are passed on to the CDC 3300 computer system. The system, which can sample up to 192 data channels or 96 pairs of data channels in specified addressable/sequential modes, consists of the following units:

1. 192 channel patch panel, expandable to 320 channels;

2. Two 96 channel multiplexers, expandable to 160 channels with a 50,000-channel or sample per second (sps) maximum sampling rate;

3. Two analog-to-digital converters with differential input, 100-nanosecond aperture sample and hold amplifiers, and 12-bit resolution, capable of 60,000 conversions per second; and

4. Control and interface logic with two 12-bit communication channels, a 100-ksps control oscillator which yields 50, 25, 12, and 6.25 ksps system sampling rates, and a special 96-channel 100-ksps "flip-flop" mode.

57

The analog/digital data system incorporates a dual controller such that each A/D channel can be automatically addressed independently, allowing greater flexibility in submultiplexing at high sampling rates. The dual controller has two controller and interface logic units, each of which has a 12-bit communication channel; the dual controllers are synchronously operated at 50, 25, 12.5, and 6.25-ksps system sampling rates.

Characteristics of the analog signals acceptable to the system are signal input level ± 1 volt with peaks up to ±4 volts, source resistance less than 1000 ohms, and frequency range up to 10,000 Hz (nominally) or up to 25,000 Hz with reduced accuracy (sharp low-pass cutoff at 25,000 Hz).

Analog Magnetic Tape Transport System

The Sangamo Model 4784 magnetic tape transport, presently connected to the computer facility, has the following features: 14 coaxial cables to data conversion system; remote controlled in computer facility; 14 channels each FM record and reproduce electronics for 5 speeds with 14 channels direct record-reproduce electronics readily obtainable for any or all 8 speeds; 5 speeds (switchable) 1-7/8, 7-1/2, 15, 30, and 60 ips with 3.375, 13.5, 27, 54, and 108 kHz IRIG intermediate-band center frequencies, respectively, with plug-in electronics for additional 3 speeds readily obtainable; tape shuttle feature; tape speed servo control; tape loop capstan drive capability for loops up to 250 ft; voice electronics; wow and flutter compensation electronics; 16 VU meters; and up to 50 ma output current.

Digital Computer System

A Control Data Corporation CDC 3300 digital computer comprises the basic system for controlling the on-line real-time data acquisition operation, storing the acquired digital data, analyzing the data subsequent to the test, and presenting the results in printed and/or graphic form. The initial system configuration shown in Fig. 2 has the following components: magnetic core storage module with 16,384 24-bit words and a memory cycle time of 1.25 µsec per 24-bit word; floating point hardware; central processing unit with four 12-bit input/output communication channels; console and input/output typewriter; four digital magnetic tape recorders, each of which has a maximum transfer rate of 120,000 6-bit characters per second (30,000 words per second or 60,000 sps); two tape

transport controllers; high-speed card reader, which reads 1200 80-column punched cards per minute; high-speed line printer, which prints 1000 136-column lines per minute; Calcomp incremental X-Y plotter, which plots up to 300 points per second 0.01 in. apart in both the X- and Y-directions; data conversion system; and remote-controlled Sangamo 4784 14-channel FM record-reproduce magnetic tape transport system.

Some of the outstanding features of the system for data handling are true high-speed buffering capability; extremely fast 24-bit fixed point arithmetic (2.5 µsec 24-bit add, 12 µsec 24-bit multiply, 12 µsec 24-bit divide) with 48-bit arithmetic; extremely fast and reliable digital magnetic tape recorders with forward and backward read capability; and basic 24-bit word and ease of interfacing 24-bit communication channel.

ACQUISITION AND ANALYSIS OF BANDWIDTH-LIMITED RANDOM RESPONSE DATA

On-Line Acquisition Parameters

Suppose the time series x_i, $i = 1, 2, \ldots, N$ represents a periodically sampled bandwidth-limited response signal which has a maximum (Nyquist) frequency component f_N. (The Nyquist frequency f_N is that frequency which is equal to one-half the sampling rate and for which "aliasing" errors [4] will occur for those data whose frequencies are above f_N.) The required periodic sampling rate of $h = 2f_N$ samples per second yields a record length of N samples taken over a period of time T_N seconds, where

$$N = hT_N \text{ samples} \tag{1}$$

and T_N is the maximum effective record length. Choosing an effective resolution bandwidth W_e determines a period of time defined as the maximum lag length T_m, where

$$W_e \approx \frac{1}{T_m} \text{ Hz} . \tag{2}$$

Likewise, a choice of the maximum number of statistical degrees of freedom (dof) k associated with a desired confidence level will determine the required record length T_N, since

$$k \quad 2T_N W_e \quad 2T_N T_m . \tag{3}$$

Figure 3 illustrates the relationships of confidence levels with k. A maximum number of discrete time lags m can be determined from
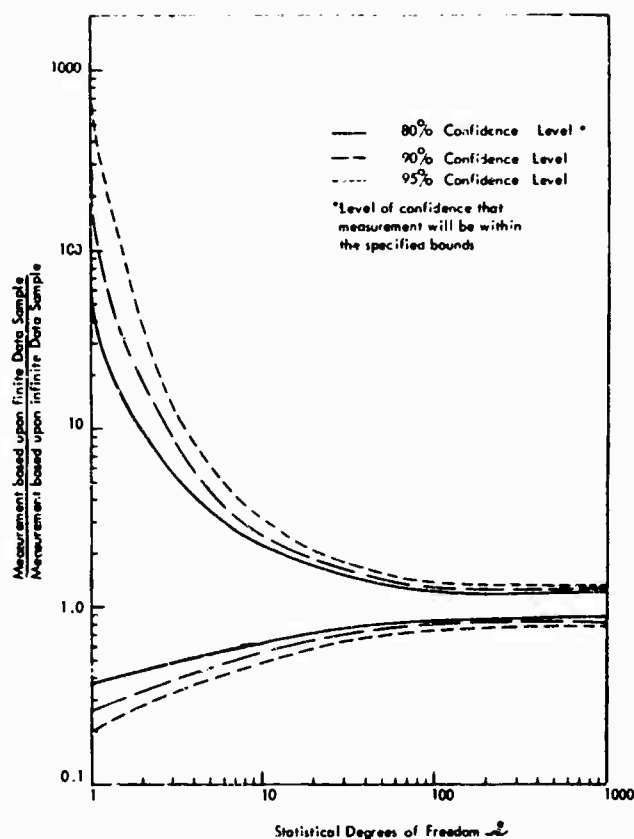
Fig. 3 - Relationship of confidence level
and statistical degrees of freedom

the maximum lag length T_m:

$$m = hT_m \text{ samples },\qquad (4)$$

which is similar to Eq. (1).

By substituting Eqs. (1) and (4) into Eq. (3), the following equation for k is obtained:

$$k = 2N/m,\qquad (5)$$

and, it is readily seen that for large k, $m \ll N$.

Sampling Requirements

The data conversion system has a fixed maximum sampling rate h, but since the data require only a sampling rate $s \quad 2f_N$ per data channel, the number of channels which can be effectively multiplexed together is given as

$$\ell = \text{integer part of } (h/s).\qquad (6)$$

Thus, the first ℓ channels are submultiplexed sequentially repeatedly until either ℓN samples

have been obtained or until T_N seconds have elapsed. Switching to the next set of ℓ channels, the process is repeated until N samples from all the channels have been acquired. Table 1 contains a chart of the maximum number of channels ℓ which can be multiplexed together for various combinations of the maximum system sampling rate h and Nyquist frequency f_N, where the individual data channel sampling rate $s = 2f_N$.

The channels within a group, which have been submultiplexed together, are related with only a constant time delay between sampled pairs of the channels within the group. This time delay is equal to the number of sample time increments separating the consecutive samples of the respective pair of channels. This sampling difference causes the subsequent computation of the crosscorrelation function to be shifted along the time axis by this incremental time delay. The resulting apparent error can be eliminated by reestablishing the time origin to account for this shift prior to computing the cross-power spectrum [5].

59

TABLE 1

Maximum Number of Channels Which Can Be Multiplexed

Nyquist Freq.[a]	Cutoff Freq.[b]	Maximum Number of Channels								
		5120 Sps	10,240 Sps	20,480 Sps	40,960 Sps	81,920 Sps	163,840 Sps	327,680 Sps	655,360 Sps	1,311,720 Sps
2.5	1	1024	2048	4096	8192	16,384	32,768	65,536	131,172	262,344
5.0	2	512	1024	2048	4096	8,192	16,384	32,768	65,536	131,172
10	4	256	512							65,536
20	8	128	256							32,768
40	16	64	128							16,384
80	32	32	64							8,192
160	64	16	32							4,096
320	128	8	16							2,048
640	256	4	8							1,024
1,280	512	2	4							512
2,560	1,024	1	2							256
5,120	2,048		1							128
10,240	4,096			1						64
20,480	8,192				1					32
40,960	16,384					1				16
81,920	32,768						1			8
163,840	65,536							1		4
327,680	131,172								1	2
655,360	262,344									1

[a] f_N, where $s = 2f_N$.

[b] f_c, where $s = 5f_c$.

Channels sampled at totally different times (i.e., in different groups) cannot be successfully related due to the large time delay between the respective channels and the complete lack of information to compute the crosscorrelation function at these extreme time delays ($m > N$). However, all of the channel pair combinations are usually not required; hence, channels which are to be interrelated are grouped together.

The data, when acquired and recorded on digital magnetic tape, are ready for retrieval, numerical filtering, analyses, and plotting.

Data Retrieval

Suppose that R random acceleration response data channels were acquired from a structure excited by applied random forces and recorded during the test on digital magnetic tape. If the R data channels were multiplexed in groups of r channels, then the records require demultiplexing to obtain and identify the separate acceleration response time series $\ddot{w}_{ni}$ ($n = 1, 2, \ldots, R$; $i = 1, 2, \ldots, N$), consisting of N samples each. Thus, the data which were sampled within the same submultiplexed groups

(during the same time) can be found for later analyses.

Numerical Filtering

The retrieved data can be numerically filtered to isolate particular bands of frequencies, such as octave bands. Of particular interest here are low-pass and bandpass filters. The low-pass and bandpass filter functions, respectively used in this report, are defined in discrete form [6] in the following equations:

$$g_k = \sqrt{\frac{1}{2\pi}} \left[1 + \cos\left(\frac{2\pi f_c t_k}{a}\right) \right] \left[\frac{\sin 2\pi f_c t_k}{t_k} \right] \quad (7)$$

and

$$g_k = \sqrt{\frac{2}{\pi}} \left[1 + \cos\left(\frac{2\pi f_c t_k}{a}\right) \right] \cdot \left[\cos 2\pi f_o t_k \left(\frac{\sin 2\pi \Delta f t_k}{t_k} \right) \right] . \quad (8)$$

where

f_c = filter cutoff frequency;

60

f_o = center frequency of passband;

f = half-width of passband;

$t_k = k \cdot s$ = incremental time;

$k = 0, 1, 2, \ldots, s \cdot 2f_c$; and

a = parameter which determines the number of zero crossings of $(\sin 2\pi f_c t_k)/t_k$ independently of f_c.

The response time series $\ddot{w}_{ni}$ is filtered to obtain the filtered time series $\tilde{\ddot{w}}_{ni}$:

$$\tilde{\ddot{w}}_{ni} = \frac{1}{\sqrt{2\pi}} \sum_{k = -s \cdot 2f_c}^{s \cdot 2f_c} \frac{1}{L} \left[\ddot{w}_{n(i+k)} \times g_k \right] . \qquad (9)$$

"Decimation"

When data, which are sampled at $s = 2f_N$ sps, are low-pass filtered with a cutoff frequency $f_c = f_N/2$, thereby removing half of the frequency content of the data, these data can be "decimated" [4] or reduced by a factor of two by computing only every other filtered data point $\tilde{\ddot{w}}_{ni}$, $i = 1, 3, 5, \ldots, N$ (N odd or N-1, N even). These "decimated" data will have an effective sampling rate s and Nyquist frequency f_N one-half that of the original unfiltered data. This process can be repeated by passing the decimated filtered data through the same filter; however, the second time through the effective sampling rate s is again reduced by 2, and, therefore, so are N, f_N and f_c. These data are in turn decimated by computing every other filtered value, and so forth.

Thus, by constructing one numerical filter function and one "decimation" process, a series of low-pass filtered data sets can be obtained, each consecutive set containing one octave less frequency range than the previous one, and also one-half as many data values at one-half the effective sampling rate. Figure 4 and Table 2 illustrate the filtering and "decimation" process.

Data Analysis

The following discussion will assume that one of the above filtered and "decimated" data sets is being analyzed and in the cases where two channels are being analyzed jointly, the corresponding low-pass data are used. The analysis procedures are the same for each set of low-pass data.

The sample mean value s_n of the nth record of the bandwidth-limited $\tilde{\ddot{w}}_{ni}$ is obtained from the equation

$$s_n = \frac{1}{N} \sum_{i=1}^{N} \tilde{\ddot{w}}_{ni} . \qquad (10)$$

where $n = 1, 2, \ldots, R$. Transforming the data record $\tilde{\ddot{w}}_{ni}$ by subtracting the sample mean value from each of the N samples of $\tilde{\ddot{w}}_{ni}$, the following equation is written:

$$\bar{w}_{ni} = \tilde{\ddot{w}}_{ni} - s_n . \qquad (11)$$

where $\bar{w}_{ni}$ is the transformed acceleration response time series with zero mean.

The crosscovariance functions $\Gamma_{np}(r/s)$ of the nth and pth data records estimated at the points $t = r/s$, $r = 0, 1, 2, \ldots, m \ll N$ are defined by the equation

$$\left. \begin{aligned} \Gamma_{np}(r/s) &= \frac{1}{N-r} \sum_{i=1}^{N-r} \bar{w}_{ni} \bar{w}_{p(i+r)} \\ \Gamma_{pn}(r/s) &= \frac{1}{N-r} \sum_{i=1}^{N-r} \bar{w}_{pi} \bar{w}_{n(i+r)} \end{aligned} \right\} . \qquad (12)$$

where r = lag number = $0, 1, 2, \ldots, m \ll N$. The crosscovariance function Γ_{np} reduces to the autocovariance function Γ_n when $n = p$. The crosscovariances Γ_{np} and Γ_{pn} can each be normalized by dividing them by

$$\sqrt{\Gamma_n(0)} \times \sqrt{\Gamma_p(0)} .$$

thus obtaining the crosscorrelation functions γ_{np} and γ_{pn}. Likewise, $\Gamma_n(r/s)/\Gamma_n(0)$ is the autocorrelation function.

Now, the one-sided cross-power spectral density function $S_{np}(f)$ is calculated at the $m + 1$ special frequencies:

$$f_j = \frac{j f_N}{m} . \qquad (13)$$

where $j = 0, 1, 2, \ldots, m$, thus providing $m/2$ independent cross-spectral estimates since spectral estimates at points less than $2f_N/m$ apart will be correlated. Therefore,

$$S_{np}\left(\frac{j f_N}{m}\right) = \left| S_{np}\left(\frac{j f_N}{m}\right) \right| e^{-i\theta_{np}\left(\frac{j f_N}{m}\right)} . \qquad (14)$$

where

61

VARIABLE BANDWIDTH OPTION   ACQUIRED DATA   SELECTIVE BANDWIDTH OPTION

Upper Octave — Bandpass Filter In Percentage BW From $f_N/2 - f_N$ And Compute Mean Square Value Per BW — Orig Digital Data — Compute Autocorrelation Over $T_m = \frac{m}{2f_N}$ Sec. — Compute Constant Bandwidth PSD's For Frequencies From $f_N/2 - f_N$ — Upper Octave

Next Lower Octave — Bandpass Filter In Percentage BW From $f_N/4 - f_N/2$ And Compute Mean Square Value Per BW — Data Filtered At $f_N/2$ And Decimated — Compute Autocorrelation Over $2T_m$ Sec. — Compute Constant Bandwidth PSD's For Frequencies From $f_N/4 - f_N/2$ — Next Lower Octave

Bandpass Filter In Percentage BW From $f_N/8 - f_N/4$ And Compute Mean Square Value Per BW — Data Filtered At $f_N/4$ And Decimated — Compute Autocorrelation Over $4T_m$ Sec. — Compute Constant Bandwidth PSD's For Frequencies From $f_N/8 - f_N/4$

Bandpass Filter In Percentage BW From $f_N/16 - f_N/8$ And Compute Mean Square Value Per BW — Data Filtered At $f_N/8$ And Decimated — Compute Autocorrelation Over $8T_m$ Sec. — Compute Constant Bandwidth PSD's For Frequencies From $f_N/16 - f_N/8$

Lowest Octave — Bandpass Filter In Percentage BW From $f_N/2^{x+1} - f_N/2^x$ And Compute Mean Square Value Per BW — Data Filtered At $f_N/2^x$ And Decimated — Compute Autocorrelation Over $2^x T_m$ Sec. — Compute Constant Bandwidth PSD's For Frequencies From $0 - f_N/2^x$ — Lowest Octave

Fig. 4 - Flow diagram of selective bandwidth analysis option and variable bandwidth analysis option

$$\left| S_{np}\left(\frac{jf_N}{m}\right)\right| = \left[C_{np}^2(jf_N,m) + Q_{np}^2(jf_N,m)\right]^{1/2}. \quad (15)$$

$$\phi_{np}(jf_N,m) = \tan^{-1}[Q_{np}(jf_N,m)/C_{np}(jf_N,m)]. \quad (16)$$

$$C_{np}(jf_N,m) = \frac{2}{s}\left[A_{np}(0)\right.$$
$$+ 2\sum_{r=1}^{m-1} A_{np}(rs)\cos\left(\frac{\pi r j}{m}\right)$$
$$\left. + (-1)^j A_{np}(m)\right]. \quad (17)$$

$$Q_{np}(jf_N,m) = \frac{4}{s}\sum_{r=1}^{m-1} B_{np}\left(\frac{r}{s}\right)\sin\left(\frac{\pi r j}{m}\right). \quad (18)$$

$$A_{np}\left(\frac{r}{s}\right) = \frac{1}{2}\left[\Gamma_{np}\left(\frac{r}{s}\right) + \Gamma_{pn}\left(\frac{r}{s}\right)\right]. \quad (19)$$

$$B_{np}\left(\frac{r}{s}\right) = \frac{1}{2}\left[\Gamma_{np}\left(\frac{r}{s}\right) - \Gamma_{pn}\right]. \quad (20)$$

$j = 0, 1, 2, \ldots, m$, and $r = 0, 1, 2, \ldots, m$.

Note from the above equations that $S_{np} = S_{pn}$ and $\phi_{np} = -\phi_{pn}$; that is, the sign of the phase angle is the only difference between the two cross-spectral density functions S_{np} and S_{pn}. When the data are from the same response point (channel), $n = p$, $B_{np} = Q_{np} = 0$, $A_{np} = \Gamma_n$, and $C_{np} = S_n$; hence, the autocovariance Γ_n and the spectral density function S_n are obtained directly from Eqs. (12) and (17).

62

TABLE 2
Table of Selective Bandwidth PSD Program — Including a Specific Analysis Example

	General Information				Example of Analysis Parameters					
Octave No.	Lower Octave Freq. (Hz)	Upper Octave Freq. (Hz)	Low-Pass Cutoff Freq. (Hz)	Channel Sampling Rate (sps)	Max. Time Lags (m)	Analysis Band-width (Hz)	Total Points per Octave (m')	Stat. Degrees of Free-dom (κ)	Reg. Total Sam-ples (N')	Total Samples Acquired (N)
1	1	2	2.5	5	—	0.5	4	12.5	500	500
2	2	4	5	10	—	0.5	8	12.5	500	500
3	4	8	10	20	—	0.5	16	12.5	500	500
4	8	16	20	40	78	0.5	32	12.5	500	500
5	16	32	39	78	78	1	32	25	1000	1,000
6	32	64	78	156	78	2	32	50	2000	2,000
7	64	128	156	312	78	4	32	100	4000	4,000
8	128	256	312	625	78	8	32	100	4000	8,000
9	256	512	625	1,250	78	16	32	100	4000	16,000
10	512	1,024	1,250	2,500	78	32	32	100	4000	32,000
11	1,024	2,048	2,500	5,000	78	64	32	100	4000	64,000
12	2,048	4,096	5,000	10,000	78	128	32	100	4000	128,000
13	4,096	8,192	12,500	25,000	—	—	—	—	—	—
14	8,192	16,384	25,000	50,000	—	—	—	—	—	—
15	16,384	32,768	50,000	100,000	—	—	—	—	—	—
16	32,768	50,000	50,000	100,000	—	—	—	—	—	—

The estimated power spectral density is frequency smoothed by Hanning's method which defines the "smoothed" $\hat{S}_n(jf_N/m)$ at the $m-1$ frequencies $f = jf_N/m$, $j = 0, 1, 2, \ldots, m$, as given by the equations

$$
\left.
\begin{aligned}
\tilde{S}_n(0) &= 0.5 S_n(0) + 0.5 S_n(f_N/m); \quad j = 0 \\
\tilde{S}_n(jf_N/m) &= 0.25 S_n[(j-1)f_N/m] \\
&\quad + 0.5 S_n(if_N/m) \\
&\quad + 0.25 S_n[(j+1)f_N/m], \\
&\qquad j = 1, 2, 3, \ldots, m-1 \\
\tilde{S}_n(f_N) &= 0.5 S_n[(m-1)f_N/m] \\
&\quad + 0.5 S_n(i_N), \quad i = m
\end{aligned}
\right\} \quad (21)
$$

The above development is given to illustrate the computational procedure. Cross-power spectral density is computed in much the same manner.

A convenient quick-look, pre-test, post-test, and/or instrumentation calibration procedure is to compute the first four statistical moments from relatively short records of data acquired from each channel during a short duration random or sinusoidal dwell excitation of the test specimen. In other words, compute

sample mean value for first statistical moment

$$
u_n = \frac{1}{N} \sum_{i=1}^{N} \ddot{w}_{ni} .
$$

sample variance (mean square value) for second statistical moment

$$
\sigma_n^2 = \Gamma_n(0) = \frac{1}{N-1} \sum_{i=1}^{N} (\ddot{w}_{ni} - u_n)^2 .
$$

sample standard deviation (rms value)

$$
\sigma_n = \sqrt{\sigma_n^2} .
$$

sample skewness (equal to 0 for a normal distribution), third statistical moment

$$
C_{ns} = \sum_{i=1}^{N} \frac{(\ddot{w}_{ni} - u_n)^3}{N \cdot \sigma_n^3} ,
$$

sample kurtosis (equal to 3.0 for a normal distribution), fourth statistical moment

$$
C_{nk} = \sum_{i=1}^{N} \frac{(\ddot{w}_{ni} - u_n)^4}{N \sigma_n^4} .
$$

63

which will indicate both the level and the quality of the analog input channels instrumentation systems, the excitation signal, and the response signals. The first three quantities are overall amplitude parameters, and the last two are amplitude probability distribution parameters.

OPERATIONAL PROCEDURES

Table 2 contains a typical set of parameters used in the selective bandwidth PSD analysis of random data. The table also contains an illustrative example of a particular analysis. Note that as the data are successively filtered (recursive filtering) at a low-pass cutoff frequency and the filtered output data are subsequently "decimated" by two before filtering again, the effective sampling rate is reduced by two. The example shows that if the lag number m is kept constant, then the resolution bandwidth in each successively lower octave is reduced by 1/2 also. Thus, the bandwidth gets narrower at low frequencies and wider at high frequencies. Another effect of this procedure is that the initial number of data values N is also reduced by 1/2 by the "decimation" process in each lower octave. The number of points N' required for analysis is determined by the statistical degrees of freedom ι required. However, in the lower frequencies the "decimated" points remaining

may be less than N', hence ι is reduced as shown in the table.

Figure 4 contains a flow diagram of the two optional analysis procedures available, that is, either the selective bandwidth analysis or the variable bandwidth analysis. The selective bandwidth analysis option yields a PSD where the constant bandwidth within each octave doubles in width in each successive higher octave. The variable bandwidth analysis option has a bank of numerical constant percentage bandpass filters within each octave. This yields a constant percentage octave PSD analysis.

Figure 5 contains two PSD plots of the same data; one plot was obtained by digital selective bandwidth analysis and the other by a 25-Hz bandwidth analog PSD analysis. Note the close agreement and the added definition at low frequencies of the digitally obtained curve. A similarly obtained digital cross-power spectral density curve is shown in Fig. 6. The absolute magnitude of the phase angle is shown separately from the sign of the phase angle for clarity.

A representative amplitude vs frequency curve obtained from a digital analysis of a sinusoidal sweep response is shown in Fig. 7. This graph is included as an illustration of the versatility of the system hardware and software.
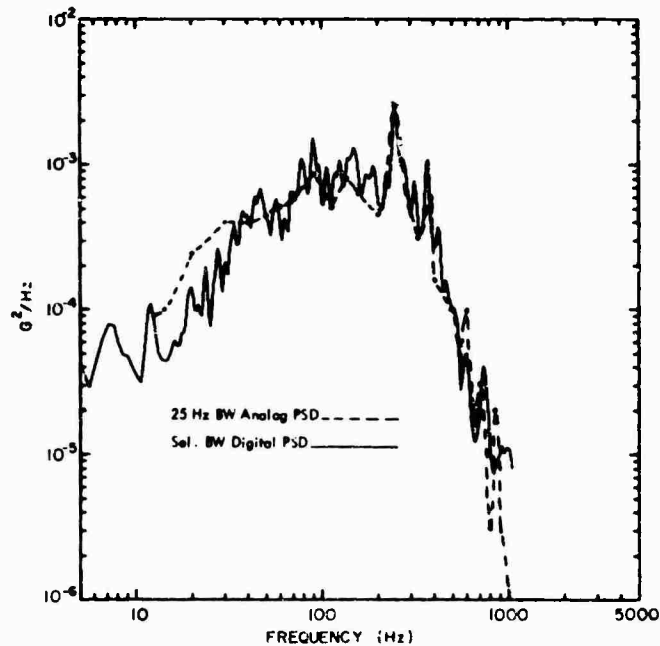
Fig. 5 - Power spectral density obtained by recursive filtering and "decimation"; 32 lags/ octave · 5 octaves plus remainder = 192 points

64
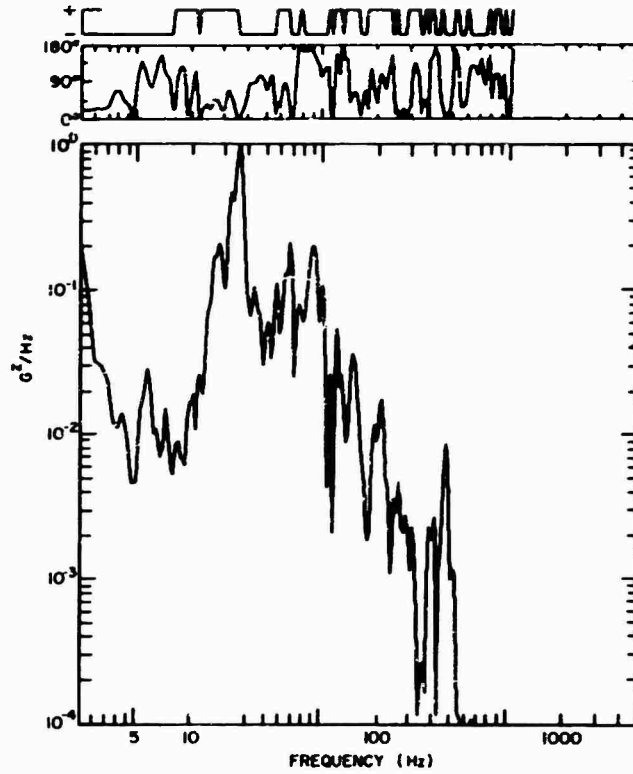
Fig. 6 - Cross-power spectral density obtained
by recursive filtering and decimation; 32 lags/
octave × 5 octaves plus remainder = 192 points
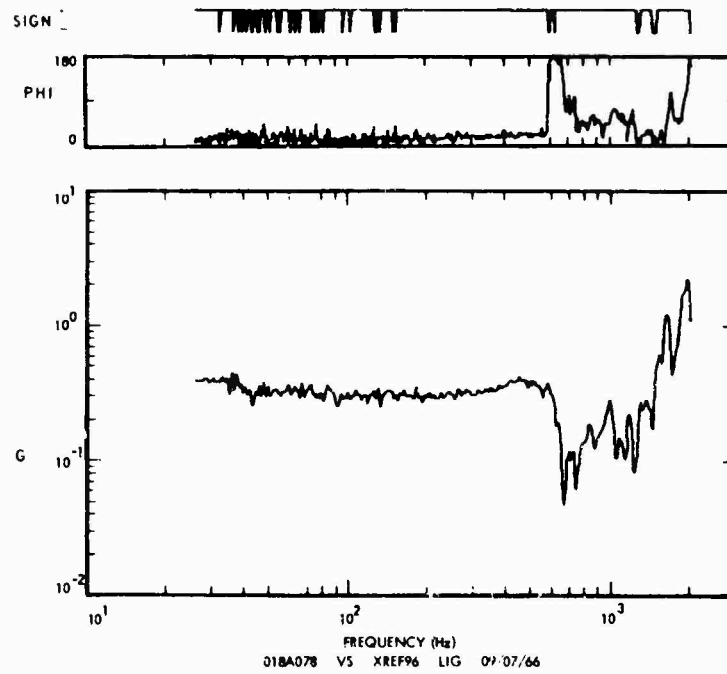
Fig. 7 - Typical acceleration amplitude and phase angle
spectra of model Saturn S-II interstage structure

65

CONCLUSION

The use of hybrid analog/digital data systems for data acquisition and subsequent analysis is expanding at a rapid rate. The flexibility afforded by the digital computer system in acquiring a large variety of dynamic response data and in the seemingly endless ways in which these data can be analyzed, reduced, and cross-interpreted comprises a highly desirable feature. Figures 5, 6, and 7 serve as excellent illustrations of the versatility of such a system.

The selective bandwidth analysis program has proven to be an accurate, efficient, and economical method for obtaining balanced resolution over a wide frequency range.

ACKNOWLEDGMENTS

REFERENCES

1. D.J. Bozich, "Utilization of a Digital Computer for On-Line Acquisition and Analysis of Acoustic and Vibration Data," Shock and Vibration Bull. No. 35, Part 4, pp. 151-180, Feb. 1966

2. D.J. Bozich, "Analog/Digital Data Systems Study for On-Line Acquisition and Analysis of Dynamic Test Data From The Vibration and Acoustic Test Facility at The Manned Spacecraft Center, Houston, Texas," Wyle Labs. Huntsville Facility Res. Staff Rept. No. WR 66-13, March 1966

3. D.J. Bozich, "Real-Time Acquisition of Acoustic and Vibration Data With an On-Line Digital Computer," 21st Ann. ISA Conf. and Exhibit, New York, No. 6.2-4-66, Oct. 24-27, 1966

4. R.B. Blackman and J.W. Tukey, The Measurement of Power Spectra. Dover Publications, New York, 1958

5. R.D. Kelly, "The Effects of Phase Errors upon the Measurement of Random Processes," Shock and Vibration Bull. No. 35, Part 4, pp. 139-150, Feb. 1966

6. R.J. Stirton, "Discrete Numerical Filters," NAVWEPS Rept. 8996, NOTS TP 3967, Jan. 1966

*   *   *

USE OF A LOW-FREQUENCY SPECTRUM ANALYZER

S. E. Lee and R. G. Tuckerman
David Taylor Model Basin
Washington, D.C.

Ship vibration problems often require immediate identification of the sources of excitation and of the vibration level in certain frequencies and mode shapes. On-board evaluation of the data is an effective tool in the analysis of the problem and in recommending remedial steps, but no instrument is available on the shelf to perform an analysis at the range from 1 to 30 cps at which most on-board vibration problems occur.

A low-frequency spectrum analyzer (LFSA) is described by which a selected signal may be analyzed simultaneously with the recording of other signals. The output of the analyzer is plotted in the form of a histogram for a frequency range from 3.50 to 23.67 cps. The LFSA has been modified for use on board ships, and its application in field studies is demonstrated.

Lee

INTRODUCTION

Studies of ship vibration are related to many types of problems including structural integrity of components, crew habitability, equipment operability, and ship's detectability. However, the importance of vibration in these areas varies. For example, in the case of detectability, fluid flow noise may be more important than vibration. Nevertheless, a better understanding of the ship's response to vibration is important in any area of concern.

Theoretical and experimental vibration studies are conducted at the David Taylor Model Basin. Theories are developed to study the dynamic response of the ship's structures, appendages, shafting, and machinery. Experimental investigations are made to determine and evaluate the actual vibration characteristics and to verify certain parameters which are necessary for the theoretical studies. To conduct both the theoretical and the experimental studies, certain special physical tools are essential. Digital and analog computers are employed in a theoretical analysis. Depending on the nature of the problems, either a digital, a direct analog (network analyzer), or an operational analog (electronic differential analyzer) computer is used. Experimental studies, especially full-scale investigations, are made in the laboratory using an ensemble of electronic analyzers, visual means, and digital computers. In recent years several special devices have been developed which enable the research engineer to obtain analyzed data during testing. Some of these devices have been described in past Symposia [1,2]. The low-frequency spectrum analyzer (LFSA) described here provides analyzed results for immediate identification of the sources of excitation.

PROBLEM

Under normal ship operating conditions, vibration may derive from many sources and is frequently difficult to analyze. Slamming in rough seas causes the ship to vibrate in one of

67

its natural modes, or propeller cavitation may cause vibrations similar to those randomly excited in superstructures by the wind.

Some sources of excitation are principally hydrodynamic. The velocity field adjacent to a propeller is generally nonuniform. As a propeller rotates, each blade experiences a varying pressure which gives rise to forces at the blade natural frequency. These forces may be transmitted to the hull through the surface, shaft bearings or the thrust block, or the combination of these. If the frequency of this quasi-periodic force or moment coincides with one of the natural frequencies of the hull, resonant vibration of the hull results. This force may be relatively small, but at lower modes of vibration the structural damping of the hull is also small, and the vibration amplitudes are magnified. It is virtually impossible to measure this varying force directly at the propeller. It is current practice to measure the varying thrust at the thrust block and the corresponding vibration of the hull at the base of the block. The response of the hull at the block may be caused by sources other than the propeller, so the response curve is irregular. Thus, the data would have to be carefully analyzed by some means such as spectrum analysis.

There is a definite need to obtain analyzed data during testing. First, if there is any change of test conditions, the vibration response may be evaluated and interpreted without delay. Second, if evaluated data are available when leaving the test vehicle, the time required to issue a report is shortened. Therefore, the research engineer can gain an

understanding of his problem or find other problems that may exist. This procedure is not new by any means, but to the author's knowledge has not been applied to low-frequency ship vibration.

LOW-FREQUENCY SPECTRUM ANALYZER

The low-frequency spectrum analyzer (LFSA) was developed under contract for the Vibration Division of the Acoustics and Vibration Laboratory, David Taylor Model Basin, by the General Kinetics Corp. The LFSA (Fig. 1) is a portable instrument, about 30 x 15 x 15 in., designed to measure vibrations of propeller blade frequency and to record the spectrum on paper tape. The output of a velocity transducer is amplified or integrated and amplified. This signal is the input to 20 1.25-cps bandwidth filters with center frequencies ranging from 3.5 to 25.7 cps. The output of each filter is rectified, averaged, and sequentially plotted by the paper recorder. These outputs are also shown on the meter on the front panel of the instrument. Effectively, the vibration signal is separated into 20 components according to frequency with amplitude proportional to the output of each of the filters.

Figure 2 is a typical frame of an analysis. The height of the first pulse represents the attenuator setting; the second pulse is a frame marker. The 20 pulses following the marker are the outputs of the 20 filters. Two empty spaces separate the frames. One frame can be scanned in 15 sec.
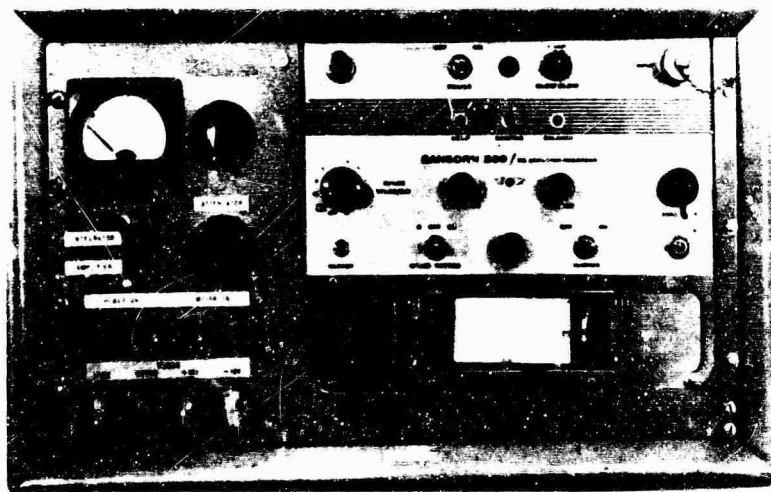
Fig. 1 - Low-frequency spectrum analyzer
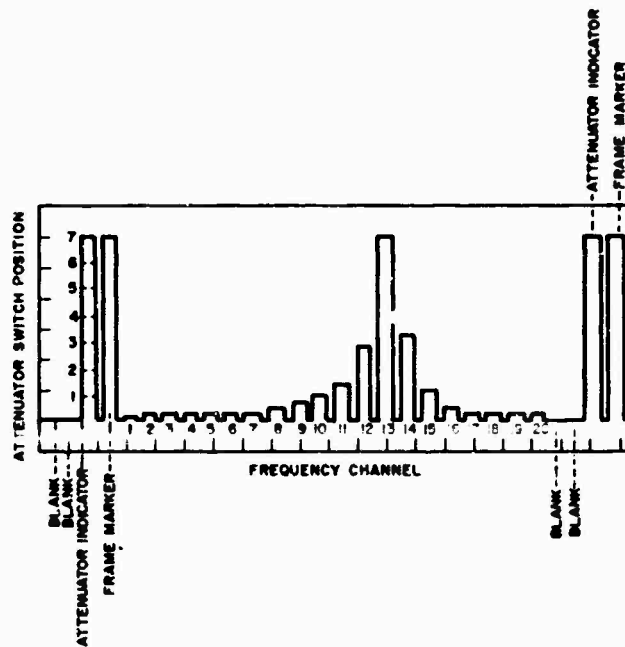
Fig. 2 - Typical scan cycle

Figure 3 is a block diagram of the LFSA system. The input signal from a vibration transducer may be attenuated up to 60 db in 10-db steps. Without any attenuation (Position 7) applied to the systems, approximately 1.6 mils of peak-to-peak vibration causes full-scale deflection on the recorder. If a velocity spectrum is desired, a switch is turned to remove the integrator from the circuit. A 24-position motor-driven switch sequentially selects the outputs of the filters and connects them to the recorder.

TEST DATA

Recently the LFSA was used on several full-scale trials and data were obtained from a transducer mounted on the propeller thrust bearing. Figure 4 is the vibration at the thrust bearing. This same signal and signals from transducers located at other positions were recorded on magnetic tape for analysis in the laboratory. Any one of these signals may be analyzed by the LFSA as it is being recorded. Figure 5 is an example of the spectrum analyzed
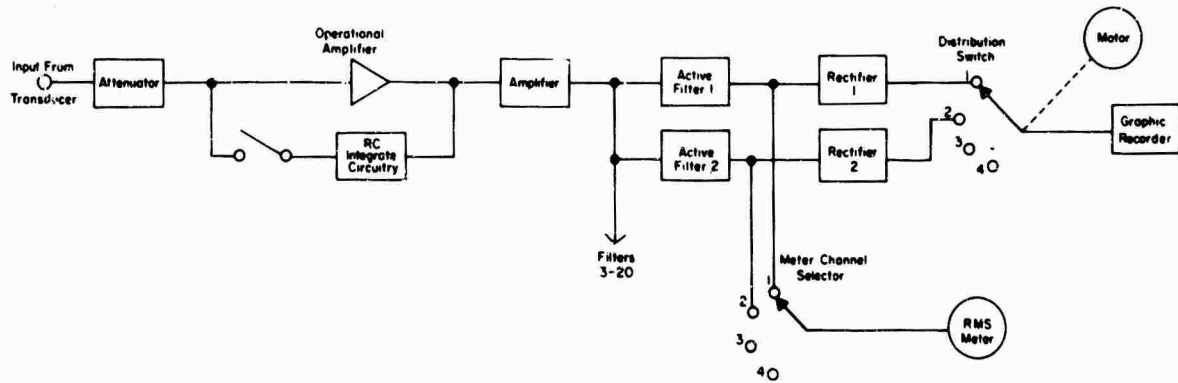
Fig. 3 - System block diagram

69
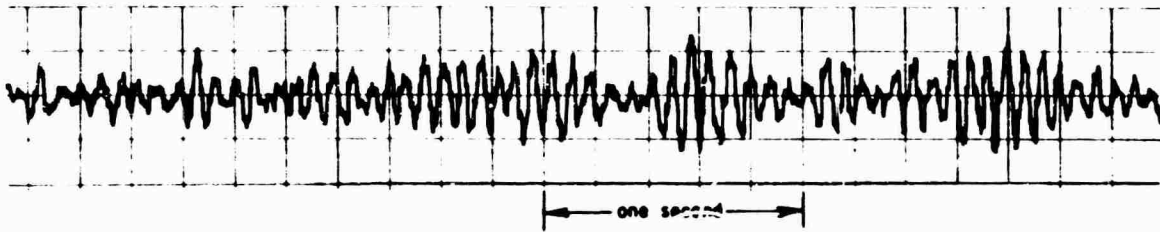
Fig. 4 - Vibration record at thrust bearing
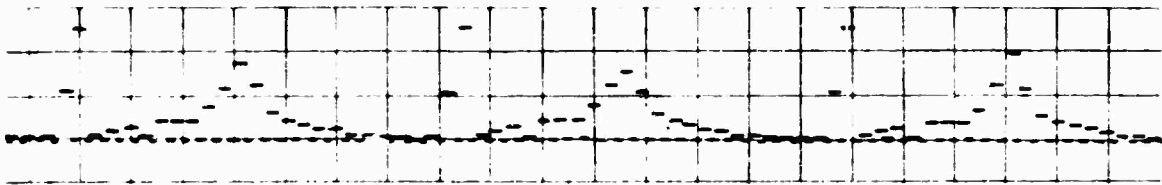
Fig. 5 - Spectrum produced by LFSA
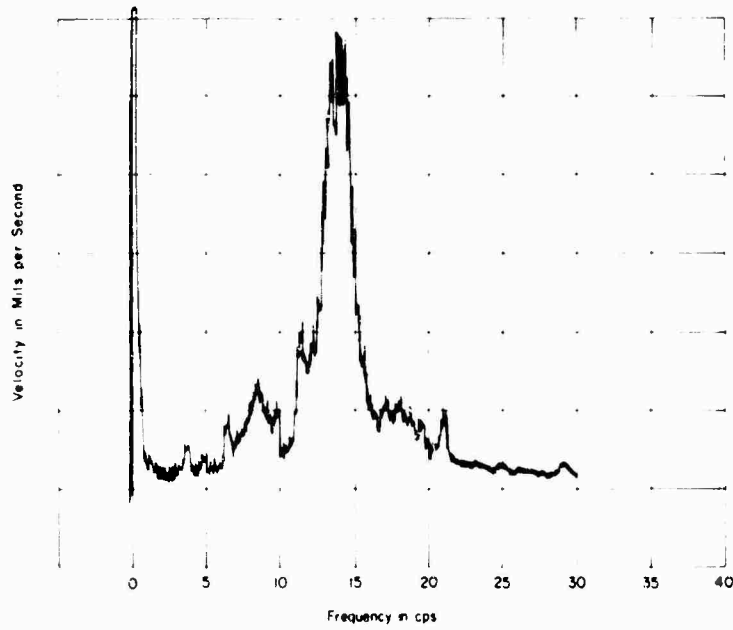
Fig. 6 - Spectrum obtained in laboratory

70

by the LFSA of the signal shown in Fig. 4. Figure 6 is the spectrum of this signal obtained in the laboratory.

Response amplitudes of the bearing at the propeller blade frequencies in the operating range are picked from the spectra of the test runs and plotted according to the propeller rotations per minute. Figure 7 compares the values obtained by the LFSA with those found in the laboratory.

CONCLUDING REMARKS

The LFSA is not a sophisticated instrument but it has under test conditions given on-site

evaluations of vibration problems. We are attempting to incorporate certain improvements to give, for instance, better resolution of the frequency components by a single sweep frequency filter instead of discrete frequency filters. Our chief goal, however, is to keep the instrument rugged enough to perform spectrum analysis of vibration data on board ship.

ACKNOWLEDGMENTS

The work presented in the paper was done with the assistance of several staff members of the Vibration Division of the David Taylor Model Basin.
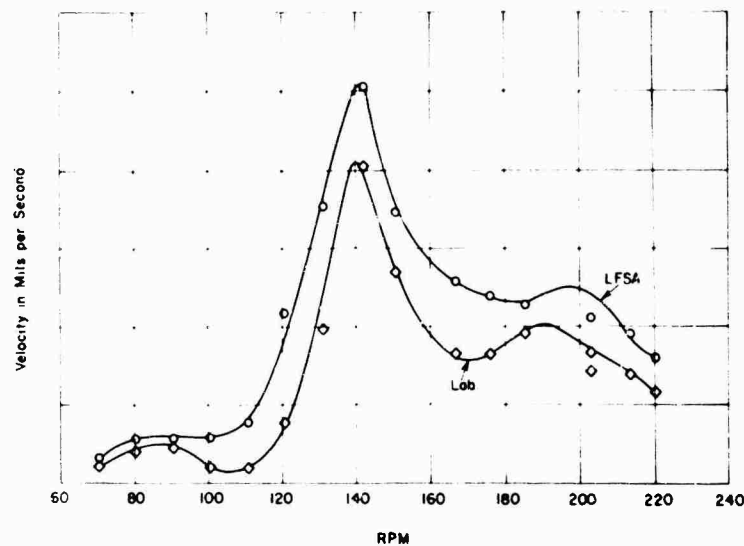
Fig. 7 - Comparison of data from
LFSA and laboratory analysis

REFERENCES

1. E. Buchmann and R. G. Tuckerman, "Model Basin Procedure for the Analysis and Presentation of Vibration Data," Shock and Vibration Bull. No. 33, Part 2, pp. 243-258, Feb. 1964

2. E. Buchmann, "Measurement and Analysis of Environmental Vibration on a Ship During any Operation and at any Sea Condition," Shock and Vibration Bull. No. 34, Part 4, pp. 1-11, Feb. 1965

*   *   *

DETECTION OF LOOSE PARTS AND FREE
OBJECTS IN SEALED CONTAINERS

M. W. Schulz
General Electric Research and Development Center
Schenectady, New York

Loose parts or free objects in electronic assemblies often are hazards
to reliable operation. This paper describes the use of the mechanical
signature obtained during a vibration test to detect the presence of
such defects without breaking the seal often found on aerospace elec-
tronic packages. In tests of packages weighing about 15 lb and of the
order of 20 in. maximum dimension, it has been possible to detect
loose particles weighing only 2 mg and "loose" screws only 1/2 turn
from completely tight.

In a typical test the package is mounted on the table of a standard vi-
bration exciter and is driven with sinusoidal acceleration of 2 g ampli-
tude at 20 Hz. Above 1 g, any loose particles will bounce around inside
the package and generate impacts which can be detected by an acceler-
ometer and displayed by an oscilloscope. Similarly, leads slapping
against each other or against nearby panels will produce impacts.

The horizontal sweep of the oscilloscope is triggered from the motion
of the exciter table. The impacts of a free object are easily seen and
readily distinguished from the slapping of leads or the rattle of con-
strained loose parts such as partially loosened covers or screws,
because impacts of bouncing particles nearly always occur at irregular
intervals and with varying amplitudes while the partially captive objects
produce a uniform regular pattern.

M. W. Schulz

The presence of loose parts or free objects
in electronic assemblies is a hazard to the re-
liable operation that is particularly important
in costly space missions. Flight failures of
hardware as well as failures during system
tests have been attributed to debris which es-
caped detection by conventional inspection.

This paper describes the use of the mechanical
signature obtained during a vibration test to de-
tect the presence of loose parts or free objects
without breaking the seal often found on aero-
space electronic packages. This simple, sen-
sitive, and effective method has been applied as
part of the quality control inspection in General
Electric's Spacecraft Department. In tests of
packages weighing about 15 lb and of the order
of 20 in. maximum dimension, it has been pos-
sible to detect loose particles weighing only
2 mg and "loose" screws only 1/2 turn from
completely tight.

Work on the method was initiated at Gen-
eral Electric's Research and Development
Center as part of a continuing program of me-
chanical signature analysis. In this program
the vibration or acoustic signals produced by a
machine are analyzed and correlated with its
operating functions to diagnose malfunctions
and detect defects. Effective techniques have
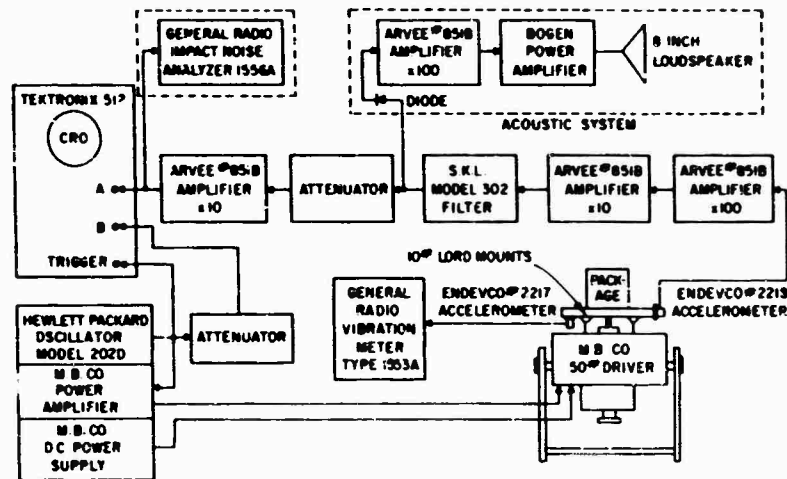
Fig. 1 - Block diagram of instrumentation

been developed for use on ball bearings ranging from small, high-speed gyro bearings to very large radar antenna bearings, for use on diesel engines, such as Army tank engines and railroad locomotive engines, and on numerous other types of machines.

Bits of wire, metal chips, scraps of insulation, solder balls, improperly secured wiring harness, loose circuit boards, and screws not completely tight can all lead to failure or malfunctioning of critical equipment. Free objects may jam relays or bridge electrical circuits; loose circuit boards or screws may permit excessive vibration and, possibly, failure of electrical connections. Such defects often are not detected by normal inspection or electrical or performance tests and loose particles are not

always picked up by the vacuum cleaner which may be used to clean up the package after assembly is completed.

All of these defects can, however, be detected by the system shown in the block diagram of Fig. 1. The instrumentation as it was set up in the laboratory is shown in Fig. 2.

In a typical test the package is mounted on the table of a standard vibration exciter and is driven with sinusoidal acceleration of 2 g amplitude at 20 to 30 Hz. The actual levels and frequency may vary for particular cases and are discussed later. Any loose particles will bounce around inside the package and generate impacts which can be detected by an accelerometer. Similarly, leads slapping against each other or
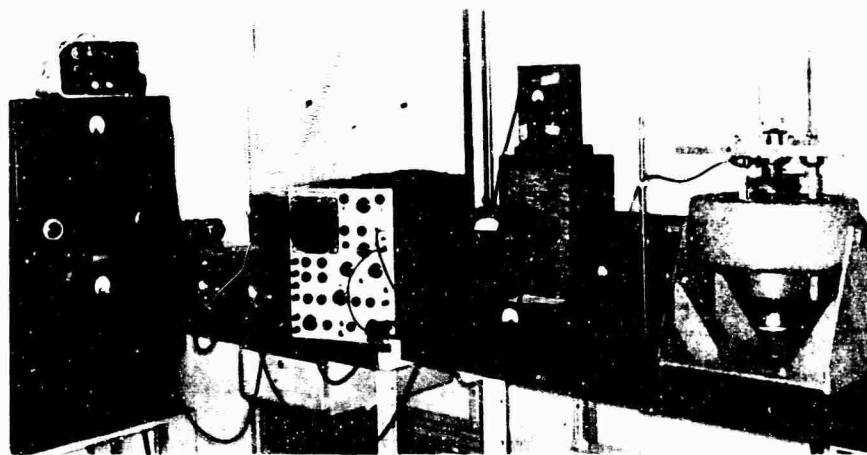
Fig. 2 - Loose part and free object detection system

74

against nearby panels will produce impacts. The acceleration signal is amplified and passed through a tunable filter to an oscilloscope, a loudspeaker, and a peak impact meter. The filter rejects the low frequency of the table motion and is adjusted for optimum signal-to-noise ratio in the range 10 to 100 kHz.

The horizontal sweep of the oscilloscope is triggered from the motion of the exciter table. The impacts of a bouncing particle are easily seen and readily distinguished from the slapping of leads or the rattle of partially loosened covers or screws. The reason is that impacts of bouncing particles nearly always occur at irregular intervals and with varying amplitudes while partially captive objects produce a regular pattern. A loose part which is restricted so that its maximum allowed displacement is about the same as the displacement of the exciter table will receive an impact on each half of the cycle to reverse its direction. A wiring harness on the other hand may be restricted in one direction by a solid panel but be free to move as far as its spring stiffness will permit in the opposite direction. Such a harness would produce an impact once per cycle. A perfect, homogeneous sphere bouncing freely on a horizontal plate which is vibrating sinusoidally in the vertical direction can be placed in a condition of stable equilibrium so that it bounces once per cycle, every other cycle, etc. The amplitude and frequency of the driver and the elastic constants of the sphere and table must be such that the velocity acquired by the sphere after rebound is just enough to provide a flight time equal to an integral number of cycles of the table motion. It has been verified experimentally that a sphere can be made to bounce in a regular pattern several minutes at a time but slight variations from the required conditions will cause the sphere to bounce in its more common irregular pattern.

For nonspherical objects, and generally for spheres as well, the pattern of impacts will be irregular. This difference in time pattern is easily seen on the oscilloscope when the sweep is triggered from the oscillator which furnishes the vibration drive signal, particularly if the oscillator signal is superimposed on the oscilloscope screen. The presence of loose items is also evidenced by the noise produced by the loudspeaker. Here, too, the bouncing particle is distinguished by its crackling type of noise as compared, for example, to the rumble of leads slapping.

An operator accustomed to the use of oscilloscopes and vibration exciters can easily learn to set the amplitude and frequency of the vibration drive as well as the optimum gain and filter settings. No special skill is required to interpret the output. Simply observing the displays produced by known loose parts is sufficient to allow one to detect them and to distinguish between the two major categories, the freely bouncing loose particle and the partially restrained loose part.

The distinct flickering, erratic character of the impacts by a free object make it relatively easy to detect even in the midst of considerable noise from loose parts slapping with regularity. Hence the method is quite sensitive to relatively small free objects. Furthermore, the signature is not strongly dependent on the structure of the package so tests can be run without prior knowledge of the characteristics of the package. Although the signal-to-noise ratio can be improved by adjusting the drive frequency and the filter passband, the tuning is not critical and is often unnecessary.

To prove the feasibility of the method, two aerospace packages were supplied for test purposes. The one shown in Fig. 3 was a "quiet" box in that it contained no loose parts of any kind. It was necessary to introduce small scraps of wire and small lead shot to demonstrate that loose particles could be detected in
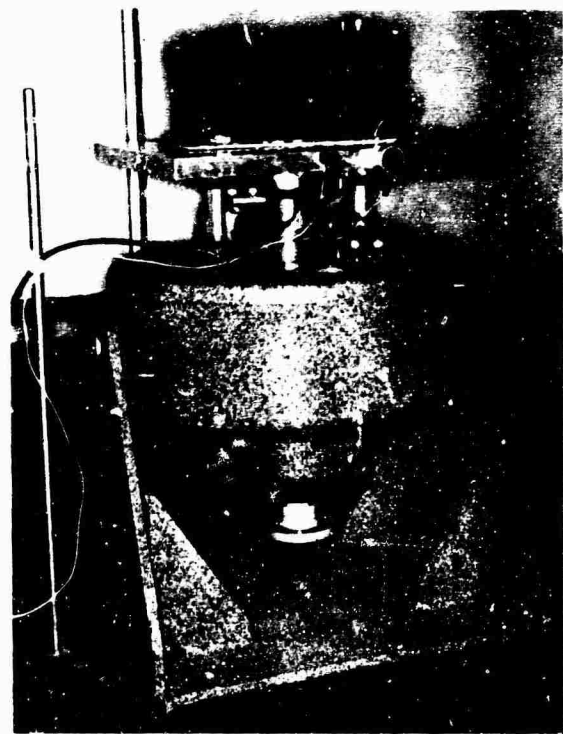
Fig. 3 - Package ready for test
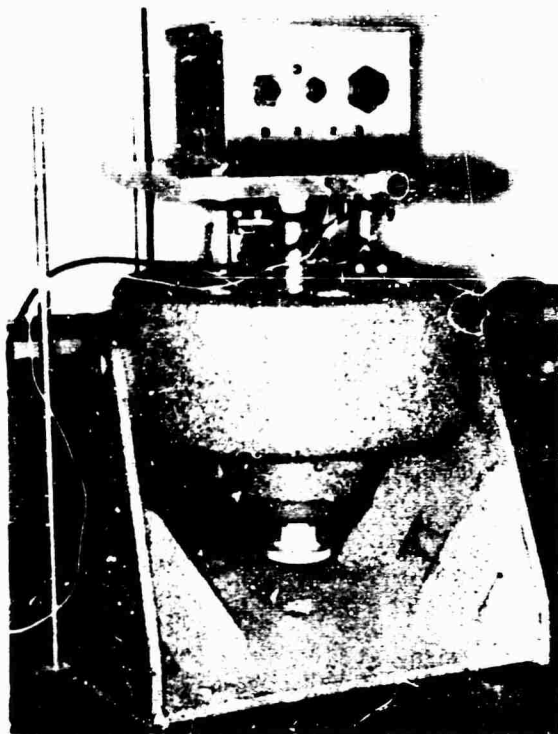
Fig. 4 - External view of second test package

this package. Figure 4 shows a somewhat larger package which also was supposed to be a "quiet" box. In this case, however, it was necessary to reduce some slapping before tests for loose particles could proceed. An interior view is shown in Fig. 5. Note that the floor of the package, as seen in this view, is a circuit board. This board is spaced from the outside shell of the package and contains connector pins for mating with a number of circuit boards which normally fill the volume, but have been removed to show the lower board. The boards which have been removed are ordinarily vertical, mate with the guides and pins visible on the lower horizontal board and are secured with two screws on each side of the box.

When initially tested with cover and vertical boards removed, an extremely high noise level was encountered. This resulted from the motion of the nuts which normally would engage the cover screws, and from variable contact between the bottom of the assembly and the platform of the shaker. These noises were eliminated by replacing screws in the nuts and using double-sided 3M tape between the bottom of the box and the platform. Further testing revealed that a loose particle was present in the assembly; some plastic particles were found
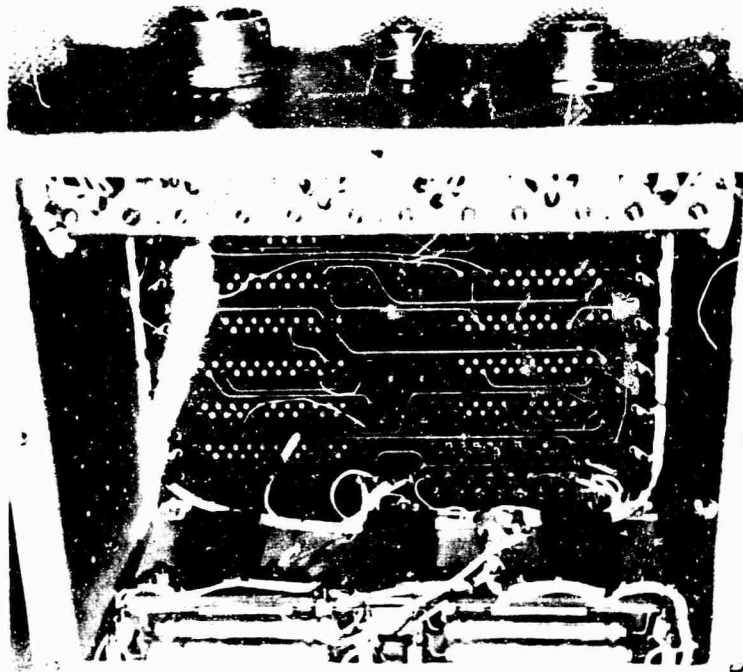
Fig. 5 - Interior view of second test package
with vertical circuit boards removed

76

trapped between the lower circuit board and the outer wall. These were extracted, and the next test showed that all the loose particles had been eliminated. The vertical circuit boards were inserted and secured. Signals were then detected indicating loose parts and improperly · secured objects. This was caused by improperly tightened screws, one of which could not be tightened because its plate nut had failed. Finally, with all screws tight, the box was re-tested and found to contain no loose parts or free objects.

The magnitude of the impact produced by a bouncing particle is proportional to the change of momentum at impact. For a fixed acceleration, the maximum velocity occurs at minimum frequency, hence a low drive frequency is usually selected. The impact is also dependent on the weight, shape, and material of the particle, as well as the material it strikes. In general, the heavier, harder and more compact the particle is, the easier it is to detect. Thus, metallic particles of a given size are easier to detect than pieces of plastic. A spherical or cubic shape will produce a larger signal than the same amount of material in the shape of a sliver or a flake. The latter two shapes produce better signals when they land on an end or an edge, respectively.

The transmission path between the point of impact and the location of the transducer also affects the detectability of loose particles. A particle hitting the bottom or some other outside surface of the container will cause an impact more easily transmitted to the accelerometer. There was some question whether a particle hitting the circuit board, shown in the bottom of the case depicted in Fig. 5, instead of the bottom of the case itself could be detected. It was found that there was about 50 percent loss of signal when particles bounced on the circuit board. Nevertheless, the two larger particles shown in Fig. 6 were detected in the midst of the residual lead slapping noise. The largest is a piece of Teflon insulation stripped from a piece of hookup wire; it weighs 3.2 mg. The second is a slug of copper wire weighing 2.4 mg. Both particles were quite easily detected when they hit the bottom of the case. The smallest particle was cut from a smaller diameter piece of wire. It weighs 1 mg and represents the threshold of detectability for particles striking the outside surfaces of reasonably "quiet" boxes of the size and type investigated here.

Much smaller particles and even tiny flakes of aluminum foil have been detected in smaller
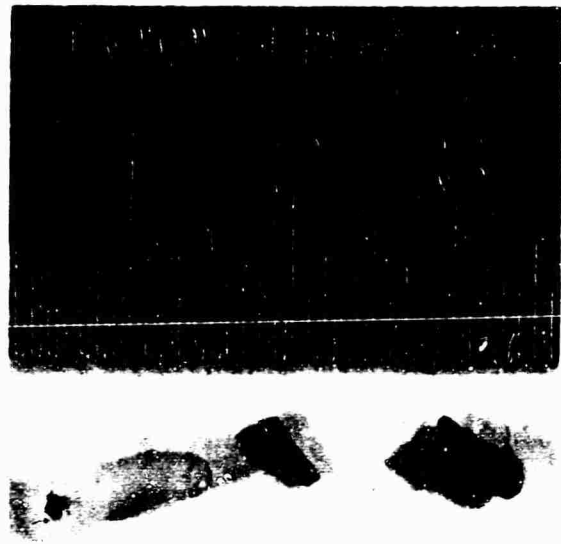
Fig. 6 - Typical free objects detected in test packages

containers mounted on a special fixture which is described later.

EQUIPMENT AND INSTRUMENTATION

The packages to be tested can be driven by any of a variety of standard vibration exciters. A level of approximately 2 g peak sinusoidal acceleration in the frequency range 10 to 50 Hz will probably be adequate, although it may be convenient to be able to apply as much as 4 or 5 g momentarily to free "loose" particles which have temporarily wedged in crevices, lodged in wiring harness, or adhered to a sticky surface. It may be necessary to support the static weight through resilient members attached to a stationary base. This was done in the system shown in Figs. 2, 3, and 4.

A 50-lb vibration exciter was used and provided more capability than was required for the packages tested. The static weight was supported by three 10-lb resilient mounts attached to the frame of the driver. The resilient mounts also provided isolation from external structure-borne noise.

Microphones as well as accelerometers have been tried to pick up the impact signals. Most of the useful information is obtained at high frequencies extending into the ultrasonic region of the spectrum. Microphones are highly directional at these frequencies. This is an advantage when one is attempting to locate the

position of a loose part or free object, but it means that the entire package must be carefully scanned. An accelerometer will detect an impact anywhere in the package and is, therefore, more convenient just to detect the presence of a defect. A microphone is more susceptible to room background noise. The accelerometer is quite sensitive to structure-borne signals such as particle impacts. Externally caused structure-borne noise was successfully blocked by the resilient mounts. The coupling between externally produced acoustic noise and the structure of the package or the table and, therefore, the accelerometer is relatively inefficient.

Attaching the accelerometer to the test package would probably give somewhat greater sensitivity but it was decided that attaching it to the drive table was satisfactory and much more convenient, permitting simpler changes from one package to the next. Another advantage was the fact that a peak in the response of the system was obtained when the resonant frequency of the accelerometer was near that of one of the major vibration modes of the table.

Figure 1 shows that a bandpass filter with variable low-frequency and high-frequency cutoffs is used. A band centered at 20 kHz, the peak response of the accelerometer and table, is a good starting point when searching for the optimum setting, but this is not the whole story because the characteristics of the loose part generating the impact influence the spectrum. For example, it has been found that some slapping noise is not as rich in the high-frequency ranges as is the impact of a loose particle. There have been cases in which a better signal-to-noise ratio has been obtained in the vicinity of 40 kHz even though the overall signal level was not as high as in some lower frequency band. Another important function of the filter is to remove the large components at the fundamental table drive frequency and its low-order harmonics. This task has been made easier by orienting the accelerometer with its least sensitive axis in the vertical direction. The accelerometer mounted on the underside of the table was connected to a vibration meter and was used to read the amplitude of the vibration drive.

The decade amplifiers are all low-noise voltage amplifiers with frequency response good to over 100 kHz.

The output of the system is given in three ways, an oscilloscope, a loudspeaker, and a peak reading meter. The display on the oscilloscope is probably the most useful. It is certainly the most sensitive to subtle changes in the amplitude and time patterns. The loudspeaker is used mainly to supplement the display on the scope but it does have the advantage of allowing the operator to watch something else while still being able to detect loose parts or particles. In the case of a noisy environment it might be necessary to use earphones. The loudspeaker, of course, does not reproduce the impact waveform but generates an audible sound which can be correlated with the presence of loose parts and a different sound for free objects.

It is difficult to record or describe the pattern seen on the scope or heard from the loudspeaker. The peak reading meter overcomes this problem since it provides a number which can be recorded and accurately described. It cannot be used alone to distinguish between a loose particle or some other loose part. The oscilloscope must be used to determine what the meter is recording. The statistical and time distribution of impact levels of bouncing particles is virtually unknown, but it was determined empirically that a 1-min sampling period would give reproducible readings for the 3- or 4-mg particles driven at about 20 Hz.

It has been mentioned before that smaller particles were detected using smaller containers and a special fixture. This fixture is shown at the front of the table in Fig. 7. An aluminum block having a resonant frequency of 70 kHz is resiliently mounted above the base of the fixture. An accelerometer is shown cemented to the front face of the block. It, too, has a resonant frequency of 70 kHz. With the bandpass filter tuned to 70 kHz, the system is extremely sensitive to the impacts of small particles. Particles were dropped into the tiny beaker cemented to the top of the block and the table was driven at 2 g at 20 Hz as before. There were no slapping noises except the minor ones produced by the lead attached to the accelerometer. Thin slivers of aluminum, small pieces of soft plastic packing material, single grains of ordinary table salt as well as bits of copper or solder were detected. A small flake of aluminum foil was detected as it bounced around and landed occasionally on its edge. It measured 75 by 125 mils by 1/4 mil thick and weighed 0.1 mg. The major difficulties were that air tended to cushion the fall of the flake, and electrostatic forces or, unless both beaker and flake were carefully cleaned, a dirt film would cause the flake to stick to the beaker. The small particles could not be handled by hand and be expected to bounce freely without sticking to the beaker at an acceleration of 2 g.

The taller plastic cylinder attached to the center of the table in Fig. 7 was used to contain
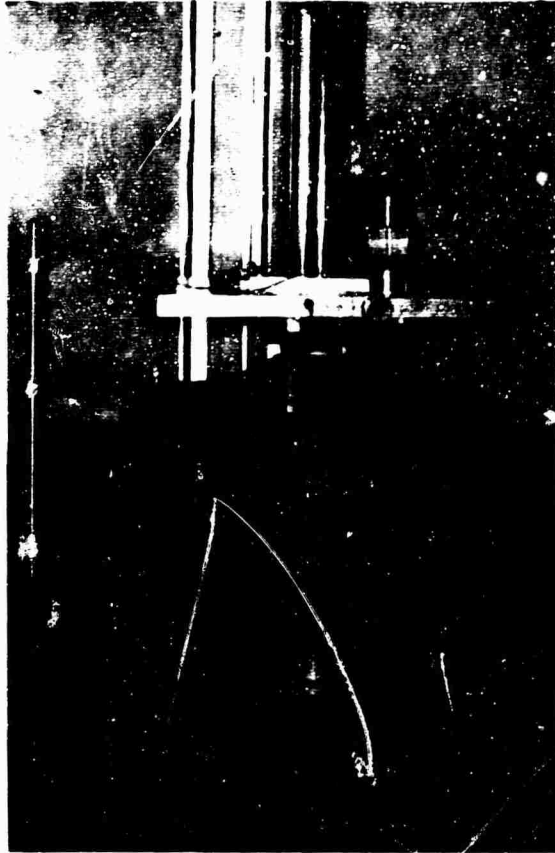
Fig. 7 - Small parts tester

bouncing particles or spheres while their be-havior was observed. The spheres were of Melmac, Teflon, lead and steel and ranged up to 5/16 in. in diameter.

TECHNIQUE FOR DETECTING LOOSE PARTICLES

The package must first be prepared for test. All external screws or bolts should be checked for tightness and made fast if possible. All other known loose parts should either be removed or fastened.

The package must be clamped securely to the vibration table. Maximum contact is de-sired between the package and the table to pro-vide the best possible transmission path for the impact signals. Thus, the maximum number of screws or bolts available should be used. If the bottom of the package is thin and flexible or is not flat it will probably be better to interpose strips of tape having adhesive on both sides to

obtain good contact between the package and the table.

A preliminary exploration is made by driv-ing the package at 2 g at various frequencies in the range 10 to 50 Hz. If there are synchro-nized impacts such as a slapping noise, a driv-ing frequency should be selected which mini-mizes them. The amplifier gains should be set high enough to obtain either substantial signal or noise. The filter should be set for a fairly wide bandwidth, for example, 10 or 15 kHz in the range of maximum sensitivity of the system. The amplitude of the vibration drive should be varied to prevent overlooking loose particles which just happen to be locked into synchronism and appear as a slapping noise. The drive am-plitude and frequency and the filter settings should be readjusted to give optimum perform-ance.

If no loose particles are detected, the threshold of detectability may be established by using calibrating particles. A container with a known size of particle is attached to the table without removing the test package. If the par-ticle can be detected, there is little likelihood that the package contains a loose particle of similar size. If the calibrating particle cannot be detected, there is too much noise in the package or the drive system and a search for the offending part must be made. The loose part must be removed or fastened before the search for loose particles is continued.

In general, it is difficult to detect a small loose particle if there is a larger one rattling about. The procedure is to detect the presence of loose particles, then open up the package and remove any particles which are found and then test again to see if there are any more, and so on until all loose particles have been removed.

APPLICATION TO PRODUCTION

A system very similar to the prototype de-scribed was set up as a quality control test fa-cility at General Electric's Spacecraft Depart-ment. The principal difference is that a larger shaker is used. The noise produced by the shaker cooling and control equipment had to be isolated from the package. The cooling fan was removed and connected through a flexible duct and the mounting fixture was provided with a high-frequency vibration isolation pad.

The problem of locating a loose part or free object has been solved by using a highly directional microphone sensitive in the frequency

79

range of 36 to 44 kHz. It is possible to deter-
mine which screw is loose or which can has the
loose particle.

A wide variety of packages have been
tested successfully, ranging from things as
small as crystal cans to as large as a 75-lb
command decoder box. There is no indication
that the limits of size have been reached.

Hundreds of boxes have been tested in the
last year. During this period there has been a
significant improvement in the failure rate,
probably due to the fact that there is now an
effective method for testing even sealed assem-
blies for loose parts and free objects.

DISCUSSION

Mr. Rommel (Lockheed-California Co.):
In the Minuteman program, a vehicle went off
course a few seconds after staging, tumbled,
and was thereafter destroyed. Audio analysis
of the accelerometer signal from the instru-
ment section indicated that either there was a
loose wrench in that area or that the tie-down
of the guidance package had broken loose.
Could your system of analysis identify the prob-
lem in a vehicle in flight?

Mr. Schulz: The type of defect is identified
by its signature when steady-state sinusoidal
vibration is applied. It is the synchronism of
one type of fault as compared to the bouncing.

Mr. Rommel: Certain work has been done
in the area of voice detection. Is such a differ-
ence in signal actually great enough to allow
identification of the problem? In one area the
problem is actually in the design, a weak tie-
down; the other, of course, is in the area of
quality control, a manufacturing problem.

Mr. Schulz: If the object is rotating in
some fashion and if there is a repetitive ap-
plied force that you can synchronize with, then
it is very easy to distinguish these signatures.
If there is nothing to synchronize with, it is
very difficult to detect the difference between
these signals because with an unsynchronized
sweep on the scope you cannot really identify
them.

Mr. Gorton (Pratt & Whitney Aircraft):
Has there been any thought given to using your
shaking technique as a production device, that
is, to take the box before the cover is put on
and vibrate it in various inverted directions to
shake the loose parts out?

Mr. Schulz: One of the recommended pro-
cedures in the test program is to shake it as
hard as you dare to dislodge stuck or wedged
parts that might come loose later. The major
application thus far has been to sealed packages,
but certainly the same tool could be used in
production. The equipment is very simple.
Most people in this kind of business have the
necessary equipment. I think the method would
be very valuable in production, but I do not know
of any use of it as yet.

Mr. Piersol (Measurement Analysis Corp.):
Many of the manufacturers of computer equip-
ment, particularly airborne and shipboard com-
puter equipment, do this as a standard routine.
One of the final factory acceptance tests is a
vibration test designed principally to get scrap
wire out of the wire bundles. This is a devas-
tating reliability problem, particularly for com-
puters that are going to be subjected to a vibra-
tion environment, and these tests have been
used for a number of years.

Mr. Weeks (Boeing Co.): Did you use ran-
dom vibration for particle detection?

Mr. Schulz: No, we used a low-frequency
sine wave. With random vibration there is no
good way to correlate the time pattern which we
are using to detect the difference between the
types of particles.

Mr. Weeks: Using a sine sweep you may
not shake loose a small particle, but with ran-
dom vibration you might. In other words the
package may pass an inspection with a sine
sweep and then fail a random vibration test
later. We have had this happen. Nothing oc-
curred during the sine sweep and then during
random vibration something happened.

Mr. Schulz: The detection system here is quite separate from any other test that the package may undergo. You can provide random tests as well. We need the sine signal at a relatively low level to provide us with the signal of the impacts and synchronization to allow us to identify the kind of defect present. I was not implying that this is taking place during the whole acceptance test. It is just a final check.

Mr. Weeks: I realize you are using this just as a check to find loose particles. Did you shake the package in only one axis?

Mr. Schulz: No. If the package is shaken in only one axis, there might be a part that is free to move in some other direction. Ordinarily we have found enough crosscoupling between modes to give a fairly high probability of detecting such loose parts. However, we turn the packages when it is convenient; it depends on the shape of the package. If it is a rectangular box, we simply turn it upside down or on one end. This is recommended because a particle which is wedged in one orientation might come loose and fall out at some other orientation.

*   *   *

COMBINED ENVIRONMENT TESTING OF SHIPBOARD ELECTRONIC EQUIPMENT AND UTILIZATION OF REGRESSION ANALYSIS

Floyd Robinson
Navy Electronics Laboratory
San Diego, California

A combined environment test was conducted on modules from the Communications Central, AN/SRC-16, to verify its effectiveness in producing failures in shipboard electronic equipment identical to those experienced in the field.

The Intermediate Frequency, Amplitude Modulation (IF/AM) Amplifier modules were subjected to 450 hours of test during which failure of a mechanical filter and unsatisfactory performance were observed. Field data on the module indicated that identical problems had occurred in the field.

A regression analysis was performed on 150 hr of recorded test data in an effort to find a technique that would aid in predicting and assessing the effects of the various environmental factors. The partial coefficients of the linear multiple regression equation were used as indicators of the environmental factor that contributed more toward the degradation of the test specimens. The results of the technique appear encouraging.

F. Robinson

INTRODUCTION

As modern shipboard electronic equipments increase in complexity, shorter, more realistic, and more economical methods are required for testing them.

It has been recognized that the time and expense involved in setting up and testing electronic equipments in an unrealistic sequence of environments could be appreciably reduced by combining the environments. Therefore, the Navy Electronics Laboratory developed an environmental test that combines vibration, humidity and temperature for assessing the reliability of shipboard electronic equipments. This combined environment test has already been conducted on commercial power supplies, manufactured by Trygon Electronics, Inc., and currently used shipboard modules from the Communications Central, AN/SRC-16.

The test results were very encouraging; however, a major problem of the combined environment test was the determination of which environmental factor contributed largely to the degradation of the test specimens.

An approach which appears promising is the utilization of regression analysis to formulate the test data in mathematical terms from which inferences are made about the effects of the environmental factors. Subsequent sections will describe the combined environment test and an analysis of 150 hr of test data recorded on the Intermediate Frequency, Amplitude Modulation (IF/AM) Amplifier module using regression analysis.

ENVIRONMENTAL CONDITIONS

The state-of-the-art of present day solid state electronic equipments renders them capable of operating at temperatures around 71 C (160°F) without any malfunctions. Therefore, the combined environment test was developed to test electronic equipment with this as an upper temperature and at a relative humidity greater than 95 percent. However, since it is essential to avoid increasing the severity of electrical and environmental stresses beyond the ultimate design strength of the hardware, thereby inducing unrealistic failures and failure modes, the environmental conditions never exceeded the design limit of the test specimens.

Since the IF/AM Amplifier modules were designed to operate in an ambient temperature of 50°C (122°F) and a relative humidity greater than 95 percent, the environmental conditions were lowered to this ambient condition for the combined environment test.

TEST CYCLE

The test cycles (Fig. 1) were 24-hr periods during which temperature and humidity were applied constantly. Vibration was applied for 23 hr of each period. During the condensation period of the cycle, the vibrator was turned off to allow normal condensation of water vapor on the surface of the components and printed circuit boards.

The frequency of vibration was varied from 5 to 40 Hz in a linear sweep cycle time of 10 min. The acceleration level was maintained at 2 g (pk) ± 5 percent between 14 and 40 Hz. In the frequency range of 5 to 14 Hz, the amplitude was held constant and the acceleration level was allowed to vary to avoid large displacements that would be detrimental to the vibrator and chamber.

The test cycle was repeated until 150 hr were accumulated on each of the three axes for a total of 450 hr of test time.

PERFORMANCE MEASUREMENTS

Performance measurements were taken at the beginning, at regular interva of 150 hr, and at the completion of the 450-hr test. To monitor the performance periodically, six measurements were taken three times daily throughout the test. These measurements consisted of recording on a log sheet the voltages at four test jacks, output power, and distortion.

The performance measurements which were made on the test bench after each 150 hr of test consisted of maximum output power, maximum undistorted output, automatic gain control, signal strength, and three conditions of harmonic distortion measurements: (a) variation of input level, (b) variation of output level, and (c) variation of modulation. These measurements were used to detect any appreciable deterioration in the various stages of the modules.

OPERATING CONDITIONS

The IF/AM Amplifier modules were operated at an input signal level of 1000 μv and a carrier frequency of 500 ± 3 kHz, modulated 30

TRANSITION PERIODS

0900 1200 1500 1800 2100 2400 0300 0600 0900

TIME
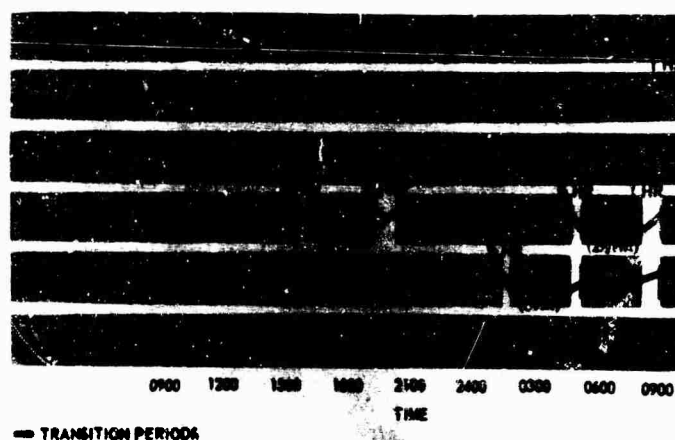
Official Photograph, U.S. Navy

Fig. 1 - Test cycle

84

percent with a 1000-Hz tone. The input voltages to the modules were held at +27 v dc and -27 v dc by two regulated Trygon power supplies. At the beginning of each axis of vibration, the output of each module was adjusted for 0 dbm ± 3 db in a 600-ohm balanced load, and the volume control was locked to prevent maladjustment as a result of vibrations.

Four IF/AM modules (Fig. 2) were installed in the environmental test chamber and two modules were located on a shelf at room temperature.
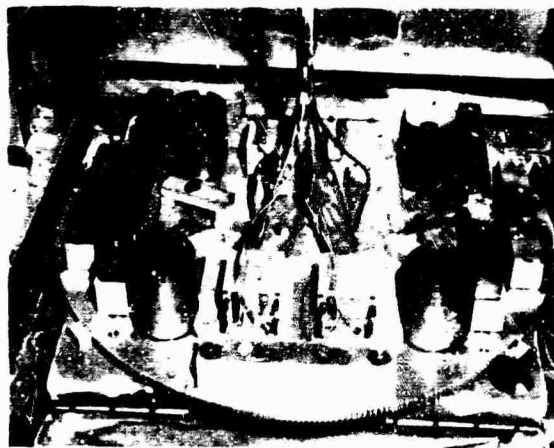
Official Photograph, U.S. Navy

Fig. 2 - Internal view of environmental chamber and vibrator, with test specimens mounted

TEST RESULTS AND ANALYSIS OF TEST DATA

The combined environment test was effective in producing failures identical to those encountered in shipboard service and problem areas that degraded the performance of the IF/AM Amplifier module.

After approximately 29 hr of combined environment test, the distortion of one module began to read out of tolerance at room temperature. The bench test measurements which were taken after the first 150 hr of test revealed high distortion values for input signal levels between 200 and 3000 μv. The output power, instead of remaining close to a previously measured value of 14.5 dbm, varied appreciably over an input signal level range of 100 to 100,000 μv. At the end of the environmental test, bench measurements revealed detuned intermediate frequency and automatic gain control circuits.

The graphs in Fig. 3 show the initial curves of the output response plotted as a function of the input signal voltage and the curves after 150 hr of environmental test for the above module.

After an accumulation of about 320 hr of test time, the output power of another module did not recover following removal of the test environments but remained at values around -29 bm. By the end of the environmental test, the module had deteriorated to the point that the output power read -52 dbm. Bench measurements revealed a defective intermediate frequency mechanical filter (Fig. 4).

The case of the mechanical filter was partially removed to determine the cause of failure. The coupling rods near the transmit transducer of the filter had flexed and collapsed, causing two disc resonators to come together. As a result, a lead wire connecting one of two terminals of the receive transducer to an external terminal was broken off from the transducer. This resulted in a loss of continuity between the two terminals.

The cause of this failure was probably vibration in the vertical and lateral axes of the mechanical filter, which caused flexing and weakening of the coupling rods. The final vibrations along the longitudinal axis of the filter then caused complete collapse of the rods. However, it is possible, of course, that the coupling rods had already been weakened by some undetermined shock prior to the test.

Unsatisfactory performance of the modules was revealed in a temperature range of 80°F to 122°F and a relative humidity of 95 percent or more.

From the beginning of the combined environment test, the four modules installed in the test chamber showed unsatisfactory performance under the above environmental conditions. In some cases, the output power of three modules dropped to values around -23 dbm and the distortion rose as high as 25 percent for a moderate input signal level of 1000 μv. The recorded data indicated a lower than normal voltage at the output of the detector. The measured voltages ranged from 20 to 160 mv rms. Normal voltage reading is around 200 mv rms for a standard input signal level of 1000 μv, modulated 30 percent with a 1000-Hz tone. However, after the removal of the test environments, the output power of three of the four modules recovered to within a tolerance of 0 dbm ±3 db in several minutes, but the other module required approximately one hour of recovery time.

85

Fig. 3 - Maximum output power curves: (a) initial
measurement, and (b) after first 150 hours of test
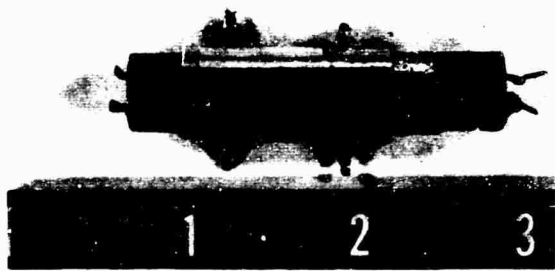
Fig. 4 - External view of defective
IF mechanical filter

The amplitude distortion of two of the four
modules installed in the environmental test
chamber is shown in Fig. 5a. Figure 5b shows
the amplitude distortions of the two modules
after removal of the test environments.

After a thorough investigation and study of
the modules and recorded test data, it was con-
cluded that the overall cause of the poor per-
formance was probably a combination of leakage
and detuning problems in the intermediate fre-
quency and automatic gain control stages.

The analysis of the test data for the second
150 hr of test also revealed the same conclusion
of leakage problems in the IF/AM Amplifier
module.

Table 1 shows the average output power of
the four modules installed in the test chamber.
However, since the test plan required three
daily recordings of test data at a temperature
level of 122°F and a relative humidity of 95 per-
cent, the number of readings that were taken
randomly at the low levels of temperature and
relative humidity will be smaller in number and
replication. Nevertheless, the test data in Table
1 will suffice in this analysis.

86
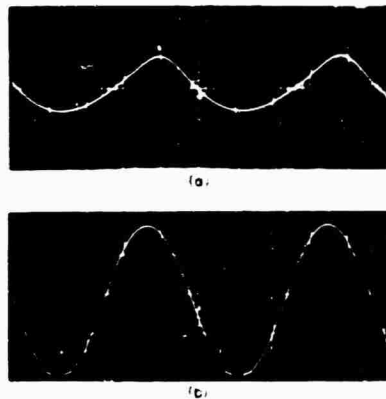
Fig. 5 - Waveform and distortion of two modules: (a) in combined environments of vibration, high temperature (122°F), and high relative humidity (95% or more), distortion readings 25% for left wave and 28% for right wave, scale factors 0.5 v/cm and 0.2 v/cm, respectively; (b) after removal of environments, distortion readings 3.3% for left wave and 4.8% for right wave, scale factor 0.5 v/cm

TABLE 1
Test Data on IF/AM Amplifier Module (Second 150-Hour Test)

Output Power* Response, Y (dbm)	Temperature, X_1 (°F)	Relative Humidity, X_2 (%)	Vibration, X_3 (g)
-6.62	122	97	2
1.30	50	87	2
-7.20	122	97	2
-7.52	122	97	2
0.77	50	87	2
-6.72	122	97	2
-7.60	122	97	2
0.35	60	97	2
-8.47	122	97	2
-7.50	122	97	2
-8.75	122	97	2
-11.30	122	97	2
-13.92	122	97	2
0.75	35	91	2
-10.70	122	97	2
-10.70	122	97	2
0.82	35	91	2
-10.95	122	97	2
-11.62	122	97	2
0.90	35	91	2
-13.62	122	97	2
-10.90	122	97	2
-10.90	122	97	2
-11.87	122	97	2
0.62	77	91	2
Total -171.39	2538	2381	—
Mean -6.84	101.5	95.2	—

*These values represent average output of four modules.

The data recorded in Table 1 are the output power and the levels of temperature, relative humidity and vibration. Notice the decrease in output power as the levels of the environmental factors are increased. This appears to imply an inverse correlation between output power and the environmental factors. In addition, the data seem to have a linear relationship. Therefore, a mathematical model of the following form is tried:

$$Y = b_0 + \sum_{i=1}^{3} b_i X_i . \qquad (1)$$

87

where

Y = mean output power in dbm,

X = ith environmental factor,

b_0 = constant, and

b_i = coefficient of ith environmental factor.

Since it was verified that vibration had no effect on the degradation of the output power during this 150-hr test, the vibration factor, X_3, was eliminated in this analysis.

The sum of squares and products of deviations of the data in Table 1 are calculated and placed in matrix form:

$$
\begin{array}{cc}
A_{ij} & g_i \\
\begin{bmatrix} 28,458.25 & 2,374.90 \\ 2,374.90 & 266.60 \end{bmatrix} & \begin{bmatrix} -3928.32 \\ 341.32 \end{bmatrix}
\end{array} \quad (2)
$$

where

$$A_{ij} = S_2 X_{i1} X_{j2} .$$

and

$$g_i = S_2 X_{i1} Y_1 .$$

Next, the inverse of the first matrix is calculated:

$$
\begin{bmatrix} 0.0001242 & -0.001106 \\ -0.001106 & 0.01326 \end{bmatrix} \begin{bmatrix} -3928.32 \\ -341.32 \end{bmatrix} \quad (3)
$$

Performing the required matrix calculus gives the following coefficients:

$$
\begin{aligned}
b_1 &= (1242 \times 10^{-7})(-3928.32) \\
&\quad + (-1106 \cdot 10^{-6})(-341.32) , \\
b_1 &= -0.1104 . \quad (4)
\end{aligned}
$$

and

$$b_2 = 0.1812 .$$

Now, the linear multiple regression equation of the test data is

$$Y = b_0 - 0.1104X_1 - 0.1812X_2 . \quad (5)$$

where

Y = mean output power in dbm,

X_1 = temperature in °F,

X_2 = relative humidity in percent, and

b_0 = constant.

The constant term of the regression equation is determined by substituting the mean values of the environmental factors and output power.

Hence,

$$b_0 = Y + 0.1104X_1 + 0.1812X_2 .$$

$$b_0 = -6.84 + (0.1104)(101.5) + (0.1812)(95.2). \quad (6)$$

$$b_0 = 21.62 .$$

Now the total multiple regression equation that gives the minimum error of estimation in the least square sense becomes

$$Y = 21.62 - 0.1104X_1 - 0.1812X_2 . \quad (7)$$

The partial regression of output power on temperatures and on relative humidity are calculated:

$$Y = 3.91 - 0.01055X_1 ,$$

and

$$Y = 18.26 - 0.264X_2 . \quad (8)$$

The analysis of variance is applied to the data in Table 1 to determine the coefficient of multiple correlation for the regression equation and the confidence limits for the coefficients of the regression equation.

Analysis of variance of data in Table 1 is given in Table 2.

The coefficient of multiple correlation, R, for the regression equation is calculated by

TABLE 2
Analysis of Variance of Data

Equation	Degrees of Freedom	Sum of Squares	Mean Squares	F Test
Regression	2	495.54	247.77	Significant at $\alpha = 0.01$ level
Residual	22	166.10	7.55	
Total	24	661.64		

taking the square root of the ratio of regression to total sum of squares:

$$R \quad \left[\frac{495.54}{561.64} \right] \quad 0.86^{-} \tag{9}$$

Since the partial coefficients of regression are used to measure the observable effects of each environmental factor on the output power it is imperative that the value of the coefficient of multiple correlation be high.

A few estimates of the output power using the above regression equation are given in Table 3. The values are within the standard error of estimation of the output power. This verifies that the regression equation gives a good fit of the test data in Table 1. However, due to the limited amount of replication of recorded test data at the lower temperatures and relative humidities the accuracy of estimation at these low levels is not as good as those levels having a high degree of replication.

95% confidence limits:

$$b_2 \cdot t \text{ (S.E.)} \quad -0.1812 \cdot 1.717 \cdot 0.1$$
$$-0.0095, -0.3529.$$

In summary, the partial coefficient of regression of the relative humidity factor had the larger magnitude of the two environmental factors in the linear multiple regression equation. Therefore, it is inferred that the relative humidity contributed largely toward the degradation of the performance of the module. This was confirmed by the simple coefficient of the partial regression equations of output power on temperature and on relative humidity. The conclusion reached in the analysis was also substantiated by the linear multiple regression equation which was calculated for the first 150-hr test:

$$Y \quad 19.73 - 0.1249X_1 - 0.1497X_2. \tag{10}$$

TABLE 3
Estimations of Output Power

Temp. Level, X_1 (°F)	Rel. Humidity Level, X_2 (%)	Observed* Output Level (dbm)	Est. Output Level (dbm)	Standard Error of Estimate (dbm)
122	97	-9.82	-9.42	
50	87	1.03	0.37	± 1.88
35	91	1.23	1.30	

*Average values of output power at levels of temperature and relative humidity.

The final calculations are the standard error (S.E.) for the regression equation coefficients and the confidence limits.

$$\text{S.E. } b_1 = 7.55 \times 1242 \times 10^{-7} = 0.0306.$$

99% confidence limits:

$$b_1 \cdot t \text{ (S.E.)} = -0.1104 \cdot (2.508)(0.0306)$$
$$= -0.0335, -0.1873;$$

95% confidence limits:

$$b_1 \cdot t \text{ (S.E.)} = -0.1104 \cdot (1.717)(0.0306$$
$$= -0.0579, -0.1629.$$

$$\text{S.E. for } b_2 = 7.55 \times 1326 \cdot 10^{-5} = 0.1.$$

99% confidence limits:

$$b_2 \pm t \text{ (S.E.)} = -0.1812 \pm 2.508 \times 0.1$$
$$= 0.0696, 0.4320;$$

where

Y = mean output power in dbm,

X_1 = temperature in °F, and

X_2 = relative humidity in percent.

The temperature did not contribute as much as the relative humidity to the degradation of the output power; however, the temperature variations resulted in condensation of the water vapor and also increased the kinetic energies at the high levels of temperature. This increased kinetic energy elevated the penetrative capability of the molecules by increasing their diffusivity. Consequently, the above effects would result in leakage and detuning problems.

CONCLUSIONS

1. The combined environment test was effective in producing failures in shipboard

electronic equipment identical to those experienced aboard ship.

2. The test revealed defective components in a short period of test time, the severity of the environmental and electrical stresses did not exceed the design limits of the module.

3. The utilization of regression analysis as an aid in assessing and predicting the effects of combined environments showed promising results.

4. The partial coefficients of regression are good indicators of the environmental factor that contributed largely to the degradation of a criterion parameter.

BIBLIOGRAPHY

Keeping, E.S., Introduction to Statistical Inference. D. Van Nostrand. New York, 1962.

Williams, E.J., Regression Analyses. John Wiley and Sons, New York, 1959.

Yule Edny, G., and M. G. Kendall, An Introduction to the Theory of Statistics. Charles Griffin and Co., London, 1947.

DISCUSSION

Mr. Rense (Measurement Analysis Corp.): Did you consider using nonlinear regression techniques to fit your data, especially after you suspected that there were crossproduct terms or synergistic effects?

Mr. Piersol (Measurement Analysis Corp.): I was going to ask the same question. You did have a pretty good correlation coefficient but it was not equal to 1, so I wondered if you expected nonlinear effects.

Mr. Robinson: I did not expect nonlinear effects in this condition. I attempted to use a curvilinear regression equation but I could not get it to give me the high correlation with the observed value that I got with a linear regression equation.

*   *   *

ANALYSIS OF RANDOM VIBRATIONS WITH AID OF OPTICAL SYSTEMS*

Ching-u Ip
Aerospace Corporation
San Bernardino, California

In the testing of missile systems, much random data such as vibrations and fluctuating pressures have to be processed. The conventional analog or digital methods of data processing can be expensive and tedious in some cases. This report shows, on a theoretical basis, that optical systems can be used to process and analyze random data to obtain items such as power spectral density and cross-power spectral density, and auto- and crosscorrelation functions.

INTRODUCTION

Data processing using coherent optical systems has been attempted by a number of research workers [1-4]. Its application has been mostly in the field of electrical communication engineering. The same coherent optical correlator can perhaps be applied to analyze rocket noise data and the subsequent structural responses or random vibration problems in general. It is the purpose of this paper to justify the optical correlator on a theoretical basis. In doing so it is necessary to present briefly Kirchhoff's light diffraction theory, Fraunhofer diffraction pattern, and Abbe's theory of image formulation, so that applied mathematicians who otherwise are unfamiliar with physical optics can be convinced that, at least theoretically, many random data such as acoustical pressure, atmospheric turbulence, and random vibrations of structures can be processed quickly and en masse by optical methods.

LIGHT AND WAVE MOTION

In the old elastic solid theory of the propagation of light, it is assumed that the light disturbance consists of vibration of a medium called "aether," the vibrations being perpendicular to the direction of propagation. The "aether" is not defined. In terms of the present electromagnetic theory of light, the vibrating "aether" is replaced by oscillatory electric and magnetic fields. For example, a transverse linear oscillation of the "aether" becomes an electric field along a given line (the magnitude varying sinusoidally) plus an associated magnetic field.

A monochromatic light wave propagating in the z-direction can be described by a function of E,

$$E = A(x,y) \cos[\omega t + \phi(x,y)]. \qquad (1)$$

where A is the amplitude of E, ω is the light frequency, t is time, and ϕ is the phase angle. The function E is simply a quantity which varies sinusoidally and is such that the square of its amplitude is proportional to the intensity of the light.

HUYGENS-FRESNEL PRINCIPLE, INTEGRAL THEOREM OF KIRCHHOFF

According to Huygens' principle it is supposed that every point on a wave front acts as a point source of a secondary disturbance which gives rise to spherical wavelets, and the wave front at any later instant may be regarded as the envelope of these wavelets. Fresnel's extension is able to account for diffraction by supplementing Huygens' construction with the postulate that the secondary wavelets mutually interfere according to the principle of superposition.

---

*This paper was not presented at the Symposium.

Kirchhoff's work shows that the Huygens-Fresnel principle may be regarded as an approximate form of a certain integral theorem which expresses the solution of the general wave equation.

The general equation of wave motion of light is given by

$$\nabla^2 F = \frac{\partial^2 F}{\partial x^2} + \frac{\partial^2 F}{\partial y^2} + \frac{\partial^2 F}{\partial z^2} = \frac{1}{c^2} \frac{\partial^2 F}{\partial t^2} . \qquad (2)$$

where c is the speed of light. If the disturbance is not monochromatic it may be resolved into its components, each of which satisfies Eq. (2).

Consider the component of frequency ν, wavelength $\lambda = 2\pi c / \omega$. Let the solution of the wave equation be of the form,

$$F = \psi(x, y, z) e^{-i\omega t} \qquad (3)$$

Now one has

$$\nabla^2 F = e^{-i\omega t} \nabla^2 \psi \qquad (4)$$

and

$$\frac{\partial^2 F}{\partial t^2} = -\omega^2 \psi e^{-i\omega t} . \qquad (5)$$

From Eqs. (4), (5) and (3) one obtains

$$\nabla^2 \psi + k^2 \psi = 0 \qquad (6)$$

where $k = \omega / c$.

If ψ_1 and ψ_2 are two continuous single-valued functions whose derivatives are continuous, Green's theorem (see Appendix) states that

$$\int_v (\psi_1 \nabla^2 \psi_2 - \psi_2 \nabla^2 \psi_1)\, dv = \int_s \left(\psi_1 \frac{\partial \psi_2}{\partial n} - \psi_2 \frac{\partial \psi_1}{\partial n} \right) ds . \qquad (7)$$

where v is the volume bounded by the surface s, and n denotes differentiation along the inward normal.

Suppose one requires the disturbance at the point P. One can take the closed surface s to surround P and put ψ_1 equal to ψ, the complex amplitude. Also it is convenient to take

$$\psi_2 = \frac{1}{r} e^{ikr}$$

where r is the radial distance measured from P as origin. ψ_2 becomes infinite at P, and so P

must be excluded from the volume of integration. To do this, take a small sphere with center P. Green's theorem may now be applied to ψ_1 and ψ_2 where the volume of integration is the volume enclosed between s and σ which together constitute the surface of integration (Fig. 1). Differentiating ψ_2 one obtains

$$\left. \begin{array}{l} \frac{\partial \psi_2}{\partial r} = e^{ikr} \left(\frac{ik}{r} - \frac{1}{r^2} \right) \\[2mm] \frac{\partial^2 \psi_2}{\partial r^2} = e^{ikr} \left(\frac{2}{r^3} - \frac{2ik}{r^2} - \frac{k^2}{r} \right) \end{array} \right\} \qquad (8)$$
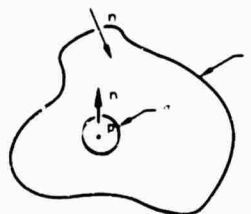
Fig. 1 - Region of integration

Writing ∇^2 in spherical polar coordinates, one has

$$\nabla^2 \psi_2 = \frac{\partial^2 \psi_2}{\partial r^2} + \frac{2}{r} \frac{\partial \psi_2}{\partial r} = -\frac{k^2}{r} e^{ikr} = -k^2 \psi_2 . \qquad (9)$$

Substituting the results of Eqs. (9) and (6) into the volume integral of Green's theorem in Eq. (7), one obtains

$$\int_v (\psi_1 \nabla^2 \psi_2 - \psi_2 \nabla^2 \psi_1)\, dv = \int_v (-k^2 \psi_1 \psi_2 + k^2 \psi_1 \psi_2)\, dv = 0. \qquad (10)$$

Hence, the surface integral in Eq. (7) is zero.

Consider the surface integral over σ. Over this surface the inward normal from the volume of integration is directed radially from P so that $\frac{\partial}{\partial n}$ becomes $\frac{\partial}{\partial r}$. Suppose the surface element $d\sigma$ on σ subtends, at P, a solid angle $d\Omega$, such that

$$d\sigma = r^2 d\Omega \qquad (11)$$

The surface integral over σ in Green's theorem then becomes

$$\int \left[\psi_1 \frac{\partial \psi_2}{\partial r} - \psi_2 \frac{\partial \psi_1}{\partial r} \right] = \int \left[\psi_1 \frac{\partial}{\partial r} \left(\frac{e^{ikr}}{r} \right) - \frac{e^{ikr}}{r} \frac{\partial \psi_1}{\partial r} \right] r^2 d\Omega$$

$$(12. \; \text{Cont.})$$

$$\int \left[e^{ikr} \left(\frac{ik}{r} - \frac{1}{r^2} \right) - \frac{e^{ikr}}{r} \frac{\cdot}{\cdot r} \right] ds \qquad \cdot \quad$$

$$\int_{\text{around } P} \left[ik r \ e^{ikr} - e^{ikr} \ r e^{ikr} \frac{\cdot}{\cdot r} \right] d \quad \textbf{(12)}$$

Assuming . is always finite, only the second term of the integrand in Eq. (12) does not approach zero as $r \to 0$. If collapses around P, the value of .. on and inside may be assumed to be constant and equal to $._2$, its value at P. Then

$$\int_{\substack{\cdot \\ r \to 0}} \left(._1 \frac{._2}{\cdot n} - ._2 \frac{._1}{\cdot n} \right) ds \quad - _P \int d.. \quad -4^{\cdot \cdot}_P \quad \textbf{(13)}$$

As shown above, the surface integral over the total surface of the volume of integration is zero, or

$$\int_{\cdot + \cdot} \quad \int_{\cdot} + \int_{\cdot} \quad 0 . \quad \textbf{(14)}$$

It then follows that

$$\int_{\cdot} \left[._1 \frac{._2}{\cdot n} - ._2 \frac{._1}{\cdot n} \right] ds \quad 4^{\cdot \cdot}_P \quad \textbf{(15)}$$

Hence,

$$._P \quad \frac{1}{4^{\cdot \cdot}} \int_{\cdot} \left[\cdot \frac{\cdot}{\cdot n} \left(\frac{e^{ikr}}{r} \right) - \frac{e^{ikr}}{r} \frac{\cdot}{\cdot n} \right] ds . \quad \textbf{(16)}$$

This is one form of the integral theorem of Kirchhoff.

So far only monochromatic waves have been considered. One can derive the general form of Kirchhoff's theorem which applies to waves that are not necessarily monochromatic.

Let $E(x, y, z, t)$ be a solution of the wave equation

$$\cdot^2 E - \frac{1}{c^2} \frac{\cdot^2 E}{\cdot t^2}$$

Now assume that E can be represented in the form of a Fourier integral,

$$F(x, y, z, t) \quad \frac{1}{\sqrt{2^{\cdot \cdot}}} \int_{\cdot}^{\cdot \tau} ..(x, y, z) e^{\cdot i \cdot t} d . \quad \textbf{(17)}$$

Then, the inverse Fourier transform gives

$$..(x, y, z) \quad \frac{1}{\sqrt{2^{\cdot \cdot}}} \int_{\cdot}^{\cdot \tau} F(x, y, z, t) e^{i \cdot t} dt . \quad \textbf{(18)}$$

Since $F(x, y, z, t)$ is assumed to satisfy the general wave equation, Eq. (2), ..(x, y, z) will satisfy the time independent equation, Eq. (6). One can apply the Kirchhoff's integral theorem, Eq. (16), to each Fourier component.

$$.._P \quad \frac{1}{4^{\cdot \cdot}} \int_{\cdot} \left[.. \frac{\cdot}{\cdot n} \left(\frac{e^{ikr}}{r} \right) - \frac{e^{ikr}}{r} \frac{\cdot}{\cdot n} \right] ds . \quad \textbf{(19)}$$

Substituting Eq. (19) into Eq. (17) gives

$$E_P \quad \frac{1}{4^{\cdot \cdot}} \int_{\cdot} ds \frac{1}{\sqrt{2^{\cdot \cdot}}} \int_{\cdot}^{\cdot \tau} \left[.. \frac{\cdot}{\cdot n} \left(\frac{e^{-i \cdot (t - \frac{r}{c})}}{r} \right) \right.$$
$$\left. - \frac{e^{-i \cdot (t - \frac{r}{c})}}{r} \frac{\cdot .._{\cdot}}{\cdot n} \right] d.$$

$$\frac{1}{4^{\cdot \cdot}} \int_{\cdot} ds \frac{1}{2^{\cdot \cdot}} \int_{-\tau}^{+\tau} \left[.. e^{-i \cdot (t - \frac{r}{c})} \frac{\cdot}{\cdot n} \frac{1}{r} \right.$$

$$+ \frac{i \cdot}{r c} .._{\cdot} e^{-i \cdot (t - \frac{r}{c})} \frac{\cdot r}{\cdot n}$$

$$\left. - \frac{e^{-i \cdot (t - \frac{r}{c})}}{r} \frac{\cdot .._{\cdot}}{\cdot n} \right] d. \quad \textbf{(20)}$$

Now the expression

$$\frac{1}{\sqrt{2^{\cdot \cdot}}} \int_{-\tau}^{+\tau} .._{\cdot} e^{-i \cdot (t - \frac{r}{c})} d. \quad [E]_{t - \frac{r}{c}} \quad \textbf{(21)}$$

is the value of E at the element ds at time

$$\left(t - \frac{r}{c} \right) :$$

it is referred to as the retarded value of E. Equation (20) then becomes

$$E_P \quad \frac{1}{4^{\cdot \cdot}} \int_{\cdot} \left\{ [E]_{t - \frac{r}{c}} \frac{\cdot}{\cdot n} \left(\frac{1}{r} \right) - \frac{1}{r c} \left[\frac{\cdot E}{\cdot t} \right]_{t - \frac{r}{c}} \frac{\cdot r}{\cdot n} \right.$$
$$\left. - \frac{1}{r} \left[\frac{\cdot E}{\cdot n} \right]_{t - \frac{r}{c}} \right\} ds \quad \textbf{(22)}$$

which is the general form of Kirchhoff's theorem.

93

FRESNEL-KIRCHHOFF DIFFRACTION FORMULA

Consider a monochromatic wave, from a point P_o, propagated through an opening in a plane opaque screen, and let P be the point at which the light disturbance is to be determined. The linear dimensions of the opening, although large compared to the wavelength, are assumed to be small compared to the distances of both P_o and P from the screen. To find the disturbance at P, one applies Kirchhoff's integral theorem to the closed surface S which comprises the opening A, a portion B of the nonilluminated side of the screen, and a portion C of a sphere of radius R centered at P (Fig. 2).
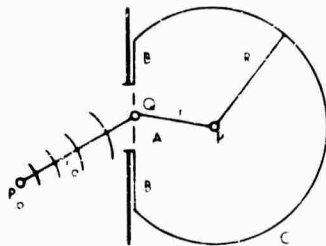
Fig. 2 - Light disturbance through opening of screen

$$\cdot P \quad \frac{1}{4} \int_{A+B+C} \left[\cdot \frac{\cdot}{n}\left(\frac{e^{ikr}}{r}\right) - \frac{e^{ikr}}{r} \frac{\cdot}{n} \right] ds \quad (23)$$

The difficulty is encountered here that the values of . and . n on A and B are never known exactly. According to St. Venant's principle, one may assume that . and . n are zero over B, the part covered by the screen, except in the immediate neighborhood of the rim of the opening, over A, the opening, . and . n have the values obtained in the absence of the screen. Kirchhoff accordingly set (Fig. 3) on A and B, respectively,

$$
\left.
\begin{array}{l}
\frac{ae^{ikr_0}}{r_0}, \quad \frac{\cdot}{n} \quad \frac{ae^{ikr_0}}{r}\left[ik \quad \frac{1}{r_0}\right]\cos(n \cdot r_0) \\[3mm]
0, \quad \frac{\cdot}{n} \quad 0
\end{array}
\right\} \quad (24)
$$

where a is a constant. These approximations are called Kirchhoff's boundary conditions.

It remains to consider the contribution from the spherical portion C. Now one assumes that the radiation field does not exist at all times but that it is produced by a source that begins to radiate at some particular instant of time $t \quad t_o$. Then at any time $t \cdot t_o$, the field fills a region

of space the outer boundary of which is at distance $c(t - t_o)$ from P_o, c being the velocity of light. Hence, if radius R is chosen so large that at the time when the disturbance at P is considered, no contributions from C could have reached P. Thus, the integral over C will vanish. Substituting Eq. (24) into Eq. (23) gives

$$
\begin{aligned}
\cdot P \quad &\frac{1}{4} \int_A \left\{ \frac{\cdot}{n}\frac{ae^{ikr_0}}{r_0} \frac{\cdot}{n}\left(\frac{e^{ikr}}{r}\right) \right. \\
&\left. - \frac{e^{ikr_0}}{r_0}\left[ik - \frac{1}{r_0}\right]\cos(n_1 r_0) \right\} ds \\[3mm]
&\frac{1}{4} \int_A \left\{ \frac{ae^{ikr_0}}{r_0}\frac{e^{ikr}}{r}\left(ik - \frac{1}{r}\right)\frac{\cdot r}{n} \right. \\
&\left. - \frac{e^{ikr}ae^{ikr_0}}{rr_0}\left(ik - \frac{1}{r_0}\right)\cos(n_1 r_0) \right\} ds \\[3mm]
&\frac{1}{4} \int_A \frac{ae^{ik(r_0+r)}}{r_0 r}\left[\left(ik - \frac{1}{r}\right)\cos(n_1 r)\right. \\
&\left. - \left(ik - \frac{1}{r_0}\right)\cos(n_1 r_0)\right] ds \quad (25)
\end{aligned}
$$

Neglecting $1 \quad r$ and $1 \quad r_0$ terms compared with the k terms, one obtains

$$\cdot P \quad \frac{1}{4} \int_A \frac{ik\, ae^{ik(r_0+r)}}{r_0 r}\left[\cos(n_1 r) - \cos(n_1 r_0)\right] ds \quad (26)$$

Putting $k \quad 2 \quad \cdot$, one has

$$\cdot P \quad \frac{-i a}{2} \int_A \frac{e^{ik(r_0+r)}}{r_0 r}\left[\cos(n_1 r_0) - \cos(n_1 r)\right] ds \quad (27)$$

which is known as Fresnel-Kirchhoff's diffraction formula.

FRAUNHOFER DIFFRACTION PATTERN

In Fresnel-Kirchhoff's diffraction formula, $r_0 \cdot r$ will, in general, change by many wavelengths as the element d explores the domain of integration, so that the factor $e^{ik(r_0+r)}$ will oscillate rapidly. The factor

$$\cos(n_1 r_0) - \cos(n_1 r) .$$

94

on the other hand, will not vary appreciably and can, therefore, be taken outside the integral.

From Fig. 3, one notices that if the linear dimensions of the opening are small compared to the distances of P_0 and P from the screen, then both the angles $(n_1 r_0)$ and $-(n_1 r)$ will be approximately equal to $\cdot$, the angle between the line $P_0 P$ and the normal to the screen. Here

$$\cos(n_1 r_0) - \cos(n_1 r) - \cos(n_1 r_0)$$

$$+ \cos \cdot - (n_1 r) \quad 2 \cos \cdot \quad (28)$$
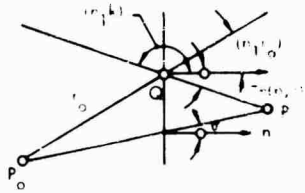
Fig. 3 - Geometry illustrating Fresnel-Kirchoff formula

Equation (27) now becomes

$$_r P \quad \frac{-i a \cos \cdot}{\cdot r_0 r} \int_A e^{ik(r_0 + r)} ds . \quad (29)$$

Consider a Cartesian reference system with origin O in the aperture and with the axes Ox and Oy in the plane of the aperture (Fig. 4). If $(x_0 \cdot y_0 \cdot z_0)$ and (x, y, z) are the coordinates of P_0 and P, respectively, and $(\cdot, \cdot)$ the coordinates of a point O in the aperture, we have

$$\left. \begin{array}{l} r_0^2 = (x_0 - \cdot)^2 + (y_0 - \cdot)^2 + z_0^2 \\ \\ r^2 = (x - \cdot)^2 + (y - \cdot)^2 + z^2 \end{array} \right\} . \quad (30)$$
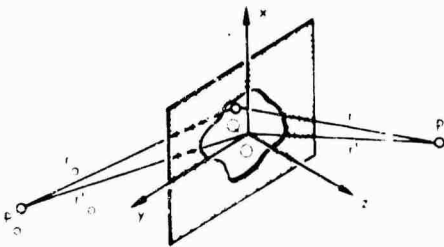
Fig. 4 - Diffraction at aperture in plane screen

Let r_0 and r' be the distances of P_0 and P from the origin. Then

$$\left. \begin{array}{l} r_0'^2 \quad x_0^2 + y_0^2 + z_0^2 \\ \\ r'^2 \quad x^2 + y^2 + z^2 \end{array} \right\} \quad (31)$$

so that

$$\left. \begin{array}{l} r_0^2 \quad r_0'^2 - 2(x_0 \cdot + y_0 \cdot) + \cdot^2 + \cdot^2 \\ \\ r^2 \quad r'^2 \quad 2(x \cdot + y \cdot) + \cdot^2 + \cdot \end{array} \right\} \quad (32)$$

Since $\cdot \cdot$ are small compared with $r_0 \cdot r'$, one can expand r_0 and r in a power series, and neglecting quadratic and higher terms, one obtains

$$\left. \begin{array}{l} r_0 \quad \left[r_0' - \left\{ 2(x_0 \cdot + y_0 \cdot) - (\cdot^2 + \cdot^2) \right\} \right]^{1/2} \\ \\ \qquad \quad r_0' - \dfrac{x_0 \cdot + y_0 \cdot}{r_0'} \\ \\ r \quad r' - \dfrac{x \cdot + y \cdot}{r'} \end{array} \right\} . \quad (33)$$

If we denote by $(\cdot_0, m_0)$ and $(\cdot, m)$ the direction cosines

$$\left. \begin{array}{ll} \cdot_0 = -\dfrac{x_0}{r_0'} , & \cdot = \dfrac{x}{r'} , \\ \\ m_0 = -\dfrac{y_0}{r_0'} , & m = \dfrac{y}{r'} \end{array} \right\} . \quad (34)$$

then Eq. (33) becomes

$$\left. \begin{array}{l} r_0 = r_0' + \cdot_0 \cdot + m_0 \cdot \\ \\ r = r' - \cdot \cdot - m \cdot \end{array} \right\} \quad (35)$$

Thus,

$$e^{ik(r_0 + r)} \quad \exp[ik(r_0' + r') + ik(\cdot_0 - \cdot)\cdot + ik(m_0 - m)\eta] \quad (36)$$

$$\quad e^{ik(r_0' + r')} e^{ik[(\cdot_0 - \cdot)\cdot + (m_0 - m)\cdot]} .$$

Substituting Eq. (35) into Eq. (28) and noting that the factors r_0 and r outside the integral can be approximated by r_0' and r', one obtains the Fraunhofer diffraction formula,

$$\cdot P \quad \frac{-i a e^{ik(r_0' + r')}}{\cdot r_0' r'} \cos \cdot \iint_A e^{ik[(\cdot_0 - \cdot)\cdot + (m_0 - m)\cdot]} d\cdot d\cdot$$

$$C \iint_A e^{ik[p\cdot + q\cdot]} d\cdot d\cdot . \quad (37)$$

95

where p ···· , q ·· ··, and C is the constant outside the integral.

To understand in more physical terms why Fraunhofer phenomena are observed in the focal plane of a well-corrected lens, let us compare the two situations illustrated in Fig. 5. In Fig. 5a a pencil of rays from an infinitely distant point is incident upon the aperture in the direction specified by the direction cosines ·, ‾ ·, n_0. The effect observed at a distant point P in the direction ·, ‾, ‖ may be regarded as arising from the superposition of plane waves originating at each point of the aperture (Huygens-Fresnel principle). These waves are called diffracted waves and the corresponding wave normals the diffracted rays.

If now a well-corrected lens is placed behind the screen (Fig. 5b), all the light diffracted in the (·‾ n) direction will be brought to a focus p' in the focal plane of the lens.
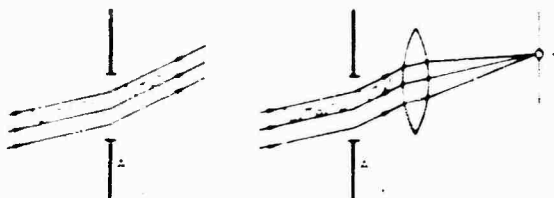
F .. 5 - Comparison of two cases of Fraunhofer diffraction

FOURIER TRANSFORM RELATIONSHIP IN COHERENT OPTICAL SYSTEM

Consider the optical system in Fig. 6 [5]. By coherency, one means that the relative phases of the light waves in various parts of the system are invariant with time. This requires that the illumination be derived from a point source of light. A point source and a collimating lens are used to produce a plane wave front which impinges on the signal film located in plane I. Let the transmissivity of the signal film be $T(x_1, y_1)$ so that the disturbance which passes the signal film is

$$F_1 \quad TA(x_1, y_1) \cos(\quad t \cdot \quad)$$
$$\quad \cdot_1(x_1, y_1) \cos(\quad t \cdot \quad). \tag{38}$$

where (x_1, y_1) is the amplitude of the wave after leaving the plane I.
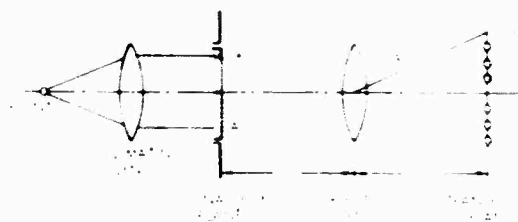
Fig. (- Two-dimensional signal analyzer

An objective lens is placed at its focal length f from each of the two planes I and II. We then have

$$x_2 \quad p f \cdot \quad y_2 \quad q f \tag{39}$$

Considering plane I as the aperture plane in the diversion of the Fraunhofer diffraction formula, one now has for the disturbance not a uniform plane wave but a function of x_1 and y_1. Thus, the constant C in Eq. (37) is replaced by $\cdot_1(x_1, y_1)$.

The amplitude of the disturbance at plane II is given by (see Eq. 37)

$$\cdot_2 \quad \iint_A \cdot_1(x_1, y_1) e^{-ik(px_1 + qy_1)} dx_1 dy_1 \tag{40}$$

Setting

$$\left. \begin{array}{l} k \quad \dfrac{2\pi}{\cdot} \\[2mm] \cdot \quad \dfrac{2\pi x_2}{f} \\[2mm] \cdot \quad \dfrac{2\pi y_2}{f} \end{array} \right\} \tag{41}$$

and substituting Eq. (39) into Eq. (40), one obtains

$$\cdot_2 \quad \iint_A \cdot_1(x_1, y_1) e^{\cdot \cdot (x_1 \cdot \cdot y_1 \cdot)} \cdot dy_1 \tag{42}$$

Since $\cdot_1(x_1, y_1)$ is zero outside the aperture of the signal film plane, one can extend the limits of integration to ·. Hence, one obtains

$$\cdot(x, y) \quad \int \int \cdot_1(x_1, y) \quad \cdot \cdot \cdot \cdot dx_1 dy_1 \tag{43}$$

Conversely,

$$\cdot_1(x_1,y_1) \quad \int \int \cdot_2(x,y) \cdot^{1(\cdot x_1 \cdot \cdot y_1)} \cdot_x d_y \tag{44}$$

That is, the Fraunhofer pattern is the Fourier transform of the amplitude across the diffracting aperture and vice versa.

From Eq. (43) it is seen that for every value of $\cdot_x$ or $\cdot_y$, there is a corresponding value of $\cdot_2$. The spectra of successive orders of the Fraunhofer diffraction pattern are denoted in Fig. 6 by $\ldots S_{-2}, S_{-1}, S_0, S_1, S_2 \ldots$.

The addition of a cylindrical lens, which has focal power in one dimension only, to the optical system shown in Fig. 6 will effect a one-dimensional Fourier transformation (Fig. 7). Thus,

$$\cdot_2(\cdot y) \quad \int_{-\tau}^{+\tau} \cdot_1(x_1,y_1) e^{-i \cdot y y_1} dy_1 \tag{45}$$

and

$$\cdot_1(x_1 \quad x_2,y_1) \quad \int_{-\tau}^{+\tau} \cdot_2(\cdot y) e^{i \cdot y y_1} d_y . \tag{46}$$
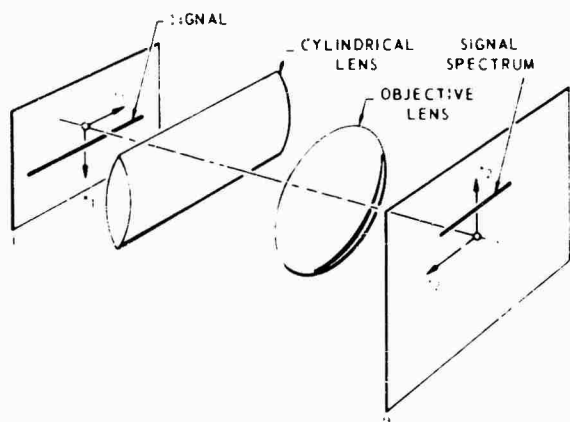
Fig. 7 - One-dimensional signal analyzer

DATA ANALYSIS OF ACOUSTICAL OR VIBRATION DATA

Both the acoustical pressures caused by a rocket jet and the resulting structural vibrations can be considered as random time series. In the analysis of the random vibrations of the structure, quantities such as power spectral density, autocorrelation function, and crosscorrelation function often enter the picture.

Consider, as an example, the acoustical pressures $p_1(t)$ and $p_2(t)$ which are measured by microphones at locations 1 and 2. If T is an arbitrarily chosen period of time in the two random time series, the power spectral density, autocorrelation function, and crosscorrelation function, respectively, can be defined as follows:

$$
\left.
\begin{aligned}
S_p(\ ) &\quad \lim_{T \to \infty} \frac{2}{T} \left| \int_{-T/2}^{T/2} p(t) e^{-i \cdot t} dt \right|^2 \\
\cdot(\cdot) &\quad \lim_{T \to \infty} \frac{1}{T} \int_{-T/2}^{T/2} p(t)\, p(t-\cdot)\, dt \\
R_{12}(\cdot) &\quad \lim_{T \to \infty} \frac{1}{T} \int_{-T/2}^{T/2} p_1(t)\, p_2(t-\cdot)\, dt
\end{aligned}
\right\} . \tag{47}
$$

where $\cdot$ is the angular frequency, and $\cdot$ is a time delay.

The acoustical pressure can be plotted as a time series with pressure vs time or as a one-dimensional spatial series with pressure p vs distance y_1, where $y_1 \quad v_{tape} t$, and v_{tape} is the speed of the recording tape. Furthermore, if this information is transcribed to a signal film by a light-intensity modulating oscilloscope, the information will appear as a line (with dots, or resolution elements, of variable intensities) (Fig. 8). The pressures at different locations, $p_1, p_2, p_3 \ldots$ can be put on the same signal film as different signal channels.

Now the period T chosen is necessarily finite. If one assumes that T is sufficiently large, then the quantities in Eq. (47) will be
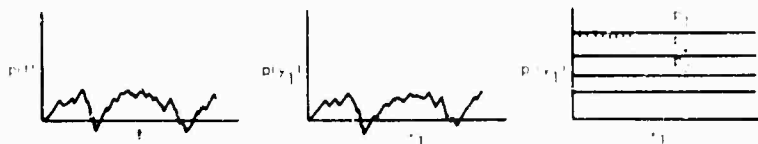
Fig. 8 - Transcribing acoustical pressure signal

given approximately by the integrals times a constant. If one equates $p(x_1)$ to $_1(x_1)$ in Eq. (45), and also recalls that $_{1}(x_1)$ is the amplitude of one frequency component of the light disturbance, and that the intensity of light is proportional to the square of the disturbance, the light intensities (measured by a microdensitometer) in the frequency plane II (Fig. 7) represent the power spectrum of the sound pressure.

The optical system in Fig. 9 can be used to obtain both the autocorrelation and crosscorrelation functions. One makes two copies of the data film by recording two films simultaneously. In this correlator, the light source is imagined as a line passing through the optical axis and lying in plane I. The channel $_{m}$ which is to be crosscorrelated is made to coincide with the line image of the source.

Thus, the amplitude of the light disturbance in plane II is

$$R_{m,n}( ) = \int_A {}_{m}(y)\, {}_{n}(y-)\, dy . \tag{48}$$

which is proportional to the crosscorrelation function. Here $ $ is the displacement in the y-direction of one of the films with respect to the other. The integration is carried out over the aperture length A.

A note is inserted here concerning the dc component of the signal. As seen in Fig. 8, the acoustical pressure has positive and negative values, whereas the light signal can only be positive, hence a dc bias is incorporated. Let $_{b}$ denote the bias signal. Then the crosscorrelation function becomes

Fig. - Multiple-channel spectrum analyzer

The spectrum of the signal $_{m}$ is formed in plane II, where the d-c term is blocked out. This spectrum then is used as a source to illuminate simultaneously all channels recorded on the data film in plane I'. The optics between planes I and I' effectively image the signal $_{m}$ in plane I on each of the signals lying in plane I'. Thus, the disturbance transmitted through each channel in plane I' is equal to the products $_{m} \times _{n}$.

The optics which follow plane I' collect the light over the length of each signal and display the crosscorrelation between $_{m}$ and $_{n}$.

$$\int_A [{}_{b}+ {}_{m}(y)][{}_{b}+ {}_{n}(y-)]\, dy$$

$$\int_A {}_{b}^2\, dy + \int_A ({}_{b} {}_{m} + {}_{b} {}_{n})\, dy$$

$$+ \int_A {}_{m}(y)\, {}_{n}(y-)\, dy . \tag{49}$$

The last term is the desired crosscorrelation. Now $_{m}$ and $_{n}$ have various frequency components, none of which has zero frequency. Thus, their crosscorrelation with $_{b}$ will be zero.

98

The term

$$\int_{\cdot} \, \cdot \cdot \mathrm{d}s$$

is the dc term which appears at the center of the optical axis, and has to be blocked out.

ACKNOWLEDGMENTS

The ideas presented in this report were originally conceived while the author was in the employ of Martin Company, Denver Division. The author wishes to express his gratitude to Dr. H. L. Cox of the Martin Company for his comments and suggestions during the formative stage of this work.

The author acknowledges the aid of a number of Aerospace personnel during the development of the ideas and preparation of the manuscript. Particular thanks are due to Eli Howard for his constructive criticism and Mary Allan for her patience and assistance during manuscript preparation.

REFERENCES

1. E. L. O'Neill, "Spatial Filtering in Optics," IRE Trans. on Information Theory, pp. 56-65, June 1956

2. P. Elias, D. Grey, and D. Robinson, "Fourier Treatment of Optical Processes," J. Opt. Soc. Am., pp. 127-134, Feb. 1952

3. J. Rhodes, "Analysis and Synthesis of Optical Images," Am. J. Physics, pp. 337-343, Jan. 1953

4. L. J. Cutrona, E. N. Leith, C. J. Palermo, and L. J. Porcello, "Optical Data Processing and Filtering Systems," IRE Trans. on Information Theory, pp. 386-400, June 1960

5. "Proposed Study of Optical Method of Analysis as Applied to Acoustical and Vibration Data," Goodyear Aircraft Co. Document GERA-639, Nov. 1961

BIBLIOGRAPHY

Born, M. and Wolf, E., "Principles of Optics," Pergamon Press, 1959

Longhurst, R. S., "Geometrical and Physical Optics," Longmans, 1957

Appendix

GREEN'S THEOREM IN ITS FIRST FORM

Let the vector field A be differentiable inside the closed surface S to establish the value of $\mathrm{div}\ A$ everywhere in the interior. Gauss's theorem states that:

$$\int_v \, \cdot \cdot A \, dv \quad \int_s A \cdot ds \quad \int_s A_n ds. \quad (A-1)$$

where n is the outward normal associated with the surface element ds, A_n is the magnitude of the component of A in the n direction, and v in the volume considered.

Let U and V be two scalar point functions satisfying the necessary continuity requirements (existence of the second and continuity of the first partial derivatives). Let A in Eq. (A-1) be

$$A \quad U \cdot V - V \cdot U. \quad (A-2)$$

such that

$$A_n \quad U \frac{\cdot V}{n} - V \frac{\cdot U}{n}. \quad (A-3)$$

From the following formula in vector analysis,

$$\cdot \cdot (\cdot B) \quad \cdot \cdot \cdot B \cdot \cdot \cdot \cdot B. \quad (A-4)$$

where $\cdot$ is any scalar, and B any vector, we obtain

$$\cdot \cdot U \cdot V \quad \cdot V \cdot \cdot U \cdot U \cdot \cdot \cdot V. \quad (A-5)$$

and

$$\cdot \cdot V \cdot U \quad \cdot U \cdot \cdot V \cdot V \cdot \cdot \cdot U. \quad (A-6)$$

Finding $\cdot \cdot A$ from Eqs. (A-2), (A-5) and (A-6), we have $\cdot \cdot A \quad \cdot \cdot U \cdot V - \cdot \cdot V \cdot U$. Hence,

99

$$\nabla \cdot \mathbf{A} = U \nabla \cdot V - V \nabla \cdot U$$

$$U \nabla^2 V - V \nabla^2 U \qquad \text{(A-7)}$$

By substituting Eq. (A-7) into Eq. (A-1),

$$\int_V (U \nabla^2 V - V \nabla^2 U)\, dv = \int_S \left(U \frac{\partial V}{\partial n} - V \frac{\partial U}{\partial n} \right) ds \qquad \text{(A-8)}$$

which constitutes Green's theorem in its first form.

*   *   *

COMPUTER PROGRAM FOR DYNAMIC DESIGN ANALYSIS METHOD

John H. Avila
David Taylor Model Basin
Washington, D.C.

A computer program is described which performs the computations
associated with the dynamic design analysis method as developed at the
Naval Research Laboratory. The program uses the influence coefficient
matrix or stiffness matrix associated with a lumped mass system, to-
gether with the masses, to generate the normal modes of vibration and
the fundamental frequencies. Of primary importance is the fact that
this routine accepts up to 60 degrees of freedom and is generally un-
affected by repeated frequencies or frequencies which lie close together.

There are capabilities for treating externally redundant systems of
certain types, alleviating the work of computing influence coefficient
matrices for these cases. Examples of such systems are given.

One valuable routine included in this program can examine the input
matrix of influence coefficients (or stiffnesses) and test for positive
definiteness, i.e., if all eigenvalues associated with the structure model
are positive. Furthermore, if the test establishes the existence of
negative eigenvalues, the routine locates certain areas of the input
matrix where errors are likely to be present. Several checks are de-
scribed for determining the reliability of the output.

J. H. Avila

MATHEMATICAL THEORY

Basic Problem

The theory of normal mode vibration has
been well developed and is available from sev-
eral sources. Of particular interest are re-
ports by O'Hara and Cunniff [1,2], from which
most of the mathematical treatment here is
derived. The development here is intended to
provide the mathematical background on which
the computer program described is based.

We are given a system of n masses in
space, each mass with the capability of dis-
placement in each of the three directions of the
coordinate axes. Let the influence coefficient
d_{ij}^{rs} be defined as the deflection of the ith mass
in the rth direction due to a unit force at the
jth mass in the sth direction. Here r, s are
indices representing one of the coordinate di-
rections. Let x_j^r denote the absolute displace-
ment of the jth mass in the rth direction.

Let us assume we have a freely vibrating
structure on a fixed base (so that motion rela-
tive to the base is absolute motion). Then the
only forces present are inertial forces, and
therefore, if we are interested in the displace-
ment of the ith mass in the rth direction we
have

$$x_j^r = -\sum_{s=1}^{3} \sum_{i=1}^{n} d_{ji}^{rs} m_i \ddot{x}_i^s . \qquad (1)$$

For response in all three directions at the jth
mass, we again get Eq. (1), replacing r by 1, 2,
and 3. In matrix notation this is written as
follows:

$$\begin{pmatrix} x^1 \\ x^2 \\ x^3 \end{pmatrix} = -\begin{pmatrix} d^{11} & d^{12} & d^{13} \\ d^{21} & d^{22} & d^{23} \\ d^{31} & d^{32} & d^{33} \end{pmatrix} \begin{pmatrix} m & 0 & 0 \\ 0 & m & 0 \\ 0 & 0 & m \end{pmatrix} \begin{pmatrix} \ddot{x}^1 \\ \ddot{x}^2 \\ \ddot{x}^3 \end{pmatrix} \quad (2a)$$

where d^{ij} is a square submatrix of order n representing the deflections in the ith direction due to unit forces in the jth direction, and m is a diagonal submatrix $(m_1, m_2, \dots, m_n)$ of masses. The full matrix (d^{ij}) is called the influence coefficient matrix; the full matrix of masses is known simply as the mass matrix.

We write Eq. (2a) as

$$x = -DM\ddot{x} \qquad (2b)$$

A standard technique in solving Eq. (2a) is to let $x = \sin(\omega t + \phi)x$, where x is a vector of $3n$ constants. We then find that solving Eq. (2b) is equivalent to solving

$$DMx = \frac{1}{\omega^2} x \qquad (3)$$

for $\omega \neq 0$, which is now recognized as a standard matrix eigenvalue problem.

From the physical nature of the problem, the matrix D is positive, definite, and symmetric. It is well known [3] that there exist $3n$ linearly independent eigenvectors corresponding to $3n$ eigenvalues (not necessarily distinct). We denote the eigenvectors by x_k and the eigenvalues by $1/\omega_k^2$, $k = 1, 2, \dots, 3n$. The first problem, therefore, is one of finding the $1/\omega_k^2$ and x_k associated with Eq. (3).

Some Useful Information
About Eigenvectors

The eigenvectors of Eq. (3) satisfy an orthogonality relationship of the form

$$\begin{aligned} (x_k . Mx_l) &= 0, \quad k \neq l \\ (x_k . Mx_k) &\neq 0. \end{aligned} \qquad (4)$$

Here we use the notation $(x.y)$ to denote the inner product (dot product) of two vectors. Thus,

$$(x.y) = \sum x_i y_i .$$

where x_i, y_i denote the ith components of the vectors x and y.

From this property of the eigenvectors, it can be shown that the eigenvectors are linearly independent, and hence that they form a basis for the space E^{3n}. This property enables us to check the computations at the end of the computer run in the following way.

Let 1^r denote the vector whose rn components are 1 and whose remaining $2n$ components are zero. Thus, 1^2 denotes the vector whose first n components are zero, the second n components are each 1, and the last n components are zero. Since the eigenvectors form a basis of E^{3n}, there exist constants c_i such that

$$1^r = \sum_{i=1}^{3n} c_i x_i \qquad (5)$$

From Eq. (5) we obtain, employing the orthogonality of the vectors,

$$(1^r . Mx_j) = c_j(x_j . Mx_j) .$$

and, thus,

$$c_j = \frac{(1^r . Mx_j)}{(x_j . Mx_j)} .$$

Therefore,

$$1^r = \sum_i \frac{(1^r . Mx_i)}{(x_i . Mx_i)} x_i . \qquad (6)$$

From Eq. (6) we can easily obtain

$$(1^s . M1^r) = \sum_i \frac{(1^r . Mx_i)(1^s . Mx_i)}{(x_i . Mx_i)} .$$

It is clear that the left side of this equation is zero for $r \neq s$. On the other hand, if $r = s$, then the left side is precisely

$$\sum_{i=1}^{n} m_i .$$

Therefore,

$$\sum_{i=1}^{n} m_i = \sum_{i=1}^{3n} \frac{(1^r . Mx_i)^2}{(x_i . Mx_i)} , \quad r = 1, 2, 3 . \qquad (7)$$

We use this check to verify the accuracy of x_i. The sum on the right is often referred to as the sum of the modal masses in the rth direction. The quantity

$$m_i^r \frac{(1^r . Mx_i)^2}{(x_i . Mx_i)}$$

is called the modal mass in the ith direction for the ith mode. In the actual computer calculations, this result perhaps is the most important for verification purposes. The computations are roughly as good as the check in Eq. (7) provides. If m_i^r is very close to the total mass of the structure, then one can expect that the computations are accurate; otherwise little confidence should be placed in the output data.

Applications

Once the eigenvalues and eigenvectors associated with Eq. (3) are known, one may calculate the response of the structure. As a preliminary step note that for the one-dimensional case (one mass, one direction of motion) the problem becomes one of solving

$$\ddot{x} + {}^2x = 0 . \tag{8}$$

As is well known, the solution is given by

$$x(t) = x(0) \cos t + \frac{\dot{x}(0)}{} \sin t . \tag{9}$$

Suppose now we return and attempt a solution of Eq. (2b) by a function of the form

$$x(t) = \sum_{j=1}^{3n} q_j(t) x_j . \tag{10}$$

where x_j are the eigenvectors. This arises naturally from our original search for a solution, which led to the eigenvalue problem, and the linearity of the differential equations, which implies that linear combinations of solutions are again solutions.

Substituting Eq. (10) into Eq. (2b), we have

$$\sum_j q_j x_j \qquad \sum_j \ddot{q}_j DM \ddot{x}_j \qquad - \sum_j \frac{1}{{}^2} \ddot{q}_j x_j .$$

Therefore,

$$\sum_j \frac{1}{{}^2} (\ddot{q}_j + {}_j^2 q_j) x_j = 0 .$$

If we compute the inner product of each side of this equation with Mx_k and use the orthogonality relationships, we get

$$\ddot{q}_k + {}_k^2 q_k = 0 . \quad k = 1,2,\dots,n .$$

and using Eq. (9), we see that

$$q_k(t) \quad q_k(0) \cos {}_k t + \frac{\dot{q}_k(0)}{{}_k} \sin {}_k t .$$

To get the solution in terms of the initial conditions for x, we use Eq. (10) and compute the inner product again with Mx_k to get

$$(x(0) . Mx_k) \quad q_k(0)(x_k . Mx_k) .$$

from which we can write

$$q_k(0) \quad \frac{(x(0) . Mx_k)}{(x_k . Mx_k)} . \tag{11a}$$

Similarly,

$$\dot{q}_k(0) \quad \frac{(\dot{x}(0) . Mx_k)}{(x_k . Mx_k)} . \tag{11b}$$

Thus, the final solution can be written

$$x(t) \quad \sum_j \left[\frac{(x(0) . Mx_j)}{(x_j . Mx_j)} \cos {}_j t \right] x_j$$
$$+ \sum_j \left[\frac{(\dot{x}(0) . Mx_j)}{{}_j(x_j . Mx_j)} \sin {}_j t \right] x_j . \tag{12}$$

Consider the problem of determining the solutions when applied forces on a structure are present. If the applied forces are assumed to be independent of the reaction of the structure, the equations of motion are given by

$$x \quad - DM\ddot{x} + Df . \tag{13}$$

where f is a vector in F^{3n} whose kth component represents the force on the kth mass in the first direction if $k \cdot n$, the force on the $(k-n)$th mass in the second direction for $n \cdot k \cdot 2n$, and the force on the $(k-2n)$th mass in the third direction for $2n \cdot k \cdot 3n$.

We will require the knowledge of the solution in the one-dimensional case just as we did for the freely vibrating structure. In the one-dimensional case we have

$$\ddot{x} + {}^2x \quad f(t) .$$

which has as its solution, incorporating the initial conditions,

$$x(t) \quad x(0) \cos t + \frac{\dot{x}(0)}{} \sin t$$
$$+ \frac{1}{} \int_0^t f(s) \sin (t-s) \, ds .$$

We use Eq. (10) again as a starting point on the $3n$ dimensional problem. From this we obtain

$$\sum_i c_i x_i \qquad \sum_j \ddot{q}_j DM x_j \cdot Df .$$

We use the fact that x_j is an eigenvector to obtain

$$\sum_j \left(q_j \cdot \frac{1}{2} \ddot{q}_j \right) x_j \qquad Df \qquad (14)$$

Since the n vectors x_j are linearly independent, we can express any vector in E^{3n} as a linear combination of these. This in turn enables us to write

$$Df \qquad \sum_j c_j x_j . \qquad (15)$$

where the scalars c_j are functions of time if f is. Taking the inner product with $M x_k$ and using the orthogonality relationships, we can solve for c_k:

$$c_k \qquad \frac{(Df . M x_k)}{(x_k . M x_k)} .$$

Symmetric matrices, such as D, have the property that if x and y are each vectors in E^{3n}, then $(Dx.y) \quad (x.Dy)$. This property is easily verified by expanding both sides. Thus,

$$(Df . M x_x) \qquad (f . DM x_k) \qquad \frac{1}{2} (f . x_k) .$$

which implies

$$c_k \qquad \frac{(f . x_k)}{{}_k^2 (x_k . M x_k)} \qquad (16)$$

Equation (15) now becomes

$$Df \qquad \sum_j \frac{(f . x_j)}{{}_j^2 (x_j . M x_j)} x_j .$$

Replacing this value for Df in Eq. (14) and combining terms, we get

$$\sum_j \frac{1}{2} \left[\ddot{q}_j \cdot {}_j^2 q_j \qquad \frac{(f . x_j)}{(x_j . M x_j)} \right] x_j \qquad 0 . \qquad (17)$$

Once again we utilize the orthogonality relationships to get

$$\ddot{q}_j \cdot {}_j^2 q_j \qquad \frac{(f . x_j)}{(x_j . M x_j)} \qquad j \quad 1, 2, \ldots, 3n. \qquad (18)$$

This is the same equation as the one-dimensional problem above; thus, the solutions are given by

$$\eta_j(t) \quad q_j(0) \cos {}_j t \cdot \frac{\dot{q}_j(0)}{{}_j} \sin {}_j t$$

$$\cdot \frac{1}{{}_j (x_j . M x_j)} \int_0^t (f . x_j) \sin {}_j (t-s) ds . \qquad (19)$$

Equations (11a) and (11b) still hold for $q_j(0)$ and $\dot{q}_j(0)$ so that the solution is known in terms of the initial conditions $x(0)$ and $\dot{x}(0)$.

Let us suppose that we have a structure mounted on a base, and that the base is subjected to a motion $z(t)$ which is a vector (z^1, z^2, z^3) with three components along the three coordinate axes. Recall Eq. (1) and remember that the inertial forces depend on the absolute acceleration of the masses, so that since the relative displacement of the jth mass x_j is given as the difference between the absolute displacement (relative to some fixed coordinate system, such as the earth) and the displacement of the base, we have

$$x_j^r \qquad \sum_{s=1}^3 \sum_{i=1}^n d_{ji}^{rs} m_i (\ddot{x}_i \cdot \ddot{z}^s) . \qquad (20)$$

where x_j^r is the displacement of the jth mass in the rth direction relative to the base. In matrix notation this is represented by the following:

$$\begin{pmatrix} x^1 \\ x^2 \\ x^3 \end{pmatrix} \quad \begin{pmatrix} d^{11} & d^{12} & d^{13} \\ d^{21} & d^{22} & d^{23} \\ d^{31} & d^{32} & d^{33} \end{pmatrix} \begin{pmatrix} m & 0 & 0 \\ 0 & m & 0 \\ 0 & 0 & m \end{pmatrix} \begin{pmatrix} \ddot{x}^1 \cdot \ddot{z}^1 \\ \ddot{x}^2 \cdot \ddot{z}^2 \\ \ddot{x}^3 \cdot \ddot{z}^3 \end{pmatrix} .$$

where, for example, x^1 is the column vector with components $x_1^1, x_2^1, \ldots, x_n^1$ representing the relative displacement of each mass in the first direction, for example, the direction of the x-axis, and where $\ddot{z}^1$ is the vector $(\ddot{z}^1, \ddot{z}^1, \ldots, \ddot{z}^1)$ whose n components are each the first component of the vector representing the acceleration of the base in the first direction.

Rewrite Eq. (20) in the form

$$x \qquad - DM \ddot{x} - DM \ddot{z} \qquad (21)$$

and compare this with Eq. (13). This is equivalent to Eq. (13) if f is replaced by $-M\ddot{z}$. Therefore, we can write the solution immediately from Eqs. (10) and (19) as

104

$$x(t) = \sum_j \left[q_j(0) \cos \omega_j t + \frac{\dot{q}_j(0)}{\omega_j} \sin \omega_j t \right] x_j$$

$$- \sum_j \left[\frac{1}{\omega_j (x_j, Mx_j)} \int_0^t (M\ddot{z}, x_j) \sin \omega_j (t-s) ds \right] x_j .$$

$$(22)$$

where $q_j(0)$ and $\dot{q}_j(0)$ can again be represented by Eqs. (11a) and (11b).

COMPUTER PROGRAM

Preliminary

The computer program was written for an IBM 7090 computer with a 32K memory, operating under the IBSYS monitor, version 13. The programming language employed was FORTRAN IV. The program was written, however, with the awareness that many users may have to modify parts of the program to use it on their systems. Consequently, this program is compatible (following minor revisions) with other systems which have FORTRAN capability.

Program Description

The user specifies his input data on cards. The input consists of the number of directions to be considered, the number of masses, options, the weight of each mass, and finally the influence coefficient or stiffness matrix.

The options include the ability to use as input the stiffness matrix instead of the influence coefficient matrix, the capability to have the computer determine the influence coefficient matrix for certain externally redundant structures, and the capability to suppress the positive definite test. Each of these options is explained below.

If the stiffness matrix is supplied, the program inverts to get the influence coefficient matrix. The computations are all done with the influence coefficient matrix.

There is a routine in the program designed to treat certain types of externally redundant structures by partially generating the influence coefficient matrix. Two simple examples will demonstrate the method and the type of structure.

Consider the two structures in Figs. 1 and 2. Figure 1 represents a statically indeterminate beam which has been treated as a three-mass system as shown. Figure 2 shows a cantilever

beam treated as a two-mass system. The influence coefficient matrix is to be obtained for each of the two structures. The following procedure was developed by G. J. O'Hara to simplify the process and actual computations.
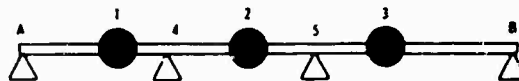
Fig. 1 - Redundant structure, routine A
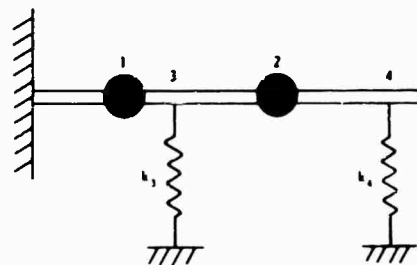
Fig. 2 - Redundant structure, routine B

In Fig. 1 we first remove the supports 4 and 5 to make the beam statically determinate. Let x_i denote the deflection at the point i and f_i denote the force at the point i. Then for the determinate beam

$$x_i = c_{i1}f_1 + c_{i2}f_2 + c_{i3}f_3 + c_{i4}f_4 + c_{i5}f_5, \quad i = 1,2,\ldots,5 .$$

$$(23)$$

where c_{ij} is the deflection at point i due to a unit force at point j for the determinate beam.

Now for the indeterminate beam, we need add only the boundary conditions $x_4 = x_5 = 0$. By doing this we can solve for f_4 and f_5 in the last two equations of Eq. (23) and substitute back to get x_1, x_2, and x_3.

The situation in Fig. 2 is similar. We generate a system of four equations in four unknown deflections at the four points, neglecting temporarily the effect of the springs. Finally, we accommodate the springs with the boundary conditions that the deflections at points 3 and 4 are given by

$$x_3 = \frac{f_3}{k_3}, \quad x_4 = \frac{f_4}{k_4}$$

We can now subtract f_3/k_3 from c_{33} and f_4/k_4 from c_{44} to get zeros on the left in the last two

105

equations. Let us now compute the true influence coefficient matrix. The influence coefficient $\cdot_{ij}$ is the deflection at mass i due to a unit force at mass j. Thus we apply in turn a unit force at mass 1, 2, etc., and the force needed at the auxiliary points to satisfy the boundary conditions and note the resulting solutions of Eq. (23).

Once the input is supplied, the user can utilize a routine which was written specifically to check the input matrix for errors. This routine can examine a matrix and determine whether or not it has positive definiteness (if all the eigenvalues are positive). In the event this condition does not exist, the routine then locates certain areas in the matrix where errors are present. The advantages of such a routine are apparent for large matrices where the elements have been calculated by hand.

The determination of eigenvalues is done with the aid of a routine available through the IBM users library which employs the QR transform method. The results of this routine have proven to be extremely reliable and accurate. This routine has worked well for repeated eigenvalues or for eigenvalues which were not well separated.

Once the eigenvalues have been determined, the mode shapes (eigenvectors) are then obtained. Here the procedure is perhaps different from most routines of this nature in that iteration is not employed. The advantage of such an approach is that no accuracy is lost in obtaining succeeding mode shapes by employing the orthogonality condition at each stage, so the final mode shape is as accurately computed as the first. The actual method employed is to obtain a nontrivial solution to the problem

$$\left(DM - \frac{1}{2} 1 \right) x \quad 0$$

by a typical Gaussian elimination method. The problem of repeated eigenvalues was treated in this program. The method used was to require that successive mode shapes satisfy the orthogonality condition with respect to the mode shapes previously calculated for the particular eigenvalue. Some justification is appropriate for this effort. It is generally felt that only in cases of symmetry do repeated eigenvalues occur. The following example shows this not to be the case.

Consider the three-mass system shown in Fig. 3. Assume that all masses have a value of 1 (in any convenient system of units). Let $k_1 = 10/28$, $k_2 = 6/28$, $k_3 = 2/28$, $k_4 = 22/28$, $k_5 = 16/28$, and $k_6 = 3/28$. From this we obtain the stiffness matrix
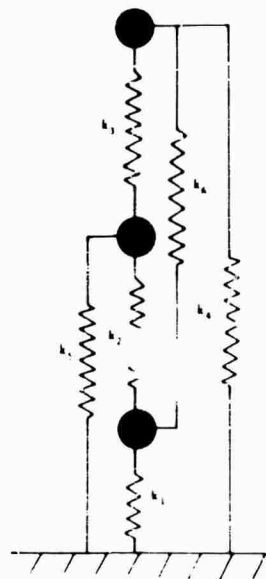
Fig. 3 - Three-mass system

$$\frac{1}{28} \begin{pmatrix} 27 & -2 & -3 \\ -2 & 24 & -6 \\ -3 & -6 & 19 \end{pmatrix}$$

and invert it to obtain the influence coefficient matrix

$$\frac{1}{42} \begin{pmatrix} 45 & 6 & 9 \\ 6 & 54 & 18 \\ 9 & 18 & 69 \end{pmatrix}.$$

From this we can obtain normalized mode shapes as

$$\frac{1}{\sqrt{42}} \begin{pmatrix} 5 \\ -4 \\ 1 \end{pmatrix}, \quad \frac{1}{\sqrt{3}} \begin{pmatrix} 1 \\ 1 \\ -1 \end{pmatrix}, \quad \frac{1}{\sqrt{14}} \begin{pmatrix} 1 \\ 2 \\ 3 \end{pmatrix}.$$

corresponding respectively to eigenvalues of 1, 1, and 2.

Except for the fact that the masses are the same, which was chosen for convenience, there is a definite lack of symmetry. Yet the eigenvalue 1 is repeated. Note the following, however. If we examine the vectors

$$\frac{1}{\sqrt{5}} \begin{pmatrix} 2 \\ -1 \\ 0 \end{pmatrix} \text{ and } \frac{1}{\sqrt{70}} \begin{pmatrix} -3 \\ -6 \\ 5 \end{pmatrix}$$

106

we see they also will serve as an orthogonal pair of eigenvectors associated with the eigenvalue of 1. In fact any linear combination of two such vectors (i.e., either these two or the two above) will produce another eigenvector with the eigenvalue 1. The program provides one such pair. The situation is the same for higher multiplicity of the eigenvalues; any linear combination of eigenvectors for the repeated eigenvalue is again an eigenvector.

Physically, this means that at the frequency corresponding to a repeated eigenvalue, the actual normal mode of vibration will be a linear combination of the vectors given in the computations. The actual combination will depend on the particular base notation or set of applied forces.

In the computer calculations, if, at any time, a zero or negative eigenvalue is encountered, the mode shape is computed but no other computations are performed for that mode and a note is made in the output. The reason for this is that a negative eigenvalue indicates that the structure behaves as

$$y(t) = e^{it}x .$$

where x and y are n-dimensional vectors and $i > 0$. The ith component of i denotes the motion of the ith mass (assume one direction of motion). This, however, implies that the structure will collapse in this mode. Thus, either an error has been made in the input or the model itself does not accurately portray the real structure. Normally, a zero eigenvalue denotes an error also, although there are situations in which they may legitimately occur.

Output

Although forces, stresses, and displacements are some of the chief quantities desired by the engineer using the program, these generally depend on a "design acceleration" factor, which is often classified. As a result, this program prints the quantities necessary for these computations without this factor, which the user can then insert by simply multiplying by a constant. For each mass the product of the weight multiplied by the mode shape and a "participation factor" is printed for each direction of input base motion. The participation factor is a quantity associated with each mode and each direction. For example, the participation factor associated with mode i in the v-direction is defined

$$P_y \quad \frac{(i^2 . Mx_j)}{(x_j . Mx_j)} .$$

where i^2 is as defined previously. Thus, if P_x, P_y, P_z denote the three participation factors (assuming we are considering three-directional motion), we print out the three quantities $m_i v x_{ia} P_x$, $m_i v x_{ia} P_y$, $m_i v x_{ia} P_z$, for each mode i and each mass i. The actual display for three-directional motion would be as shown in Fig. 4 Here we have let v_{ia} and z_{ia} denote the deflections in the v and z directions, respectively. Also we denote v_{ia} as w_i. The actual computation of forces involving these quantities are described in Refs. 1 and 2.

$w_1{}^x{}_{1a}P_x$	$w_1{}^y{}_{1a}P_x$	$w_1{}^z{}_{1a}P_x$
$w_2{}^x{}_{2a}P_x$	$w_2{}^y{}_{2a}P_x$	$w_1{}^z{}_{2a}P_x$
.	.	.
.	.	.
.	.	.
$w_n{}^x{}_{na}P_x$	$w_n{}^y{}_{na}P_x$	$w_n{}^z{}_{na}P_x$
$w_1{}^x{}_{1a}P_y$	$w_1{}^y{}_{1a}P_y$	$w_1{}^z{}_{1a}P_y$
$w_2{}^x{}_{2a}P_y$	$w_2{}^y{}_{2a}P_y$	$w_2{}^z{}_{2a}P_y$
.	.	.
.	.	.
.	.	.
$w_0{}^x{}_{na}P_y$	$w_n{}^y{}_{na}P_y$	$w_n{}^z{}_{na}P_y$
$w_1{}^x{}_{1a}P_z$	$w_1{}^y{}_{1a}P_z$	$w_1{}^z{}_{1a}P_z$
$w_2{}^x{}_{2a}P_z$	$w_2{}^x{}_{2a}P_z$	$w_2{}^z{}_{2a}P_z$
.	.	.
.	.	.
$w_n{}^x{}_{na}P_z$	$w_n{}^y{}_{na}P_z$	$w_n{}^z{}_{na}P_z$

Fig. 4 - Display for three-directional motion

Also given as output, as already mentioned, are the participation factors for each input direction, depending on how many directions have been considered from the beginning. In addition, the so-called effective mass or modal mass and weight are given for each mode, and a running total is kept. This enables the engineer to take into account as many modes as he wishes or as few as he needs, and he can see all of the modes present in the model.

The total modal weight can be compared to the total weight of the structure as a check on the computations as described in the mathematical section. Similarly, the trace of the matrix and the sum of the eigenvalues are printed as a check on the accuracy of the eigenvalue calculations. (The trace of a matrix is the sum of the diagonal elements along the main diagonal.) In all cases tested, these checks have shown that the method is quite accurate. For example,

107

in a test run for a single-direction system of 59 masses, the total mass was 59.00 and the total modal mass was 59.43. For the same run, the trace was equal to 849.37, and the sum of the eigenvalues was equal to 849.36.

Running Time; Additional Information

This program has a relatively short running time. The test case of 59 degrees of freedom ran 12.66 min, but a slightly longer time should be allowed for a problem of this size since the matrix tested for this case was sparse. Another problem with 8 degrees of freedom required 1.06 min. This should give a fair guide to the time required.

Copies of the program together with more detailed information on input preparation and other facts of this nature are available upon request on an individual basis from the David

Taylor Model Basin, Applied Mathematics Laboratory (Code 872), Washington, D.C. 20007.

SAMPLE RUN

Figures 5 through 11 give selected pages of output from a sample problem. As Fig. 5 indicates, the problem involved two directions of motion and four masses. The computations for the first and eighth modes of vibration are given. The program took 1.06 min of computer time.

ACKNOWLEDGMENT

The author wishes to acknowledge the very patient assistance of G. J. O'Hara in obtaining an understanding of normal mode theory and for his valuable suggestions in the development of this program.

```
INPUT DATA
      NUMBER OF DIRECTIONS     NO. OF MASSES
           2                        4

      INFLUENCE COEFFICIENT MATRIX INPUT


   INPUT MATRIX


   ROW  1      0.29761E-03    0.            0.17850E-04    0.17850E-04
               0.             0.           -0.17850E-04   -0.17850E-04

   ROW  2      0.            0.50925E-03    0.27770E-04    0.27770E-04
               0.13880E-04    0.13880E-04   0.27770E-04    0.27770E-04

   ROW  3      0.17850E-04    0.27770E-04   0.16710E-04   -0.12300E-05
               0.19200E-05   -0.19200E-05  -0.40000E-07    0.12300E-05

   ROW  4      0.17850E-04    0.27770E-04  -0.12300E-05    0.16710E-04
              -0.19200E-05    0.19200E-05   0.12300E-05   -0.40000E-07

   ROW  5      0.            0.13880E-04    0.19200E-05   -0.19200E-05
               0.93300E-05   -0.16000E-05  -0.19200E-05    0.19200E-05

   ROW  6      0.            0.13880E-04   -0.19200E-05    0.19200E-05
              -0.16000E-05    0.93300E-05   0.19200E-05   -0.19200E-05

   ROW  7     -0.17850E-04    0.27770E-04  -0.40000E-07    0.12300E-05
              -0.19200E-05    0.19200E-05   0.16710E-04   -0.12300E-05

   ROW  8     -0.17850E-04    0.27770E-04   0.12300E-05   -0.40000E-07
               0.19200E-05   -0.19200E-05  -0.12300E-05    0.16710E-04
```

Fig. 5 - Output from sample problem

108

```
MATRIX OF WEIGHTS (DIAGONAL)
            0.15050E 03    0.20060E 03    0.57300E 02    0.8675CE 02


MATRIX OF MASSES (CIAGONAL)
            0.38990E 00    0.51969E 00    0.14845E 00    0.22474E 00


TOTAL MASS SUM =   0.12828E 01
TCTAL WEIGHT SUM =   0.49515E 03

SCALE PRODUCT, MASS MATRIX   X   INFL. COEFF. MATRIX


ROW  1      0.37146E 01    0.          0.84825E-01    0.12842E 00
            0.          0.         -0.84825E-01   -0.12842E 00

ROW  2      0.          0.84722E 01    0.13197E 00    0.19979E 00
            0.17324E 00    0.23092E 00    0.13197E 00    0.19979E 00

ROW  3      0.22280E 00    0.46200E 00    0.79408E-01   -0.88493E-02
            0.23965E-01   -0.31942E-01   -0.19008E-03    0.88493E-02

ROW  4      0.22280E 00    0.46200E 00   -0.58451E-02    0.12022E 00
           -0.23965E-01    0.31942E-01    0.58451E-02   -0.28778E-03

ROW  5      0.          0.23092E 00    0.91241E-02   -0.13813E-01
            0.11045E 00   -0.26618E-01   -0.91241E-02    0.13813E-01

ROW  6      0.          0.23092E 00   -0.91241E-02    0.13813E-01
           -0.19971E-01    0.15522E 00    0.91241E-02   -0.13813E-01

ROW  7     -0.22280E 00    0.46200E 00   -0.19008E-03    0.88493E-02
           -0.23965E-01    0.31942E-01    0.79408E-01   -0.88493E-02

ROW  8     -0.22280E 00    0.46200E 00    0.58451E-02   -0.28778E-03
            0.23965E-01   -0.31942E-01   -0.58451E-02    0.12022E 00
SCALE =   0.32013E 05
```

Fig. 6 - Output from sample problem

REFERENCES

1. G. J. O'Hara and P. F. Cunniff, "Elements
   of Normal Mode Theory," NRL Rept. 6002,
   Nov. 15, 1963

2. G. J. O'Hara and P. F. Cunniff, "Normal
   Mode Theory for Three-Directional Motion,"
   NRL Rept. 6170, Jan. 5, 1965

3. Jack Indritz, Methods in Analysis. Mac-
   Millan, New York, 1963

DISCUSSION

Mr. Hooper (Boeing-Vertol): I was expecting some discussion of the effect of external applied forces. Do you have another program which this one feeds into to give the effect of external forces?

Mr. Avila: No, we do not have a program yet. This is, of course, a logical sequel to this program, and we are writing one now which uses the output from this program to compute the response for applied forces.

Mr. Hooper: Are you working with aircraft companies on this? Every aircraft manufacturer must have at least one program that does the same thing, and unless you are

109

```
                       DAVID TAYLOR MODEL BASIN
                     APPLIED MATHEMATICS LABORATORY
                       PROBLEM NO.  840-325


          MODAL COMPUTATION TABLES        MODE   1

          FREQUENCY =              0.6130E 02 RAD/SEC
                   =              0.9756E 01 CYCLES/SEC
          FREQUENCY SQUARED =   0.3757E 04 (RAD/SEC) SQUARED

          SUM OF (MASS X MODE SHAPE SQUARED) FOR MODE =   0.5226E 00




          G/OMEGA SQUARED =   0.10273E 00

     MODE   1    MODE SHAPE



     MASS       ------------- MODE SHAPE ----------------
     NUMBER   X-DIRECTION    Y-DIRECTION    Z-DIRECTION
        1     -0.68576E-07    0.27391E-01
        2      0.10000E 01    0.27541E-01
        3      0.54709E-01    0.54761E-01
        4      0.55027E-01    0.54974E-01
```

Fig. 7 - Output from sample problem

working closely together, I suspect there is repetition.

Mr. Avila: There undoubtedly is. This program did not take months and months to write. The primary reason for its form is that it actually provides the specific quantities needed for the dynamic design analysis method. These then need only be multiplied by some factor to get the actual numbers for the method. We looked at other similar programs, but some of them were fairly specific to the systems involved, and it was felt that it would be easier to put some routines together to get the results here than to modify a program.

Mr. Dobson (Knolls Atomic Power Lab.): Do you represent the mass matrix as a diagonal?

Mr. Avila: Yes, it is a simple diagonal matrix with no gyroscopic effects or the like.

110

MODE 1 PARTICIPATION FACTORS
           WGT * MODE SHAPE * PARTICIPATION FACTORS

PARTICIPATION FACTOR FOR X DIRECTION = 0.10336E 01
                         Y DIRECTION = 0.87015E-01

**** NOTE THAT WGT * MODE SHAPE INCLUDES G FACTOR.
     I.E. WGT * MODE SHAPE = G * MASS * MODE SHAPE

   MASS   ----- WGT * MODE SHAPE * P FACTOR ----- FOR X   INPUT MOTION
   NUMBER X-DIRECTION   Y-DIRECTION   Z-DIRECTION
     1 -0.10667E-04   0.42608E 01
     2   0.20734E 03   0.57102E 0
     3   0.32401E 01   0.32432E 01
     4   0.49339E 01   0.49292E 01

   MASS   ----- WGT * MODE SHAPE * P FACTOR ----- FOR Y   INPUT MOTION
   NUMBER X-DIRECTION   Y-DIRECTION   Z-DIRECTION
     1 -0.89806E-06   0.35870E 00
     2   0.17455E 02   0.48073E 00
     3   0.27278E 00   0.27304E 00
     4   0.41537E 00   0.41497E 00
   SUM   0.23365E 03   0.19671E 02

EFFECTIVE
   MASS   0.55832E 00   0.39571E-02
   WEIGHT   0.21551E 03   0.15274E 01

TOTALS---
UP TO AND INCLUDING THIS MODE

MODAL MASS 0.55832E 00   0.39571E-02

MODAL WGT   0.21551E 03   0.15274E 01

Fig. 8 - Output from sample problem

111

```
                        DAVID TAYLOR MODEL BASIN
                        APPLIED MATHEMATICS LABORATORY
                        PROBLEM NO.  840-325


        MODAL COMPUTATION TABLES        MODE    8

        FREQUENCY =             0.7977E 03 RAD/SEC
                   =             0.1270E 03 CYCLES/SEC
        FREQUENCY SQUARED =   0.6363E 06 (RAD/SEC) SQUARED

        SUM OF (MASS X MODE SHAPE SQUARED) FOR MODE =  0.3410E 00




        G/OMEGA SQUARED =   0.60665E-03

MODE    8      MODE SHAPE



MASS     ------------- MODE SHAPE -------------
NUMBER   X-DIRECTION    Y-DIRECTION    Z-DIRECTION
   1      0.66700E-02    0.28216E 00
   2     -0.55154E-01    0.15896E 00
   3      0.76306E 00    0.10000E 01
   4      0.34909E 00    0.38291E 00

                   Fig. 9 - Output from sample problem
```

```
MODE   8  PARTICIPATION FACTORS
          WGT * MODE SHAPE * PARTICIPATION FACTORS



PARTICIPATION FACTOR FOR X DIRECTION =  0.48584E 00
                          Y DIRECTION =  0.12526E 01



**** NOTE THAT WGT * MODE SHAPE INCLUDES G FACTOR.
     I.E.  WGT * MODE SHAPE = G * MASS * MODE SHAPE


   MASS     ----- WGT * MODE SHAPE * P FACTOR ----- FOR   X    INPUT MOTION
   NUMBER X-DIRECTION    Y-DIRECTION    Z-DIRECTION
     1     0.48770E 00    0.20631E 02
     2    -0.53753E 01    0.15492E 02
     3     0.21242E 02    0.27839E 02
     4     0.14713E 02    0.16138E 02


   MASS     ----- WGT * MODE SHAPE * P FACTOR ----- FOR   Y    INPUT MOTION
   NUMBER X-DIRECTION    Y-DIRECTION    Z-DIRECTION
     1     0.12574E 01    0.53191E 02
     2    -0.13859E 02    0.39942E 02
     3     0.54768E 02    0.71774E 02
     4     0.37933E 02    0.41608E 02
    SUM    0.11117F 03    0.28661E 03


EFFECTIVE
  MASS       0.80487E-01    0.53501E 00
  WEIGHT     0.31068E 02    0.20651E 03


TOTALS---
UP TO AND INCLUDING THIS MODE

MODAL MASS    0.12828E 01    0.12828E 01


MODAL WGT     0.49515E 03    0.49515E 03
```

Fig. 10 - Output from sample problem


```
    TRACE =     0.12858E 02     SUM DF EIGENVALUES =     0.12858E 02
      NORMAL COMPLETION
```

Fig. 11 - Output from sample problem

*   *   *

113

COMPUTER PROGRAM FOR GENERAL SHIP
VIBRATION CALCULATIONS*

Francis M. Henderson
David Taylor Model Basin
Washington, D.C.

A digital computer program was developed at the Applied Mathematics
Laboratory, David Taylor Model Basin, for calculating the approximate
steady-state response to harmonic forces and natural frequencies of a
system of slender, moderately nonuniform beams with elastic couplings.
This system is used to represent a ship hull connected elastically to its
propulsion system and to flexibly mounted units (i.e., machinery) which
may influence the vibration. The program handles vertical, horizontal,
longitudinal (extensional), torsional, coupled vertical-torsion, and
horizontal-torsion vibration.

Finite-difference equations are used to approximate the systems of
steady-state differential equations which the beam system satisfies in
each type of vibration. The difference equations are set up by the
computer according to a set of lumped elastic and inertial parameters
and options supplied as input to the program. These equations are
solved (with free-end conditions on each beam) for the mode shapes
corresponding to natural frequencies or response patterns for arbi-
trary frequencies of the exciting forces. Solutions are given in terms
of displacement, moment and rotation at discrete points in the beam
system.

The program provides for automatic calculation of added mass as a
function of frequency and consideration of various forms of damping,
including hysteretic and viscous, and frequency-proportional exciting
forces and moments. The program is being extended to include calcu-
lation of critical whirling speeds of propeller shafts. A set of sample
problems is included.

INTRODUCTION

In 1962, CONESCO, Inc., under a contract
with the U.S. Naval Bureau of Ships, began a
detailed analysis of the hull structure for the
ballistic-missile submarine SSB(N)598 GEORGE
WASHINGTON [1]. Their study of the structural
response of the hull in bending required the aid
of a digital computer program which could take
into account the influence on vibration of (a) the
propulsion system represented as a mass-
elastic system connected to the hull, (b) flexibly
mounted units throughout the hull, (c) added
mass of surrounding water as a function of fre-
quency, and (d) various types of damping. For
this purpose a new computer program was

developed and coded by E. H. Cuthill of the Applied
Mathematics Laboratory, David Taylor Model
Basin. This computer code, General Bending
Response Code 1 (GBRC1) [2], allowed a wide
variety of descriptions of the mathematical
model for the hull and was sufficiently general
to apply not only to bending calculations but
also to longitudinal (extensional) and torsional
calculations as well. The author has augmented
GBRC1 to produce a second computer code,
GBRC2, for application to coupled torsion-
bending hull vibration problems, and current
work is directed toward a second expansion of
the original program to produce GBRC3, which
will be used in calculating critical whirling
speeds of propeller shafts. These computer

---

*This paper was not presented at the Symposium.

codes can be used either as self-contained units or as subprograms of one computer package, referred to as the General Bending Response Program.

This paper outlines the development of the various systems of finite-difference equations for the General Bending Response Program and discusses their generalized matrix form for application to beam-spring systems. The computer method for solving these equations in the nonhomogeneous (forced response) and homogeneous (free response) cases is considered briefly, and several sample problems typical of those to which the program has been applied are presented.

PARTIAL DIFFERENTIAL EQUATIONS FOR BEAM

The partial differential equations which form the basis for GBRC1 and GBRC2 are obtained from the equations derived [3, Chap. 3, Sect. B] for torsion horizontal bending motion of a slender, moderately nonuniform beam approximation to the ship hull. The beam is described as having three principal types of flexibility: bending, shear and torsion. Figure 1 shows the coordinate system orientation for the beam. The x-axis is defined as parallel to the keel and passing through a point halfway between the main deck and keel at the midship section. The y-axis is always in the plane of bending. For the purposes of the General Bending Response Program, we augment the partial differential equations to include a damping coefficient and externally acting forces, moments, and torques. The resulting equations are

$$\frac{\partial V(x,t)}{\partial x} \quad \mu(x)\frac{\partial^2 y(x,t)}{\partial t^2} - r(x)\frac{\partial V(x,t)}{\partial t}$$

$$\cdot \mu(x) z(x) \frac{\partial^2 \varphi(x,t)}{\partial t^2} \cdot P(x,t). \quad (1)$$

$$\frac{\partial M(x,t)}{\partial x} \quad V(x,t) \cdot I_{\mu z}(x)\frac{\partial^2 \varphi(x,t)}{\partial t^2} \cdot Q(x,t). \quad (2)$$

$$\frac{\partial \varphi(x,t)}{\partial x} \quad \frac{M(x,t)}{FI(x)} \quad (3)$$

$$\frac{\partial \varphi(x,t)}{\partial x} \quad \frac{T(x,t) \cdot V(x,t) \bar{z}(x)}{GJ_n(x)} \quad (4)$$

$$\frac{\partial y(x,t)}{\partial x} \quad \varphi(x,t) - V(x,t)\left[\frac{1}{KAG(x)} \cdot \frac{\bar{z}(x)^2}{GJ_n(x)}\right]$$

$$\frac{\bar{z}(x) \cdot I(x,t)}{GJ_n(x)} \quad (5)$$
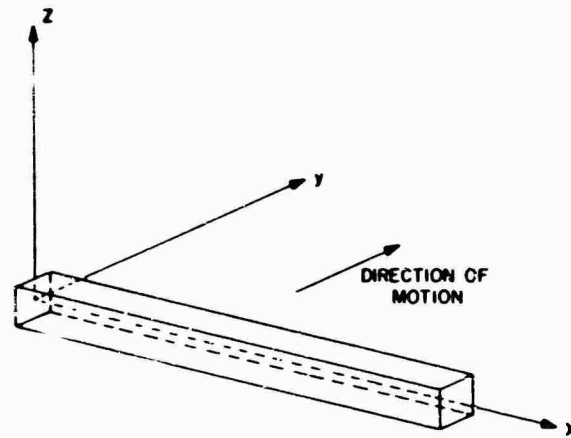
Fig. 1 - Orientation of coordinate system

and

$$\frac{\partial T(x,t)}{\partial x} \quad \mu(x) z(x) \frac{\partial^2 y(x,t)}{\partial t^2} - I_{\varphi x}(x)\frac{\partial^2 \varphi(x,t)}{\partial t^2}$$

$$\cdot U(x,t). \quad (6)$$

The notation for these equations is

- t = time;

- x = distance in longitudinal direction measured from origin of coordinates;

- y = displacement normal to x in plane of bending;

- φ = angular displacement relative to z-axis;

- V = shearing force in direction of bending (y-direction);

- M = bending moment;

- ψ = rotation of cross section with respect to x-axis;

- T = total moment on cross section taken about x-axis;

- μ = effective mass per unit length;

- $I_{\mu z}$ = effective rotary inertia per unit length;

- z = vertical distance from x-axis to center of mass;

- $\bar{z}$ = distance from x-axis to center of horizontal shear (assumed to be centroid of area of cross section of hull);

116

KAG = shearing rigidity, where K is numerical factor dependent on geometry of cross section ($K \leq 1$), A is cross-sectional area, and G is shear modulus of elasticity;

EI = bending rigidity, where E is Young's modulus of elasticity and I is areal moment of inertia of any cross section about principal axis perpendicular to plane of bending;

GJ_e = effective torsional rigidity with respect to longitudinal axis, where J_e is effective areal polar moment of inertia of cross section about its shear center;

I_{xx} = diametral mass moment of inertia about x-axis of section of length Δx;

P = external forcing function acting in y-direction;

Q = external forcing moment about axis parallel to z;

U = external forcing torque about x-axis; and

c = damping coefficient.

These equations are derived for small motions of the beam. The terms z and $\bar{z}$ are required because, in general, a horizontal plane of elastic and inertial symmetry does not exist for the ship hull.

TIME-INDEPENDENT DIFFERENTIAL EQUATIONS FOR BEAM

If the externally acting forces, moments, and torques in Eqs. (1) through (6) are sinusoidal functions of time, they can be expressed as

$$P(x,t) = e^{i\omega t} P(x),$$

$$Q(x,t) = e^{i\omega t} Q(x),$$ (7)

$$U(x,t) = e^{i\omega t} U(x).$$

Then for the steady-state condition, we can also write

$$y(x,t) = e^{i\omega t} y(x),$$

$$\psi(x,t) = e^{i\omega t} \psi(x),$$ (8)

$$V(x,t) = e^{i\omega t} V(x),$$ (Cont.)

$$M(x,t) = e^{i\omega t} M(x).$$

$$z(x,t) = e^{i\omega t} z(x),$$ (8)

$$T(x,t) = e^{i\omega t} T(x).$$

We note that $y(x)$, $V(x)$, $M(x)$, $z(x)$, and $T(x)$ are complex-valued functions whose absolute values indicate the lengths of vectors rotating with time in the complex plane at a common angular frequency of ω rad/sec. Substituting Eqs. (8) into Eqs. (1) through (6), we can obtain the following time-independent equations:

$$\frac{dV(x)}{dx} = \mu(x)\omega^2 y(x) - ic(x)\omega y(x)$$
$$- \mu(x)\omega^2 z(x) - \omega^2 z(x) + P(x).$$ (9)

$$\frac{dM(x)}{dx} = V(x) - \omega^2 I_{zz}(x)\psi(x) + Q(x).$$ (10)

$$\frac{dy(x)}{dx} = \psi(x) - \frac{V(x)}{KAG(x)} - \frac{V(x)\bar{z}(x)^2}{GJ_e(x)} - \frac{\bar{z}(x)T(x)}{GJ_e(x)}.$$ (11)

$$\frac{d\psi(x)}{dx} = \frac{M(x)}{EI(x)}.$$ (12)

$$\frac{dz(x)}{dx} = \frac{T(x)}{GJ_e(x)} - \frac{V(x)\bar{z}(x)}{GJ_e(x)}.$$ (13)

and

$$\frac{dT(x)}{dx} = -\mu(x)z(x)\omega^2 y(x) + I_{xx}(x)\omega^2 z(x) + U(x).$$ (14)

GENERAL BENDING RESPONSE CODE 1

Difference Equations, Lumped Parameter Representation of Beam

The first code developed in the series handled only vibrations of the hull in which there was no coupling between deflection and rotation of the cross sections. The differential equations for this condition are obtained by dropping terms involving T, z, $\dot{z}$ and $\bar{z}$ from Eqs. (9) through (14). This gives

$$\frac{dV(x)}{dx} = \mu(x)\omega^2 y(x) - ic(x)\omega y(x) + P(x).$$ (15)

$$\frac{dM(x)}{dx} = V(x) - I_{zz}(x)\omega^2 \psi(x) + Q(x).$$ (16)

$$\frac{dy(x)}{dx} = \psi(x) - \frac{V(x)}{KAG(x)}.$$ (17)

and

$$\frac{d\theta(x)}{dx} = \frac{M(x)}{EI(x)} \qquad (18)$$

Cuthill, in an analysis of Eqs. (15) through (18) for GBRC1 [2, Sect. II], obtains for the beam as subdivided in Fig. 2 a set of linear, finite-difference equations in the variables y (deflection) and M (moment) and generalizes these equations for application to systems of beams with elastic couplings. The difference equations are

$$\alpha_{n-1,n} y_{n-1} + \beta_{n-1,n} M_{n-1} + (\gamma_{n,n+1} + \gamma_{n-1,n}) y_n$$
$$+ (\delta_{n,n+1} + \delta_{n-1,n}) M_n + \alpha_{n,n+1} y_{n+1} - \beta_{n,n+1} M_{n+1}$$
$$= P_n + \epsilon_{n,n+1} Q_{n,n+1} + \epsilon_{n-1,n} Q_{n-1,n} \qquad (19)$$

and

$$\zeta_{n-1,n} y_{n-1} - \eta_{n-1,n} M_{n-1} + (\theta_{n,n+1} + \theta_{n-1,n}) y_n$$
$$+ (\lambda_{n,n+1} + \lambda_{n-1,n} + \mu_n) M_n - \nu_{n,n+1} y_{n+1} + \xi_{n,n+1} M_{n+1}$$
$$= -\rho_{n,n+1} Q_{n,n+1} + \sigma_{n-1,n} Q_{n-1,n} \qquad (20)$$

where $n = 1, 2, \ldots, N$, N being the number of intervals into which the beam is divided. The conditions for free ends on the beam will be included in these equations when $n = 1$ and $n = N$. The notation for these equations is given in the following section.

L DENOTES LENGTH OF BEAM
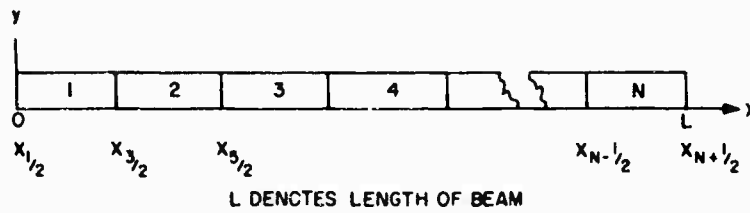
Fig. 2 - Subdivision of beam

Matrix Formulation of Finite-Difference Equations

The matrix formulation of Eqs. (19) and (20) is

$$Az = P \qquad (21)$$

where

$$A = \begin{vmatrix} A_{11} & A_{12} & 0 & & 0 \\ A_{21} & A_{22} & A_{23} & 0 & \\ 0 & A_{32} & A_{33} & A_{34} & 0 \\ & & & & A_{N-1,N} \\ 0 & & 0 & A_{N,N-1} & A_{N,N} \end{vmatrix} \qquad (22)$$

$$z = \begin{vmatrix} y_1 \\ M_1 \\ y_2 \\ M_2 \\ \cdot \\ \cdot \\ y_N \\ M_N \end{vmatrix} \qquad (23)$$

and P is a column vector whose elements form the right-hand side of Eqs. (19) and (20). The elements of the column vector P represent the forces and moments acting externally at discrete points along the subdivided beam. The elements $A_{i,j}$ of A are $2 \cdot 2$ submatrices.

The connections between adjacent sections in the subdivided beam of Fig. 2 give off-diagonal submatrices of the form

$$A_{n,n+1} = \begin{vmatrix} -\alpha_{n,n+1} & -\beta_{n,n+1} \\ \zeta_{n,n+1} & -\eta_{n,n+1} \end{vmatrix}$$

for $n = 1, 2, \ldots, N-1$ and their respective symmetric counterparts below the main diagonal

$$A_{n,n-1} = \begin{vmatrix} -\alpha_{n-1,n} & \beta_{n-1,n} \\ \zeta_{n-1,n} & -\eta_{n-1,n} \end{vmatrix}$$

for $n = 2, 3, \ldots, N$. The notation is

$$\alpha_{n,n+1} = \left[1 + \left(\frac{I_z}{KAG}\right)^2_{n,n+1}\right] \cdot \frac{1}{(\Delta x)_{n,n+1}}$$

$$\beta_{n,n+1} = (I_z)^2_{n,n+1} \tau_{n,n+1}$$

$$\gamma_{n,n+1} = \frac{1}{(KAG)_{n,n+1}} \tau_{n,n+1}$$

118

for $n = 1, 2, 3, \ldots, N$ 1, with the subscripts indicating an averaging of parameters ove. the interval x_n to x_{n+1} with

$$x_n \quad \frac{1}{2}(x_{n+1\ 2} + x_{n-1\ 2})\ .$$

The d. .l submatrices for $n = 2, 3, \ldots, N$ 1 are

$$A_{n,n} \quad \begin{vmatrix} n \cdot\ \cdots\ n \cdot\ \cdot n+1 & n,n+1\ \cdot\ n-1,n \\ \cdot_{n,n+1}\ \cdot\ n-1,n & n \cdot\ \cdot n-1,n\cdot\ \cdot\ n,n+1 \end{vmatrix}.$$

and for n 1 and n N, respectively,

$$A_{1,1} \quad \begin{vmatrix} \cdot_1 \cdot\ \cdot_{1\ 2} & \cdot_{1\ 2} \\ \cdot_{1\ 2} & 1\ \cdot\cdot_{1,2} \end{vmatrix}$$

and

$$A_{N,N} \quad \begin{vmatrix} N \cdot\ \cdot N-1,N & \cdot N-1,N \\ \cdot_{N-1,N} & N \cdot\ \cdot N-1,N \end{vmatrix}.$$

with notation

$$\cdot_n \quad (\ldots x)_n\ ,\ ^2 - \cdot(c\ \cdot x)_n\ \cdots\ n\ 1,2,\ldots,N\ .$$

$$\cdot_n \quad \left(\frac{\cdot x}{EI}\right)_n\ \cdots\ n\ 2,3,\ldots,N-1\ .$$

where the subscripts indicate averaging of parameters over the section length $\cdot x$ and $(\ldots x)_n$ is the effective mass for section n of the ship (see Appendix A).

By giving sufficiently large numerical values to $\cdot_1$ $(\cdot x\ EI)_1$ and $\cdot_N$ $(\cdot x\ EI)_N$ in the diagonal submatrices $A_{1,1}$ and $A_{N,N}$, we can insure i it the moments M_1 and M_N calculated at the end sections of the divided beam will be small enough to satisfy, for practical purposes, the end conditions or moment for a beam with free ends. We note that the diagonal submatrices $A_{n,n}$ can be expressed

$$A_{n,n} \quad - \begin{vmatrix} -\cdot_{n-1,n} & -\cdot_{n-1,n} \\ -\cdot_{n-1,n} & -\cdot_{n-1,n} \end{vmatrix} - \begin{vmatrix} -\cdot_{n,n+1} & -\cdot_{n,n+1} \\ -\cdot_{n,n+1} & -\cdot_{n,n+1} \end{vmatrix}$$

$$\cdot \begin{vmatrix} \cdot_n & 0 \\ 0 & \cdot_n \end{vmatrix}\ . \quad (24)$$

i.e., the negative sum of the off-diagonal submatrices in the nth row plus the matrix

$$\begin{vmatrix} \cdot_n & 0 \\ 0 & \cdot_n \end{vmatrix}\ D_n$$

of parameters for the nth section of the beam. Therefore, Eq. (24) has a form which can be generalized to give the diagonal submatrices in the A-matrix expression for beam-spring systems.

Generalized Matrix Formulation and Damping

The matrix formulation discussed in the preceding section can be generalized for application to systems of beams with various types of elastic connections. Each beam is subdivided as illustrated in Fig. 2. The matrix equation for the general beam system is again Eq. (21), with

$$A \quad \begin{vmatrix} A_{11} & A_{12} & A_{13} & \cdots & A_{1N} \\ A_{21} & A_{22} & A_{23} & \cdots & A_{2N} \\ \cdots & \cdots & \cdots & \cdots & \cdots \\ \cdots & \cdots & \cdots & \cdots & \cdots \\ \cdots & \cdots & \cdots & \cdots & \cdots \\ A_{N1} & A_{N2} & A_{N3} & \cdots & A_{NN} \end{vmatrix}\ . \quad (25)$$

z as given by Eq. (23), and P being the column vector of all external forces and moments acting on the system. The $A_{n\ m}$ are $2 \cdot 2$ submatrices and will have some nonzero elements when the sections numbered n and m, respectively, are connected to one another in the beam system. For example, if sections n and m are adjacent beam sections or if they are members of separate beams, but connected through a rigid arm, as shown in Fig. 3,

$$A_{n,m} \quad \begin{vmatrix} -\cdot_{n,m} & -\cdot_{n,m} \\ -\cdot_{n,m} & -\cdot_{n,m} \end{vmatrix}\ . \quad (26)$$

where $\ldots$ are as defined in the previous section. If n and m are connected by a spring, as shown in Fig. 4,
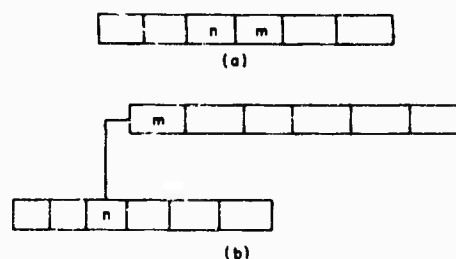
Fig. 3 - Rigidly connected beam elements
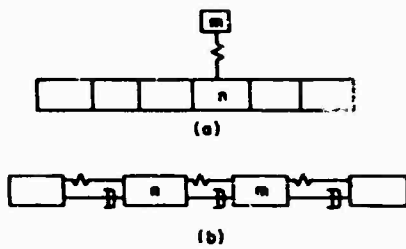
Fig. 4 - Spring connections:
(a) beam with sprung mass,
and (b) mass-spring system

Fig. 5 - Ground connections

Fig. 6 - Model for
Rayleigh damping

$$A_{n,m} = \begin{vmatrix} (k_{n,m} + i\omega c_{n,m} + i\omega^2 \tilde{c}_{n,m}) & 0 \\ 0 & 0 \end{vmatrix} . \quad (27)$$

where $k_{n,m}$ is the spring constant for the connection, $c_{n,m} = (c\Delta x)_{n,m}$ is a viscous damping coefficient associated with the connection, and $\tilde{c}_{n,m} = (\tilde{c}\Delta x)_{n,m}$ is a viscous damping constant proportional to the frequency ω of vibration. Each diagonal submatrix $A_{n,n}$ is represented by a generalization of Eq. (24) in which the summation now takes in all off-diagonal submatrices in the nth row of A-matrix,

$$A_{n,n} = - \sum_{\substack{m=1 \\ m \neq n}}^{N} A_{n,m} + D_n . \quad (28)$$

where

$$D_n = \begin{vmatrix} \delta_n & 0 \\ 0 & \zeta_n \end{vmatrix} .$$

If a section n is connected to a rigid foundation (ground) as indicated in Fig. 5, we add to the corresponding diagonal submatrix $A_{n,n}$ the matrix

$$\begin{vmatrix} -k_n - ic_n\omega & 0 \\ 0 & 0 \end{vmatrix} , \quad (29)$$

where k_n is the spring constant for the ground connection and $c_n = (c\Delta x)_n$ is the associated damping coefficient. Through this type of connection we incorporate Rayleigh damping [3, Chap. 4, Sect. A and B] terms (viscous and proportional to mass) into the generalized matrix. The typical ground connection given in the model for this type of hull damping is shown in Fig. 6. For these connections, Eq. (29) has the form

$$\begin{vmatrix} -ic_n\omega & 0 \\ 0 & 0 \end{vmatrix} , \quad (30)$$

where the damping coefficient c_n is expressed as

$$c_n = (\mu\Delta x)_n C . \quad (31)$$

or for frequency-dependent Rayleigh damping [3, Chap. 4, Sect. A and B],

$$c_n = (\mu\Delta x)_n \omega C \quad (32)$$

with C a constant. In the latter case, the damping coefficient c_n will combine with the effective mass in Eq. (28) which is generated for $A_{n,n}$ giving

$$\delta_n = (\mu\Delta x)_n \omega^2 - ic_n\omega = \omega^2 (\mu\Delta x)_n (1 - Ci) .$$

This type of damping can, therefore, be specified to the program through a complex scaling, $(1 - Ci)$, of mass. In general, the damping coefficients for connections $c_{n,m}$ and $\tilde{c}_{n,m}$ in Eq. (27) and for ground connections c_n in Eqs. (29) and (30), except when used in the frequency-dependent Rayleigh sense, will be given explicitly in the input data to the program. Hysteretic damping terms [1, Sect. 5] are entered into the generalized matrix by providing for a complex-valued scaling of input parameters involving either of the moduli of elasticity, E or G, defined previously. In particular, these parameters are $(\Delta x/EI)_n$ and $(\Delta x/KAG)_{n,n+1}$ for bending vibrations or $k_n = (\Delta x/AE)_n$ for

120

longitudinal vibrations. With this generalized matrix formulation, GBRC1 can set up the finite-difference equations for vertical, horizontal, longitudinal (extensional) or torsional vibration calculations, depending on the set of inertial and elastic parameters supplied as input. Typical sets of parameters for some of these types of vibration are seen in the sample problems in Appendix B. As an example of this generalized formulation, we have, for the beam-system of Fig. 7, the matrix equation

$$
\begin{vmatrix}
A_{11} & A_{12} & A_{13} & 0 & 0 & 0 \\
A_{21} & A_{22} & 0 & 0 & 0 & 0 \\
A_{31} & 0 & A_{33} & A_{34} & A_{35} & 0 \\
0 & 0 & A_{43} & A_{44} & 0 & 0 \\
0 & 0 & A_{53} & 0 & A_{55} & A_{56} \\
0 & 0 & 0 & 0 & A_{65} & A_{66}
\end{vmatrix}
\cdot
\begin{vmatrix}
Y_1 \\ M_1 \\ Y_2 \\ M_2 \\ Y_3 \\ M_3 \\ Y_4 \\ M_4 \\ Y_5 \\ M_5 \\ Y_6 \\ M_6
\end{vmatrix}
=
\begin{vmatrix}
0 \\ 0 \\ 0 \\ 0 \\ 0 \\ 0 \\ 1 \\ 0 \\ 0 \\ 0 \\ 0 \\ 0
\end{vmatrix}
$$
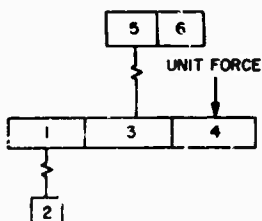
Fig. 7 - Typical connected beam elements

EQUATIONS AND MATRIX FORMULATION GBRC2

The second computer code in this series extends the capabilities of GBRC1 to steady-state vibrations of beam spring systems where bending and torsional motions are coupled. For this program we derive from Eqs. (9) through (14) a set of 3N (N being the number of sections on the subdivided beam) finite-difference equations in terms of deflection y, moment M and rotation ϕ to be evaluated at each beam section. The finite-difference equations are then generalized for a system of beams with elastic connections. The generalized equations are

$$A'z' = P'.$$

where

A' symmetric matrix of coefficients,

$$
z' =
\begin{vmatrix}
Y_1 \\ M_1 \\ \phi_1 \\ Y_2 \\ M_2 \\ \phi_2 \\ \cdot \\ \cdot \\ \cdot \\ Y_N \\ M_N \\ \phi_N
\end{vmatrix}
, \text{ and}
$$

P' = column vector of forces, moments and torques acting externally on the beam system.

The equations for each beam section having a free end will include the required conditions on shear V, bending moment M and total moment about the x-axis T.

EQUATIONS AND MATRIX FORMULATION, GBRC3

A third computer code currently being developed will extend the range of the General Bending Response Program to the calculation of the forced whirling response and critical whirling speeds of propeller shafts.

As a basis for this code, we use the set of partial differential equations derived by Jasper [4] for a whirling shaft. Since the whirling motion is treated theoretically as a coupling of flexural vibrations in two perpendicular planes of the shaft (xy and xz planes where x is the shaft longitudinal axis) we can obtain for each plane a system of four time-independent equations which have essentially the form of Eqs. (15) through (18). Treating these equations as in GRRC1 leads to the corresponding set of generalized difference equations in terms of deflections and moments in both planes. The matrix form of the difference equations is

$$A''z'' = P''.$$

where A is the generalized matrix of coefficients and

121

$$z^* = \begin{bmatrix} y_1 \\ M_{1(xy)} \\ z_1 \\ M_{1(xz)} \\ y_2 \\ M_{2(xy)} \\ z_2 \\ M_{2(xz)} \\ \vdots \\ y_N \\ \ddot{M}_{N(x,)} \\ z_N \\ M_{N(xz)} \end{bmatrix}$$

with y, $M_{(xy)}$ and z, $M_{(xz)}$ denoting the deflection and bending moment, respectively, in the xy and xz planes; N is the number of shaft sections and P is the vector of forces and moments acting externally at discrete points along the shaft.

SOLUTION OF EQ. (21)

Forced Response

For this type of calculation the computer program sets up the matrix A and vector P for each specified frequency ω of the exciting forces and then premultiplies P by the inverse of A to give the required steady-state solution. In particular, we obtain (assuming damping in the system) the real and imaginary components of the vectors, Eq. (8), associated with deflection, moment and rotation at each beam section (the real component representing the actual physical quantity), the amplitude of each vector and its phase angle with the respect to the vectors of exciting forces.

Undamped Natural Frequencies

In this case, the program calculates the approximate eigenvalues (natural frequencies) and corresponding eigenvectors (modal columns) of the homogeneous problem given by Eq. (21), where all elements of P are zero. The values of deflection, moment and rotation calculated at each section in the beam system are relative to

a unit deflection at section 1. Bounds on the number of natural frequencies to be computed are supplied with the input data.

PROGRAM INFORMATION

The component subprograms of the General Bending Response Program (GBRC1, -2, -3) are in FORTRAN II language as modified for compatibility with FORTRAN IV. These programs have been designed for the IBM 7090 computer, and the Stromberg-Carlson 4020 Microfilm Recorder at the Applied Mathematics Laboratory is used to plot calculated results.

Computer running times recorded during a series of vertical and longitudinal response calculations with GBRC1 range from 0.04 min/frequency for 20 sections with a matrix half-bandwidth of 3 elements to 0.80 min/frequency for 40 sections with a matrix half-bandwidth of 23 elements and 1.22 min/frequency for 74 sections with a matrix half-bandwidth of 19 elements. The term "min/frequency" denotes the average time to compute the response for each frequency of the exciting forces. Coupled bending-torsion response calculations with GBRC2 indicate a computer time of 0.08 min/frequency for a 20-section hull with a matrix half-bandwidth of 5 elements.

The maximum number of sections which may be specified for the beam system is 80 for bending, longitudinal or torsional calculations. For coupled bending-torsion calculations, we allow at present a maximum of 53 sections but anticipate expanding this to 80 sections to maintain consistency in the problem description.

SAMPLE CALCULATIONS

For purposes of illustration, we base these calculations on hypothetical beam-spring models which are described with a small number of sections and connections. The inertial and elastic parameters defined for each model appear with the associated computer output in Appendix B. In actual practice, these parameters will be either specified with consistent units of measurement or provided with suitable scaling factors in the data to bring the respective units into consistency. The calculated results will then be in the system of units as determined by the input data.

Sample Problem 1

The damped vertical bending response of a beam with one sprung mass, as shown in Fig.

122

3, is computed for two frequencies of the exciting force. The damping is assumed to be the frequency-dependent Rayleigh type, so an imaginary scaling factor for mass is provided as indicated in the section on generalized matrix formulation and damping for GBRC1.
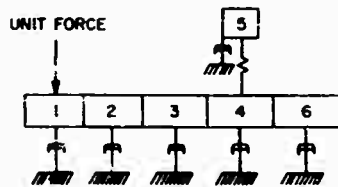
Sample Problem 2

The first natural frequency and the mode shape of vertical vibration are computed for the beam system of Fig. 8 with the damping and exciting force removed.

Sample Problem 3

The damped longitudinal response of the mass-spring system in Fig. 9 is computed for two frequencies of the exciting force.

Fig. 8 - Model for sample problem 1
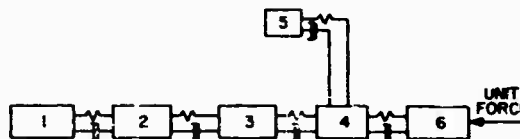
Fig. 9 - Model for sample problem 3

REFERENCES

1. F.E. Reed and E.H. Cuthill, "Ship Hull Vibrations - 5: Analysis of Hull Structure as Applied to SSB(N)598 GEORGE WASHINGTON," CONESCO Rept. No. F-111-2, March 1963

2. E.H. Cuthill and F.M. Henderson, "Description and Usage of General Bending Response Code 1 (GBRC1)," DTMB Rept. 1925, July 1965

3. R.T. McGoldrick, "Ship Vibration," DTMB Rept. 1451, Dec. 1960

4. Norman H. Jasper, "A Theoretical Approach to the Problem of Critical Whirling Speeds of Shaft-Disk Systems," DTMB Rept. 827, Sect. IV and V, Dec. 1954

Appendix A

EFFECTIVE MASS

The expression $(\mu \Delta x)_n$ denotes the effective mass for section n of the ship [1, App. C; 2, Sect. III]. It consists of the mass m_n of the section and a virtual mass term which takes into account the effects of surrounding water. The virtual mass term is given by the expression $J(\omega) \bar{m}_n$, where $\bar{m}_n$ is the water inertia for the nth section and J is the longitudinal inertia coefficient [1, App. C]. Since J is a function of the response pattern for the particular system (hull, shaft, etc.) with which the nth section is associated, we say that J is a frequency-dependent term and have denoted it $J(\omega)$. The effective mass can then be written

$$(\mu \Delta x)_n = m_n + J(\omega) \bar{m}$$ (A-1)

The formulation for J is that given for an infinitely long circular cylinder which is undergoing vertical vibration while immersed in water [A-1]:

$$J = \frac{K_1(\alpha)}{K_1(\alpha) + \alpha K_0(\alpha)},$$ (A-2)

where K_0 and K_1 are the first and second modified Bessel functions of the second kind, and

$$\alpha = \frac{\pi c}{d}$$ (A-3)

with d the distance between nodes on the amplitude curve for the cylinder and c the radius of the cylinder. For the automatic computation of J we utilize the power series approximation for J as a function of α [1, App. C]:

$$J = 0.0609 + \frac{0.715}{\alpha} - \frac{0.9093}{\alpha^2} + \frac{0.00297}{\alpha^3} + \dots,$$ (A-4)

where $0.6 < \alpha < 4$, or the approximation

$$J = 1.030 + 1.56 \frac{r}{d} \qquad \text{(A-5)}$$

for $0 < \frac{r}{d} < 0.6$. The automatic calculation of the effective mass terms $(\mu \lambda x)_n$ for the hull and/or any other system is handled by the General Bending Response Program as follows. An initial J for the system is specified as input data along with the radius of the approximating cylinder and section water inertias $\bar{m}_n$. The initial J is used until a frequency is reached at which the deflection curve for the system has at least two nodes on the x-axis. Having determined the average distance d between these nodes, the program then calculates r from Eq. (A-3) using the cylinder radius, and J from Eq. (A-4) or (A-5). The water inertia $\bar{m}_n$ for each section in the system is multiplied by this value of J and added to the section masses to give the new effective mass values for use in calculating the next frequency of response.

The automatic calculation of J is an optional feature of the program. In cases where the option is not specified, a value of unity is automatically assigned to J for each system so that the effective mass becomes

$$(\mu \lambda x)_n = m_n + \bar{m}_n.$$

REFERENCE

A-1. R.C. Leibowitz and E.H. Kennard, "Theory of Freely Vibrating Nonuniform Beams, including Methods of Solution and Application to Ships," DTMB Rept. 1317, App. B, May 1961

Appendix B

COMPUTER OUTPUT FOR SAMPLE PROBLEMS

GBBC1 JULY 25, 1966
SAMPLE PROBLEM 1.

DATA CONTROL CARD

NO	TYPE
1	10
1	21
1	30
1	41
1	42
1	43
1	51
2	53

CASE TITLE—VERTICAL BENDING. DAMPED RESPONSE

OPTION DATA
21   1   3   3   -0   -0   -0   -0   -0   -0

GENERAL DATA — NUMBER OF SECTIONS   6
                FREQUENCY RANGE FROM   1.000 CPS   TO   2.000 CPS
                FREQUENCY INTERVAL   1.000 CPS

REAL PARTS OF SCALING FACTORS

SECTION-END COMMON-SYSTEM	MASS	WATER INERTIA	DX/EI(N)	DX(N,N+1)	DX/KAG(N,N+1)	(MZ*DX(N,N+1))	P(N)
1 1	1.0000E 00	-0.	(0.0000E-05	1.0000E 00	3.0000E-06	-0.	1.0000E 00

(IMAGINARY PARTS OF SCALING FACTORS

SECTION-END COMMON-SYSTEM	MASS	WATER INERTIA	DX/EI(N)	DX(N,N+1)	DX/KAG(N,N+1)	(MZ*DX(N,N+1))	P(N)
1 (	-3.0000E-02	-0.	-0.	-0.	-0.	-0.	-0.

PARAMETER VALUES FOR EACH SECTION — UNSCALED

SECTION-END COMMON-SYSTEM	MASS	WATER INERTIA	DX/EI(N)	DX(N,N+1)	DX/KAG(N,N+1)	(MZ*DX(N,N+1))	P(N)
1 1	2.3500E 00	-0.	1.2890E 01	1.5000E 01	2.1300E 00	-0.	1.0000E 00
2 -0	4.0000E 00	-0.	2.0100E 00	1.6000E 01	5.0000E-01	-0.	-0.
3 -0	6.0600E 00	-0.	1.0200E 00	1.6000E 01	3.3000E-01	-0.	-0.
4 -0	1.1300E 01	-0.	5.7000E-01	-0.	-0.	-0.	-0.
5 -0	2.6800E-01	-0.	9.0000E-01	-0.	-0.	-0.	-0.
6 2	6.7600E 00	-0.	3.9000E-01	-0.	-0.	-0.	-0.

REAL PARTS OF SCALING FACTORS

N	M	SYSTEM K(N,M)	C(N,M)	DX(N,M)	DX/KAG(N,M)	(MZ*DX(N,M))	Q(N,M)
1	1	1.0000E 05	1.0000E 00	-0.	1.0000E 00	(0.0000E-06	-0.	-0.

PARAMETER VALUES FOR SPECIAL CONNECTIONS

N	M	SYSTEM K(N,M)	C(N,M)	DX(N,M)	DX/KAG(N,M)	(MZ*DX(N,M))	Q(N,M)
1	6	(-0.	-0.	1.5000E 01	2.5000E-01	-0.	-0.
1	5	3.1900E-01	-0.	-0.	-0.	-0.	-0.

125

GERCI

SAMPLE PROBLEM 1.

VERTICAL BENDING.   DAMPED RESPONSE

FREQUENCY	DEFLECTION	MOMENT	DEFLECTION	MOMENT	DEFLECTION	MOMENT	DEFLECTION	MOMENT	DEFLECTION	MOMENT
CPS	SECTION 1		SECTION 3		SECTION 6		SECTION			
1.00	4.307E-03	9.756E-07	1.468E-03	9.686E 00	1.352E-03	9.787E-07				
2.00	1.068E-03	2.428E-07	3.746E-04	9.744E 00	3.401E-04	2.460E-07				

GERCI

SAMPLE PROBLEM 1.

VERTICAL BENDING.   DAMPED RESPONSE

FREQUENCY   1.00 CPS

STATION	DEFLECTIONS				MOMENTS			
	REAL PART	IMAG PART	ABS VALUE	PHASE ANGLE	REAL PART	IMAG PART	ABS VALUE	PHASE ANGLE
1	-4.3047E-03	-1.2947E-04	4.3066E-03	-1.7828E 02	9.7514E-07	2.9290E-08	9.7559E-07	1.7208E 00
2	-2.8548E-03	-8.5528E-05	2.8560E-03	-1.7828E 02	9.0041E 00	-4.6228E-04	9.0041E 00	-2.9416E-03
3	-1.4673E-03	-4.4514E-05	1.4680E-03	-1.7829E 02	9.6855E 00	-5.8352E-04	9.6855E 00	-3.6519E-03
4	-1.1718E-04	-3.4999E-06	1.1724E-04	-1.7829E 02	5.3974E 00	-3.5368E-04	5.3974E 00	-3.7548E-03
5	-1.1722E-04	-3.4999E-06	1.1727E-04	-1.7829E 02	0.	0.	0.	0.
6	1.3511E-03	4.0444E-05	1.3517E-03	1.7146E 00	-9.7824E-07	-2.9296E-08	9.7868E-07	-1.7828E 02

GERCI

SAMPLE PROBLEM 1.

VERTICAL BENDING.   DAMPED RESPONSE

FREQUENCY   2.00 CPS

STATION	DEFLECTIONS				MOMENTS			
	REAL PART	IMAG PART	ABS VALUE	PHASE ANGLE	REAL PART	IMAG PART	ABS VALUE	PHASE ANGLE
1	-1.0678E-03	-3.2370E-05	1.0683E-03	-1.7826E 02	2.4273E-07	7.3243E-09	2.4284E-07	1.7283E 00
2	-7.1658E-04	-2.1381E-05	7.1689E-04	-1.7829E 02	9.0506E 00	-1.8689E-03	9.0506E 00	-1.1632E-02
3	-3.7447E-04	-1.1129E-05	3.7464E-04	-1.7830E 02	9.7442E 00	-2.3604E-03	9.7442E 00	-1.3879E-02
4	-2.9090E-05	-8.7683E-07	2.9703E-05	-1.7831E 02	5.4329E 00	-1.4312E-03	5.4329E 00	-1.5093E-02
5	-2.9722E-05	-8.7481E-07	2.9742E-05	-1.7831E 02	0.	0.	0.	0.
6	3.4000E-04	1.0110E-05	3.4015E-04	1.7033E 00	-2.0586E-07	-7.3236E-09	2.4596E-07	-1.7829E 02

GERCI JULY 25, 1964
SAMPLE PROBLEM 1.

DATA CONTROL CARD

.C TYPE

START NEW DATA SET

126

GERCI JULY 23, 1964
SAMPLE PROBLEM 2.

DATA CONTROL CARD

NC TYPE
1   10
1   20
1   21
1   30
1   41
0   43
1   51
2   53
X   70

CASE TITLE-VERTICAL BENDING.   NATURAL FREQUENCIES

OPTION DATA
20 -0 -0 -0 -0 -0 -0 -0   1

OPTION DATA
21   1   3   6 -0 -0 -0 -0 -0

GENERAL DATA - NUMBER OF SECTIONS   6
               FREQUENCY RANGE FROM   1.000 CPS TO   30.000 CPS
               FREQUENCY INTERVAL   1.000 CPS

REAL PARTS OF SCALING FACTORS

SECTION-END CONDN-SYSTEM	MASS	WATER INERTIA	DX/EI(N)	DX(N,N+1)	DX/KAG(N,N+1)	(RZ+DX(N,N+1)	P(N)
1	1.0000E 00	-0.	10.0000E-09	1.0000E 00	10.0000E-06	-0.	-0.

PARAMETER VALUES FOR EACH SECTION - UNSCALED

SECTION-END CONDN-SYSTEM	MASS	WATER INERTIA	DX/EI(N)	DX(N,N+1)	DX/KAG(N,N+1)	(RZ+DX(N,N+1)	P(N)
1	2.3500E 00	-0.	1.2890E 01	1.5000E 01	2.1300E 00	-0.	-0.
2 -0 1	4.8900E 00	-0.	2.0100E 00	1.4000E 01	5.0000E-01	-0.	-0.
3 -0 1	6.8800E 00	-0.	1.0200E 00	1.4000E 01	3.3000E-01	-0.	-0.
4 -0 1	1.1300E 01	-0.	5.7000E-01	-0.	-0.	-0.	-0.
5 -0 1	2.6600E-01	-0.	9.0000E-01	-0.	-0.	-0.	-0.
6 2	6.7800E 00	-0.	3.9000E-01	-0.	-0.	-0.	-0.

REAL PARTS OF SCALING FACTORS

N	M	SYSTEM	K(N,M)	C(N,M)	C(N,M)/W	DX(N,M)	DX/KAG(N,M)	(RZ+DX(N,M)	Q(N,M)
1			1.0000E 05	-0.	-0.	1.0000E 00	10.0000E-06	-0.	-0.

PARAMETER VALUES FOR SPECIAL CONNECTIONS

N	M	SYSTEM	K(N,M)	C(N,M)	C(N,M)/W	DX(N,M)	DX/KAG(N,M)	(RZ+DX(N,M)	Q(N,M)
2	6	1	-0.	-0.	-0.	1.5000E 01	2.5000E-01	-0.	-0.
4	5	1	3.1900E-01	-0.	-0.	-0.	-0.	-0.	-0.

AFREQ= 1

127

GERC1

SAMPLE PROBLEM 2.

VERTICAL BENDING.   NATURAL FREQUENCIES

FREQUENCY CPS	DEFLECTION SECTION 1	MOMENT	DEFLECTION SECTION 3	MOMENT	DEFLECTION SECTION 6	MOMENT	DEFLECTION SECTION	MOMENT	DEFLECTION	MOMENT
23.61	1.000E 00	1.252E-04	3.575E-01	1.064E 06	3.084E-01	1.784E-04				

GERC1

SAMPLE PROBLEM 2.

VERTICAL BENDING.   NATURAL FREQUENCIES

FREQUENCY   23.61 CPS

STATION	DEFLECTIONS			MOMENTS				
	REAL PART	IMAG PART	ABS VALUE	PHASE ANGLE	REAL PART	IMAG PART	ABS VALUE	PHASE ANGLE
1	1.0000E 00	0.	1.0000E 00	0.	-1.2510E-04	0.	1.2510E-04	-1.0215E 04
2	-2.8947E-01	0.	2.8947E-01	0.	7.7584E 05	0.	7.7584E 05	0.
3	-3.5746E-01	0.	3.5746E-01	0.	1.0638E 06	0.	1.0638E 06	0.
4	-7.3534E-02	0.	7.3534E-02	0.	6.8638E 05	0.	6.8638E 05	0.
5	-8.9610E-02	0.	8.9610E-02	0.	0.	0.	0.	0.
6	3.0845E-01	0.	3.0845E-01	0.	-1.7839E-04	0.	1.7839E-04	0.

GERC1 JULY 25. 1964
SAMPLE PROBLEM 2.

DATA CONTROL CARD

AC TYPE

START NEW DATA SET

128

GBRC1 JULY 25, 1964
SAMPLE PROBLEM 3.

DATA CONTROL CARD

NO TYPE
1   10
1   21
1   30
1   41
6   43
1   51
5   53

CASE TITLE-LONGITUDINAL RESPONSE

OPTION DATA
21 1 3 6 -0 -0 -0 -0 -0 -0

GENERAL DATA - NUMBER OF SECTIONS 6
FREQUENCY RANGE FROM 1.000 CPS TO 2.000 CPS
FREQUENCY INTERVAL 1.000 CPS

REAL PARTS OF SCALING FACTORS

SECTION-END CONDN-SYSTEM	MASS	WATER INERTIA	DX/EI(N)	DX(N,N+1)	DX/KAG(N,N+1)	IMZ*DX(N,N+1)	P(N)
1	1.0000E 00	-0.	-0.	-0.	-0.	-0.	1.0000E 00

PARAMETER VALUES FOR EACH SECTION - UNSCALED

SECTION-END CONDN-SYSTEM		MASS	WATER INERTIA	DX/EI(N)	DX(N,N+1)	DX/KAG(N,N+1)	IMZ*DX(N,N+1)	P(N)
1	-0	1	3.1300E 00	-0.	-0.	-0.	-0.	-0.
2	-0	1	5.0700E 00	-0.	-0.	-0.	-0.	-0.
3	-0	1	9.2300E 00	-0.	-0.	-0.	-0.	-0.
4	-0	1	7.8900E 00	-0.	-0.	-0.	-0.	-0.
5	-0	1	7.9000E-01	-0.	-0.	-0.	-0.	1.0000E 00
6	-0	1	8.8100E 00	-0.	-0.	-0.	-0.	

REAL PARTS OF SCALING FACTORS

N	M	SYSTEM	K(N,M)	C(N,M)	OX(N,M)	C(N,M)/B	OX(N,M)	IMZ*DX(N,M)	Q(N,M)
	1	1	1.0000E 05	1.0000E 00	-0.	-0.	-0.	-0.	-0.

PARAMETER VALUES FOR SPECIAL CONNECTIONS

N	M	SYSTEM	K(N,M)	C(N,M)	OX(N,M)	C(N,M)/B	OX(N,M)	IMZ*DX(N,M)	Q(N,M)
1	2	1	2.3500E 00	2.6500E 01	-0.	-0.	-0.	-0.	-0.
2	3	1	7.5100E 00	1.5000E 01	-0.	-0.	-0.	-0.	-0.
3	4	1	6.4900E 00	3.1200E 01	-0.	-0.	-0.	-0.	-0.
4	6	1	1.0800E 01	2.0000E 01	-0.	-0.	-0.	-0.	-0.
	5	1	3.4500E-02	9.3000E 00	-0.	-0.	-0.	-0.	-0.

GBRC1

SAMPLE PROBLEM 3.

LONGITUDINAL RESPONSE

FREQUENCY CPS	DEFLECTION SECTION 1	MOMENT	DEFLECTION SECTION 3	MOMENT	DEFLECTION SECTION 6	MOMENT
1.00	7.203E-04	0.	7.256E-04	0.	7.242E-04	0.
2.00	1.823E-04	0.	1.816E-04	0.	1.802E-04	0.

GBRC1

SAMPLE PROBLEM 3.

LONGITUDINAL RESPONSE

FREQUENCY   1.00 CPS

STATION	DEFLECTIONS				MOMENTS			
	REAL PART	IMAG PART	ABS VALUE	PHASE ANGLE	REAL PART	IMAG PART	ABS VALUE	PHASE ANGLE
1	-7.2632E-04	-2.1327E-09	7.2632E-04	-1.8000E 02	0.	0.	0.	0.
2	-7.2594E-04	-2.4022E-09	7.2594E-04	-1.8000E 02	0.	0.	0.	0.
3	-7.2563E-04	-2.4405E-09	7.2563E-04	-1.8000E 02	0.	0.	0.	0.
4	-7.2486E-04	-2.6704E-09	7.2486E-04	-1.8000E 02	0.	0.	0.	0.
5	-7.3147E-04	1.1029E-07	7.3147E-04	1.7999E 02	0.	0.	0.	0.
6	-7.2416E-04	-3.7519E-07	7.2416E-04	-1.8000E 02	0.	0.	0.	0.

GBRC1

SAMPLE PROBLEM 3.

LONGITUDINAL RESPONSE

FREQUENCY   2.00 CPS

STATION	DEFLECTIONS				MOMENTS			
	REAL PART	IMAG PART	ABS VALUE	PHASE ANGLE	REAL PART	IMAG PART	ABS VALUE	PHASE ANGLE
1	-1.8236E-04	-4.5779E-09	1.8236E-04	-1.8000E 02	0.	0.	0.	0.
2	-1.8196E-04	-5.1117E-09	1.8196E-04	-1.8000E 02	0.	0.	0.	0.
3	-1.8164E-04	-5.1821E-09	1.8164E-04	-1.8000E 02	0.	0.	0.	0.
4	-1.8087E-04	-5.6266E-09	1.8087E-04	-1.8000E 02	0.	0.	0.	0.
5	-1.8765E-04	2.3235E-07	1.8765E-04	1.7993E 02	0.	0.	0.	0.
6	-1.8018E-04	-5.7955E-09	1.8018E-04	-1.8000E 02	0.	0.	0.	0.

GBRC1 JULY 23, 1964
SAMPLE PROBLEM 3.

DATA CONTROL CARD

NC TYPE

END GBRC1 RUN

130

MATHEMATICAL MODEL AND COMPUTER PROGRAM
FOR TRANSIENT SHOCK ANALYSIS*

Anthony C. Melodia
David Taylor Model Basin
Washington, D.C.

A computer program is given for a mathematical model used for computing shock and residual shock spectra of linear elastic structures responding to transient forces and foundation motions. A wide range of output options, from tabulated results to a four-coordinate log-log grid, are possible. Included in the mathematical analysis of the shock spectra is a refinement in determining maximum responses which results in a more accurate shock spectrum. The program is written in FORTRAN IV for the IBM 7090 and includes plotting subroutines for the General Dynamics SC 4020 printer plotter. The program is also coded without the SC 4020 subroutines.

INTRODUCTION

This report is based on work done to develop a series of programs applicable to static and dynamic structural analysis. O'Hara's [1] techniques for shock analysis are reduced to a computer code. The program generates various forms of shock and residual shock spectra, where a single-degree-of-freedom linear oscillator is the mathematical model for response to a transient force or a foundation motion. The spectra are used to find the displacement of a structure caused by an arbitrarily prescribed transient motion to its base, such as the response of buried structures to an underground blast or of structures within a vehicle during ballistic impact. In addition, if the input shock function to the program is an acceleration, the residual shock spectrum generated is also the Fourier spectrum of the system.

The program is written in IBSYS FORTRAN IV, version 13, and executed on an IBM 7090 in conjunction with a Stromberg-Carlson 4020 printer-plotter. In the Appendix, coding is furnished without reference to the plotter, thus making the program more adaptable for other FORTRAN IV compilers.

MATHEMATICAL SYMBOLS

C Linear damping factor in $C\ddot{X}$ in Eq. (1)

F_c Fourier cosine transform value at

F_s Fourier sine transform value at

f Frequency, cps

h Increment of time

M Mass

p Damped natural frequency of linear system

S_n First forward difference at n

S_n^2 Second forward difference at n

t Time, sec

X Relative displacement $(y-z)$ or response displacement

$\dot{X}$ True response velocity

ωX Pseudo-response velocity

$\omega^2 X$ Pseudo-response acceleration

Y Absolute displacement of linear oscillator from its equilibrium position

Z Displacement of foundation from its equilibrium position

α Ratio of damping to critical linear damping or damping coefficient

ω Undamped natural frequency of linear system, rad/sec

*This paper was not presented at the Symposium.

131

MATHEMATICAL ANALYSIS

The mathematical model for shock analysis is the simple linear oscillator. The general differential equation for the motion in Fig. 1 is

$$M\ddot{Y} + C\dot{X} + KX = F(t). \qquad (1)$$

where X is the relative displacement $Y - Z$, $C\dot{X}$ is the damping term, and KX is the restoring force, based on Hooke's law. Now using standard notation, where C is less than the critical damping factor, let

$$\omega^2 = \frac{K}{M}.$$

$$\zeta = \frac{C}{2M}.$$

and

$$p = \omega\sqrt{1 - \zeta^2}.$$
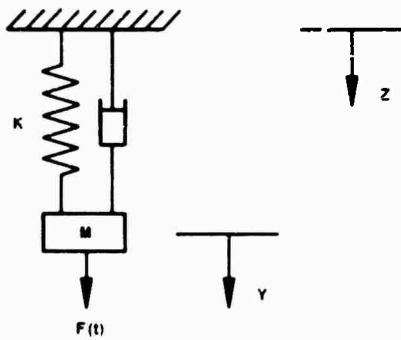
Fig. 1 - Linear oscillator

Substitution of the above expressions into Eq. (1) yields the following equation:

$$\ddot{Y} + 2\zeta\dot{Y} + \omega^2 Y = 2\zeta\dot{Z} + \omega^2 Z + \frac{F(t)}{M}. \qquad (2)$$

There are two types of motion that are of interest, either no applied force ($F(t) = 0$) and foundation motion, or no foundation motion ($Z = 0$) and an applied force. The remainder of this section will describe mainly the first case, where $F(t) = 0$. The latter case, where $Z = 0$, will be dealt with only at the end. When $F(t) = 0$, Eq. (2) becomes

$$\ddot{Y} + 2\zeta\dot{Y} + \omega^2 Y = 2\zeta\dot{Z} + \omega^2 Z.$$

or since $Y - Z = X$,

$$\ddot{X} + 2\zeta\dot{X} + \omega^2 X = -\ddot{Z}. \qquad (3)$$

Using Laplace transforms, the solution to Eq. (3) is found to be

$$X(t) = X(0) \, e^{-\zeta\omega t} \left(\cos pt + \frac{\zeta}{\sqrt{1 - \zeta^2}} \sin pt\right)$$

$$+ \dot{X}(0) \frac{e^{-\zeta\omega t} \sin pt}{p}$$

$$- \frac{1}{p}\int_0^t \ddot{Z}(T) \, e^{-\zeta\omega(t-T)} \sin p(t-T) \, dT. \qquad (4)$$

while the derivative of Eq. (4) is

$$\dot{X}(t) = e^{-\zeta\omega t} X(0) \left[-\zeta\omega\left(\cos pt + \frac{\zeta}{\sqrt{1 - \zeta^2}} \sin pt\right)\right.$$

$$\left.- p \sin pt + \frac{p\zeta \cos pt}{\sqrt{1 - \zeta^2}}\right]$$

$$+ \frac{\dot{X}(0) \, e^{-\zeta\omega t}}{p} (-\zeta\omega \sin pt + p \cos pt)$$

$$+ \frac{1}{p}\int_0^t \ddot{Z}(t) \, e^{-\zeta\omega(t-T)} \left[\zeta\omega \sin p(t-T)\right.$$

$$\left.- p \cos p(t-T)\right] \, dT. \qquad (5)$$

Equation (4) gives the relative response displacement of the mass to the shock $\ddot{Z}(t)$. The solution of the differential equation is not yet useful, because the integral has to be evaluated. Now, if the solution were known at $t = t_1$, the values of relative displacement X and relative velocity $\dot{X}$ could be considered initial values at t_1 for the solution at $t_1 + \Delta t$, using Eqs. (4) and (5) again. A convenient procedure followed in the numerical solution of the differential equation consists of subdividing the time record into equal increments, each of duration $\Delta t = h$ sec, so the method of evaluating $X(t)$ at each point will require the same equations. Of course, the values of X and $\dot{X}$ at the beginning of the time record must be given to use the above procedure for solving the differential equation. A parabolic approximation for $\ddot{Z}(t)$ between 0 and h is substituted in Eqs. (4) and (5), and the integrals are evaluated. In addition, the approximation for $\ddot{Z}(t)$ at any point in the time record will go through the preceding point as well as the successive point. If the time is subdivided into enough intervals h, no sudden peaks of $\ddot{Z}$ should be missed by the approximating parabola for $\ddot{Z}$.

A useful change in notation $X(ih) = X_i$ and $\ddot{Z}(ih) = \ddot{Z}_i$, where $\ddot{Z}_i$ is the $(i+1)$th point in the time record, $i = 0, 1, 2, 3, \ldots, k$, and $k + 1$ is the number of points in the time record.

132

The parabola passing through $\ddot{Z}_{n-1}$, $\ddot{Z}_n$, $\ddot{Z}_{n+1}$ yields the equation

$$\ddot{Z}(t) = \frac{(\ddot{Z}_{n+1} - 2\ddot{Z}_n + \ddot{Z}_{n-1})}{2h^2}\, t^2 + \frac{(\ddot{Z}_{n+1} - \ddot{Z}_{n-1})}{2h}\, t + \ddot{Z}_n \tag{6}$$

for $(n-1)h \leq t \leq (n+1)h$. Equation (6) can be simplified by letting $S_n = \ddot{Z}_{n+1} - \ddot{Z}_n$ and $S^2_{n-1} = S_n - S_{n-1} = \ddot{Z}_{n+1} - 2\ddot{Z}_n + \ddot{Z}_{n-1}$:

$$\ddot{Z}(t) = \ddot{Z}_n + \frac{S_n t}{h} + \frac{S^2_{n-1}}{2}\left(\frac{t^2}{h^2} - \frac{t}{h}\right). \tag{7}$$

Now, using Eq. (7) in the integral in place of $\ddot{Z}(t)$ in Eq. (4), integrating by parts from 0 to h, and finally substituting h for t in the other terms of Eq (4), the final equation for the response at each point in the time record is

$$X_{n+1} = X_n e^{-\zeta \omega h}\left(\cos ph + \frac{\zeta}{\sqrt{1-\zeta^2}}\sin ph\right)$$

$$+ \dot{X}_n \frac{e^{-\zeta \omega h}\sin ph}{\sqrt{1-\zeta^2}}$$

$$- \frac{\ddot{Z}_n}{\omega}\left[1 - e^{-\zeta \omega h}\left(\cos ph + \frac{\zeta}{\sqrt{1-\zeta^2}}\sin ph\right)\right]$$

$$- \frac{S_n}{\omega}\left[1 - \frac{2\zeta}{\omega h}(1 - e^{-\zeta \omega h}\cos ph)\right.$$

$$\left. - \frac{(1 - 2\zeta^2)\, e^{-\zeta \omega h}\sin ph}{ph}\right]$$

$$- \frac{S^2_{n-1}}{2\omega}\left\{-\frac{4\zeta}{\omega h} - \left[\frac{2(1-4\zeta^2)}{\omega^2 h^2} - \frac{2\zeta}{\omega}\right]\right.$$

$$\cdot (1 - e^{-\zeta \omega h}\cos ph)$$

$$\left. + \left[\frac{1-2\zeta^2}{\omega h} + 2\zeta\frac{(3-4\zeta^2)}{\omega^2 h^2}\right]\frac{e^{-\zeta \omega h}\sin ph}{\sqrt{1-\zeta^2}}\right\}. \tag{8}$$

Using the same method in developing Eq. (8), Eq. (5) is transformed into

$$\dot{X}_{n+1} = -\omega X_n \frac{e^{-\zeta \omega h}\sin ph}{\sqrt{1-\zeta^2}}$$

$$+ \dot{X}_n e^{-\zeta \omega h}\left(\cos ph - \frac{\zeta}{\sqrt{1-\zeta^2}}\sin ph\right) \tag{9}$$
(Cont.)

$$- \frac{\ddot{Z}_n}{\omega}\frac{e^{-\zeta \omega h}\sin ph}{\sqrt{1-\zeta^2}}$$

$$- \frac{S_n}{\omega}\left[\frac{1}{\omega h} - \frac{e^{-\zeta \omega h}}{h}\left(\cos ph + \frac{\zeta}{\sqrt{1-\zeta^2}}\sin ph\right)\right]$$

$$- \frac{S^2_{n-1}}{\omega}\left\{\frac{2}{\omega h} - \left(\frac{1}{\omega h} + \frac{4\zeta}{\omega^2 h^2}\right)(1 - e^{-\zeta \omega h}\cos ph)\right.$$

$$\left. - \left[\frac{2(1 - 2\zeta^2)}{\omega^2 h^2} - \frac{\zeta}{\omega h}\right]\frac{e^{-\zeta \omega h}\sin ph}{\sqrt{1-\zeta^2}}\right\}. \tag{9}$$

The response X is scaled by ω in Eq. (8) because ωX is a meaningful quantity, as will be explained later. Consider a time record of $\ddot{Z}$ versus time; the initial values must be given before Eqs. (8) and (9) can be used; i.e., $X(t_0)$ and $\dot{X}(t_0)$ must be known. Also, S_0 for $t = t_0 + h$ is $\ddot{Z}(t_0 + h) - \ddot{Z}(t_0)$, and S^2_{n-1} where $n = 1$ becomes $\ddot{Z}(2h + t_0) - 2\ddot{Z}(h + t_0) + \ddot{Z}(t_0)$.

The maximum or minimum response for each frequency over a given range of frequencies is of more interest to the engineer than the response X at each point in the time record for a particular frequency. Essentially, for the given range of frequencies, one obtains the maximum response as a function of frequency. The maximum and minimum response $X\omega$ for each frequency is selected from the values of $X\omega$ for the complete time record. The refinement of the maximum and minimum (a more accurate estimate) is achieved by first noting that the product of $\dot{X}_{max}$ (the derivative of the chosen X_{max}) and $\dot{X}_{max-h}$ (the derivative of X_{max-h}) is positive if X_{max} reaches its true maximum between X_{max} and X_{max+h} and negative if the true maximum occurs between X_{max} and X_{max-h} (Fig. 2).

Equation (8) is used after it is determined whether the true maximum or minimum is within the range of X_{max-h}, X_{max} or X_{max}, X_{max+h}. $X\omega$ is then evaluated at intervals of $0.2h$, and then the largest $X\omega$ in the subinterval is taken as the more accurate (refined) maximum. The same method is used for computing the refined minimum value of $X\omega$.

The shock spectrum is usually the plot of maximum $X\omega$ vs f, where f is $2\pi\omega$; the residual shock spectrum is a plot of $\sqrt{(X\omega)^2 + \dot{X}^2}$ vs f, where $\sqrt{(X\omega)^2 + \dot{X}^2}$ is the residual response (in velocity units) at the end of the time record, i.e., at the beginning of residual time, which is computed only when there is no damping.

133

Notational Information: $X_{max} = X(nh)$

$X_{max+1} = X((n+1)h)$

$X_{max-1} = X((n-1)h)$

POSSIBILITY 1
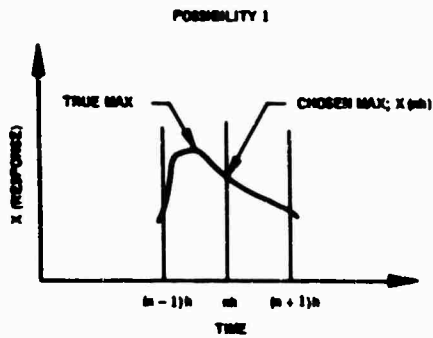
$\dot{X}((n-1)h) \cdot \dot{X}(nh)$ is negative, so true maximum occurs between X_{max-1} and X_{max}.

POSSIBILITY 2
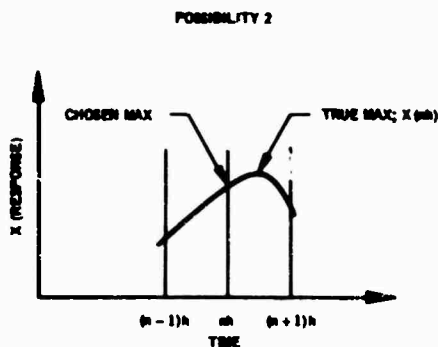
$\dot{X}((n-1)h) \cdot \dot{X}(nh)$ is positive, so true maximum occurs between X_{max} and X_{max+h}.

Fig. 2 - Maximum response refinement

When $\omega = 0$, equations for X and $\dot{X}$ as already presented become meaningless, even though X at $\omega = 0$ has physical meaning. New equations are derived from Eqs. (8) and (9) by L'Hopital's rule. In Eqs. (8) and (9), ω is set equal to zero, and when an indeterminant form is encountered L'Hopital's rule is used yielding

$$X_{n+1} = X_n + \dot{X}_n h - \frac{\ddot{Z}_n h^2}{2} - \frac{S_n h^2}{6} + \frac{h^2}{24} S_{n-1}^2 \quad (10)$$

$$\dot{X}_{n+1} = -\ddot{Z}_n h - S_n \frac{h}{2} + \frac{S_{n-1}^2 h}{12} . \quad (11)$$

Damping plays no role in these equations.

An added feature of the residual shock spectrum solution is that, if the input shock function is an acceleration $\ddot{Z}$, the Fourier spectrum is

identical to the residual shock spectrum. The Fourier spectrum magnitude at ω is $(F_c^2 + F_s^2)^{1/2}$, where

$$F_c = -X\omega \sin \omega t - \dot{X} \cos \omega t$$

and

$$F_s = X\omega \cos \omega t - \dot{X} \sin \omega t .$$

By substitution, $(F_c^2 + F_s^2)^{1/2}$ becomes

$$[(X\omega)^2 + \dot{X}^2]^{1/2} .$$

which is the residual shock spectrum magnitude for ω. The Fourier spectrum is not necessarily equivalent to the residual shock spectrum when the input shock spectrum is $\dot{Z}$. Thorough discussions of Fourier spectra are given by O'Hara [1] and Gertel and Holland [2]. The author is presently finishing a program dealing with Fourier spectra, computing the Fourier spectrum magnitude, the phase angle, the Fourier cosine transform, and the Fourier sine transform. A detailed description of Fourier spectra will be contained in a subsequent report.

Until now the input shock function was assumed to be $\ddot{Z}$ (foundation acceleration), so the necessary equations for an input function which is the foundation velocity $\dot{Z}$ will now be considered.

$$S_n = \dot{Z}_{n+1} - \dot{Z}_n .$$

$$S_{n-1}^2 = S_n - S_{n-1} = \dot{Z}_{n+1} - 2\dot{Z}_n + \dot{Z}_{n-1} . \quad (12)$$

$$\dot{Z}(t) = \dot{Z}_n + S_n \frac{t}{h} + \frac{S_{n-1}^2}{2}\left(\frac{t^2}{h^2} - \frac{t}{h}\right) .$$

where $\ddot{Z}$ is replaced by $\dot{Z}$.

$$X_{n+1} = X_n \cdot e^{-\zeta\omega h}\left(\cos ph + \frac{\zeta}{\sqrt{1-\zeta^2}} \sin ph\right)$$

$$+ \frac{\dot{X}_n e^{-\zeta\omega h} \sin ph}{\sqrt{1-\zeta^2}} - \frac{S_n}{\omega h}\left[1 - e^{-\zeta\omega h}\left(\cos ph + \frac{\zeta}{\sqrt{1-\zeta^2}} \sin ph\right)\right]$$

$$- \frac{S_{n-1}^2}{\omega h}\left\{\frac{1}{2} - \frac{2\zeta}{\omega h} + e^{-\zeta\omega h}\left[\left(\frac{1}{2} - \frac{2\zeta}{\omega h}\right) \cos ph\right.\right.$$

$$\left.\left. - \left(\frac{1 - 2\zeta^2}{\omega h} - \frac{\zeta}{2}\right)\frac{\sin ph}{\sqrt{1-\zeta^2}}\right]\right\} . \quad (13)$$

134

$$\dot{X}_{n+1} \quad -X_n \cdot e^{-z\omega h} \frac{\sin ph}{\sqrt{1-z^2}}$$

$$+ \dot{X}_n e^{-z\omega h} \left(\cos ph - \frac{z}{\sqrt{1-z^2}} \sin ph \right)$$

$$- \frac{S_n}{zh} \frac{e^{-z\omega h} \sin ph}{\sqrt{1-z^2}} - \frac{S_{n-1}^2}{zh} \left\{ \frac{1}{zh} - e^{-z\omega h} \right.$$

$$\left. \cdot \left[\frac{\cos ph}{h} \cdot \left(\frac{z}{zh} + \frac{1}{2} \right) \frac{\sin ph}{\sqrt{1-z^2}} \right] \right\} . \quad (14)$$

Equation (13) is obtained from Eq. (4) by integrating by parts, substituting Eq. (12) for $\dot{Z}(t)$ into the new integral, integrating again by parts, and finally substituting h for t in the other terms of Eq. (4). Equation (14) is obtained in a similar manner, using Eq. (5) in place of Eq. (4).

When $\omega = 0$,

$$X_{n+1} = X_n + \dot{X}_n h - \frac{S_n h}{2} + \frac{S_n^2 h}{12}$$

and

$$\dot{X}_{n+1} = \dot{X}_n - S_n .$$

The rest of the calculations using $\dot{z}$ are the same as those using $\ddot{z}$, except that for the $\dot{z}$ input, the residual shock spectrum is not necessarily identical to the Fourier spectrum.

Finally, to solve a problem in which there is an applied force $F(t)$ but no foundation motion, we must solve the differential equation

$$\ddot{X} + 2z\omega \dot{X} + \omega^2 X = \frac{F(t)}{M} . \quad (15)$$

Equations (15) and (3) are the same except for their right-hand members, so if the input function is an applied force $F(t)$, then since

$$\ddot{Z}(t) = - \frac{F(t)}{M} ,$$

all of the F_i's are scaled by $-1/M$ and the input function is treated as if it were $\ddot{Z}(t)$. The output would correctly be the response to $F(t)$.

IMPORTANT FORTRAN VARIABLES (EXCLUDING INPUT VARIABLES)

Dimensioned

Z $\ddot{z}$ or $\dot{z}$

S S_i, first forward difference where
$S_i \quad Z_{i+1} - Z_i$

S2ND S_i^2, second forward difference where
$S_i^2 = Z_{i+1} - 2Z_i + Z_{i-1}$

XØMEGA $X\omega$, and X when $\omega = 0$, response displacement times natural frequency

X   X, response displacement, used for plotting in IP1, also used for plotting Y (acceleration)

XDØT $\dot{X}$, response velocity

ØSCIL   F, frequency

VEL   Maximum absolute value of $X\omega$ for each ω

RESID $\sqrt{(X\omega)^2 + \dot{X}^2}$, at the start of residual time

Undimensioned

A1 $10^{LØP}$, the value of the first A-line drawn on the four-coordinate graph (lower left-hand corner)

D1 $10^{LØP}$, the value of the first D-line drawn on the four-coordinate graph (upper left-hand corner)

IER   Number of points out of range when plotting response (X) vs time in IP1

IERA   Number of points out of range when plotting response velocity ($\dot{X}$) vs time in IP1

IERB   Number of points out of range when plotting $-X\omega^2$ vs time in IP2

IERR   Number of points out of range when plotting the input function Z

OUTLINE OF PROGRAM

The Roman numeral headings correspond to the comment cards in the program listing. The flow chart (Fig. 3) should aid in understanding the ensuing outline. $\emptyset$ is used to denote an alphabetic O in FORTRAN.

I. Input — Data are read, such as the forcing function $\dot{z}$ or $\ddot{z}$, output options, and other constants. IP3 (four-coordinate grid option) is checked for zero; if not zero, IP1 and IP2 (other plots) are deleted even if they are requested.

Fig. 3 - Flow chart

136
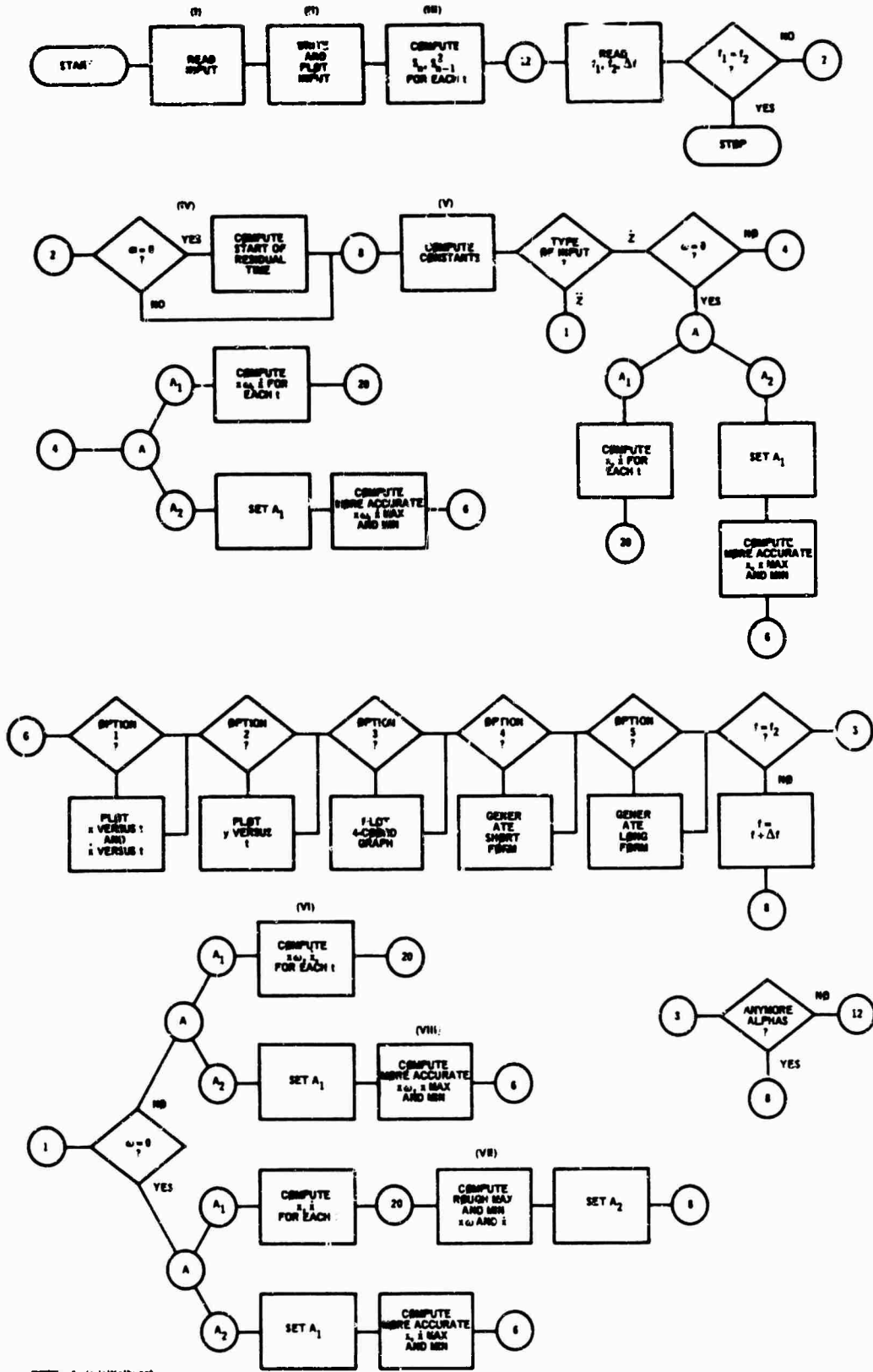
II. Write and Plot Input Data — The time T corresponding to each Z is generated using H. Each Z and corresponding T are written. From statement 110 to 123, Z vs T is plotted.

III. Compute S(N) and S2ND(N) for Each Time T — Each S and S2ND are computed. A frequency card is read, i.e., FREQ1, FREQ2, DELTAF. If FREQ1 = FREQ2, the blank card was read, indicating the run is finished. If FREQ1 $\neq$ FREQ2 the program continues. The number of frequencies is computed from the card just read; i.e., NØFREQ = (FREQ2 - FREQ1)/DELTAF.

IV. Damped or Undamped — If undamped, find number of residual points. The large DØ-loop, which is indexed for each alpha, is executed. IALPHA is set equal to one if no damping is present ($\cdot$ 0), or set equal to two if there is damping ($\cdot$: 0). If no damping is present, the start of residual time is computed, i. ., T(KH).

V. Compute Constants — Many mathematical expressions repeatedly used in the program are computed. IF REQ is set equal to one if the frequency is zero or to two if the frequency is not zero. Finally, there is a major branch in the program, depending on whether (a) Z $\dot{Z}$ and frequency is zero, (b) Z $\dot{Z}$ and frequency is not zero, (c) Z $\ddot{Z}$ and frequency is zero, and (d) Z $\ddot{Z}$ and frequency is not zero. Of these possibilities, only (b) is assumed in the rest of the discussion.

VI. Compute XØMEGA (N), XDØT for Velocity Input — More constants and mathematical expressions are evaluated. N XØMEGA's and XDØT's are computed in a DØ-loop ending at statement 210. Then there is transfer to preliminary calculations.

VII. Preliminary Calculations for Minimum and Maximum Response — Maximum and minimum XØMEGA's are determined; then control is transferred to statement 225. Statements 225 to 235 inclusive contain the "efinement calculations for maximum and minimum X . Then from statements 211 through 215 the different output features, selected in the input, are executed.

VIII. Restart with New Frequency, Restart with New Alpha, or Stop — FREQ and FREQ2 are compared; if equal, the end of the alpha DØ-loop is reached (statement 800), and either the entire calculation is restarted for a new alpha or the next frequency card is read. If FREQ $\neq$ FREQ2, then FREQ is incremented by DELTAF, and the calculations for XØMEGA, XDØT, etc., are repeated.

FORTRAN INPUT VARIABLES

Z — Shock function which is dimensioned, either acceleration or velocity

T — Initial time, really T(I), usually zero

TZERØ — Starting time of residual shock, i.e., end of transient

H — Time increment into which record is subdivided

X0 — Response displacement at time T, usually zero

N — Number of points, i.e., number of Z's; must not exceed the dimensioned value for Z in the DIMENSIØN statement

XDØT0 — Response velocity at time T, usually zero

ISZ — If ISZ 0, then Z $\dot{Z}$; if ISZ $\neq$ 0, then Z $\ddot{Z}$

IP1 — Output option one, if IP1 0, ignored; if IP1 : 0, plots of response displacement vs time and response velocity vs time are generated for each frequency and each alpha

IP2 — Output option two, if IP2 - 0, ignored; if IP2 : 0 a plot of negative pseudo-response acceleration vs time is generated for each frequency and each alpha

IP3 — Output option three, if IP3 0, ignored; if IP3 $\neq$ 0, a four-coordinate, log-log graph is produced for each range of frequencies submitted, as well as for each alpha, consisting of response displacement vs frequency, pseudo-response velocity vs frequency, pseudo-response acceleration vs frequency, and if no damping (alpha = 0) residual response velocity vs frequency. If IP3 is used, i.e., IP3 $\neq$ 0, then the program will inhibit IP1 and IP2.

IP4 — Output option four is ignored if IP4 0; if IP4 $\neq$ 0 tabulation of results is generated (see output for explanation).

IP5 — Output option five is ignored if IP5 0; if IP5 $\neq$ 0 tabulation of results, more extensive than IP4, is generated (see output for explanation).

137

ALPHA   Damping coefficient, dimensioned

NALPHA   Number of damping coefficients submitted, which must not be greater than the dimension of ALPHA in the DIMENSIØN statement

FREQ1   Initial frequency, cps

FREQ2   Last frequency, cps

DELTAF   Frequency increment

INPUT

The input is read into the computer mostly in the form of FORTRAN NAMELISTS; consequently, the format for the data is not very restrictive. The data are usually on punched cards. If the shock function Z is available on an analog tape, it must be converted to digitized tape or to cards before the program can be used. Of course, the NAMELISTS can be replaced by regular format statements, which would be mandatory if the program is converted to FORTRAN II.

ZAZA1 through ZAZA4 are NAMELIST names, each containing one or more variables. (See any IBM FORTRAN IV manual for an explanation of NAMELISTS.) The data cards are arranged in the following order: $DATA card, $ZAZA1 data, $ZAZA2 data, $ZAZA3 data, $ZAZA4 data, frequency cards, and system cards, END ØF FILE, $IBSYS, $RESTØRE, and END ØF FILE.

There is no limit to the number of frequency ranges that can be handled, at one card per range. The last card must be blank. The frequency cards are read under format statement 920, i.e., 3F20.8, so the decimal point of the first number FREQ1 is in column 12, that of the second number FREQ2 in column 32, and that of the last number DELTAF in column 52. FREQ1 must not equal FREQ2; therefore, the first number on the frequency card must be less than the second number. The number of frequencies, (FREQ2 - FREQ1) / DELTAF, must not exceed the storage capacity of the variable ØSCIL when using IP3, which is now dimensioned for 1,000 words.

If IP1 through IP5 are set equal to zero, the only output that will result is a plot of the input function, a tabulation of the input function, and a tabulation of S_i and S_i^2.

If the shock function, Z, is not on cards but is generated from a formula inserted into the

program, the READ (5, ZAZA1) statement must be deleted from the program.

The physical units for most of the quantities used in this program are assumed to be consistent. The units for the input quantities determine the units for the output values except where specified; for example, the input frequencies should be in cycles per second.

OUTPUT

The output from the program is composed of a plot and tabulation of the input shock function, a printout of each S_k and S_k^2, and the input options. If the printed S_k and S_k^2 are not desired, the statement immediately following statement 200 in the program should be removed.

An example graph of an input function is shown in Fig. 4. Figures 5 and 6 are examples of IP1, which is a plot of X vs time and $\dot{X}$ vs time for each frequency and each alpha (damping coefficient). IP2 is illustrated in Fig. 7, which is a plot of $\ddot{X}$ vs time for each frequency and each alpha. The quantity $-\ddot{X}$ is equivalent to the negative pseudo-response acceleration when $\ddot{Z} = 0$, because $\ddot{Y} = \ddot{X}$ when $\ddot{Z} = 0$.

IP3, illustrated in Figs. 8 and 9, is a four-coordinate log-log grid which is a plot of velocity vs frequency, with acceleration lines having negative slope and velocity lines having positive slope superimposed on an originally two-coordinate grid. The value of the A lines increases logarithmically from left to right, and the line labeled A in the lower left corner of the grid corresponds to the value for A printed in the lower right margin. The value of the D lines decreases downward logarithmically, and the line labeled D in the upper left corner of the grid corresponds to the value for D printed in the lower right margin. The shock spectrum is the starred plot ($\dot{X}$ vs f); the residual shock spectrum, $\sqrt{(\dot{X}_o)^2 + \ddot{X}^2}$ vs f, plotted only when $\alpha = 0$, is the plot of zero points. One complete four-coordinate graph is generated for each frequency range and damping coefficient α. Hence, for any given frequency within the plotted range, the pseudo-acceleration A, the pseudo-velocity, and the displacement D can be read from the starred curve; provided there is no damping, the residual shock spectrum magnitude can also be read from the zero curve.

IP4 (Short Form) is, for each frequency range and damping coefficient, a tabulation of frequency, the maximum value between the pseudo-velocity $\dot{X}_o$ and the residual response $\sqrt{(\dot{X}_o)^2 + \ddot{X}^2}$, and, if no damping is present, the residual response.
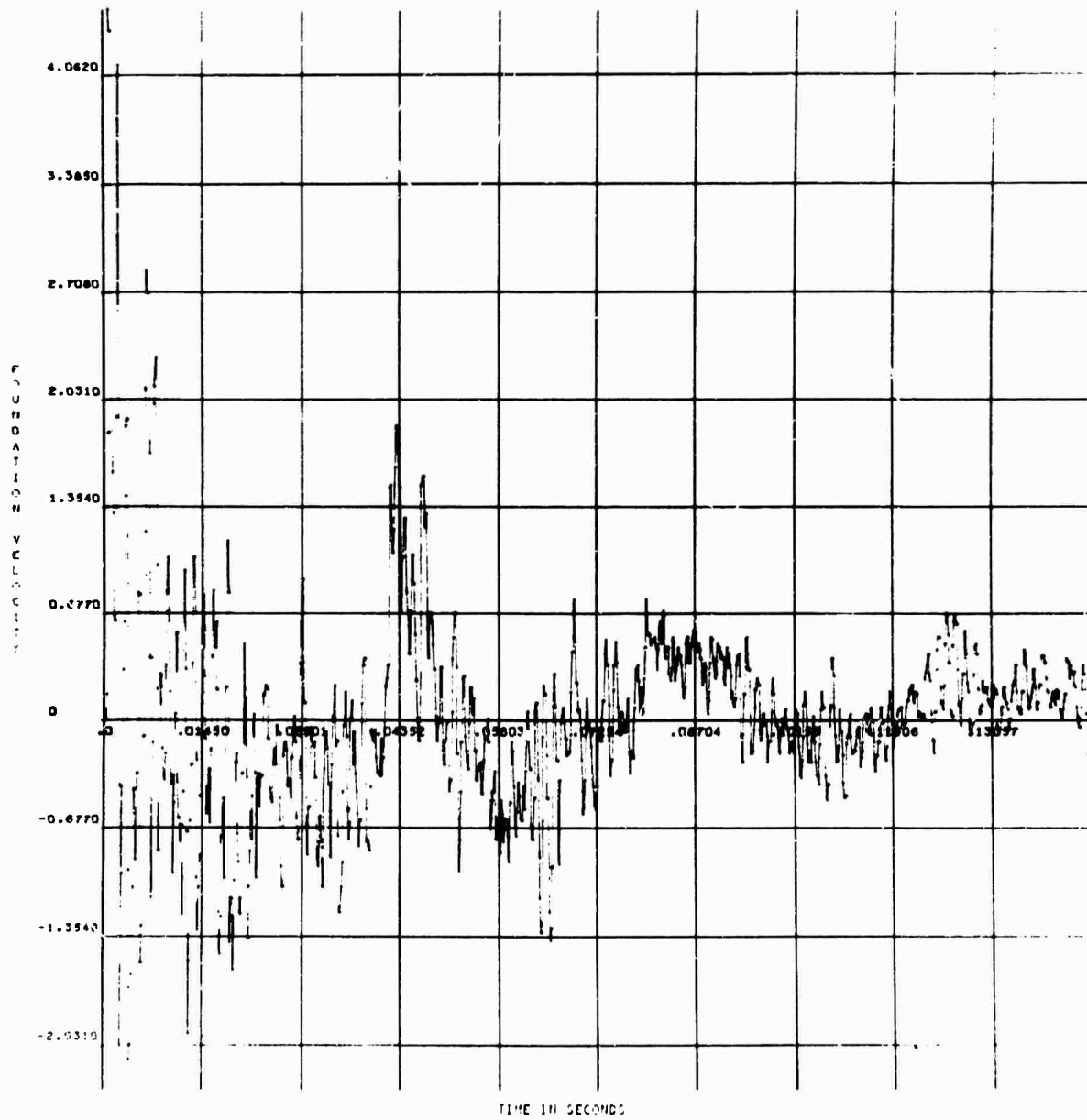
Fig. 4 - Plot of sample input function
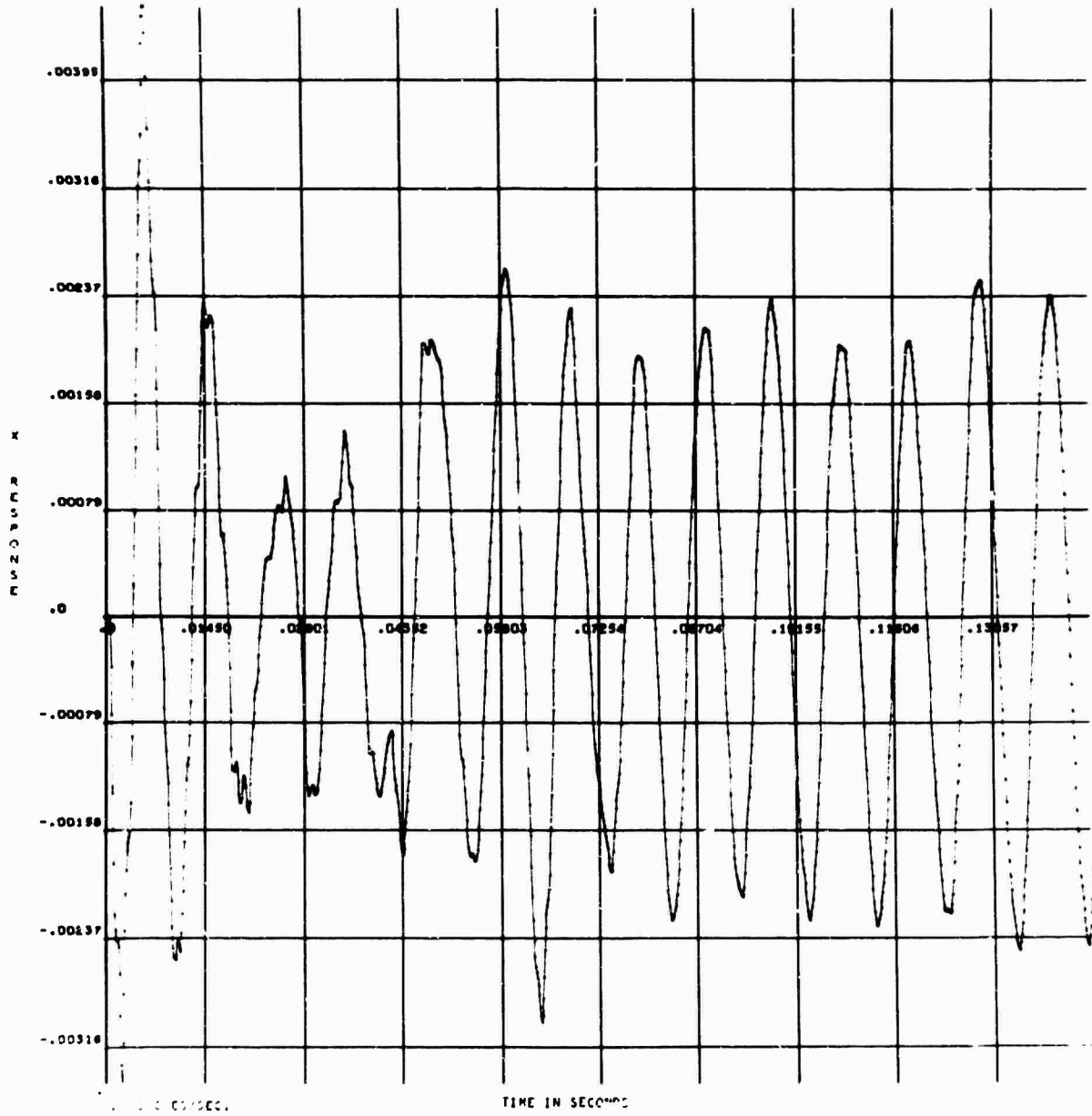
Fig. 5 - Response X vs time for sample function at fixed frequency

140
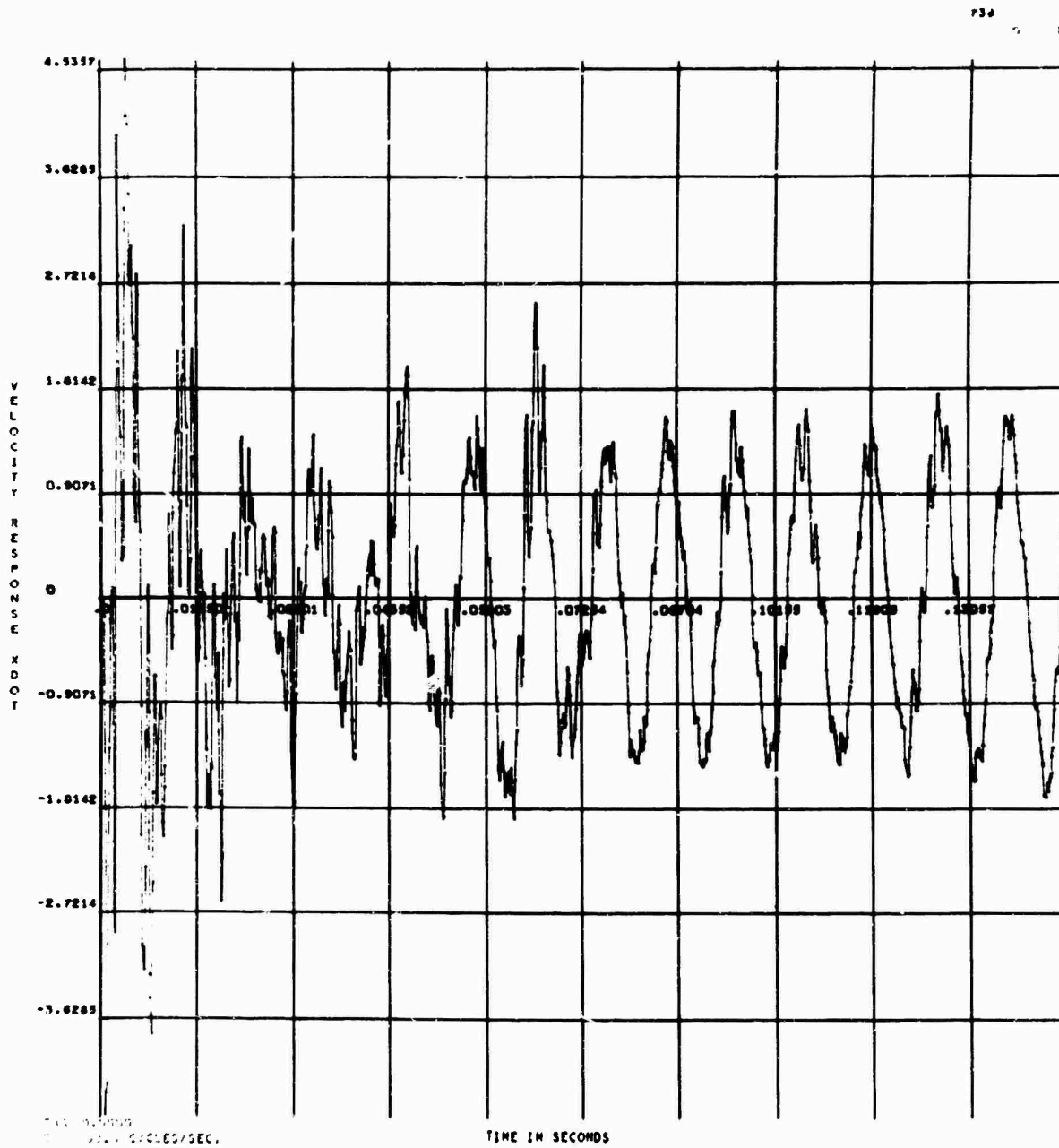
Fig. 6 - Response velocity $\dot{x}$ vs time for sample function at fixed frequency
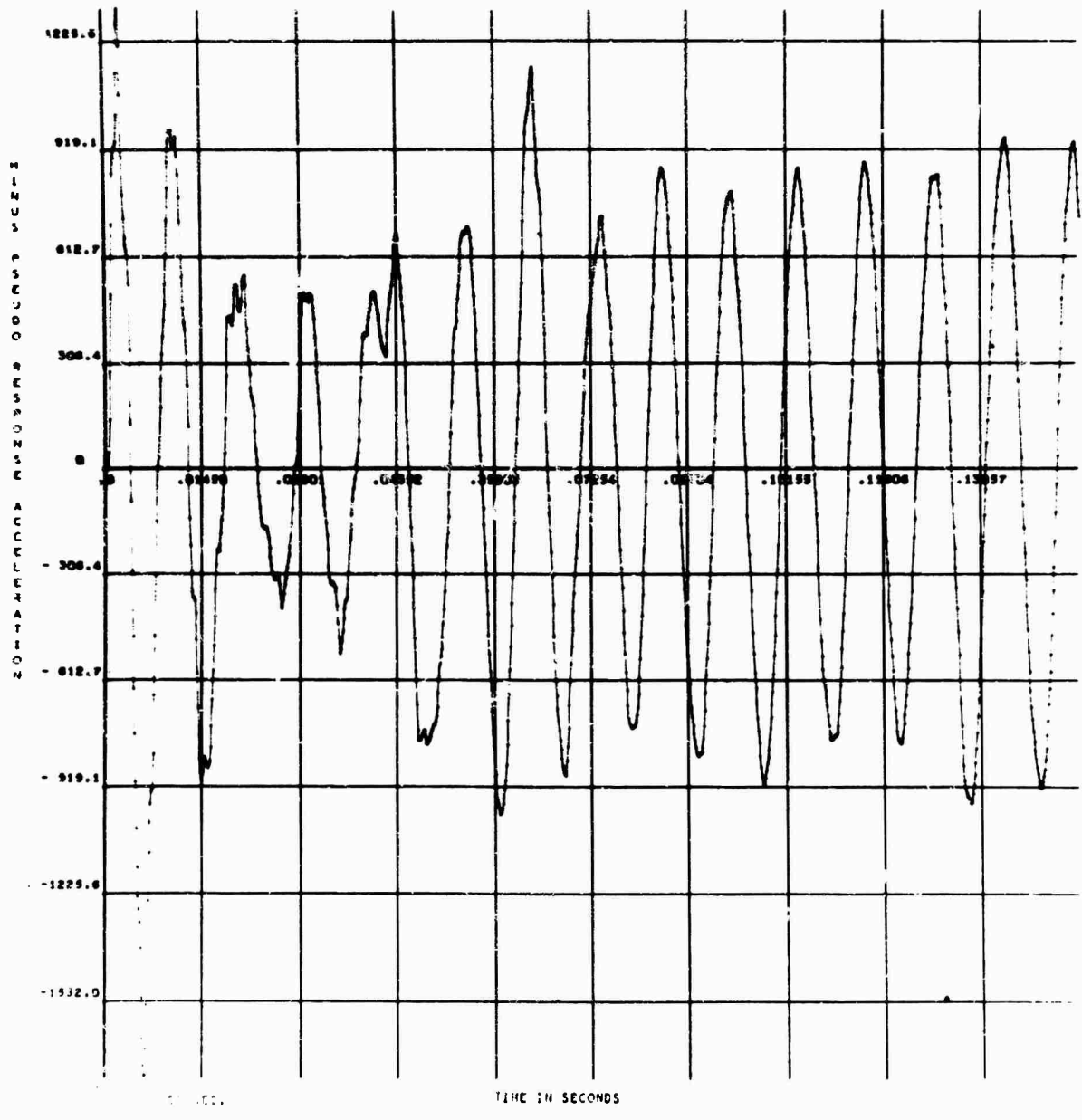
Fig. 7 - Negative pseudo-response acceleration $(-\omega^2 x)$ vs time
for sample function at fixed frequency

142
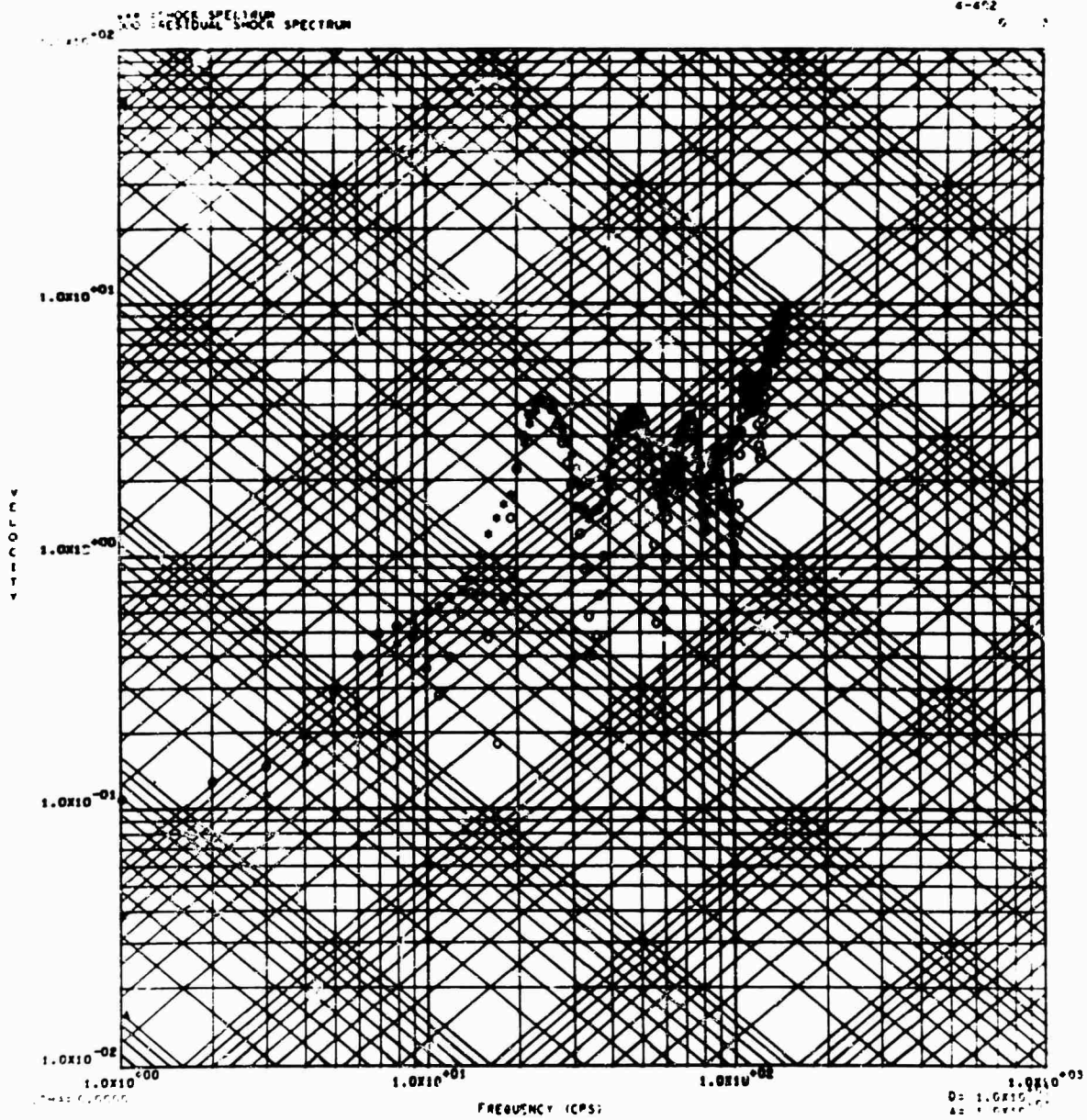
Fig. 8 - Four-coordinate grid of sample function (1-150 cps)

143
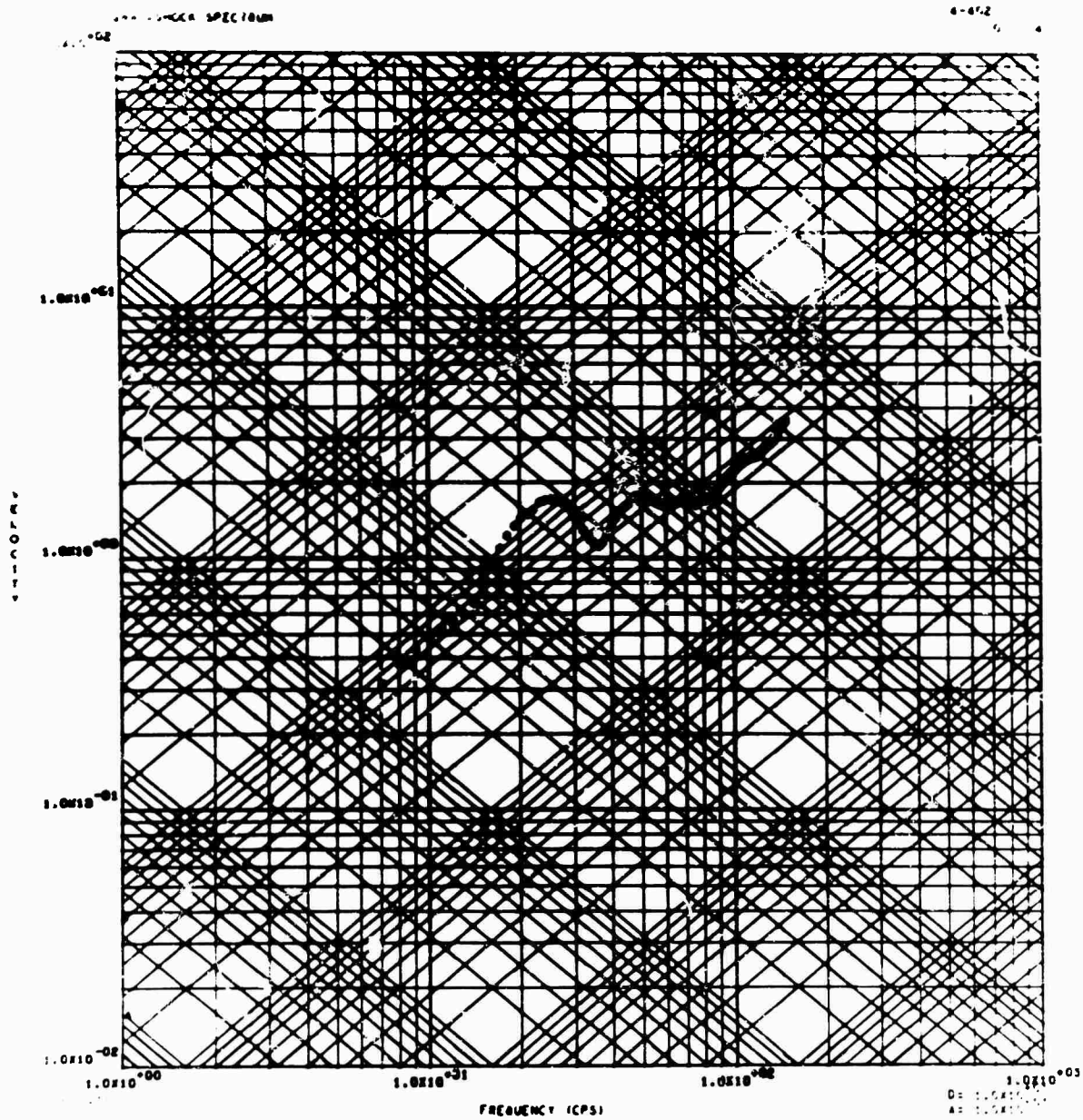
Fig. 9 - Four-coordinate grid of sample function with damping (1-150 cps)

IP5 (Long Form) is, for each frequency range and damping coefficient, a tabulation of frequency, maximum positive pseudo-velocity, minimum negative pseudo-velocity, and, if no damping is present, the residual response.

One method for using the various graphical outputs is first to generate the log-log grid (shock spectrum) from IP3, and then select from the shock spectrum the important frequencies.

Next, these frequencies are used as input in running the program a second time for IP1 and/or IP2 to produce response vs time plots for each desired frequency.

OPERATING INSTRUCTIONS

The subroutines required are from the plotting package written by North American

144

Aviation for the Stromberg-Carlson 4020. If the SC 4020 is not available, the alternate deck is used, in which no SC 4020 subroutines are given and there are only two output options, IP4 and IP5.

No input tapes, except for unit 5, are required; the program is run under IBSYS version 13. Three output tapes are needed for the program: one for the SC 4020, if used, one for logical tape unit 6, and one for logical tape unit 8. IP4 is written on unit 8, and IP5 is written on unit 6.

An approximation of the running time of the program, using the data from Fig. 1, is

about 5 min, including compiling time. The running time for the program is increased considerably if more than a few frequencies are used with IP1 and IP2.

Most of the memory is used (32K); see the dimension statement of the program listing for the array sizes which influence the amount of memory needed.

ACKNOWLEDGMENT

The author wishes to thank George J. O'Hara for his expert guidance and advice on the engineering analysis and the organization of the program.

REFERENCES

1. G.J. O'Hara, "A Numerical Procedure for Shock and Fourier Analysis," NRL Rept. 5772, June 1962

2. M. Gertel and R. Holland, "Definition of Shock Design and Test Criteria Using Shock and Fourier Spectra of Transient Environments," Allied Research Associates, Document No. DYN-65-1, Oct. 1965

Appendix

PROGRAM LISTINGS

LISTING OF PROGRAM WITHOUT 4020 SUBROUTINES

```
$EXEFUTE        IBJOB
$IBJOB          MAP,FIOCS                                    MELODIA
$IBFTC SNERD    LIST,NODECK
C         PROGRAMMER------ANTHONY MELODIA---------*--
C-- - *-         APPLIED MATHEMATICS LABORATORY----------
C------DAVID TAYLOR MODEL BASIN, WASHINGTON D.C.---------- -
C--------TELEPHONE NUMBER---AREA CODE 301, 995-1514-------- --
C
C
      DIMENSION Z(2500),T(2500),S(2500),S2ND(2500),XOMEGA(2500),
     1XDOT(2500),ALPHA(25)
      NAMELIST/ZAZA1/Z/ZAZA2/T,TZERO,                   H,      X0,N,
     1XDOT0,ISZ/ZAZA3/IP4,IP5/ZAZA4/ALPHA,NALPHA
      WRITE(6,900)
      PI=3.1415927
      READ(5,ZAZA1)
      READ(5,ZAZA2)
      READ(5,ZAZA3)
      READ(5,ZAZA4)
C
C------- -- WRITE AND PLOT INPUT DATA------------- *
      DO 100 I=2,N
  100 T(I)=T(I-1)+H
      IF(ISZ)104,105,104
  104 WRITE(6,901)
      GO TO 106
  105 WRITE(6,902)
  106 CONTINUE
      WRITE(6,903)  (Z(I),T(I),I=1,N)
C
C------- --COMPUTE S(N) AND S2ND(N) FOR EACH TIME,T--------
      S(1)=Z(2)-Z(1)
      S2ND(1)=Z(3)-2.*Z(2)+Z.1.
      K=N-1
      DO 200 I=2,K
      S(I)=Z(I+1)-Z(I)
  200 S2ND(I)=Z(I+1)-2.*Z(I)+Z(I-1)
      WRITE(6,917) (I,S(I),S2ND(I),I=1,N)
C
  190 READ(5,920) FREQ1,FREQ2,DELTAF
      IF(ABS(FREQ1-FREQ2)-.1E-20) 801,801,191
  191 CONTINUE
C------DAMPED OR UNDAMPED,IF UNDAMPED FIND NUMBER OF RESIDUAL POINTS-------
      DO 800 IX=1,NALPHA
      NIN=1
      FREQ=FREQ1
      IF(ABS(ALPHA(IX))-.1E-09)201,201,202
  201 IALPHA=1
      GO TO 222
  202 IALPHA=2
  222 GO TO (203,207),IALPHA
  203 TT=TZERO-T(1)
      IF(AMOD(TT,H)-H/2.)205,204,204
  204 KH=TT/H+1.000001
      GO TO 207
  205 KH=TT/H+.000001
  207 CONTINUE
C
C---------COMPUTE CONSTANTS-------
      OMEGA=FREQ*2.*PI
```

```
      RADCAL=SQRT(1.-ALPHA(IX)**2)
      OH=OMEGA*H
      P=OMEGA*RADCAL
      EX=EXP(-ALPHA(IX)*OH)
      COSPH=COS(P*H)
      SINPH=SIN(P*H)
      A2OH=2.*ALPHA(IX)/OH
      RECOH=1./OH
      ALPHA2=ALPHA(IX)**2
      X12=1.-2.*ALPHA2
      FACT1=EX*SINPH/RADCAL
      FACT2=EX*COSPH+FACT1*ALPHA(IX)
      IF(ABS(FREQ)-.1E-20)220,220,221
  220 IFREQ=1
      GO TO 223
  221 IFREQ=2
  223 IF(ISZ)300,208,300
  208 GO TO (400,209),IFREQ
  209 CONTINUE
C
C-----COMPUTEXOMEGA(N),XDOT FOR VELOCITY INPUT-----------
      GO TO(224,225),NIN
  224 XOMEGA(1)=OMEGA*XO
      FACT3=RECOH*(1.-FACT2)
      FACT4=RECOH*(.5-2.*ALPHA(IX)*RECOH+EX*((.5+2.*ALPHA(IX)*RECOH)
     1*COSPH-(X12*RECOH-ALPHA(IX)/2.)*SINPH/RADCAL))
      FACT5=EX*COSPH-ALPHA(IX)*FACT1
      FACT6=RECOH*FACT1
      FACT7=(RECOH**2)*(1.-EX*(COSPH+(ALPHA(IX)+OH/2.)*SINPH/RADCAL))
      XDOT(1)=XDOTO
      DO 210 I=2,N
      XOMEGA(I)=XOMEGA(I-1)*FACT2+XDOT(I-1)*FACT1-S(I-1)*FACT3-S2ND(I-1)
     1*FACT4
  210 XDOT(I)=-XOMEGA(I-1)*FACT1+XDOT(I-1)*FACT5-S(I-1)*FACT6-S2ND(I-1)*
     1FACT7
      GO TO 756
  225 CONTINUE
      KRO=KMX+KOOK
      KRA=KMN+KICK
      DO 235 I=2,5
      VA=I-1
      TA=VA*.2*H
      COSPT=COS(P*TA)
      SINPT=SIN(P*TA)
      EXT=EXP(-ALPHA(IX)*OMEGA*TA)
      FACTR1=EXT*(COSPT+ALPHA(IX)*SINPT/RADCAL)
      FACTR2=EXT*SINPT/RADCAL
      FACTR3=(1.-FACTR1)*RECOH
      FACTR4=(TA/H-.5-A2OH+(ALPHA(IX)/2.-X12*RECOH)*FACTR2+(.5+A2OH)
     1*EXT*COSPT)*RECOH
      XMAXO    =XOMEGA(KRO)*FACTR1+XDOT(KRO)*FACTR2-S(KRO)*FACTR3
     1-S2ND(KRO)*FACTR4
      IF(XMAX-XMAXO    )229,230,230
  229 XMAX=XMAXO
  230 XMINO    =XOMEGA(KRA)*FACTR1+XDOT(KRA)*FACTR2-S(KRA)*FACTR3
     1-S2ND(KRA)*FACTR4
      IF(XMIN-XMINO    )235,235,232
  232 XMIN=XMINO
  235 CONTINUE
      NIN=1
```

147

```
    214 IF(IP4)650,215,650
    215 IF(IP5)700,785,700
C
C------COMPUTE XOMEGA(N), XDOT(N), FOR ACCELERATION INPUT---------
    300 CONTINUE
        GO TO(350,305),IFREQ
    305 CONTINUE
        GO TO(308,325),NIN
    308 XOMEGA(1)=OMEGA*X
        ECOS1=1.-EX*COSPH
        DFACT3=(1.-FACT2)/OMEGA
        DFACT4=(1.-A2OH*ECOS1-X12*FACT1*RECOH)/OMEGA
        DFACT5=(-4.*ALPHA(IX)-(2.*(1.-4.*ALPHA2)/OM-2.*ALPHA(IX))*ECOS1+
       1(X12+2.*ALPHA(IX)*(3.-4.*ALPHA2)/OM)*FACT1)*RECOH/(2.*OMEGA)
        DFACT6=(1.-ECOS1)-FACT1*ALPHA(IX)
        DFACT7=FACT1/OMEGA
        DFACT8=(1.-FACT2)*RECOH/OMEGA
        DFACT9=(2.-(1.+4.*ALPHA(IX)*RECOH)*ECOS1-(2.*X12*RECOH-ALPHA(IX))
       1*FACT1)*RECOH/(2.*OMEGA)
        XDOT(1)=XDOTC
        DO 310 I=2,N
        XOMEGA(I)=XOMEGA(I-1)*FACT2+XDOT(I-1)*FACT1-Z(I-1)*DFACT3-S(I-1)
       1*DFACT4-S2ND(I-1)*DFACT5
    310 XDOT(I)=-XOMEGA(I-1)*FACT1+XDOT(I-1)*DFACT6-Z(I-1)*DFACT7
       1       -S(I-1)*DFACT8-S2ND(I-1)*DFACT9
        GO TO 750
    325 CONTINUE
        KRO=KMX+KOOK
        KRA=KMN+KICK
        H2=H**2
        DO 335 I=2,5
        VA=I-1
        TA=VA*.2*H
        COSPT=COS(P*TA)
        SINPT=SIN(P*TA)
        EXT=EXP(-ALPHA(IX)*OMEGA*TA)
        FACTR1=EXT*(COSPT+ALPHA(IX)*SINPT/RADCAL)
        FACTR2=EXT*SINPT/RADCAL
        FACTR3=(1.-FACTR1)/OMEGA
        FACTR4=(TA/H-A2OH*(1.-EXT*COSPT)-X12*FACTR2*RECOH)/OMEGA
        FACTR5=(TA**2/H2-TA/H-(2.*(1.-4.*ALPHA2)*RECOH**2-A2OH)*
       1(1.-EXT*COSPT)+(X12*RECOH+2.*ALPHA(IX)*(3.-4.*ALPHA2)*RECOH**2)
       2*FACTR2)/(2.*OMEGA)
        XMAXO=XOMEGA(KRO)*FACTR1+XDOT(KRO)*FACTR2-Z(KRO)*FACTR3
       1-S(KRO)*FACTR4-S2ND(KRO)*FACTR5
        IF(XMAX-XMAXO   )329,330,330
    329 XMAX=XMAXO
    330 XMINO=XOMEGA(KRA)*FACTR1+XDOT(KRA)*FACTR2-Z(KRA)*FACTR3
       1-S(KRA)*FACTR4-S2ND(KRA)*FACTR5
        IF(XMIN-XMINO   )335,335,332
    332 XMIN=XMINO
    335 CONTINUE
        NIN=1
        GO TO 214
C
C------FREQ1=ZERO FOR FOUNDATION ACCELERATION---------
    350 GO TO(352,365),NIN
    352 XOMEGA(1)=XO
        XDOT(1)=XDOTC
        H2=H**2
```

148

```fortran
      DO 360 I=2,N
      XOMEGA(I)=XOMEGA(I-1)+H*XDOT(I-1)-Z(I-1)*H2/2.-S(I-1)*H2/6.+
     1S2ND(I-1)*H2/24.
  36  XDOT(I)=-Z(I-1)*H-S(I-1)*H2/2.+S2ND(I-1)*H/12.
      GO TO 756
 365  CONTINUE
      NIN=1
      GO TO 214
C
C-------COMPUTE X, XDOT FOR OMEGA=ZERO-----VELOCITY INPUT
 40   GO TO(402,425),NIN
 402  XOMEGA(1)=XO
      XDOT(1)=XDOTO
      DO 410 I=2,N
      XOMEGA(I)=XOMEGA(I-1)+XDOT(I-1)*H-S(I-1)*H*.5+S2ND(I-1)*H/12.
 410  XDOT(I)=XDOT(I-1)-S(I-1)
      GO TO 756
 425  CONTINUE
      NIN=1
      GO TO 214
C
C-------- *   SHORT FORM----------
  65  CONTINUE
      IF(ABS(FREQ-FREQ1)-.1E-04)651,651,652
 651  WRITE(8,912) ALPHA(IX)
 652  GO TO(658,655),IALPHA
 655  XOMAX=AMAX1(ABS(XMAX),ABS(XMIN))
      GO TO(668,669),IFREQ
 653  RMAX=SQRT(XOMEGA(KH)**2+XDOT(KH)**2)
      XOMAX=AMAX1(ABS(XMAX),ABS(XMIN),ABS(RMAX))
      GO TO(681,678),IFREQ
 668  WRITE(8,906) FREQ,XOMAX
      GO TO 215
 669  WRITE(8,905) FREQ,XOMAX
      GO TO 215
 678  WRITE(8,907) FREQ,XOMAX,RMAX
      GO TO 215
 681  WRITE(8,908) FREQ,XOMAX,RMAX
      GO TO 215

C--------LONG FORM---------
 700  CONTINUE
      IF(ABS(FREQ-FREQ1)-.1E-04)701,701,702
 701  WRITE(6,915) ALPHA(IX)
 702  GO TO(704,705),IALPHA
 704  RMAX=SQRT(XOMEGA(KH)**2+XDOT(KH)**2)
      GO TO(743,742),IFREQ
 705  GO TO(726,727),IFREQ
 726  WRITE(6,916) FREQ,XMAX,XMIN
      GO TO 785
 727  WRITE(6,910) FREQ,XMAX,XMIN
      GO TO 785
 742  WRITE(6,912) FREQ,XMAX,XMIN,RMAX
      GO TO 785
 743  WRITE(6,911) FREQ,XMAX,XMIN,RMAX
      GO TO 785

C------ PRELIMINARY CALCULATIONS FOR MIN. AND MAX. RESPONSE----------
 756  GO TO (758,757),IALPHA
 757  NX=N
```

149

```
                  GO TO 759
          758 NX=KH
          759 XMAX=XOMEGA(1)
                  KMX=1
                  XMIN=XOMEGA(1)
                  KMN=1
                  DO 760 I=2,NX
                  IF(XMAX-XOMEGA(I))761,762,762
          761 XMAX=XOMEGA(I)
                  KMX=I
          762 IF(XMIN-XOMEGA(I))760,765,765
          765 XMIN=XOMEGA(I)
                  KMN=I
          760 CONTINUE
                  IF(KMX-1)771,770,771
          770 KMX=KMX+1
          771 IF(KMX-NX)773,772,773
          772 KMX=KMX-1
          773 IF(KMN-1)775,774,775
          774 KMN=KMN+1
          775 IF(KMN-NX)777,776,777
          776 KMN=KMN-1
          777 CONTINUE
                  IF(XDOT(KMX-1)*XDOT(KMX))778,778,779
          778 KOOK=-1
                  GO TO 781
          779 KOOK=0
          781 CONTINUE
                  IF(XDOT(KMN-1)*XDOT(KMN))783,783,784
          783 KICK=-1
                  GO TO 950
          784 KICK=0
          950 NIN=2
                  GO TO 207
      C
      C-------EITHER RESTART WITH NEW FREQ. OR RESTART WITH NEW ALPHA OR STOP
          785 CONTINUE
                  IF(ABS(FREQ-FREQ2)-.1E-03)800,755,755
          755 FREQ=FREQ+DELTAF
                  GO TO 207
          800 CONTINUE
                  GO TO 190
          801 WRITE(6,909)
                  STOP
      C
          900 FORMAT(1H1,49X,22HSHOCK SPECTRUM PROGRAM//50X,21HAPPLIED MATH LAB
             1DTMB,////)
          901 FORMAT(40X,38HFOUNDATION ACCELERATION VS TIME(INPUT)//18X,23HFOUND
             IATION ACCELERATION,36X,15HTIME IN SECONDS)
          902 FORMAT(42X,35HFOUNDATION VELOCITY VS TIME (INPUT)//20X,19HFOUNDATI
             ION VELOCITY,35X,15HTIME IN SECONDS)
          903 FORMAT(1X,F35.9, 44X,F20.9)
          905 FORMAT(15X,F10.5,29X,F12.7)
          906 FORMAT(10X,11HFIRST FREQ=,F10.5,7X,13HMAX RESPONSE=,F12.7/)
          907 FORMAT(15X,F10.5,2(29X,F12.7))
          908 FORMAT(10X,11HFIRST FREQ=,F10.5,7X,13HMAX RESPONSE=,F12.7,12X,
             117HMAX RES RESPONSE=,F12.7)
          909 FORMAT(///38X,25HPROGRAM RAN TO COMPLETION)
          910 FORMAT(10X,F10.5,3(18X,F12.7))
          911 FORMAT(5X,11HFIRST FREQ=,F10.5,9X,9HMAX RESP=,F12.7,10X,9HMIN RESP
```

```
       1=,F12.7,7X,15HMAX RESID RESP=,F12.7)
   912 FORMAT(1H1,55X,10HSHORT FCRM//45X,20HDAMPING COEFFICIENT=,F10.8///
      1/9X,22HFREQUENCY(CYCLES/SEC,),19X,20HMAX RESPONSE X OMEGA,18X,26HM
      2AX RESID RESPONSE X OMEGA)
   915 FORMAT(1H1,55X,9HLONG FORM//45X,20HDAMPING COEFFICIENT=,F10.8////
      17X,16HFREQ(CYCLES/SEC),12X,20HMAX RESPONSE X OMEGA,10X,20HMIN RESP
      2ONSE X OMEGA,8X,22HMAX RESID RESP X OMEGA)
   916 FORMAT(4X,11HFIRST FREQ=,F10.5,10X,9HMAX RESP=,F12.7,10X,9HMIN RES
      1P=,F12.7)
   917 FORMAT(1H1,18X,1HI,38X,4HS(I),34X,7HS2ND(I)//
      1(17X,I4,34X,F12.7,28X,F12.7))
   918 FORMAT(1H1,50X,19HINTERMEDIATE VALUES/19X,1HI,35X,9HXOMEGA(I),
      13)X,7HXDOT(I)//
      2(17X,I3,34X,F12.7,26X,F12.7))
   920 FORMAT(3F20.8)
   921 FORMAT(6F15.6)
       END
```

317

```
$RESTORE
$*       CHARACTRON OUTPUT TAPE ON B9
$ATTACH          B9
$AS              SYSLB
$EXECUTE         IBJOB
$IBJOB           MAP,FIOCS                                  MELODIA
$IBFTC SNERD   LIST,NODECK
C        PROGRAMMER------ANTHONY MELODIA--------- --
C-------          APPLIED MATHEMATICS LABORATORY-------------
C-----DAVID TAYLOR MODEL BASIN, WASHINGTON D.C.---------- *
C--------TELEPHONE NUMBER---AREA CODE 301, 995-1514----------    *
C
C
      DIMENSION Z(2000),T(2000),S(2000),S2ND(2000),XOMEGA(2000),X(2000),
     1XDOT(2000),ALPHA(25),OSCIL(1000) ,VEL(1000),RESID(1000)
      EQUIVALENCE (RESID,X(1)),(VEL,X(1001))
      NAMELIST/ZAZA1/Z/ZAZA2/T,TZERO,                         H,      XO,N,
     1XDOTO,ISZ/ZAZA3/IP1,IP2,IP3,IP4,IP5/ZAZA4/ALPHA,NALPHA
      WRITE(6,900)
      PI=3.1415927
      READ(5,ZAZA1)
      READ(5,ZAZA2)
      READ(5,ZAZA3)
      READ(5,ZAZA4)
      IF(IP3)50,51,50
   50 IP1=0
      IP2=0
   51 CONTINUE
C
C---------- WRITE AND PLOT INPUT DATA----------- --
      DO 100 I=2,N
  100 T(I)=T(I-1)+H
      IF(ISZ)104,105,104
  104 WRITE(6,901)
      GO TO 106
  105 WRITE(6,902)
  106 CONTINUE
      WRITE(6,903) (Z(I),T(I),I=1,N)
      ZMIN=Z(1)
      ZMAX=Z(1)
      DO 110 I=2,N
      IF(ZMAX-Z(I))108,109,109
  108 ZMAX=Z(I)
      GO TO 110
  109 IF(ZMIN-Z(I))110,110,107
  107 ZMIN=Z(I)
  110 CONTINUE
      CALL CAMRAV(35)
      ZN=N
      DX=H*ZN/10.
      DY=(ZMAX-ZMIN)/10.
      CALL GRID1V(1,T(1),T(N),ZMIN,ZMAX,DX,DY,1,1,1,1,6,6)
      CALL APLOTV(N,T,Z,1,1,1,42,IERR)
      IF(IERR)115,116,115
  115 WRITE(6,904) IERR
  116 CONTINUE
      NN=N-1
      DO 120 I=1,NN
      CALL LINEV(NXV(T(I)),NYV(Z(I)),NXV(T(I+1)),NYV(Z(I+1)))
  120 CONTINUE
```

```
      CALL PRINTV(-15,15HTIME IN SECONDS,452,6)
      IF(ISZ)121,122,121
  121 CALL APRNTV(0,-14,-23,23HFOUNDATION ACCELERATION,4,696)
      GO TO 123
  122 CALL APRNTV(0,-14,-19,19HFOUNDATION VELOCITY,4,664)
  123 CONTINUE
C
C---------COMPUTE S(N) AND S2ND(N) FOR EACH TIME,T--------
      S(1)=Z(2)-Z(1)
      S2ND(1)=Z(3)-2.*Z(2)+Z(1)
      K=N-1
      DO 200 I=2,K
      S(I)=Z(I+1)-Z(I)
  200 S2ND(I)=Z(I+1)-2.*Z(I)+Z(I-1)
      WRITE(6,917) (I,S(I),S2ND(I),I=1,N)
C
  190 READ(5,920) FREQ1,FREQ2,DELTAF
      IF(ABS(FREQ1-FREQ2)-.1E-20) 801,801,191
  191 CONTINUE
      IF(IP3)192,195,192
  192 TEMP=FREQ2-FREQ1
      IF(AMOD(TEMP,DELTAF)-DELTAF/2.)193,194,194
  193 NOFREQ=TEMP/DELTAF
      GO TO 195
  194 NOFREQ=TEMP/DELTAF+1.0001
  195 CONTINUE
C------DAMPED OR UNDAMPED,IF UNDAMPED FIND NUMBER OF RESIDUAL POINTS--------
      DO 800 IX=1,NALPHA
      NIN=1
      INI=0
      FREQ=FREQ1
      IF(ABS(ALPHA(IX))-.1E-09)201,201,202
  201 IALPHA=1
      GO TO 222
  202 IALPHA=2
  222 GO TO (203,207),IALPHA
  203 TT=TZERO-T(1)
      IF(AMOD(TT,H)-H/2.)205,204,204
  204 KH=TT/H+1.000001
      GO TO 207
  205 KH=TT/H+.000001
  207 CONTINUE
C
C--------COMPUTE CONSTANTS------
      OMEGA=FREQ*2.*PI
      RADCAL=SQRT(1.-ALPHA(IX)**2)
      OH=OMEGA*H
      P=OMEGA*RADCAL
      EX=EXP(-ALPHA(IX)*OH)
      COSPH=COS(P*H)
      SINPH=SIN(P*H)
      A2OH=2.*ALPHA(IX)/OH
      RECOH=1./OH
      ALPHA2=ALPHA(IX)**2
      X12=1.-2.*ALPHA2
      FACT1=EX*SINPH/RADCAL
      FACT2=EX*COSPH+FACT1*ALPHA(IX)
      IF(ABS(FREQ)-.1E-20)220,220,221
  220 IFREQ=1
      GO TO 223
```

```
  221 IFREQ=2
  223 IF(ISZ)300,208,300
  208 GO TO (400,209),IFREQ
  209 CONTINUE
C
C------COMPUTEXOMEGA(N),XDOT FOR VELOCITY INPUT-----------
      GO TO(224,225),NIN
  224 XOMEGA(1)=OMEGA*XO
      FACT3=RECOH*(1.-FACT2)
      FACT4=RECOH*(.5-2.*ALPHA(IX)*RECOH+EX*((.5+2.*ALPHA(IX)*RECOH)
     1*COSPH-(X12*RECOH-ALPHA(IX)/2.)*SINPH/RADCAL))
      FACT5=EX*COSPH-ALPHA(IX)*FACT1
      FACT6=RECOH*FACT1
      FACT7=(RECOH**2)*(1.-EX*(COSPH+(ALPHA(IX)+OH/2.)*SINPH/RADCAL))
      XDOT(1)=XDOTO
      DO 210 I=2,N
      XOMEGA(I)=XOMEGA(I-1)*FACT2+XDOT(I-1)*FACT1-S(I-1)*FACT3-S2ND(I-1)
     1*FACT4
  210 XDOT(I)=-XOMEGA(I-1)*FACT1+XDOT(I-1)*FACT5-S(I-1)*FACT6-S2ND(I-1)*
     1FACT7
      GO TO 756
  225 CONTINUE
      KRO=KMX+KOOK
      KRA=KMN+KICK
      DO 235 I=2,5
      VA=I-1
      TA=VA*.2*H
      COSPT=COS(P*TA)
      SINPT=SIN(P*TA)
      EXT=EXP(-ALPHA(IX)*OMEGA*TA)
      FACTR1=EXT*(COSPT+ALPHA(IX)*SINPT/RADCAL)
      FACTR2=EXT*SINPT/RADCAL
      FACTR3=(1.-FACTR1)*RECOH
      FACTR4=(TA/H-.5-A2OH+(ALPHA(IX)/2.-X12*RECOH)*FACTR2+(.5+A2OH)
     1*EXT*COSPT)*RECOH
      XMAXO   =XOMEGA(KRO)*FACTR1+XDOT(KRO)*FACTR2-S(KRO)*FACTR3
     1-S2ND(KRO)*FACTR4
      IF(XMAX-XMAXO   )229,230,230
  229 XMAX=XMAXO
  230 XMINO   =XOMEGA(KRA)*FACTR1+XDOT(KRA)*FACTR2-S(KRA)*FACTR3
     1-S2ND(KRA)*FACTR4
      IF(XMIN-XMINO   )235,235,232
  232 XMIN=XMINO
  235 CONTINUE
      IIN=1
  211 IF(IP1)500,212,500
  212 IF(IP2)550,213,550
  213 IF(IP3)600,214,600
  214 IF(IP4)650,215,650
  215 IF(IP5)700,785,700
C
C------COMPUTE XOMEGA(N), XDOT(N), FOR ACCELRATION INPUT--------
  300 CONTINUE
      GO TO(350,305),IFREQ
  305 CONTINUE
      GO TO(308,325),NIN
  308 XOMEGA(1)=OMEGA*XO
      ECOS1=1.-EX*COSPH
      DFACT3=(1.-FACT2)/OMEGA
      DFACT4=(1.-A2OH*ECOS1-X12*FACT1*RECOH)/OMEGA
```

154

```
      DFACT5=(-4.*ALPHA(IX)-(2.*(1.-4.*ALPHA2)/OH-2.*ALPHA(IX))*FCOS1+
     1(X12+2.*ALPHA(IX)*(3.-4.*ALPHA2)/OH)*FACT1)*RECOH/(2.*OMEGA)
      DFACT6=(1.-ECOS1)-FACT1*ALPHA(IX)
      DFACT7=FACT1/OMEGA
      DFACT8=(1.-FACT2)*RECOH/OMEGA
      DFACT9=(2.-(1.+4.*ALPHA(IX)*RECOH)*ECOS1-(2.*X12*RECOH-ALPHA(IX))
     1*FACT1)*RECOH/(2.*OMEGA)
      XDOT(1)=XDOTO
      DO 310 I=2,N
      XOMEGA(I)=XOMEGA(I-1)*FACT2+XDOT(I-1)*FACT1-Z(I-1)*DFACT3-S(I-1)
     1*DFACT4-S2ND(I-1)*DFACT5
  310 XDOT(I)=-XOMEGA(I-1)*FACT1+XDOT(I-1)*DFACT6-Z(I-1)*DFACT7
     1          -S(I-1)*DFACT8-S2ND(I-1)*DFACT9
      GO TO 756
  325 CONTINUE
      KRO=KMX+KOOK
      KRA=KMN+KICK
      H2=H**2
      DO 335 I=2,5
      VA=I-1
      TA=VA*.2*H
      COSPT=COS(P*TA)
      SINPT=SIN(P*TA)
      EXT=EXP(-ALPHA(IX)*OMEGA*TA)
      FACTR1=EXT*(COSPT+ALPHA(IX)*SINPT/RADCAL)
      FACTR2=EXT*SINPT/RADCAL
      FACTR3=(1.-FACTR1)/OMEGA
      FACTR4=(TA/H-A2OH*(1.-EXT*COSPT)-X12*FACTR2*RECOH)/OMEGA
      FACTR5=(TA**2/H2-TA/H-(2.*(1.-4.*ALPHA2)*RECOH**2-A2OH)*
     1(1.-EXT*COSPT)+(X12*RECOH+2.*ALPHA(IX)*(3.-4.*ALPHA2)*RECOH**2)
     2*FACTR2)/(2.*OMEGA)
      XMAXO=XOMEGA(KRO)*FACTR1+XDOT(KRO)*FACTR2-Z(KRO)*FACTR3
     1-S(KRO)*FACTR4-S2ND(KRO)*FACTR5
      IF(XMAX-XMAXO  )329,330,330
  329 XMAX=XMAXO
  330 XMINO=XOMEGA(KRA)*FACTR1+XDOT(KRA)*FACTR2-Z(KRA)*FACTR3
     1-S(KRA)*FACTR4-S2ND(KRA)*FACTR5
      IF(XMIN-XMINO   )335,335,332
  332 XMIN=XMINO
  335 CONTINUE
      NIN=1
      GO TO 211
C
C------FREQ1=ZERO FOR FOUNDATION ACCELERATION---------
  350 GO TO(352,365),NIN
  352 XOMEGA(1)=X0
      XDOT(1)=XDOTO
      H2=H**2
      DO 360 I=2,N
      XOMEGA(I)=XOMEGA(I-1)+H*XDOT(I-1)-Z(I-1)*H2/2.-S(I-1)*H2/6.+
     1S2ND(I-1)*H2/24.
  360 XDOT(I)=-Z(I-1)*H-S(I-1)*H/2.+S2ND(I-1)*H/12.
      GO TO 756
  365 CONTINUE
      NIN=1
      GO TO 211
C
C------COMPUTE X, XDOT FOR OMEGA=ZERO-----VELOCITY INPUT
  400 GO TO(402,425),NIN
  402 XOMEGA(1)=X0
```

```
      XDOT(1)=XDOT0
      DO 410 I=2,N
      XOMEGA(I)=XOMEGA(I-1)+XDOT(I-1)*H-S(I-1)*H*.5+S2ND(I-1)*H/12.
  410 XDOT(I)=XDOT(I-1)-S(I-1)
      GO TO 756
  425 CONTINUE
      NIN=1
      GO TO 211
C
C---------PLOT X VS. T AND XDOT VS. T------------
  500 GO TO(505,510),IFREQ
  505 DO 506 I=1,N
  506 X(I)=XOMEGA(I)
      GO TO 518
  510 DO 515 I=1,N
  515 X(I)=XOMEGA(I)/OMEGA
  518   XMX=X(1)
        XDMX=XDOT(1)
        XMN=X(1)
        XDMN=XDOT(1)
      DO 530 I=2,N
      IF(X(I)-XMX )521,521,520
  520   XMX=X(I)
  521 IF(X(I)-XMN )522,523,523
  522   XMN=X(I)
  523 IF(XDOT(I)-XDMX )525,525,524
  524   XDMX=XDOT(I)
  525 IF(XDOT(I)-XDMN )526,530,530
  526   XDMN=XDOT(I)
  530 CONTINUE
      DY=(XMX -XMN )/10.
      CALL GRID1V(1,T(1),T(N),XMN, XMX, DX,DY,1,1,1,1,6,6)
      CALL APLOTV(N,T,X,1,1,1,42,IER)
      IF(IER)531,532,531
  531 WRITE(6,913) IER,FREQ
  532 NN=N-1
      DO 535 I=1,NN
      CALL LINEV(NXV(T(I)),NYV(X(I)),NXV(T(I+1)),NYV(X(I+1)))
  535 CONTINUE
      CALL PRINTV(-15,15HTIME IN SECONDS,452,6)
      CALL PRINTV(-23,23HFREQ=        CYCLES/SEC.,20,3)
      CALL LABLV(FRFQ,60,3,6,1,4)
      CALL PRINTV(-8,8HALPHA=   ,20,17)
      CALL LABLV(ALPHA(IX),72,17,6,1,1)
      CALL APRNTV(0,-14,-11,11HX   RESPONSE,4,600)
      DY=(XDMX -XDMN )/10.
      CALL GRID1V(1,T(1),T(N),XDMN, XDMX, DX,DY,1,1,1,1,6,6)
      CALL APLOTV (N,T,XDOT, 1,1,1,42,IERA)
      IF(IERA) 538,539,538
  538 WRITE(6,914) IERA,FREQ
  539 DO 540 I=1,NN
      CALL LINEV(NXV(T(I)),NYV(XDOT(I)),NXV(T(I+1)),NYV(XDOT(I+1)))
  540 CONTINUE
      CALL PRINTV(-15,15HTIME IN SECONDS,452,6)
      CALL PRINTV(-23,23HFREQ=        CYCLES/SEC.,20,3)
      CALL LABLV(FREQ,60,3,6,1,4)
      CALL PRINTV(-8,8HALPHA=   ,20,17)
      CALL LABLV(ALPHA(IX),72,17,6,1,1)
      CALL APRNTV(0,-14,-22,22HVELOCITY RESPONSE XDOT,4,688)
      GO TO 212
```

```
C
C---------PLOT Y(ACCELERATION) VS. TIME-----------
  550 CONTINUE
      GO TO(213,551),IFREQ
  551 CONTINUF
  560 DO 562 I=1,
  562 X(I)=-XOMEGA(I)*OMEGA
      XMX=X(1)
      XMN=X(1)
      DO 566 I=2,N
      IF(XMX -X(I))563,564,564
  566 XMX=X(I)
  564 IF(XMN -X(I))566,566,565
  565 XMN=X(I)
  566 CONTINUF
      DY=(XMX -XMN )/10.
      CALL GRID1V(1,T(1),T(N),XMN, XMX, DX,DY,1,1,1,1,6,6)
      CALL APLOTV(N,T,X,1,1,1,42,IERB)
      IF(IERB)570,571,570
  570 WRITE(6,919) IERB,FREQ
  571 NN=N-1
      DO 575 I=1,NN
      CALL LINEV(NXV(T(I)),NYV(X(I)),NXV(T(I+1)),NYV(X(I+1)))
  575 CONTINUE
      CALL PRINTV(-15,15HTIME IN SECONDS,452,6)
      CALL PRINTV(-23,23HFREQ=         CYCLES/SEC.,20,3)
      CALL LABLV(FREQ,60,3,6,1,4)
      CALL PRINTV(-8,8HALPHA=   ,20,)7)
      CALL LABLV(ALPHA(IX),72,17,6,1,1)
      CALL APRNTV(0,-14,-34,34HMINUS PSEUDO RESPONSE ACCELERATION,
     14,844)
      GO TO 214
C
C
C----*-- -       FOUR COORDINATE GRID------
  600 CONTINUE
      INI=1+INI
      OSCIL(INI)=FREQ
      VEL(INI)=AMAX1(ABS(XMAX),ABS(XMIN))
      GO TO (601,602),IALPHA
  601 RESID(INI)=SQRT(XOMEGA(KH)**2+XDOT(KH)**2)
      IF(RESID(INI)-.1E-19)604,604,602
  602 IF(FREQ-.1E-19)604,604,603
  603 IF(VEL(INI)-.1E-19)604,604,605
  604 NOFREQ=NOFREQ-1
      INI=INI-1
  605 IF(ABS(FREQ-FREQ2)-.1E-09)606,606,214
  606 CONTINUF
      CALL SMXYV(1,1)
      FRQSML=OSCIL(1)
      VELSML=VEL(1)
      RESSML=RESID(1)
      DO 616 I=2,NOFREQ
      IF(OSCIL(I)-FRQSML)611,612,612
  611 FRQSML=OSCIL(I)
  612 IF(VEL(I)-VFL SML)613,614,614
  613 VELSML=VEL(I)
  614 IF(RESID(I)-RESSML)615,615,616
  615 RESSML=RESID(I)
  616 CONTINUE
```

157

```
      ORDSML=AMINI(VELSML,RESSML)
C
C-------TO FIND THE LIMITS FOR THE (4X3) CYCLES------------
C
      IF(ALOG10(ORDSML))620,621,621
  620 LOGORD=ALOG10(ORDSML)-1.
      GO TO 622
  621 LOGORD=ALOG10(ORDSML)
  622 IF(ALOG10(FRQSML))623,624,624
  623 LOGFRQ=ALOG10(FRQSML)-1.
      GO TO 625
  624 LOGFRQ=ALOG10(FRQSML)
  625 ORDSML=10.**LOGORD
      OROLG=ORDSML*10.**4
      FRQSML=10.**LOGFRQ
      FRQLG=FRQSML*10.**3
C-----PLOT LOG-LOG GRID FOR VELOCITY VS FREQUENCY-------
      CALL GRIDIV(1,FRQSML,FRQLG,ORDSML,ORDLG,1.0,1.0,1,1,1,1,-2,-2)
C-----TO FIND LARGEST 1X10 TO THE PTH POWER LINE FOR X--------
      OMSTRT=2.*PI*FRQSML
      TEMP=ALOG10(ORDLG/OMSTRT)
      IF(TEMP)627,628,628
  627 LCP=TEMP-1.
      GO TO 629
  628 LOP=TEMP
  629 D1=10.**LOP
      V1=OMSTRT*D1
      WIG=10.*ORDSML
      XMARGN=NXV(FRQLG)-NXV(FRQSML)
      YMARGN=NYV(ORDLG)-NYV(WIG)
      SLOPE=YMARGN/XMARGN
      IXCOR=4+NXV(FRQSML)
      CALL PRINTV(-1,1HD,IXCOR,NYV(V1))
      CALL PRINTV(-2,2HD=,900,17)
      CALL LABLV(D1,924,17,-2,1,3)
C------DRAW LINES UP FROM V1-----------
      VIS=0.
      DO 632 I=1,9
      VIS=VIS+V1
      IF(ORDLG-VIS)647,630,630
  630 XTCH=NYV(ORDLG)-NYV(VIS)
      ITCH=XTCH/SLOPE
      ITCH=NXV(FRQSML)+ITCH
      KITCH=NYV(ORDLG)
      CALL LINEV (NXV(FRQSML),NYV(VIS),ITCH,KITCH)
  632 CONTINUE
C-------DRAW LINES FROM V1 DOWN----------
  647 DO 638 J=1,20
      LAL=LOP-J
      LAN=LAL+1
      DLAN=10.**LAN
      DLAL=10.**LAL
      DO 638 I=1,9
      FFTI=I
      VIS=OMSTRT*DLAN-OMSTRT*DLAL*EFTI
      IF(VIS-ORDSML)639,633,633
  633 KITCH=NYV(ORDLG)-NYV(VIS)
      IYMARG=YMARGN
      IF(IYMARG-KITCH)635,634,634
  634 ZITCH=KITCH
```

158

```
      ITCH=ZITCH/SLOPE
      GO TO 637
  635 ITCH=XMARGN
      YITCH=YMARGN
  637 ITCH=(ITCH+NXV(FRQSML)
      KITC= K(TC +NYV(VIS)
      CALL LINEV (NXV(FRQSML),NYV(VIS),ITCH,KITCH)
C 9 CONTINUE
C- ---DRAW FROM THE RIGHT ORDINATE THE REMAINING X-LINES-----
  639 OMLAST=2.*PI*FROLG
      LEFT2=J
      LEFT1=EFT1
      DO 641 J=LEFT2,30
      LAL=LOP-J
      LAN=LAL+1
      DLAN=10.**LAN
      DLAL=10.**LAL
      DO 640 I=LEFT1,9
      EFT1=I
      VIS=OMLAST*DLAN-OMLAST*DLAL*EFTI
      IF(VIS-ORDSML)642,636,636
  636 KITCH=NYV(VIS)-NYV(ORDSML)
      CAPT=KITCH
      ITCH=CAPT/SLOPE
      ITCH=NXV(FRQLG)-ITCH
      KITCH=NYV(ORDSML)
      CALL LINEV (NXV(FRQLG),NYV(VIS), ITCH, KITCH)
  640 CONTINUE
      LEFT1=1
  641 CONTINUF
  642 CONTINUE
C---------PLOT POINTS--------
      CALL APLOTV(NOFREQ,OSCIL,VEL,1,1,1,44,LIT)
      IF(LIT)643,644,643
  646 WRITE(6,922) LIT,ALPHA(IX)
  644 GO TO (648,646),IALPHA
  648 CALL APLOTV(NOFREQ,OSCIL,RESID,1,1,1,38,KIT)
      CALL PRINTV(-28,28HOOO =RESIDUAL SHOCK SPECTRUM,NXV(FRQSML),1006
      IF(KIT)645,646,645
  645 WRITE(6,923) KIT,ALPHA(IX)
  646 CONTINUE
      CALL PRINTV(-15,15HFREQUENCY (CPS),452,6)
      CALL APRNTV(0,-14,-8,8HVELOCITY,9,576)
      CALL PRINTV(-8,8HALPHA=  ,20,17)
      CALL LABLV(ALPHA(IX),72,17,6,1,1)
      CALL PRINTV(-19,19H*** =SHOCK SPECTRUM,NXV(FRQSML),1015)
C------- --  GENERATION OF ACCELERATION GRID-------
C---------- TO FIND A1------------
      TEMP=ALOG10(ORDSML*OMSTRT)
      IF(TEMP)850,851,851
  350 LOP=TEMP
      GO TO 853
  851 LOP=TEMP+1.
  853 A1=10.**LOP
      V1=A1/OMSTRT
      CALL PRINTV(-1,1HA,IXCOR,NYV(V1))
      CALL PRINTV(-2,2HA=,900,4)
      CALL LABLV(A1,924,4,-2,1,3)
C------DRAW LINES DOWN FROM A1-------
      KITCH=NYV(ORDSML)
```

159

```
      DO 856 I=1,9
      FFT1=I-1
      VIS=V1*(1.-.1*EFT')
      IF(ORDSML-VIS)855,855,857
  855 XTCH=NYV(VIS)-NYV(ORDSML)
      ITCH=XTCH/SLOPE
      ITCH=ITCH+NXV(FROSML)
      CALL LINEV (NXV(FROSML),NYV(VIS),ITCH, KITCH)
  856 CONTINUE
C---------DRAW LINES FROM A1 UP-------------
  857 DO 870 J=1,20
      LAN=LOP+J-1
      ALAN=10.**LAN
      DO 870 I=2,10
      FFT1=I
      VIS=ALAN/OMSTRT*EFT1
      IF(VIS-ORDLG)858,858,871
  858 KITCH=NYV(VIS)-NYV(OPDSML)
      IYMARG=YMARGN
      IF(IYMARG-KITCH)862,861,861
  861 ZITCH=KITCH
      ITCH=ZITCH/SLOPE
      KITCH=NYV(ORDSML)
      GO TO 868
  862 ITCH=XMARGN
      KITCH=NYV(VIS)-IYMARG
  868 ITCH=ITCH+NXV(FROSML)
      CALL LINEV (NXV(FROSML),NYV(VIS),ITCH, KITCH)
  870 CONTINUF
C--------DRAW FROM THE RIGHT ORDINATE ,REMAINING A-LINES---------
  871 LEFT2=J
      LEFT1=EFT1
      KITCH=NYV(ORDLG)
      DO 875 J=LEFT2,30
      LAN=LOP+J-1
      ALAN=10.**LAN
      DO 874 I=LEFT1,10
      EFT1=I
      VIS=ALAN/OMLAST*EFT1
      IF(VIS-ORDLG)872,872,876
  872 CAPT=NYV(ORDLG)-NYV(VIS)
      ITCH=CAPT/SLOPE
      ITCH=NXV(FROLG)-ITCH
      CALL LINEV (NXV(FROLG),NYV(VIS), ITCH,KITCH)
  874 CONTINUF
      LEFT1=2
  875 CONTINUE
  876 CONTINUE
      GO TO 214
C
C---------- SHORT FORM----------
  650 CONTINUE
      IF(ABS(FREQ-FREQ1)-.1E-04)651,651,652
  651 WRITE(8,912) ALPHA(IY)
  652 GO TO(658,655),IALPHA
  655 XOMAX=AMAX1(ABS(XMAX),ABS(XMIN))
      GO TO(668,669),IFREQ
  658 RMAX=SQRT(XOMEGA(KH)**2+XDOT(KH)**2) .
      XOMAX=AMAX1(ABS(XMAX),ABS(XMIN),ABS(RMAX))
      GO TO(681,678),IFREQ
```

160

```
      668 WRITE(8,906) FREQ,XOMAX
          GO TO 215
      669 WRITE(8,905) FREQ,XOMAX
          GO TO 215
      678 WRITE(8,907) FREQ,XOMAX,RMAX
          GO TO 215
      681 WRITE(8,908) FREQ,XOMAX,RMAX
          GO TO 215
C
C---------LONG FORM---------
      700 CONTINUE
          IF(ABS(FREQ-FREQ1)-.1F-04)701,701,702
      701 WRITE(6,915) ALPHA(IX)
      702 GO TO(704,705),IALPHA
      704 RMAX=SQRT(XOMEGA(KH)**2+XDOT(KH)**2)
          GO TO(743,742),IFPEQ
      705 GO TO(726,727),IFPEQ
      726 WRITE(6,916) FREQ,XMAX,XMIN
          GO TO 785
      727 WRITE(6,910) FREQ,XMAX,XMIN
          GO TO 785
      742 WRITE(6,910) FREQ,XMAX,XMIN,RMAX
          GO TO 785
      743 WRITE(6,911) FREQ,XMAX,XMIN,RMAX
          GO TO 785
C
C--------PRELIMINARY CALCULATIONS FOR MIN. AND MAX. RESPONSE---------
      756 GO TO (758,757),IALPHA
      757 NX=N
          GO TO 759
      758 NX=KH
      759 XMAX=XOMEGA(1)
          KMX=1
          XMIN=XOMEGA(1)
          KMN=1
          DO 760 I=2,NX
          IF(XMAX-XOMEGA(I))761,762,762
      761 XMAX=XOMEGA(I)
          KMX=I
      762 IF(XMIN-XOMEGA(I))760,765,765
      765 XMIN=XOMEGA(I)
          KMN=I
      760 CONTINUE
          IF(KMX-1)771,770,771
      770 KMX=KMX+1
      771 IF(KMX-NX)773,772,773
      772 KMX=KMX-1
      773 IF(KMN-1)775,774,775
      774 KMN=KMN+1
      775 IF(KMN-NX)777,776,777
      776 KMN=KMN-1
      777 CONTINUE
          IF(XDOT(KMX-1)*XDOT(KMX))778,778,779
      778 KOOK=-1
          GO TO 781
      779 KOOK=0
      781 CONTINUF
          IF(XDOT(KMN-1)*XDOT(KMN))783,783,784
      783 KICK=-1
          GO TO 950
```

```
    784 KICK=0
    950 NIN=2
        GO TO 207
C
C-------EITHER RESTART WITH NEW FREQ. OR RESTART WITH NEW ALPHA OR STOP
    785 CONTINUE
        IF(ABS(FREQ-FREQ2)-.1E-03)800,755,755
    755 FREQ=FREQ+DELTAF
        GO TO 207
    800 CONTINUE
        GO TO 190
    801 WRITE(6,909)
        CALL FRAMEV
        STOP
C
    900 FORMAT(1H1,49X,22HSHOCK SPECTRUM PROGRAM//50X,21HAPPLIED MATH LAB
       1DTMB,///)
    901 FORMAT(40X,38HFOUNDATION ACCELERATION VS TIME(INPUT)//18X,23HFOUND
       1ATION ACCELERATION,36X,15HTIME IN SECONDS)
    902 FORMAT(42X,35HFOUNDATION VELOCITY VS TIME (INPUT)//20X,19HFOUNDATI
       1ON VELOCITY,35X,15HTIME IN SECONDS)
    903 FORMAT(1X,F35.9, 44X,F20.9)
    904 FORMAT(47H  PLOTTING ERROR NUMBER OF POINTS OUT OF RANGE=,I2//)
    905 FORMAT(15X,F10.5,29X,F12.7)
    906 FORMAT(10X,11HFIRST FREQ=,F10.5,7X,13HMAX RESPONSE=,F12.7/)
    907 FORMAT(15X,F10.5,2(29X,F12.7))
    908 FORMAT(10X,11HFIRST FREQ=,F10.5,7X,13HMAX RESPONSE=,F12.7,12X,
       117HMAX RES RESPONSE=,F12.7)
    909 FORMAT(///38X,25HPROGRAM RAN TO COMPLETION)
    910 FORMAT(10X,F10.5,3(18X,F12.7))
    911 FORMAT(5X,11HFIRST FREQ=,F10.5,9X,9HMAX RESP=,F12.7,10X,9HMIN RESP
       1=,F12.7,7X,15HMAX RESID RESP=,F12.7)
    912 FORMAT(1H1,55X,10HSHORT FORM//45X,20HDAMPING COEFFICIENT=,F10.8///
       1/9X,22HFREQUENCY(CYCLES/SEC.),19X,20HMAX RESPONSE X OMEGA,18X,26HM
       2AX RESID RESPONSE X OMEGA)
    913 FORMAT(59H  PLOTTING ERROR FOR X VS T, NUMBER OF POINTS OUT OF RAN
       1GE=,I2,6H FREQ=,F10.7//)
    914 FORMAT(1X,I2,43H POINTS OUT OF RANGE FOR XDOT VS TIME,FREQ=,F10.7
       1//)
    915 FORMAT(1H1,55X,9HLONG FORM//45X,20HDAMPING COEFFICIENT=,F10.8////
       117X,16HFREQ(CYCLES/SEC),12X,20HMAX RESPONSE X OMEGA,10X,20HMIN RESP
       2ONSE X OMEGA,8X,22HMAX RESID RESP X OMEGA)
    916 FORMAT(4X,11HFIRST FREQ=,F10.5,10X,9HMAX RESP=,F12.7,10X,9HMIN RES
       1P=,F12.7)
    917 FORMAT(1H1,18X,1HI,38X,4HS(I),34X,7HS2ND(I)//
       1(17X,I4,34X,F12.7,28X,F12.7))
    918 FORMAT(1H1,50X,19HINTERMEDIATE VALUES/19X,1HI,35X,9HXOMEGA(I),
       151X,7HXDOT(I)//
       2(17X,I3,34X,F12.7,28X,F12.7))
    919 FORMAT(1X,I2,43H POINTS OUT OF RANGE FOR Y    VS TIME,FREQ=,F10.7
       1//)
    920 FORMAT(3F20.8)
    921 FORMAT(6F15.6)
    922 FORMAT(1X,I2,49H POINTS OUT OF RANGE FOR VEL VS. FREQ WITH ALPHA=,
       1F10.8)
    923 FORMAT(1X,I2,50H POINTS OUT OF RANGE FOR RESIDUAL PLOT WITH ALPHA=
       1,  F10.8)
        END
```

*   *   *

162

TRANSPORTATION ENVIRONMENTAL MEASUREMENT
AND RECORDING SYSTEM

Frank J. Holley
NASA Goddard Space Flight Center
Greenbelt, Maryland

The newly developed Transportation Environmental Measurement and Recording System (TEMARS) is a complete, unified system for the measurement of critical environmental parameters. It can operate continuously and unattended for over two weeks. The primary considerations in the system design were economy, universal compatibility, maximum reliability, and practical weight, volume, and power consumption. To meet these requirements, most of the electronics are molecular electronic devices which convert analog data from transducers into preanalyzed digital form for recording in IBM computer-compatible format on a cartridge incremental digital tape recorder. The recorded information includes the direction, magnitude, duration, and time occurrence of transient vibration or shock above predetermined threshold levels, as well as periodic measurements of quasi-static phenomena such as temperature and humidity. The existing system is based on using triaxial piezoresistive accelerometers with dc response to time duration measurements of 2 msec and three low-speed data channels for the periodic recording of quasi-static environmental data. The volume of the system is slightly over 1 cu ft with a weight of approximately 35 lb. Over 100,000 complete sets of data can be recorded with the present 300-ft tape recorder capacity.

F. J. Holley

INTRODUCTION

One of the major problems in military and space programs is the determination of environmental parameters in the handling and shipment of specific or sensitive equipment by the four primary modes of transportation [1]. Many methods and types of measurement equipment have been developed to obtain significant data relative to transportation environment. Previous approaches to this basic problem range from the use of simple mechanical shock measurement devices which only indicate that some preset shock level has been exceeded to large complex analog or digital acquisition systems. Often these systems require a full-time instrumentation crew and sometimes an auxiliary carrier [2] to accommodate the equipment and personnel (Fig. 1). The simple devices, even with various recording schemes [3], cannot adequately measure or define the various modes of transportation environment, while the large systems require considerable expenditure in time, equipment, and personnel and usually can only be justified for a limited number of major or priority projects (Fig. 2).

After a careful survey of available methods and equipment, the design and development of a new unified system was deemed necessary to meet basic requirements for obtaining in-transit environmental data during all handling and transportation modes. The design and development of the TEMARS was initiated by Goddard Space Flight Center under contract with the Endevco Corporation.

163

Fig. 1 - Instrumentation van and spacecraft transporter
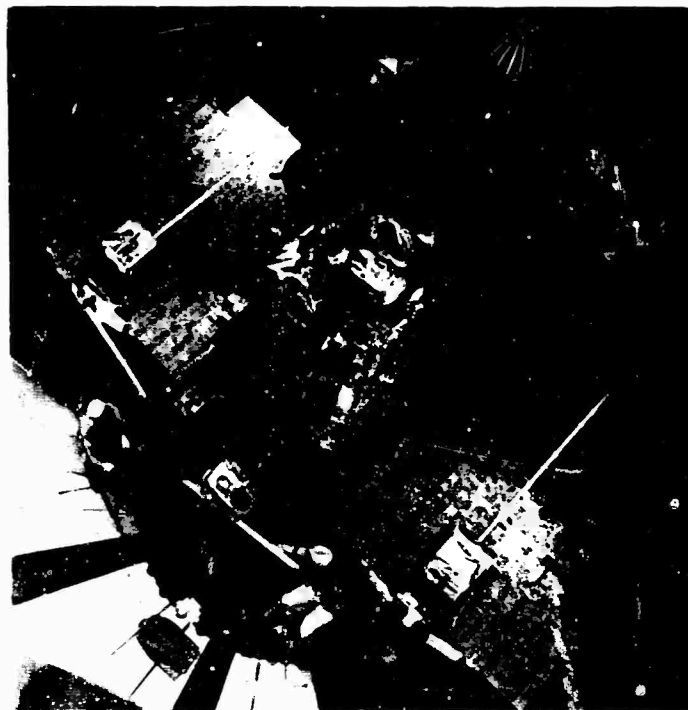
Fig. 2 - OGO spacecraft

The basic considerations in the design of the TEMARS required a self-contained unattended system for the automatic measurement and digital recording of significant time—correlated in-transit environmental parameters for periods of more than two weeks. The direction, magnitude, duration, and time of occurrence of acceleration data above selected levels would be automatically recorded on magnetic tape in IBM computer-compatible format. Quasi-static data, such as temperature and humidity, would also be recorded at periodic intervals.

SYSTEM DESCRIPTION

The TEMARS is a self-contained digital recording system in a portable metal housing, as shown in Fig. 3, measuring $14-1/8 \times 15-5/8 \times 11$ in. and weighing 35 lb. For installation in locations subject to high shock, a special shock isolation fixture can be used as shown in Fig. 4. The functional equipment of the system consists of the following major items: accelerometers, auxiliary transducers, electron unit, magnetic tape recorder, and power source.

164
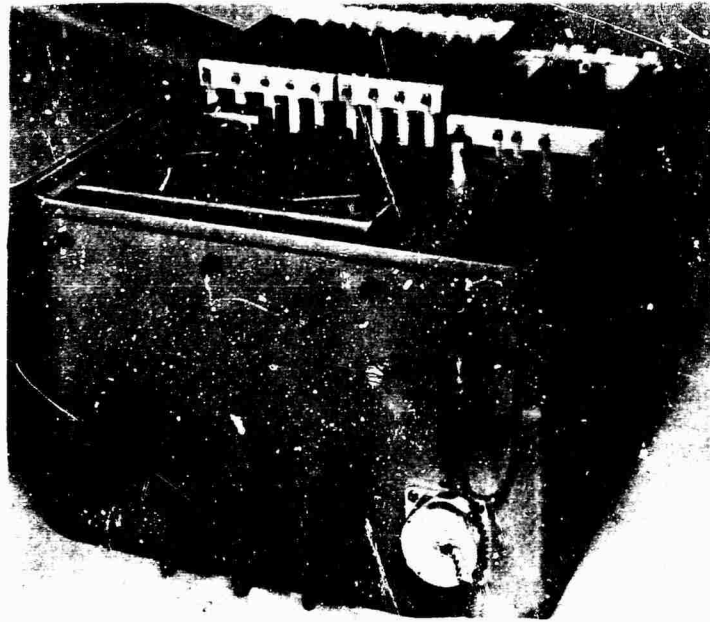
Fig. 3 - TEMARS recording system
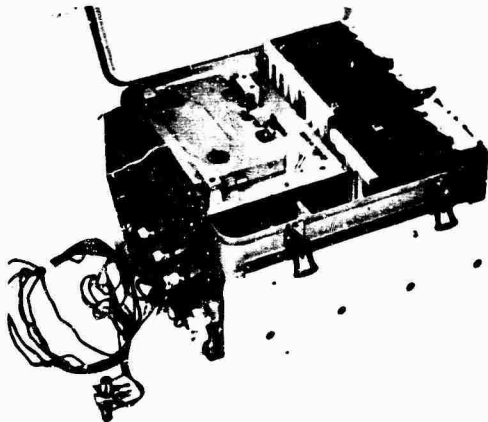
Fig. 4 - TEMARS with shock isolation
fixture and accelerometers

Fig. 5 - Triaxially mounted piezo-
resistive accelerometer

The accelerometers, as shown in Fig. 5,
are piezoresistive strain gages [4, 5] that are
normally mounted remotely in a triaxial config-
uration. They are the Endevco model 2262 [6]
with a flat frequency response between 0 and
750 Hz, and they weigh 28 gm (1.0 oz.).

Four auxiliary transducers or inputs can
be selected by the user to meet his special en-
vironmental measurement requirements for

165

quasi-static data such as temperature and humidity. Other parameters such as speed or mileage could also be recorded at periodic intervals.

The electronics unit contains all electronic circuits to condition, sample, digitize, and provide recorder outputs for triaxial acceleration and auxiliary transducer measurements. Maximum use of solid state devices and integrated circuits, as shown in Fig. 6, provides great reliability with minimum size, weight, and power consumption. All electronics are contained in a card cage assembly with the following replaceable printed circuit card modules:

1. Three conditioning amplifier modules containing the x-, y-, and z-axes accelerometer amplifiers, scaling and threshold controls, and threshold sensing circuits;

2. Two dual conditioning amplifier modules containing sensitivity and range controls for the auxiliary transducer channels;

3. Memory card module containing the diode logic, polarity memory, pulse width-to-amplitude converter, and multiplex circuits;

4. Programmer module containing the sampling commander and analog-to-digital converter circuits;

5. Output write gate module containing the analog-to-digital clock, output memory register, and write logic circuits;

6. Time register module containing the Accutron clock mechanism and time register circuits; and

7. Power supply module consisting of a wired-in assembly which generates the five voltages necessary for the operation of the system.

The magnetic tape recorder is a 7-track incremental digital recorder [6], Kennedy Corp; model 340 SE. It records on a 300-ft magnetic tape cartridge at a packing density of 200 7-bit characters per inch at a maximum speed of 200 characters per second. Special low-power circuitry is incorporated for the standby or the quiescent mode of operation.

The power source is presently an external 12-v storage battery with a 120-amp-hr capacity to provide system operation for more than two weeks. The transportation vehicle's standard automotive battery could be used to meet TEMARS power source requirements. An internal rechargeable Ni-Cd or Ag-Cd battery is now in the design stage to meet requirements for either interim handling operations or complete self-contained operation for the entire transportation period.

SYSTEM OPERATION

The TEMARS system provides for input signals from triaxial piezoresistive accelerometers and responds only when an acceleration
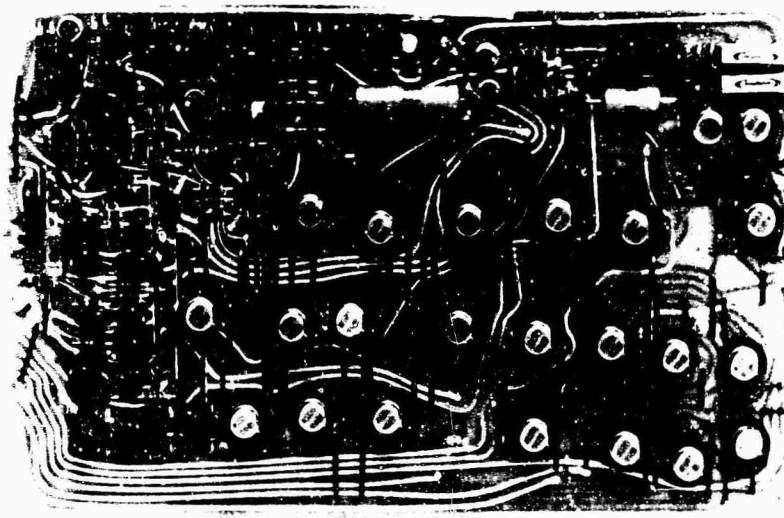

Fig. 6 - Programmer module

166

along any axis exceeds a preset threshold level. When this threshold is exceeded, the polarity, peak amplitude, and time duration of the shock pulse are stored in analog form in channel A. After the shock input has passed, these data, for each of three axes, are converted to digital form and the digitized values are recorded in IBM-compatible format on the integral incremental magnetic tape transport.

To preserve a history of closely spaced shock impulses, a second analog storage channel B retains the peak amplitudes, polarities, and time duration of a second shock pulse which may occur during the 20-msec time period the data in the first channel are being digitized and recorded.

The internal clock mechanism also triggers an alternate recording cycle at 15-min intervals. At this time, quasi-static input data from the auxiliary transducers such as temperature or humidity sensors are digitized and recorded. This alternate cycle also permits the time history of shock data to be resolved to ±7.5 min.

Figure 7 shows the functional block diagram of the TEMARS system. Shock data from the input accelerometers are amplified by the signal conditioners (Fig. 8, which provide normal (X) and inverted complementary (X) outputs. Scaling controls in these signal conditioning circuits permit full-scale output of ±5 v to correspond to input levels ranging from 5 to 30 g in six steps. Threshold controls in each circuit allow the lower level threshold to be varied from 5 to 50 percent of selected full-scale range in ten steps.

If the input shock on any of three axes exceeds the preset threshold value, as determined by the threshold detector circuits, the input signal polarity is detected by the polarity sensing circuits which, in turn, control the diode gates. These diode gates select either the normal or the inverted signal conditioner outputs on each of the three axes to provide a positive analog signal output regardless of input polarity to accommodate the analog-to-digital converter. Simultaneously, the three input signal polarities are stored in the polarity memory.

The positive output signal from each of the diode logic circuits is peak detected, and the peak analog values are maintained on storage capacitors C_{xa}, C_{ya}, C_{za}.

When the initial input signal exceeds the threshold level, a gate signal is generated and maintained until the input falls below the

threshold. This gate signal, in the pulse width-to-analog converter, causes a constant current generator to charge a capacitor C_{va} linearly. At the end of the input shock period, the voltage value stored on the capacitor is proportional to the time duration of the input shock signal.

The basic analog storage cycle is now complete, and digital processing of the four signals (X, Y, Z and time) now begins, as shown in Fig. 9. To permit the capture of other input data which may occur before processing is complete, the A and B channel switch is now set. This circuit enables a duplicate memory consisting of a portion of the polarity memory, C_{xb}, C_{yb}, C_{zb}, and their associated control circuits.

Processing of each of the four stored analog signals occurs sequentially under the control of the sampling commander. The program sequence consists of converting the value on C_{xa} to digital form, recording on magnetic tape, and then converting the value on C_{ya} to digital form, etc.

If a second input occurs, its peak values stored on C_{xb}, C_{yb}, C_{zb}, and C_{wb} are then inserted into the output format immediately following the first values. If no second event occurs, the program cycle terminates.

The stored analog data are switched, one variable at a time to the input of the analog-to-digital converter. The data are then converted to digital form by generating a linear sawtooth voltage concurrent with a 100-kHz clock pulse train. The clock pulses are accumulated in a counter, which starts at the beginning of the linear waveform and stops when the amplitude of the sawtooth equals the amplitude of the stored voltage. Thus, the value standing in the counter at the end of the conversion cycle is proportional to the amplitude of the input voltage.

At the completion of the conversion cycle, the digital data are transferred to the memory register, where they form 5 bits of the output word. The 6th bit, controlled by the sampling commander, corresponds to the polarity of the digitized signal. Time is digitized to 6-bit accuracy since no sign indication is required. These 6 bits form one word of the output data and are recorded in parallel on magnetic tape. A parity bit, selected by the recorder to make the total number of recorded bits an odd number, is added in the 7th bit position by the recorder circuits.

Quasi-static data such as temperature and humidity are sampled and converted every 15
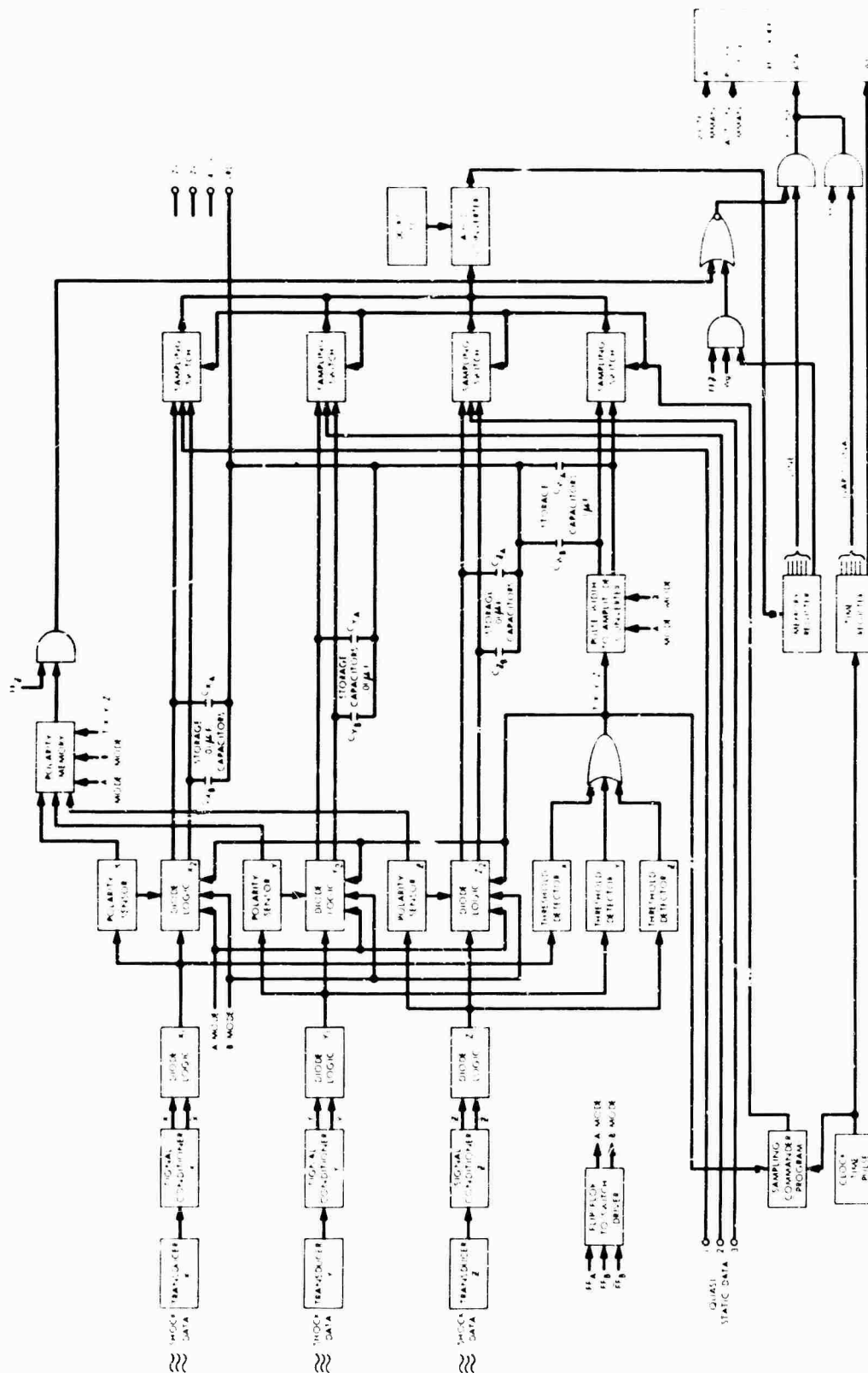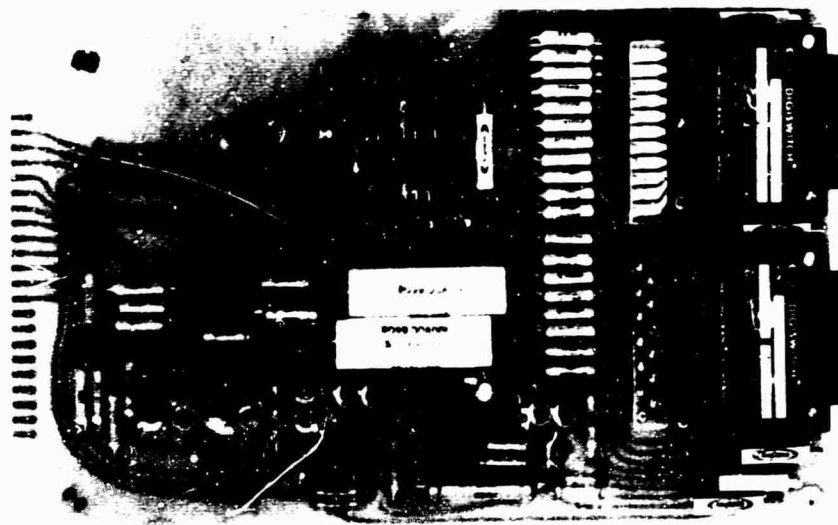
Fig. 7 - TEMARS functional diagram

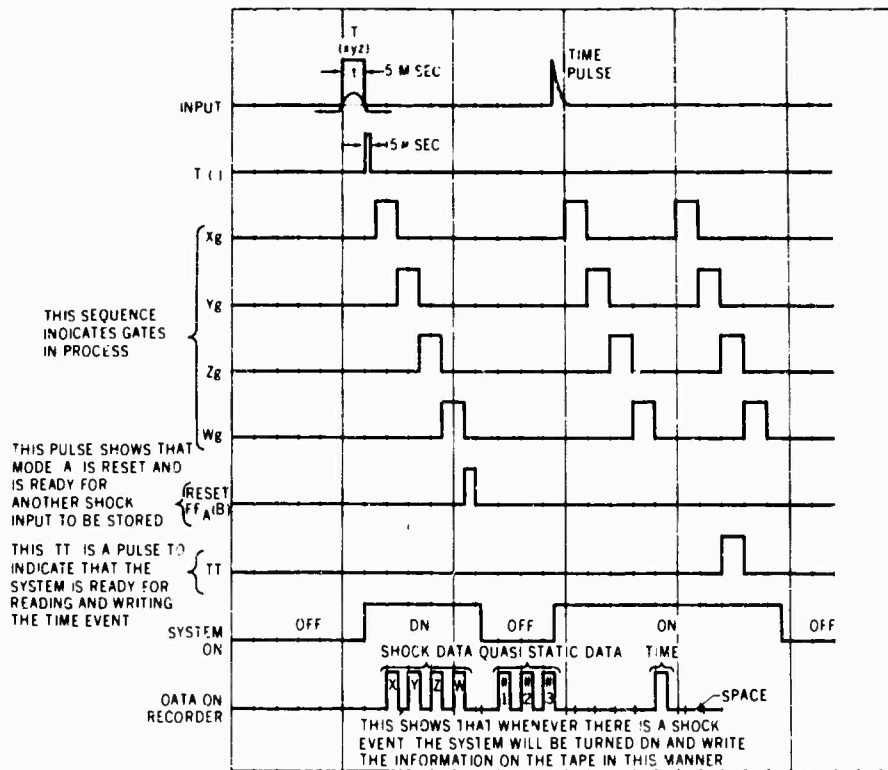Fig. 8 - Accelerometer signal conditioner

Fig. 9 - TEMARS time program

169

min under control of the sampling commander. At 15-min intervals, the integral Accutron clock mechanism (Fig. 10) provides a command to the commander which, in the absence of shock data, generates an alternate program to sample each of the quasi-static inputs sequentially and record their digital values on tape, along with the contents of the time register.

The 15-min clock pulses are accumulated in the time register, which resets to zero after 48 input pulses, the equivalent of 12 hr. This counter reset pulse sends a signal to the recorder gap generator, which generates a 3/4-in. interrecord gap on tape to aid in computer processing and time identification.

SYSTEM PERFORMANCE

The primary factor affecting overall system performance is presently related directly to the magnetic tape recorder. With the present 7-track incremental digital magnetic tape recorders, TEMARS performance specifications are as follows:

1. Shock Data

a. Amplitude ranges — normal sensitivity (12-v transducers excitation voltage), ranges of 5, 7.5, 10, 15, 20, and 30 g full scale; 2 × sensitivity (24-v transducer excitation voltage),

ranges of 2.5, 3.75, 5, 7.5, 10, and 15 g full scale. The full scale of each gain range corresponds to a full-scale binary number of 31 (5 bits) with the 6th bit indicating polarity and the 7th bit for parity. The resolution is 3.3 percent with an accuracy of ±1 part in 31 of full scale.

b. Duration — 126 msec full scale corresponding to a binary number of 63 (6 bits) without polarity indication. The resolution is 1.67 percent with an accuracy of ±1 part in 63 of full scale.

c. Threshold level — ten selective threshold levels in 5 percent increments from 5 to 50 percent of full scale within a tolerance of ±2 percent on each level.

2. Quasi-Static Data

Provisions for up to 4 channels of data with a 5-v full scale corresponding to the binary number 63 (6 bits) and a resolution of 1.67 percent of full scale with an accuracy of ±1 part in 63 of full scale.

3. Time

An internal clock generates 15-min time pulses, with a nominal accuracy of ±1.5 sec/day, which are recorded on the tape with the quasi-static data. A 3/4-in. interrecord gap is generated every 12-hr time period.

Fig. 10 - Time register module

4. Data Storage Capacity

The magnetic tape cartridge accommodating 300 ft of 1/2-in. tape provides for the storage of 720,000 7-bit characters or approximately 100,000 sets of recorded data.

FUTURE PERFORMANCE CAPABILITY

The present performance of TEMARS can be increased in accuracy, resolution, speed, and storage capability by the use of an incremental digital recorder compatible with the new IBM 360 computer system. Characteristics of two recorders are compared in Table 1. As indicated, performance can be improved by a factor of 3 to 16 with the availability of these recorders for TEMARS.

CONCLUSIONS

The design concepts of TEMARS enable acquisition of significant data on the environmental conditions encountered during the transportation of critical or sensitive equipment. Most additional or specialized requirements can be readily accommodated with only minor modification or replacement of an existing module. Each item in the system, from transducer to recorder, takes advantage of available equipment

TABLE 1
IBM Computer-Compatible Formats

Characteristics	Standard[a]	360[b]
Tape tracks	7	9
Information density (characters/in.)	200	800
Recording speed (characters/sec)	200	600
Tape supply (ft)	300	1200[c]

[a] TEMARS incremental digital magnetic tape recorder (cartridge).
[b] Design goals for recorders now under development.
[c] Reel.

to provide a completely unified and compact system that is compatible with standard computer data reduction and analysis techniques.

ACKNOWLEDGMENTS

REFERENCES

1. R. W. Schock and W. E. Paulson, "A Survey of Shock and Vibration Environments in Four Major Modes of Transportation," Shock and Vibration Bull. No. 35, Part 5, pp. 1-19, Feb. 1966

2. H. E. Krachman, "The Vibration Monitoring of the OGO-C Spacecraft During Transportation to WTR," TRW Rept. 2322-6017-RU-000, Oct. 1965

3. J. W. Schlue, "The Dynamic Environment of Spacecraft Surface Transportation," Shock and Vibration Bull. No. 35, Part 5, pp. 21-36, Feb. 1966

4. D. E. Lovelace, "Development and Application of a Piezoresistive Strain Gage Accelerometer," J. Environ. Sci., Vol. 7, No. 16, 1964

5. W. E. Wall, "Piezoresistive Strain Gage Accelerometers Increase Spectrum of Shock and Vibration Measurements," Shock and Vibration Bull. No. 35, Part 4, pp. 17-20, Feb. 1966

6. W. E. Wall, "Piezoresistive Strain Gage Accelerometers With Subcritical Damping and High Overload Capabilities," Proc. 12th Nat. ISA Aerospace Symp., p. 269-274, May 1966

BIBLIOGRAPHY

Cromer, E. G., Jr., "Incremental Magnetic Tape Recorders," Electronic Instrument Dig., pp. 7-12, Aug. 1966

DISCUSSION

Mr. Venetos (USA Natick Laboratories): How long will the recorder ope. ate before the batteries have to be recharged?

Mr. Holley: Operation is based on a storage battery supply, and the recorder will run more than one week on 120 mamp 'hr. With a design change and using integrated circuits, we hope to reduce the current drain considerably.

Mr. Venetos: Will the recorder also measure humidity?

Mr. Holley: Yes.

Mr. Venetos: Have you selected a humidity transducer yet?

Mr. Holley: We are presently considering a hydrodynamic transducer, mainly because it will operate off the existing power supply without any modification. The input to the analog-to-digital converter in this system requires a high-volt signal, and this would provide a 5-v output.

Mr. Rommel (Lockheed-California Co.): What g level did you use as a threshold to trigger the recorder?

Mr. Holley: The threshold is variable.

Mr. Rommel: What did you use on the OGO?

Mr. Holley: The OGO had a specification essentially based on a probability figure. The maximum duration they were concerned with roughly was under 5 g at 95 percent. The example I have given in OGO was taken from a Goddard requirement to obtain environmental data during shipment. In other words, this recorder presently is scheduled for shipment on the Isis satellite from Montreal, but it has not been used on the OGO project.

Mr. Rommel: Would 1/2 g be a nominal threshold level?

Mr. Holley: Between 1/2 and 1 g is probably a realistic level, depending on the quantity of data and the fineness of resolution desired. There has been work done on Saturn, for example, with a maximum level of less than 1-1/2 g, so the resolution of the instrument would be considerable, from 1/2 to 1-1/2 g. It depends on the project requirements. For a survey, you would probably want the maximum dynamic range and resolution without running out of tape before the time had elapsed.

Mr. Rommel: What frequency response were you able to acquire with this system?

Mr. Holley: The basic system is limited in the period measurement for a binary number of 63, that is, from 2 to 120 msec resolving power. With the other recording system, we shall go probably from 2 to 512 msec, but the electronics are not frequency limited and the accelerometer we are using could record accurately down to approximately 1-msec duration.

Mr. Rommel: And the tape recorder?

Mr. Holley: The tape recorder is limited only by the time it takes to process the data. Presently it takes 20 msec to complete 3 channels. With higher stepping, we could shorten the time to 5 msec. Data that come in while we are processing the information are stored in the auxiliary or redundant channel, so it is a flip-flop system.

Mr. Rommel: You are working at relatively low frequency then?

Mr. Holley: We are going from about 2 to 126 msec, so this would be from the regions of 4 to 8 cps to about 250 to 500 cps. But the system responds to dc.

*   *   *

172

DEVELOPMENT OF VELOCITY SHOCK RECORDER
FOR MEASUREMENT OF SHIPPING ENVIRONMENTS

Matthew A. Venetos
U. S. Army Natick Laboratories
Natick, Massachusetts

The primary purpose of this study was to develop a velocity shock recorder capable of measuring and recording the shock environment, in terms of impact velocity or drop height, to which containers are subjected in shipment, handling, and storage. The performance requirements and electromechanical operation of a recorder developed during a preliminary investigation are discussed. In-house investigations to determine the duration of the shock inputs to be expected in typical container handling situations are described. This shock duration information was used to determine the required natural frequency of the velocity transducer. The problems encountered in the design and development of a suitable velocity transducer are described, as are in-house efforts to develop a sliding rod magnet transducer satisfactory for the measurement of shock durations up to 30 msec and of the response to those velocity components of angular impacts parallel to the sensitive axis of the transducer.

M. A. Venetos

INTRODUCTION

One of the major problems in the development of effective packaging and container systems is the lack of reliable information on conditions encountered by supplies during shipment, handling, and storage. Container design in the past has been chiefly based on observations and experience gained over a long period of time on the actual field performance of many types of containers of varied size and construction. Although many containers presently used in our supply system may have excellent protective qualities, they may be overpackaging, wasting materials and labor.

At the present time there is no direct method of evaluating, with a high degree of certainty, the suitability of new types of containers prior to their introduction into the supply system. One procedure currently used is to evaluate from trial field shipments. However, such test shipments are both costly and time consuming. Another method is to compare the performance of a new item with that of a container which has already proved to be suitable. However, there is a risk of overpackaging if the standard of comparison is an overprotective pack.

In an attempt to correct this situation, the U.S. Army Natick Laboratories has initiated a project on the establishment of design criteria for containers. One of the primary goals of the project is to develop recording devices for the measurement of important environmental conditions, such as shock, temperature, humidity, precipitation, and superimposed loading experienced by containers in shipment, handling, and storage.

The overall program on container design criteria comprises five distinct work phases:

1. Determination of the environmental parameters to be measured;

2. Design and development of instrumentation suitable for measuring and recording the required information;

3. Survey of domestic and overseas shipping, handling, and storage conditions with instrumented containers;

4. Analysis and reduction of data on supply line conditions to a form suitable for container design purposes; and

5. Development of reliable performance tests for containers based on the measured environmental data.

Although several environmental conditions will be considered in the long-range program, current efforts are being concentrated on the determination of shock inputs experienced by shipping containers. Past experience has shown that the shock environment produced during the manual handling of containers is more damaging than that associated with the mode of transport. Moreover, quantitative information is lacking chiefly in the handling area. It was decided, therefore, to investigate this area first.

APPROACH

Since the shock environment can be expressed in many different forms, the form most useful to the packaging engineer had to be determined. Since the greatest damage to a container and its contents is likely to occur when the container is dropped during handling operations, impact velocity and equivalent drop height were felt to be very representative of the shock environment. The importance of drop height is reflected in the fact that many standard test procedures utilize the free-fall impacting of containers. A knowledge of the impact velocity of a container is also useful in the design of protective cushioning, since the impact energy absorbed can be readily calculated from the impact velocity (KE = 1/2 MV^2). In view of these considerations, the decision was made to develop a shock recorder for the measurement of container impact velocity.

DETERMINATION OF CONTAINER IMPACT SHOCK DURATIONS

Essential to the design of the recorder was a knowledge of the duration of the shock inputs to be expected in typical container handling situations, since this information would be needed to establish the required natural frequency of the velocity transducer to be used in the shock

recorder. This information was obtained by dropping an instrumented container on impact surfaces typical of those to be encountered during shipment. The surfaces selected were concrete, packed sand, and a standard wood pallet base. Since shock input durations will be affected not only by the nature of the impact surface but also by the orientation of the container at impact, both corner and flat face drops were made. These two attitudes were selected because they would establish the minimum and maximum values of pulse duration to be encountered. At impact the penetration of the relatively sharp corner of the container into the impact surface will extend the duration of the shock input, whereas the larger bearing or contact area associated with a flat drop will result in a greater decelerating force and consequently a shorter stopping time.

The test container for the determination of impact pulse duration was designed to correspond to a typical supply pack in dimensions (16-1/4 ×12-3/16 ×9-3/8 in.), weight (45 lb), and exterior appearance. The basic skeletal structure of the case was formed from metal angles bolted together in a rectangular framework. Six plywood panels of 3/4-in. thickness were bolted to the metal framework to increase the rigidity of the case and to separate the sharp edges of the metal framework from the fiberboard shipping container into which the entire assembly was placed. A large wooden block was fastened to the interior of the framework to provide a rigid support on which the accelerometers could be mounted for both the flat and corner drops. The block was divided into two segments by a plane passing through the geometric center of the container assembly and perpendicular to a line extending from a corner to the geometric center. For corner drops an accelerometer was mounted on the surface of the plane at the point where it intersects the geometric center of the assembly. Crystal accelerometers were used for the measurement of the shock pulse durations. Shock pulse signals were read on an oscilloscope and recorded with Polaroid oscilloscope camera.

The initial height of drop was 18 in. and was increased by 6-in. increments until a maximum height of 36 in. was reached. Five test drops were made for each combination of drop height, container orientation and impact surface. The drops on a standard 40- × 48-in. pallet were made at two locations, the unsupported midspan of a deck board and a portion of deck board supported by a corner post block (or stringer).

In the corner drop tests the containers were suspended from one corner so that a line

passing through the impact corner and the center of gravity of the container was perpendicular to the impact surface. The flat drops were performed on a standard drop-leaf impact tester with the container side panel as the impact face. The results of these impact tests, presented in Fig. 1, indicate that the maximum pulse durations which should be expected for the type of impact surfaces investigated are approximately 30 msec. These maximum pulse durations were produced by corner drops on the midspan of a pallet deck board and into packed sand. Pulse duration information for corner drops on concrete from a height of 36 in. were not obtained because severe racking and distortion occurred in the test container. As expected the flat face drops (Fig. 2) resulted in the shortest pulse durations, with pulse times as low as 2 msec on the concrete impact surface.
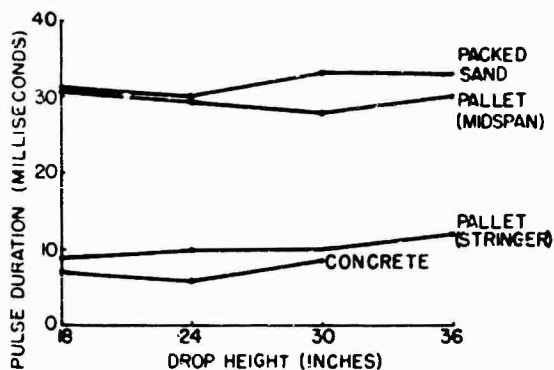

Fig. 1 - Impact pulse durations for container corner drops on typical stacking surfaces

DESIGN REQUIREMENTS

In addition to the natural frequency requirements for the recorder which could now be established from the information obtained in the pulse duration study, several other design requirements were presented to the contractor undertaking the developmental work on the recorder:

1. Self-powered recorder, capable of operating unattended for periods of at least 6 mo. The 6-mo operational period is considered minimum for military shipments.

2. Magnetic tape recording for ease of data processing. In many commercially available shock recorders, data are recorded by marks scribed on wax-coated chart paper. The amplitudes of these marks must be visually measured
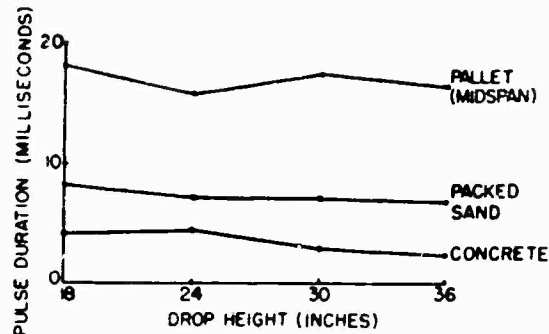

Fig. 2 - Impact pulse durations for container flat drops on typical stacking surfaces

and manually recorded to obtain the desired information. This not only is a time-consuming operation but also is susceptible to human error. In any large-scale study involving the measurement of shipping conditions over numerous supply routes and extended periods of time, the volume of data generated would create a serious processing problem. However, magnetic tape can be played back through analog-to-digital converters, and the desired information can be printed rapidly and automatically on paper tape.

3. Compact size. The recorder must fit a container that will be subjected to rough manual handling rather than to handling by mechanized equipment.

4. Data capacity of 4 channels with 5000 events per channel. A minimum of 3 channels is required for the three velocity transducers to be mounted in mutually perpendicular planes to provide measurement of impacts from any direction. A fourth channel is needed to place a timing mark on the tape each hour to pinpoint at what time and place in shipment the shock inputs occurred.

5. Adaptability to the measurement of additional parameters. The recorder unit had to be able to be readily modified to measure other important supply line parameters such as humidity, temperature, acceleration, and stacking loads.

DEVELOPMENT OF A
VELOCITY TRANSDUCER

Using as a guide the pulse duration information previously obtained, the contractor [1] analytically determined the natural frequency required for the velocity transducer. Figure 3
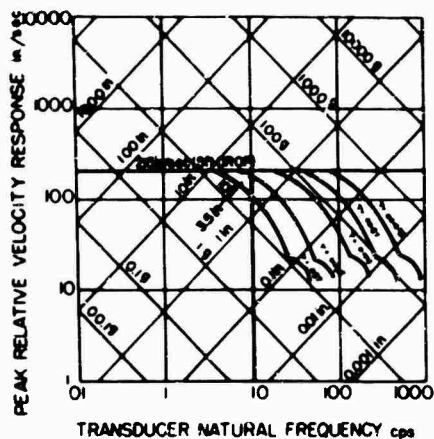
175

Fig. 3 - Response of velocity
shock recorder to half-sine
pulses of various durations

Fig. 4 - Prototype vel·· :v transducer

shows a four-coordinate nomograph of peak in-put acceleration, relative velocity, and relative displacement as a function of the natural frequency of the transducer. Shock spectrum responses are plotted for five half-sine acceleration pulses of different time durations but representative of the same velocity changes of 215 in./sec. As indicated in Fig. 3, each of the 5 curves is asymptotic to the 215-in./sec velocity line at low frequencies. The frequency at which the curves become asymptotic indicates the highest natural frequency which a transducer could have and still accurately measure the velocity change represented by a particular acceleration pulse. Based on these curves the contractor selected a design frequency of 10 cps, so half-sine acceleration inputs up to approximately 40 msec duration could be accurately measured. As our previous studies indicated, a transducer of this natural frequency would be more than adequate for the measurement of shock inputs expected in shipment.

The contractor used the principle of electromagnetic induction in designing the velocity transducers. The prototype design shown in Fig. 4 consists essentially of a coil and magnet. The C-shaped Alnico V magnet has a strength of approximately 3000 gauss. The coil, wound flat, is embedded in the nylon housing of the transducer. Note from the coil winding details illustrated in Fig. 4 that one segment of each loop of the coil is positioned so that it will be intercepted by the field of the magnet as the magnet slides along the guide rod. However, the opposite segment of each loop is arranged so that it is beyond the allowable limits of travel for the magnet and, therefore, beyond its magnetic field. If this were not the case, the
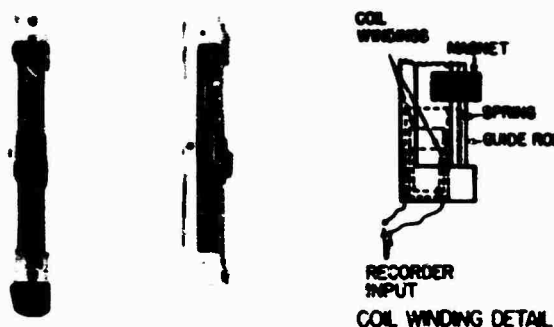
voltage induced in these outlying coil segments would be of such polarity as to cause cancellation of the signal. The magnet is mounted by four springs with one end of each attached to the magnet and the other end to a pin connection located at a midpoint on the back face of the transducer housing. Two nylon pulleys located at each end of the housing are used to change the direction of the springs. This transducer has a natural frequency of 10 cps and allows for magnet displacements of ±3.5 in. which, as indicated in Fig. 3, is sufficient for drop heights up to 5 ft. Performance testing of the transducer by the contractor revealed that the prototype design gave excellent results for vertical drops but was unsatisfactory for angle drops because of the friction developed between the nylon runner of the magnet and the guide rod. Because of this fact and the complexity and expense of fabrication, this design was discarded in favor of a cantilever beam style of transducer, as shown in Fig. 5. This transducer consists of a cantilever beam constructed of an aluminum channel and a piece of spring steel which connects to a point on the transducer housing. A coiled conductor wound around the unsupported end of the beam rests in a magnetic field produced by the permanent C magnet. At impact, the relative motion between the coil and the magnetic flux lines generates voltage. Vacuum cups were positioned on both sides of the beam. In Fig. 5, one vacuum cup is visible directly below the midpoint of the beam, while the vacuum cup on the opposite side of the beam is hidden by the beam housing. The purpose of these cups was to stop the beam momentarily at impact until tape advancement has occurred. If the beam were permitted to rebound immediately, the voltage produced of opposite polarity would erase all or most of the original signal recorded.

Performance testing of the cantilever beam transducer was conducted on a Model SM-020 AVCO shock tester. By interchanging the rubber
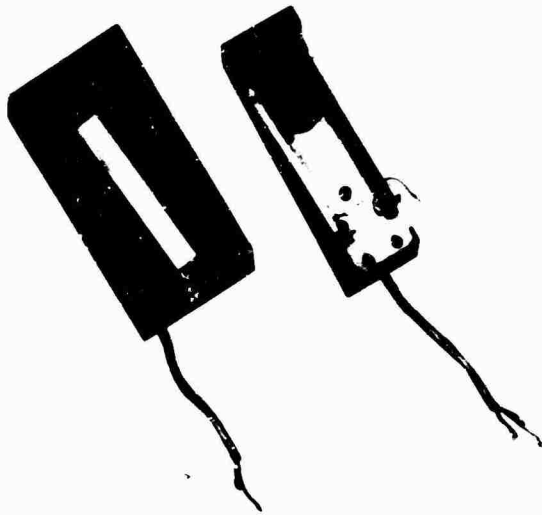
176

Fig. 5 - Cantilever beam-type
velocity transducer

| 22.6 VOLTS | 18.0 VOLTS | 13.7 VOLTS |

| 3 MILLISECOND INPUT PULSE | 6 MILLISECOND INPUT PULSE | 10 MILLISECOND INPUT PULSE |

Fig. 6 - Cantilever beam velocity trans-
ducer outputs for half-sine pulses of
various durations (12-in. drop height)

shock pads on the shock tester, the duration of
the half-sine input pulses to the transducer
could be varied from 3 to 30 msec.

The results of a series of 12-in. vertical
drop tests at varied pulse durations are pre-
sented in Fig. 6. In these tests the transducer
was aligned with its apparent sensitive axis
parallel to the direction of impact. These re-
sults showed that velocity measurements with
this transducer design were dependent on pulse
duration. At a 10-msec pulse duration, the peak
voltage output was only 61 percent of the value
obtained with a 3-msec pulse duration. After
reexamination of the transducer design, it was
concluded that the attenuation of the voltage
outputs with increased pulse duration was due
to a decrease in the number of coils being cut
by the magnetic flux lines. As the impact ac-
celeration pulse duration is increased, the coil
end of the cantilever beam is further displaced
from its equilibrium position before the maxi-
mum relative velocity is reached. However, as
the cantilever beam displacement increases, a
greater proportion of the coil begins to move
outside of the concentrated flux field lying in
the gap of the magnet, resulting in a drop-off in
signal strength. The situation was improved by
effectively increasing the gap width of the mag-
net so that all coils of the transducer would re-
main in the flux field for greater beam dis-
placements. However, because of certain design
limitations, it was not practical to increase the
gap length of the magnet to the point required
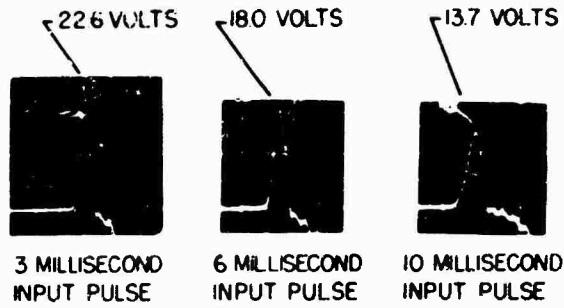for accurate velocity readings of shock inputs
up to 40 msec duration.

The results obtained on angle drops with
this transducer were equally disappointing. The
transducer was positioned on the drop table of
the shock tester so that its "apparent" sensitive
axis was at angles of 0, 30, 45, and 60 deg with
respect to the direction of impact. The dashed
lines in Fig. 7 indicate the fraction of the re-
sponse at 0-deg deviation that should have oc-
curred at the 30-, 45-, and 60-deg alignments.
However, for the 30- and 45-deg angles the
voltage signal outputs were instead greater than
those obtained when the transducer axis was
parallel to the direction of impact. Even at the
60-deg angle the response was still 45 percent
higher than the calculated value. An explanation
of these results is that the translational velocity
developed during free fall is converted into ro-
tational velocity at impact.

CALCULATED OUTPUT LEVELS

| 28 VOLTS | 36 VOLTS | .866 | 30 VOLTS | .707 | 26 VOLTS | .5 |

— 0° —— 30° —— 45° —— 60° —
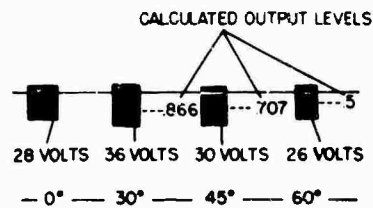
Fig. 7 - Cantilever beam ve-
locity transducer outputs for
various angles between trans-
ducer's apparent sensitive
axis and direction of impact

Because of the obvious inadequacies of the
cantilever beam transducer, an in-house effort
was undertaken to develop a new transducer. A
design (Fig. 8) which appeared to have promise
was one in which a rod magnet slides within a
rigid tube. Coil conductors are wound around
the outer circumference of the tube. The

177

$$h = \frac{v^2}{2g}$$

WHERE
h = EQUIVALENT DROP HEIGHT
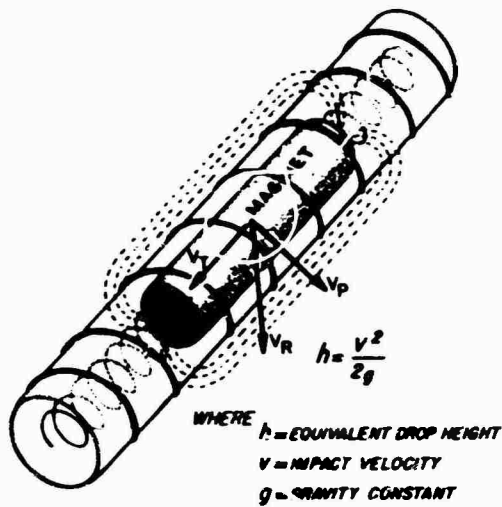V = IMPACT VELOCITY
g = GRAVITY CONSTANT

Fig. 8 - Sliding rod magnet velocity
transducer (double-ended operation)

advantages of this design were simplicity of
construction and, unlike the cantilever beam-
type transducer, the ability in angle drops to
respond only to that component of the velocity
vector V_t, parallel to the axis of the trans-
ducer. Several variations of this basic design
were evaluated. The first prototype design
(Fig. 8) incorporated a bronze spring at both
ends of the magnet and utilized magnet wire
over the full length of the tube. To prevent sig-
nal cancellation, the direction of the windings
were reversed at the midpoint of the tube. One
of the advantages of this design was that it could
be used to measure impacts in both directions
along its longitudinal axis. However, its linear
operating range was found to be limited. The
single-ended transducer shown in Fig. 9a uti-
lized a spring which acted in compression.
However, the tendency of the spring in com-
pression to buckle against the side walls of the
tube resulted in large friction forces which pro-
duced erroneous velocity readings. Therefore,
in the final design, Fig. 9b, a tension spring
was utilized. Although friction is reduced to a
minimum, this transducer design can measure
velocity in only one direction along its axis.
Therefore, a total of 6 transducers will be re-
quired to measure impact from any direction.
A combination stop and bumper is provided at
both ends of the tube to absorb impact energy
and to prevent overextension and compression
of the spring. Two metal projections located on
top of the bumper pad, adjacent to the uncon-
nected end of the magnet, serve as switch con-
tact points. These contact points are electri-
cally bridged by the end face of the magnet when
it comes in contact with them. This effectively
closes the switch and activates the circuitry

within the recording unit. After several plastic
materials were considered for the tube, graph-
ite impregnated nylon was selected because of
its low friction. The magnets used were formed
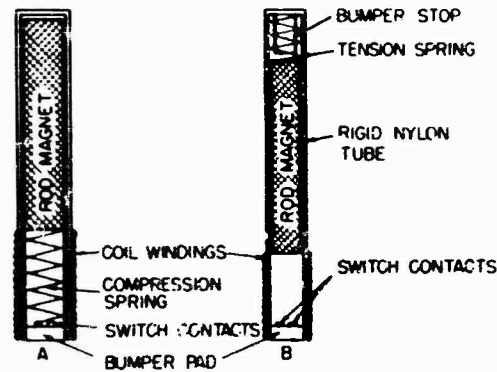from cast Alnico V with a relatively high finish.

Fig. 9 - Sliding rod magnet velocity
transducers (single-ended operation)

Because of the relatively small container
size to be instrumented, transducer length be-
came an important design consideration. For a
drop height requirement of 4 ft, a 10-cps system
would be displaced 3 in. After making further
allowances for the magnet, the spring, and the
transducer housing, the overall length of the
transducer would be approximately 9 in. How-
ever, since the maximum relative velocity will
occur before the total displacement of 3 in. is
reached, it was decided to shorten the spring
and use the bumper stops to dissipate the ki-
netic energy not absorbed by the displacement
of the spring. The length to which the springs
could be shortened and still provide accurate
measurement of maximum impact velocity was
determined experimentally. A transducer was
subjected to a series of 30-msec half-sine pulse
impacts from a height of 4 ft. A mechanical
bumper was used to limit the displacement of
the magnet to successively decreasing values
until the signal output began to drop off. By
this means it was determined that the length of
the spring must allow displacements of 2 in.

The results of the performance evaluation
of the single-ended sliding rod magnet velocity
transducer design are presented in Figs. 10 and
11, respectively, for both vertical and angular
orientation with respect to the input shock
directions.

In Fig. 10, velocity transducer output vs
drop height is plotted for half-sine pulse dura-
tions of 6, 15 and 30 msec. Drop height was
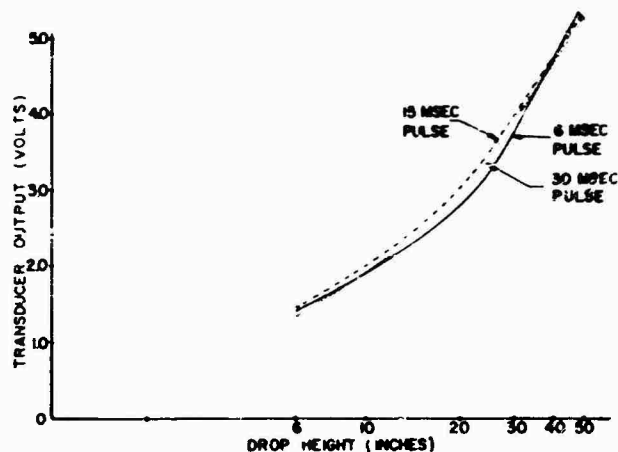varied from 6 to 48 in., and the longitudinal axis

178

Fig. 10 - Sliding rod magnet velocity transducer
output vs drop height for half-sine shock pulses
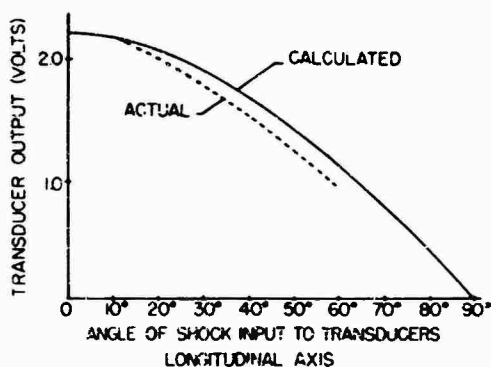of various durations

Fig. 11 - Sliding rod magnet trans-
ducer output vs angle of shock input
to transducer's longitudinal axis

of the transducer was in parallel alignment with
the direction of shock input. As indicated in
Fig. 10, there was close correspondence among
the outputs obtained from 6 to 30 msec. The
greatest deviations occurred at the approximate
midpoint of the drop height range investigated.
This deviation amounted to 9 percent at a drop
height of 24 in.

Transducer outputs obtained when the lon-
gitudinal axis of the transducer was oriented at
angles of 0, 10, 30, and 60 deg to the direction
of the shock input are presented in Fig. 11.
These values were obtained at a drop height of
12 in. and a pulse duration of 15 msec. The
solid line is a plot of the calculated output at
the various angles and, as can be seen, the ac-
tual readings obtained are in fairly close agree-
ment with the calculated values. The greatest

deviation, 15 percent, from the calculated values
occurred at the 60-deg angle drops.

DEVELOPMENT OF VELOCITY RECORDING UNIT

The recording unit is a solid-state elec-
tronic device, which in addition to the trans-
ducer section, consists of five basic elements:

1. Spring loaded magnetic tape supply and
take-up reels;

2. A 4-channel in-line tape recording head;

3. A rotary stepping motor to advance the
tape 1/16 in. for each shock input;

4. A 45-v dc power supp'y;

5. Solid-state circuitry to provide the
proper electrical triggering impulses for ad-
vancing the stepping motor; and

6. Electronic switch circuitry for the elim-
ination of undesirable secondary signal inputs.

Unlike the conventional type of tape re-
corder, recordings with this unit are made when
the tape is stationary. This resulted in a sim-
plified design and eliminated the need for a
large power supply. However, because the tape
was stationary during the recording of the sig-
nal, it was necessary to block out all but the
initial peak velocity pulse. Otherwise, the sub-
sequent pulses of opposite polarity produced by
the damped oscillation of the magnet after im-
pact would erase all or most of the initial signal
pulse from the tape. The required elimination
of all but the initial pulse is achieved by an

179

electronic switch which shorts out any signal after the initial signal for a period of 2 sec.

As shown in Fig. 12 the recording unit is shock-mounted with 6 1-in. pads of bonded fiberglass with a density of 7.5 pcf. Figure 13 is a block diagram of the velocity shock recorder. At impact a voltage proportional to the impact velocity is developed by the transducer. This voltage produces a current which flows through a resistance network into the recorder head, from which a signal is recorded on the magnetic tape. The purpose of the resistance network is to limit the induced current to less than tape saturation levels.

When the rod magnet of the transducer reaches its mechanical stop, it closes a set of contacts (transducer limit switch) which causes a series of transistors in the recorder electronics to be biased into conduction, providing a path for the power supply to discharge through the digimotor which is then actuated and advances the tape. The digimotor will continue to advance the tape until all the transducer limit switches return to an open position. However,

because of the time required for the current booster capacitor in the power supply circuit to reach the operating voltage level of the digimotor, there is an interval of 2.5 sec for the stepping intervals of the digimotor.

The electronic switch, whose function as described previously is to block temporarily all secondary signals to the recorder head after the initial signal pulse occurs, is set into operation by the current pulse associated with the operation of the digimotor. The digimotor current pulse causes a series of transistors in the electronic switch to conduct current. These transistors, connected in parallel between the transducer coil and the record head, effectively short or ground all signals before they reach the record head. This shorted condition continues to exist for a period determined by an R-C timing network in the electronic switch.

A timing circuit is also used to actuate the recorder at 1-hr intervals. A time piece in this circuit closes a switch, causing a pulse to be fed to the recorder electronics, which energizes the digimotor. Simultaneously a pulse is fed to the recorder head and recorded on magnetic tape as a timing mark.

FUTURE WORK

Some further work will be conducted on a lower frequency transducer of approximately 7 cps to determine whether the increase in accuracy warrants the required increase in transducer length.

Our studies to date on the sliding rod magnet transducer have been conducted with the transducer separated from the basic recorder unit. Since the performance of this transducer has proven to be satisfactory for both the required pulse durations and for angle drops, the shock recorder now must be evaluated as a complete unit, that is, with the transducer electrically connected to the recording unit. This evaluation will include subjecting the recorder

Fig. 12 - Velocity shock recorder unit
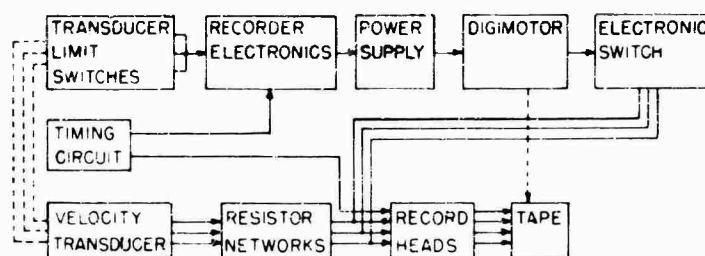
Fig. 13 - Velocity shock recorder block diagram

to programmed shock inputs as previously conducted on the transducer alone. These tests will then be followed by the free-fall drop testing of shipping containers instrumented with the recorder

Finally, after completion of the laboratory calibration of the recorder, a series of controlled field test shipments to both domestic and overs as destinations will be conducted to obtain information on the shipping environment as well as on the field performance of the velocity shock recorder.

REFERENCE

1. M. Gertel and D. Franklin, "Determination of Container Design Criteria, Final Report," Mitron R&D Corp. Nov. 1, 1964

* * *

ABSOLUTE CALIBRATION OF VIBRATION GENERATORS
WITH TIME-SHARING COMPUTER AS INTEGRAL
PART OF SYSTEM

B. F. Payne
National Bureau of Standards
Washington, D.C.

Improved shakers with a simplified ceramic moving element and a reference accelerometer now permit reciprocity calibration over a frequency range from 10 to 5000 Hz. This paper describes the present NBS shaker calibration procedure in which magnitude and phase lag measurements are made. Calibrations to 10 kHz are planned.

A teletypewriter gives access to a central time-sharing computer which can accept commands and data from punched paper tape or from the keyboard. The data may be recorded from digital measuring instruments by a special coupling system. Data reduction is rapid and permits errors to be corrected quickly. The combined use of the computer and the digital data recording system cuts the calibration time to about one-fourth that required by previous methods. Monitoring the quality of motion of the shaker by the computer makes possible improved accuracy of the calibration process. Calibration of one of the improved shakers is described.

B. F. Payne

INTRODUCTION

In calibration of vibration standards, accuracy is affected by many mechanical and electrical factors, and exact reproduction of conditions is extremely difficult. Accordingly, it is particularly important to know the results of measurements while the experimental setup is still in place. It is useful to know almost immediately if data are changing uniformly or randomly, and to assess the effects of varying the parameters to obtain optimum performance.

This paper describes a system for data collection and reduction with a time-sharing computer as an integral part of a calibration system. Data from digital instruments such as voltmeters and frequency counters are transmitted to a teletypewriter either automatically or manually. The teletypewriter prints a copy of the data and also punches a paper tape. Data from the tape can be fed into the computer through the teletypewriter, and the computed results are recorded in return by the teletypewriter. Various combinations of data sources can be read into the recording system by a switch located on the interface equipment.

Most of this paper is devoted to the application of this technique to the known reciprocity calibration of vibration exciters. The ratio circuitry is presented in a general form and other applications for the circuitry are suggested in the Appendix.

The data analysis techniques follow current practice which has been found to be useful. Additional experience with the calibration system may lead to alternative criteria for the screening of data due to bad motion and other

183

causes. Other aspects of data analysis techniques are also being investigated.

FEATURES OF TIME-SHARING COMPUTER SERVICE

A time-sharing computer gives the user a connection between the computer and his laboratory and permits him to communicate with the computer by some suitable means — usually a typewriter. By typing in or reading in taped data and commands, the user can receive answers in a matter of seconds or minutes.

The time-sharing system here is a commercial system using the BASIC language. There are other systems available which in addition to BASIC can be programmed in ALGOL and a special version of FORTRAN. The computer used in this system has a 16 K word storage and a 6-μsec memory cycle.

Changes in the program are easily made by retyping a statement number and statement for each correction since a program is recompiled on each run. New statements can be inserted between existing ones. Each user is allocated a certain amount of space in which he can store his programs and recall them later by typing out the name of the desired program. Storing the most commonly used programs provides a rapid means of access to a large amount of information. Some of the systems also have libraries of commonly used programs, called system programs, available to each user. If a laboratory has a number of instruments which are used as reference standards, a detailed calibration or performance characteristic chart can be compiled in the form of a program for each instrument. The users of the instruments use the computer efficiently by naming the program for that instrument when the calibration information is desired for a comparison test.

The remote consoles are commercial teletypewriters connected to the central computer by telephone lines. The computer time is sold to customers by the terminal hour each month; usually 25 or 50 hr is the minimum. The teletypewriter can be rented or purchased.

BASIC is a user-oriented language. It is similar in structure to FORTRAN, but does not take as much training and time to learn. The average person can learn the essentials of BASIC in 2 hr using an instruction book. For more sophisticated programming, FORTRAN and ALGOL are available.

One of the attractive features of this system is that one can program, edit, debug, store, and update at the typewriter console with only a small delay between commands. The editing commands have a higher priority than the run command, thus making it possible to debug a program very rapidly. Programs in the user's storage can be combined to form still other programs. Large segments of a program can be deleted from the current program in the working area of the computer without affecting the "saved" program in the memory area. This residual program can then be combined with another program, using the "merge" or "weave" commands, thus creating a new program which, if desired, can be renamed and saved for future use. In all this, the two original programs are unchanged and are still available for use. An application of this technique is in transferring data from one program to another, eliminating the need for re-reading in the data for the second program.

DESIGN OF IMPROVED SHAKER

For a number of years the reference in the National Bureau of Standards calibration service for vibration pickups has been a velocity sensing coil calibrated by a reciprocity method. The coil was part of the shaker used to provide motion for the pickups being calibrated. The large size and complicated structure of the shaker caused resonances and cross-axis motions which limited the accuracy which could be achieved and the frequencies at which satisfactory calibrations could be performed. Modifications of the flexures of the shaker reduced cross-axis motion but provided little significant improvement because the basic design remained unchanged. A much smaller, simpler shaker has been built specifically for calibration and has been found suitable to 5 kHz [1]. The new shaker uses an accelerometer in place of a velocity coil. This change was necessary because at the higher frequencies the velocity coil signal was lost in the noise level. Also, since most of the pickups calibrated are accelerometers, it was convenient to have a standard that was linear with acceleration instead of velocity.

The shaker is shown schematically in Fig. 1. The moving element is made from a single casting of alumina (Al_2O_3) which is ground to fit the stainless steel bearing. The driver coil is wound on and epoxied in place to make the whole moving element rigid. Pickups can be mounted on this by a 10-32 screw.
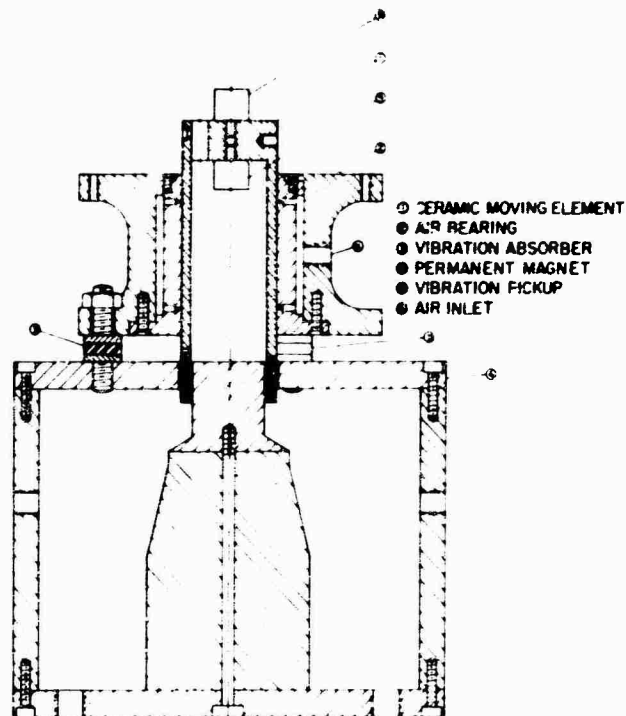
184

Fig. 1 - Electrodynamic vibration exciter
equipped with air bearing and ceramic
moving element

RECIPROCITY CALIBRATION

By the reciprocity technique, a shaker
equipped with a velocity coil or transducer is
calibrated. This shaker can then be used to
calibrate other transducers. The reciprocity
calibration is called "absolute" because it is
independent of arbitrary standards. It is based
on measurements of voltage ratio, resistance,
frequency, and mass, and is not a technique of
comparison of secondary standards. The accu-
racy attained reflects the accuracy with which
one makes the measurements and the character
of the physical motion of the exciter, for exam-
ple, whether the motion is purely sinusoidal or
distorted and whether or not one is operating
near a resonance.

Until recently the reciprocity calibration
of shakers was limited in frequency range to
10 to 2000 Hz. In large part, this limitation
was due to the complicated structure of the
shakers. With the advent of the new shakers
described earlier, it has been possible to ex-
tend the range to 5000 Hz.

The reciprocity calibration technique used
was an adaptation of the one given in Refs. 2

and 3. A brief outline of the measurements
necessary for a reciprocity calibration follows.

Experiment 1

With the shaker being driven by an oscilla-
tor and amplifier and the circuit as shown in
Fig. 2, the first set of measurements consists
of the transfer admittance given by

$$\bar{Y} = \frac{\bar{I} \text{ (driver coil)}}{\bar{E} \text{ (standard accelerometer)}} .$$

where a bar above the symbol for the variable
denotes a complex number. This ratio can be
measured by computing the current $\bar{I}$ from the
known drop in voltage across a 10-ohm resistor
in series with the driver coil and amplifier.
The quantity measured is

$$\bar{R} = \frac{\bar{E} \text{ (10-ohm resistor)}}{\bar{E} \text{ (standard accelerometer)}} .$$

Therefore,

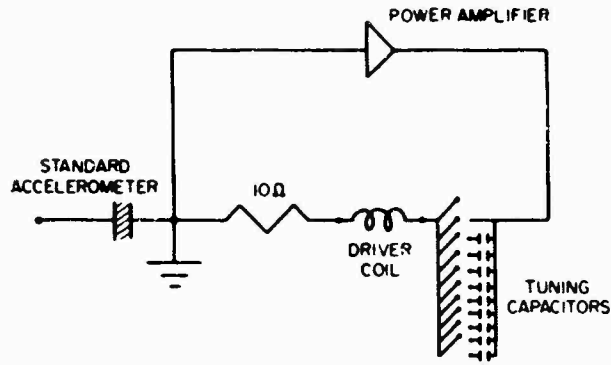$$\bar{Y} = \frac{\bar{R}}{10} \text{ mho} .$$

185

Fig. 2 - Schematic for transfer admittance
measurements and use as calibrator

A block diagram of the electrical circuit for the ratio measurements is given in Fig. 3. This shows a general circuit used for voltage ratio measurements. In the case of experiment 1, the reference signal is the voltage drop across the 10-ohm resistor and signal 2 is the voltage generated by the standard accelerometer. Both switches are in position 1. A series of such readings is taken for each frequency and consists of readings taken with incremental weights attached to the mounting table one at a time; the increments ranged from 0.1 to 0.5 lb in this calibration. Zero load readings are taken after each load. Also, the phase angle for each point is needed. In all, 22 data points for each frequency are required for a calibration.

Having measured the transfer admittance for a series of loads at a given frequency, we now plot graphs of the real and imaginary components of the ratio $\bar{W}(\bar{Y}_W - \bar{Y}_0)$ vs W, where W is the value of mass attached to the table and $\bar{Y}_W$ and $\bar{Y}_0$ are the transfer admittance for the various loads and zero load, respectively. The zero intercepts of these plots and their slopes are computed by the weighted least square method of Bouche [4], who has shown that the error in $W(\bar{Y}_W - \bar{Y}_0)$ is inversely proportional to W.

The values of $\bar{Y}_0$ used in the calculations are obtained by averaging the values of the $\bar{Y}_0$ measurements before and after each measurement of $\bar{Y}_W$. The computed values of intercept $\bar{J}$ and slope $\bar{Q}$ are used in determining the sensitivity of the standard. Figure 4 shows the shaker and readout instruments used for these measurements.
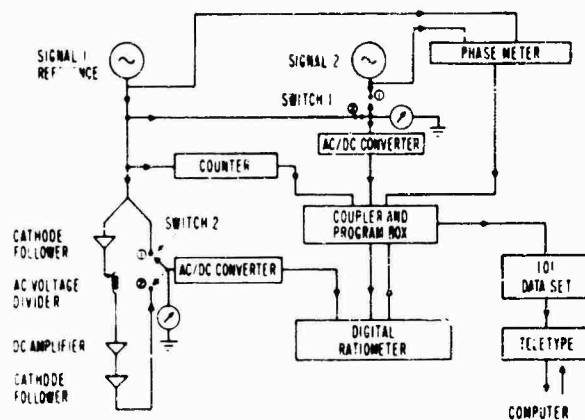

Fig. 3 - Block diagram for phase angle
and/or voltage ratio measurements for
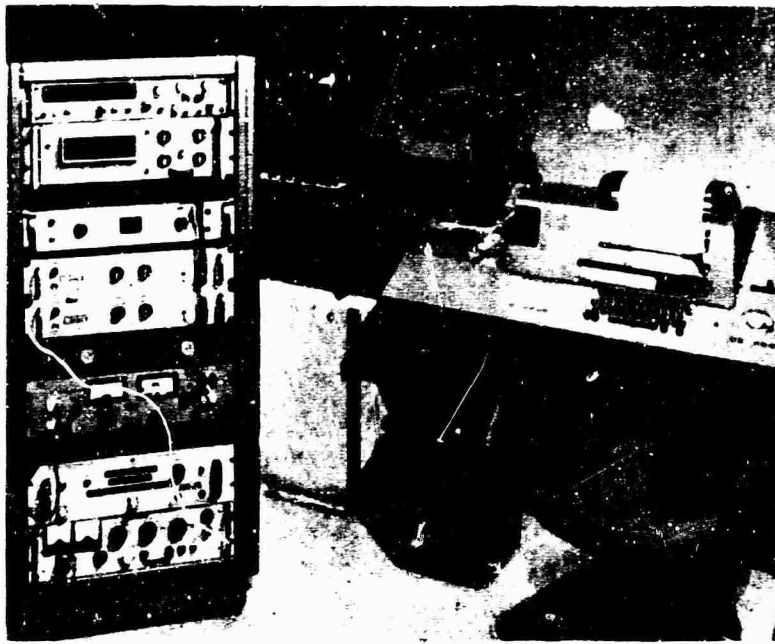two ac signals

186

Fig. 4 - Experimental setup for
obtaining transfer admittance data

Experiment 2

In this experiment, the open circuit voltage
ratio of the standard accelerometer to the
driver coil is measured when the shaker is
driven with a second shaker. The moving ele-
ment of the second shaker is connected to the
mounting table of the shaker being calibrated.
The ratio circuit is again given by Fig. 3. This
time the reference is the voltage generated by
the driver coil as it moves in the magnetic field
of the shaker. Signal 2 is the voltage generated
by the standard accelerometer. In such a case,
where both signals fall below 2 v, the reference
is amplified before being fed into the reference
channel of the ratiometer. Measurements are
usually taken every 50 Hz throughout the cali-
bration frequency range. Three sets of data
are usually taken and are used to compute the
final value used. Phase angles are also taken
here for each ratio data point. For the fre-
quency range of 10 to 2000 Hz, a Goodman's
V47 shaker was used to drive the standard
shaker. For the frequency range of 2000 to
5000 Hz, a piezoelectric shaker was used.
While driving with the piezoelectric shaker, a
matching transformer and a network of step
inductors in parallel with the driver coil was
found to be necessary to minimize the distortion
in the motion. By a careful adjustment of the
inductor bank, the distortion was kept at ap-
proximately 1 percent. Data from these two
experiments are sufficient to determine the
sensitivity of the mounting table of the shaker
in volts output of the standard accelerometer
per g (acceleration of gravity) of table acceler-
ation.

DRIVING ELECTRONICS

The oscillator provided a signal with no
more than 0.05 percent distortion and fluctua-
tions in amplitude after one hour warmup of no
more than $\pm$ 10 μv for a 0.5-v signal level, as
measured by a differential voltmeter.

The potentiometer which controlled the
amplitude of the signal to the power amplifier
had the equivalent of 10 turn resolution.

The power amplifier provided 250 watts
with less than 0.1 percent distortion. The
combined harmonic distortion of the oscillator
and amplifier was checked periodically at less
than 0.1 percent.

A matching network of capacitors, varying
from 0.1 to about 150 μf, was used to tune the
amplifier and shaker for best efficiency. Paper
or mylar-paper capacitors were used, since
they are the least noisy for this purpose.

187

MEASURING SYSTEM

The principal measurements in reciprocity calibration are ac ac ratios. The instruments available to measure such ratios have improved greatly in the last few years. Systems used earlier are described in Refs. 2, 5 and 6.

The system used for the work described here consists of the following components: (a) two ac dc voltage converters effective to frequencies as low as 1 Hz, (b) frequency counter, (c) phase meter with dc voltage output to feed into a digital voltmeter, (d) dual trace oscilloscope, (e) coupler program box, (f) digital ratiometer-voltmeter, (g) Model 101 data set, (h) Model 35 teletypewriter, (i) two high-input impedance cathode followers, (j) dc amplifier, (k) two voltmeters (3 percent) for setting levels, and (f) ac voltage divider.

The digital ratiometer used consists of two ac dc converters and a dc dc ratiometer. It measures ac voltages over the frequency range from 10 to 10,000 Hz with an accuracy of approximately 0.5 percent for voltage signals from 10 mv to 10 volts. Ratios of ac ac can be measured with greater accuracy by keeping the reference voltage (denominator) at 3 v or more. Over the frequency range from 10 to 10,000 Hz, the accuracy of the ratio will be about 0.2 percent if the numerator signal is as low as 5 mv, and it improves to about 0.1 percent if the numerator signal is above 10 mv. If the reference signal is less than 3 v, a good dc amplifier can be used in the reference branch of the ratiometer. The gain of the amplifier can be measured so accurately that the overall accuracy of the ratio is not appreciably impaired.

In using the dc amplifier in the reference branch of the circuit, we found we needed to buffer it on the ratiometer side by a cathode follower of high-input impedance (1000 megohms). A cathode follower was also used on the signal side of the dc amplifier to buffer the signal feeding into the voltage divider (Fig. 3). These cathode followers prevent loading effects which otherwise would introduce appreciable errors. For signals whose reference signal is greater than 2 v, both switches 1 and 2 are in position 1 and the ratiometer reads the ratio directly.

The procedure for obtaining voltage ratio measurements for signals whose reference drops below 2 v is as follows:

1. Set the dc amplifier to some convenient gain (usually × 30) and adjust the voltage divider to give a reference signal of 5 to 10 v.

2. With switch 1 in position 1 and switch 2 in position 2, record a voltage ratio R 1.

3. With switch 1 in position 2 and switch 2 in position 2, record a second voltage ratio R 2.

4. Program the computer to calculate the ratio R = R 1/R 2.

An alternate method for signals with low reference voltage is to measure the combined gain of the dc amplifier and cathode followers for the various frequencies of the calibration and then program the computer to make the gain corrections.

The system described above can reflect changes in ratio very quickly (5/sec in tracking mode), has an overall accuracy of at least 0.2 percent, has provision for printer output, and will feed a paper tape punch and typewriter.

INTERFACE BETWEEN MEASUR-
ING INSTRUMENTS AND
COMPUTER

In Fig. 3 the interface equipment is denoted by the coupler and program box and the data set. The coupler accepts information from the digital ratiometer, frequency counter, and phase meter. It operates on this information by coding, formatting, and transmitting it to the teletype. The data set, a standard piece of telephone hardware, permits the user to use the teletype as a device to record data, both as hard copy and on paper tape. The coupler can work with many different printout devices, including magnetic tape producing units as well as the teletypewriter. The teletypewriter, however, is an economical printer-tape punch as well as a computer outlet.

The choice of data is made by providing various format options of all the possible types of data sequences likely to be needed for a particular application. A switch on the front panel of the coupler is used to choose the format option. Each position of the switch provides a particular sequence of data to be collected and the various positions comprise all possible sequences likely to be needed for a given application. The data collection is done while the teletypewriter is disconnected from the telephone line to the computer. This is accomplished by a switch located on the teletype which either connects the telephone line or the coupler to the teletype. For data recording, the teletype is connected to the coupler.

The coupler has two modes of operation, manual and automatic. In the manual mode, one data logging cycle is executed when the command button is depressed; in the automatic mode, the coupler continues to log data one cycle after another until switched out of the automatic position. The coupler also formats the data for use on the computer. The coupler has a number of features for data formatting. Extra characters can be inserted, such as commas and decimal points. A manual data entry panel provides for manual data entries, such as run numbers or time. After the coupler logs the data, it automatically advances the statement number.

After the data are collected on the paper tape, the teletype is connected to the telephone line and the data on the paper tape are read into the computer by the tape reader located on the teletype. The results of the computer program are printed on the teletype and can also be put on tape for future use.

FROM DATA TO RESULTS—USE OF TIME-SHARED COMPUTER SYSTEM

In practice the voltage ratio experiment is performed first. Usually, three sets of ratios covering the frequency range are taken. The data, collected on tape and teletypewriter as described above, consist of frequency, voltage ratio, and phase angle. The phase angle can be recorded at the same time as the ratio, or it can be recorded in a separate run.

To measure the phase angle, a digital phase meter is used which utilizes the digital dc voltmeter part of the ratiometer. By a remote command feature, the ratiometer can be electronically switched from voltage to ratio and the input can be switched to the signal from the phase meter, so that the coupler will present to the teletypewriter voltage ratio, phase angle, and frequency.

In the voltage ratio experiment, the computer is asked to read in the ratio, phase, and frequency data points, normalize the ratio by dividing by $2 F \times 10^{-6}$ (F = frequency), and give a second-degree polynomial fit for the normalized data vs frequency. Using the constants for this fitted equation, the computer calculates and prints out the fitted voltage ratio for integral frequencies (every 50 Hz). Thus, even though the original data were taken at only approximate frequency intervals, in its final form results are for exact intervals.

After the voltage ratio is taken (experiment 2), the calibration measurements are completed by obtaining the transfer admittance (experiment 1). Figure 4 shows the shaker and equipment setup for obtaining the transfer admittance readings. First, we establish the frequency at which we wish to calibrate. In this experiment we take voltage ratio and phase with a sequence of masses attached one at a time to the shake table. After obtaining the necessary 22 data points, plus the frequency and voltage ratio from experiment 2, the data are entered into the computer to obtain the final results. The results are illustrated by an actual run given in Fig. 5. At the top of the page is the frequency, value of the standard resistor used in experiment 1, and magnitude and phase (radians) of the voltage ratio of experiment 2. Next is a printout of the data, consisting of the load attached to the table, ratio and phase angle as given for experiment 1, and the computed transfer admittance. In the following columns are the average of the zero load transfer admittances (YEO-AVE), the difference in these and the loaded transfer admittances (Y-YEOAVE), and the real and imaginary components YMR and YMI using the recorded phase angles. The YM's are the components of the quantity

$$ W = (YM) - (YEO-AVE). $$

In the next step, the computer develops a weighted least squares fit for each of the real and imaginary components YMR and YMI, respectively, vs the masses W. The J's and Q's are the intercepts and slopes, respectively, of these plots. Next the experimental and calculated YMR and YMI and the deviation (DEV) and percent deviation (YMI-DP and YMR-DEV PC) for these data are printed out. The index is a measure of how well the data fit a straight line. It is an average weighted deviation given by

$$ \text{Index} = \frac{\sum_{n=1}^{N} n \cdot m}{N}. $$

where n is the loading factor which varies directly as the mass (that is, 0.1 lb is counted once, 0.5 lb is counted 5 times); m is the percentage deviation of the YMR (since YMR contributes much more to the final answer than YMI, we are more interested in how YMR behaves); and N is the number of masses used in the sequence (in this case, five).

Next there is a second pass made; that is, the computer decides which points, if any, should be eliminated based on how far the point

```
F= 1500        R2= 10.215     VR= 1.31067    VR-PH= 1.52193

LOAD           RATIO          PHASE          YM

0              .006881        2.25           14.2269
.1             .006219        2.5            15.7413
0              .00688         2.33           14.225
.2             .005679        2.7            17.2381
0              .006881        2.33           14.2269
.3             .005222        2.79           18.7467
0              .006882        2.33           14.2248
.4             .004831        2.92           20.264
0              .006882        2.33           14.2248
.5             .004492        2.95           21.7932
0              .006885        2.33           14.2186


YEO-AVE        Y-YEOAVE       YMR            YMI
14.2279        .128041        6.57791 E-2    5.56006 E-3
14.2279        .233591        6.62036 E-2    5.15001 E-3
14.2259        .334152        6.61502 E-2    4.90075 E-3
14.2243        .453969        6.60196 E-2    4.97474 E-3
14.2217        .543394        6.58459 E-2    4.73655 E-3

J1= 5.43901 E-3                J2= .066392
Q1=-1.37130 E-3               Q2=-1.02902 E-3


LOAD      YMI-EX         YMI-CAL        YMI-DEV        YMI-DP
.1        5.56006 E-3    5.30188 E-3    2.78176 E-4    4.98517
.2        5.15001 E-3    5.16475 E-3    -1.47426 E-5   -.286263
.3        4.90075 E-3    5.02762 E-3    -1.26876 E-4   -2.58892
.4        4.97474 E-3    4.89050 E-3    8.42489 E-5    1.69353
.5        4.73655 E-3    4.75337 E-3    -1.70121 E-5   -.359181

LOAD      YMR-EX         YMR-CAL        YMR-DEV        YMR-DEV-PC
.1        6.57791 E-2    6.62891 E-2    -5.09980 E-4   -.775292
.2        6.62036 E-2    6.61862 E-2    1.73568 E-5    2.62174 E-2
.3        6.61502 E-2    6.60833 E-2    6.68957 E-5    .101127
.4        6.60196 E-2    6.59804 E-2    3.92104 E-5    5.93921 E-2
.5        6.58459 E-2    6.58775 E-2    -3.15631 E-5   -4.79348 E-2
INDEX= .107223


XXXXXXXXXXXXXXXX   SECOND PASS   XXXXXXXXXXXXXXXXXXXXXXXX

LOADING FACTOR PC DEV

1              -.775292
2              2.62173 E-2
3              .101127
4              .059392
5              -4.79349 E-2
INDEX= .107223


SUMMARY FOR 1500   HZ
           IMAGINARY      REAL          MAGNITUDE      PHASE
J          -5.43901 E-3   .066392       6.66144 E-2    -8.17401 E-2
Q          1.37130 E-3    -1.02902 E-3  1.71445 E-3    2.21455
BYP                                     .258693        2.23099

SEN- 0 LOAD                             20.1028        -3.74154
SEN- 1/2 LB                             19.9321        -3.18528
```

Fig. 5 - Calibration data sheet for
typical frequency calibration point

deviates from the straight line. The limit for selection is programmed into the computer beforehand; usually it is 2 percent. The limit of 2 percent is tentatively selected as a working rule based on experience to date. With cumulation of additional data, this figure may be adjusted upwards or downwards. Other reasonable rules for the screening or editing of data are also being investigated. A new index is then computed and is printed with the loading factor used. In this sample run, no points were omitted on the second pass.

The components of the new $\bar{J}$'s and $\bar{Q}$'s are combined to get magnitudes and phases of J and Q which, together with the voltage ratio from experiment 2, provide all the information for obtaining the sensitivity. The computer now substitutes these quantities into the equation

$$S = 2634.95 \left[\frac{\bar{R}\,\bar{J}}{\bar{j}\,F}\right]^{1/2} \left[1 + \frac{\bar{w}\bar{Q}}{\bar{J}}\right] \text{mv}/g .$$

where

j = unit imaginary vector,

w = weight attached to exciter table (lb), and

F = frequency (Hz).

Using the usual rules of complex numbers, the computer then computes sensitivities for w as zero and 1/2-lb loads from this equation.

The final summary at the bottom of the data sheet (Fig. 5) gives the pertinent information for the intercepts, slope, and sensitivities for zero and 1/2-lb loads. The sensitivities here are in millivolts per g and degrees.

The computer then fits two second-degree polynomials to each of the two sensitivity-frequency curves by the method of least squares. The interpolation formula for sensitivity for other weights is given by

$$S_w = S_0 - \frac{w}{0.5}\,(S_0 - S_{1/2}) .$$

where S_0 are the values given by the zero load second-degree equation and $S_{1/2}$ are the values given by the 1/2-lb load second-degree equation.

This sensitivity is tabulated by the computer for incremental loads which might be attached to the mounting table, usually every 0.05 lb from 0.0 to 0.5 lb for the various frequencies which are ordinarily used in a pickup calibration. These tables provide a convenient calibration listing for any load up to 1/2 lb throughout the calibration frequency range. Having established the calibration of the primary standard in millivolts output per g of acceleration, we can use the same ratio circuit to establish by comparison techniques the sensitivities of secondary standards.

Before the computer was used, not only was the calibration slower, but also some of the data handling could not have been done. For example, computing deviations and quality

indexes would not have been considered practicable.

The reciprocity technique is independent of other calibration methods and a calibration resulting from the procedures described above can be considered as equal in accuracy and resolution to a calibration derived by any other means. However, vibration measurements are subject to so many sources of error that check measurements are desirable to minimize chances of systematic error. The calibration described in this paper was checked in a number of ways, since both the shaker and the computer routine were fairly new.

The accelerometer used as the calibration standard was calibrated by the usual NBS routine: from 10 to 2000 Hz on two electrodynamic shakers using velocity sensing coils, and from 1.5 to 10 kHz by the modulated frequency interferometric technique [7]. These results were compared with the manufacturer's calibration. After the new shaker was calibrated as described above, it was used to calibrate a number of accelerometers maintained at NBS which are known to produce repeatable results on the current standard shakers. A good check at 10, 15, and 30 Hz was obtained by using the new shaker to calibrate a servo accelerometer which had been calibrated statically on a tilt table. A further check over the frequency range below 2000 Hz was obtained by using a strobe light synchronized with the motion, and a microscope with a filar micrometer eyepiece. The discrepancies between the reciprocity calibration and the check measurements were well within the estimated uncertainties of the measurements.

USE OF RECIPROCITY TECHNIQUE TO EVALUATE DESIGN

The reciprocity experiments combined with the computer can be used to evaluate design features of shakers under development. This can be seen from the data collected on the new shaker shown in Fig. 2. Figure 6 shows the frequency response for the voltage ratio experiment 2. The smoothness of the curve indicates undistorted uniaxial motion of the shaker. If distortion occurs or local resonances affect the motion, it will be reflected in these data. On the older shaker, these data would show breaks in the curve indicating bad motion.

The transfer admittance data also reflect the quality and uniformity of the motion. The scatter indices described above, taken on three
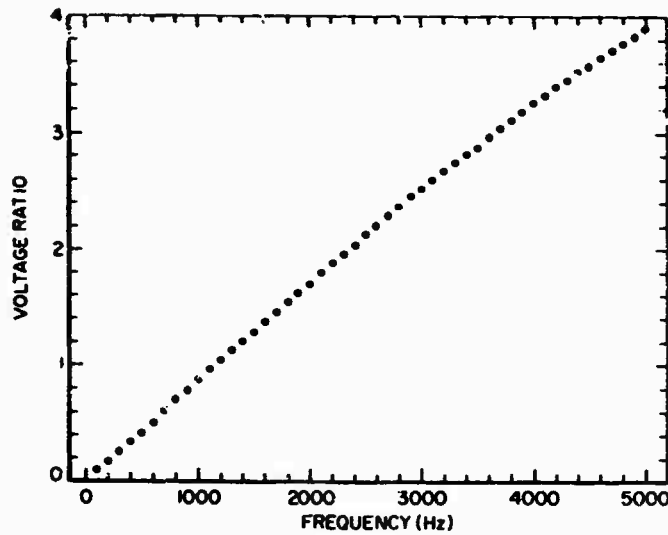
191

Fig. 6 - Voltage ratio vs frequency
for experiment 2

shakers calibrated with the readout system described here, are given in Table 1. Shakers 619 and 676 are an older modified commercial type, and the indices reflect their scatter on the first pass through the computer. On the shaker AF II, very few points were rejected by the computer with a cutoff limit of 2 percent. These data indicate that the new design of the ceramic shaker reduced the scatter by a factor of about three. Figure 7 shows the frequency response of the shaker calibrated by reciprocity using an accelerometer as the standard.

TABLE 1

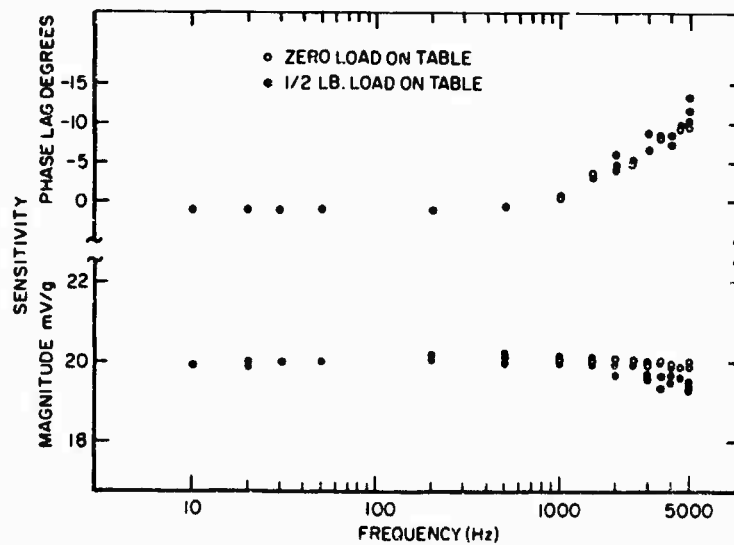| Shaker	Average Scatter Index	
	1st Pass	2nd Pass
No. 619	0.886	0.415
No. 676	1.00	0.420
AF II	0.327	0.259

Fig. 7 - Sensitivity vs frequency for Shaker AF II

192

REFERENCES

1. T. Dimoff, "Electrodynamic Vibration Standard with a Ceramic Moving Element," J. Acoust. Soc. Am., Vol. 40, No. 3, pp. 671-676, Sept. 1966

2. Samuel Levy and Raymond R. Bouche, "Calibration of Vibration Pickups by the Reciprocity Method," J. Res. NBS, Vol. 57, No. 4, pp. 227-243 (1956)

3. R. R. Bouche and L. C. Ensor, "Use of Reciprocity Calibrated Accelerometer Standards for Performing Routine Laboratory Comparison Calibrations," Shock and Vibration Bull. No. 34, Part 4, pp. 21-29, Feb. 1965

4. R. R. Bouche, "Development of Standards for the Measurement of Vibratory Motion," Ph.D. thesis, Dept. of Mech. Eng., Univ. of Maryland, Dec. 1958

5. "American Standard Methods for the Calibration of Shock and Vibration Pickups," Am. Standards Assoc., S2.2, 1959

6. J. R. Houghton, NBS Tech. Note 266, Govt. Print. Off., Dec. 1965

7. V. A. Schmidt, S. Edelman, E. R. Smith, and E. T. Pierce, "Modulated Photoelectric Measurement of Vibration," J. Acoust. Soc. of Am., Vol. 34, No. 4, pp. 455-458, April 1962

Appendix

The circuit given in Fig. 3 can also be used for the calibration of pickups by comparison with the reciprocity calibrated shaker using the standard accelerometer. The sensitivity of an unknown pickup mounted on the exciter table is given by

$$S_{unknown} = \left[\frac{E_{unknown}}{E_{standard}} G \right] \times S_{standard} \cdot$$

where G is the gain of the dc amplifier and $S_{standard}$ is the sensitivity of the standard accelerometer. The quantity in brackets is that measured by the ratiometer. Our standard accelerometer has a sensitivity of approximately 20 mv/g. By setting the dc amplifier gain on approximately 50 and using the voltage divider to correct for small variations in the sensitivity of the standard and the gain of the amplifier and cathode followers, the meter will read the sensitivity of the unknown pickup directly.

This leads to a simple means of setting the system for direct reading of sensitivity:

1. Feed the output from an oscillator into both inputs of Fig. 3. That is to say, use position 2 on both switches 1 and 2. Let the amplitude level be approximately what the output of the standard pickup would be at 5 g.

2. Pick a gain setting on the dc amplifier so that its reciprocal will be approximately the

$S_{standard}$ in the above equation (in volts per g). In our case 1/G should be 0.02.

3. Adjust the voltage divider so that the exact calibration factor of the standard accelerometer appears on the ratiometer when switch 2 is in position 2. Note this voltage divider setting.

4. Repeat step 4 for the various frequencies taken in the calibration range, noting the voltage divider setting for each frequency.

To calibrate pickups, the standard accelerometer output will be fed into channel 1 (reference); the unknown to be calibrated will be fed into channel 2. Switch 1 will be in position 1 and switch 2 in position 2. If the voltage divider is now set for the appropriate frequency, the ratiometer will read the sensitivity of the unknown directly in volts per g.

At the two lowest frequencies, 15 and 10 Hz, the reference in the system drops below 1.5 v at the lower acceleration levels if the dc amplifier is held at the same gain. Therefore, at these two frequencies, the system must be calibrated for the separate levels of acceleration. In our case this is 5, 2, 1 for 15 Hz and 2, 1, 0.5 at 10 Hz. This is especially convenient when using the coupler and teletype to record the data. Activating the command button provides a direct printout of the sensitivity.

193

DISCUSSION

Mr. Ames (Frankford Arsenal): What method is used to support the moving element in the vertical axis?

Mr. Payne: At the present time we use two methods: a flexible rubber tube or by a dc voltage imposed on the driving coil. The rubber tube works a little better than the dc suspension.

Mr. Jackman (General Dynamics/Pomona): What is the cross-axis sensitivity in your calibrations?

Mr. Payne: It runs under 2 percent over the calibration range, with some points below 1 percent.

Mr. Jackman: Is that 2 percent more or less uniform, or do you have resonances pulling up to the 2 percent?

Mr. Payne: Throughout the calibration range from 10 to 5000 Hz, we do not have any evidence of resonances. The cross-axis motion seems to have a more or less random pattern. A paper in the Journal of the Acoustical Society of America, September 1966, gives the actual experimental data on this.

*   *   *

EXPERIMENTAL TECHNIQUES FOR OBSERVING MOTION
OF EXTENDIBLE ANTENNA BOOMS

Donald J. Hershfeld
NASA Goddard Space Flight Center
Greenbelt, Maryland

Some unique experimental techniques, developed for the damping tests of 23- to 43-ft long segments of the 750-ft long extendible antenna booms used on the Radio Astronomy Explorer (RAE) satellite, are described. The booms, which are stored as a flat tape on a spool in the spacecraft and then assume a tubular shape when deployed, are extremely flexible in long lengths. High damping is desirable to insure stability of the antennas in the orbital environment. These tests were conducted by suspending segments of the boom as vertical cantilevers in a vacuum and measuring the decay rate of amplitude when the boom was released from an initially deflected configuration. Two methods were used to observe the motion of the boom: a photographic method in which time exposures of the boom tip were recorded on film, and a strain gage transducer which measured bending moments in two directions at the root end of the boom. The output signals from the strain gage transducer, when displayed on an X-Y plot, describe interesting Lissajous patterns which essentially duplicate the path traced out by the free end of the boom. These patterns are interpreted by a mathematical model of the boom which has been programmed on an analog computer.

D. J. Hershfeld

INTRODUCTION

The Radio Astronomy Explorer (RAE) satellite represents the first attempt to obtain directive measurements of electromagnetic radiation from space in a frequency range which is shielded from the earth's surface by the ionosphere. This directive capability will be achieved using a double V antenna configuration which, to measure low radio frequencies in the 0.4 to 10 Mc range, requires that each leg of

the V's be 750 to 1,000 ft long. An artist's concept of the RAE in orbit is shown in Fig. 1. In addition to serving as the prime antenna system on the RAE, these long antenna elements will also be utilized to provide gravitational gradient stabilization of the spacecraft attitude in orbit; i.e., the spacecraft will be continually oriented with one V pointing toward the earth along the local gravity gradient vector while the opposite V points toward the celestial sphere. The forces or torques necessary to achieve and maintain such an orientation are derived from the very small differences between the gravitational and the centrifugal forces acting on the long antenna elements. Associated with this technique for spacecraft attitude control is a set of libration modes or oscillations about the local vertical. These oscillations may be caused by initial conditions of misalignment with respect to local vertical or by disturbing torques due to such influences as orbital eccentricity, the earth's magnetic field, and solar radiation.

To support a study of the effects of these libration modes and of other perturbing torques

Fig. 1 - Artist's concept of Radio Astronomy
Explorer (RAE) satellite in orbit

on the pointing accuracy of the antenna system and on the overall stability of the spacecraft, it was necessary to measure experimentally the mechanical damping of these antenna elements. The extreme flexibility and light weight per unit length of these antennas required the development of some unique techniques to accomplish these measurements. This paper describes these techniques and presents some typical test results obtained thereby.

TEST OBJECTIVES

The RAE antenna element is a 2-in. wide tape of silver-plated beryllium copper, 0.002 in. thick, which has been heat treated to form an overlapping tubular shape approximately 1/2 in. in diameter. These tapes are stored in a strained, flattened condition on spools inside the satellite during launch and, upon command, are unreeled at a controlled rate. As the tapes extend, they resume their natural tubular shape.

Figure 2 shows an antenna element forming into a tubular shape as it is deployed. These antenna elements weigh approximately 0.015 lb/ft and have a bending rigidity (EI) of 2,000 lb-in^2.

To measure the damping characteristics of these antenna booms, sample segments of boom were suspended vertically as cantilever beams, initially displaced at the tip, and then released. By observing the rate at which the amplitude of the motion decreased, some measure of damping could be obtained. These tests were performed in a vacuum environment to eliminate air drag which would introduce damping considerably greater than the mechanical damping of the boom itself.

The arrangement of the test equipment and test boom is shown in Fig. 3. This figure shows a 10-ft long test boom suspended from a fixture inside the vacuum chamber. Initial deflection and release of the boom were accomplished by a "Polynoid" linear actuator and a

196
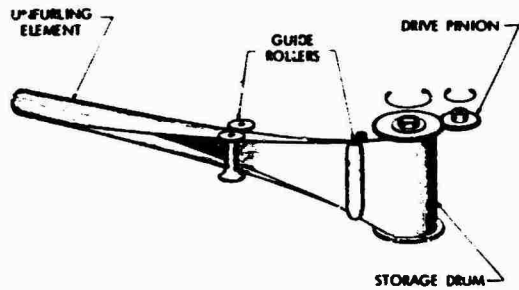
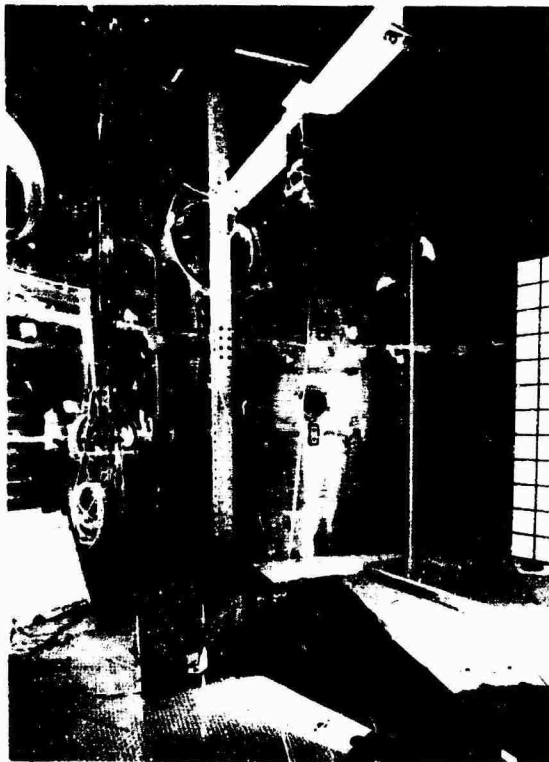Fig. 2 - Antenna element forming into
tubular shape during deployment

Fig. 3 - Test setup in GSFC dynamic
test chamber

solenoid-operated boom catching mechanism
shown in the lower part of the figure. To per-
mit initial deflection of the boom in various di-
rections relative to its cross section, the fix-
ture from which the boom is suspended could
be rotated about a vertical axis.

Because of the vacuum requirement, direct
observation of the boom motion was impractica-
ble and, therefore, some unusual experimental

techniques were developed. In chronological
order, they were the photographic technique and
the strain gage bending moment transducer.

Photographic Technique

In the photographic technique, a 70-mm
Hulcher pulse camera was located below the
boom and aligned so that it looked vertically up
at the bottom tip of the boom. Time exposures
of the motion of the boom tip were to be obtained.
However, because the period of oscillation of
the boom was about 3 to 5 seconds, all tests had
to be performed in a dark chamber with an ex-
tremely small "pinlight" attached to the tip of
the boom to provide a trace of the motion on the
film. With this technique, the camera shutter
could be left open continuously, and a trace of
the motion was obtained simply by turning the
boom tip light on and off. A frame advance sig-
nal to the camera provided a new frame of film
when required. This system could then be used
to record any number of cycles of boom motion
on one frame of film or could be used to record
single cycles of boom motion on a series of
frames.

Typical test results obtained by this photo-
graphic technique are shown in Figs. 4 and 5.
Figure 4 is a typical record of a single cycle of
motion. This exposure is one of a series of
single-cycle exposures which were recorded
while the amplitude of boom motion decreased.
By scaling and plotting the amplitudes of suc-
cessive exposures on a logarithmic scale vs
the elapsed number of cycles of motion on a
linear scale, a curve was obtained whose slope
was directly proportional to the logarithmic
decrement. These series of single-cycle expo-
sures thus provided the quantitative data needed
to evaluate the mechanical damping of the boom.
Additional qualitative information on the dy-
namic behavior of the booms was obtained by
continuous time exposures of multiple cycles of
motion on one frame such as that shown in
Fig. 5. This exposure shows some 100 oscil-
lations of the boom and required exposure time
of 5 min.

Analog Computer Simulation of
   Boom Motion

The pattern of motion shown in Fig. 5 can
be explained as the result of combining the os-
cillations of the boom in its two principal planes
of bending. Because the rigidity of the boom is
asymmetrical, the frequencies of these oscilla-
tions in the principal planes are slightly differ-
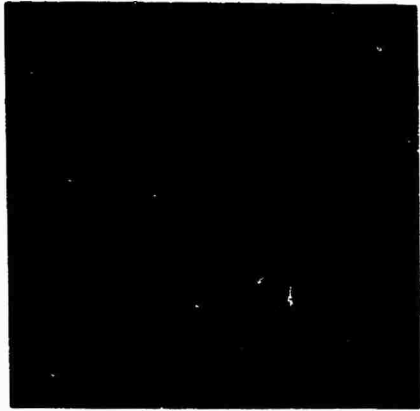ent; this difference results in a type of planar

197

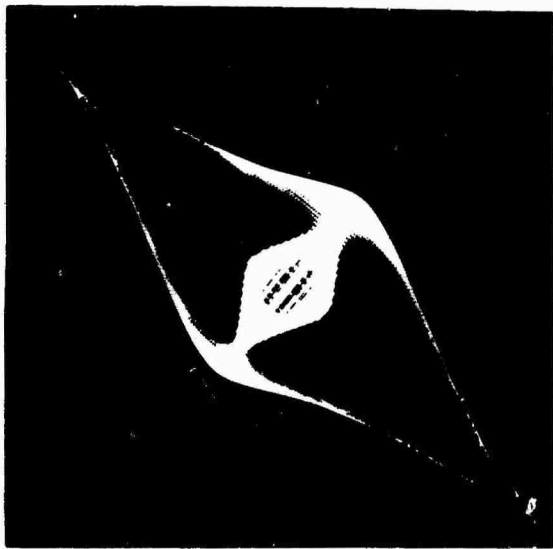Fig. 4 - Typical time exposure
of one cycle of boom tip motion

Fig. 5 - Five-minute continuous time
exposure of boom tip motion

parallelograms. The motion then describes a
pattern as shown in Fig. 5.

To verify this theory, an analog computer
program was used which consisted simply of
two uncoupled spring-mass-dashpot systems
whose natural frequencies differed only slightly,
and the displacements of the two systems were
displayed simultaneously as the X and Y coor-
dinates on an X-Y plotter. A typical plot, shown
in Fig. 6, compares well with the photographic
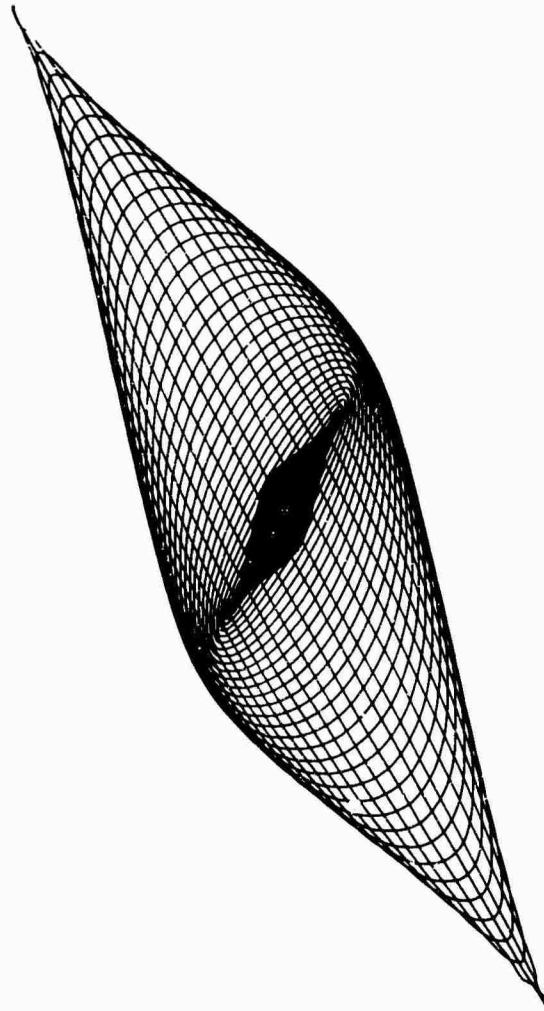time exposure of the boom tip motion in Fig. 5.

Fig. 6 - X-Y plot of analog
computer program

motion which has been discussed by Timoshenko
and Young [1]. For the case of no damping, as
described in the above reference, the motion
describes a series of ellipses which may be in-
scribed in a rectangle with sides parallel to the
principal planes. The dimensions of the rec-
tangle are determined by the initial displace-
ments in the two principal planes. The orienta-
tion and shape of the ellipse within this rectangle
changes uniformly with time at a rate propor-
tional to the difference in the two frequencies of
oscillation. When damping is introduced, the
dimensions of the rectangle are reduced with
time so that the circumscribing figure no longer
appears as a rectangle but rather as a series of

Strain Gage Bending Moment
   Transducer Technique

After the first series of boom damping
tests, it was apparent that the photographic

198

technique, while providing all necessary data for engineering analysis, did have several disadvantages which made its application somewhat cumbersome. Particularly, the number of tests which could be run was limited by the available film capacity, and the test data were not available concurrently with the conduct of the test. The strain gage bending moment transducer was proposed to overcome these disadvantages.

The measurement concept for this technique is based on the fact that the bending moment at any cross section of a beam is related to the deflection of the beam as described by its normal mode shapes. If the load distribution on the beam, and therefore its deflected mode shape, can be well defined, it is possible, at least in theory, to determine the deflection of any point along the beam by measuring the bending moment at some particular cross section. In this case, we attempted to determine the tip deflections of a cantilever beam by measuring the bending moment at the root end of the beam. Also, since the cantilever beam was free to vibrate in all directions, bending moments had to be measured in two perpendicular planes to determine the motion completely. For convenience, it was desirable that these bending moments be measured along the

principal planes of bending of the boom so that the bending strains in these planes would correspond to the uncoupled normal modes in the principal planes.

Prior experience in attempting to measure strain in the boom material indicated that it was inadvisable to apply strain gages directly to the boom itself since the strain field in this thin-wall tubular section is extremely complex. Instead, it was decided to instrument the mandrel on which the booms are mounted for these tests. The mandrel thus became a bending moment transducer.

This bending moment transducer is shown in Fig. 7. Essentially, the transducer consists of a 1/2-in. diameter aluminum rod which has been machined near one end to provide a strain section 1/4 in. square, approximately 1/2 in. long. Four strain gages, one mounted on each face of the strain section, are connected electrically to form two independent Wheatstone bridges which measure bending moments in two perpendicular directions. The RAE boom segments were clamped over the 1/2-in. rod. The complete transducer system was carefully calibrated by dead weight loading prior to use in the test setup.
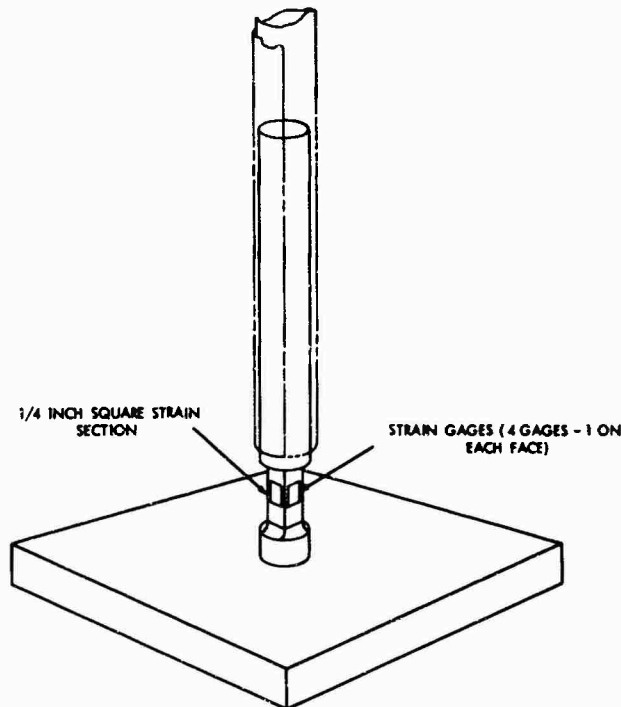

1/4 INCH SQUARE STRAIN SECTION   STRAIN GAGES (4 GAGES - 1 ON EACH FACE)

Fig. 7 - Strain gage bending moment transducer

199

The same test setup and procedure were used with the bending moment transducer as were used with the photographic technique. In fact, both techniques were applied simultaneously to compare the test data obtained. This comparison is demonstrated in Figs. 8 through 13. All of these patterns were obtained from a test of one boom segment. The difference between them is caused by the initial displacement of the boom in different directions. Figures 8 through 10 are photographic time exposures of the boom tip motion. Notice the narrowness of Figs. 8 and 10 in which the initial displacements were almost aligned with the principal planes, thereby exciting only one of the normal modes. This contrast with the broad pattern of Fig. 9 in which the initial displacement was misaligned with both principal planes by about 45 deg, thereby exciting both normal modes. Figures 11 through 13 were generated from the output voltages of the bending moment transducer system during the same tests. These voltages were initially recorded on magnetic tape and then later played back and displayed simultaneously
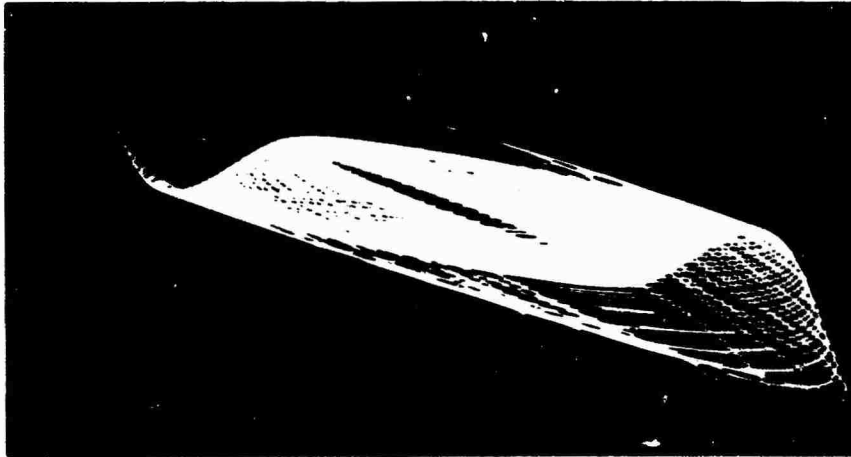

Fig. 8 - Photographic time exposure of boom tip motion after initial displacement in 0-deg direction
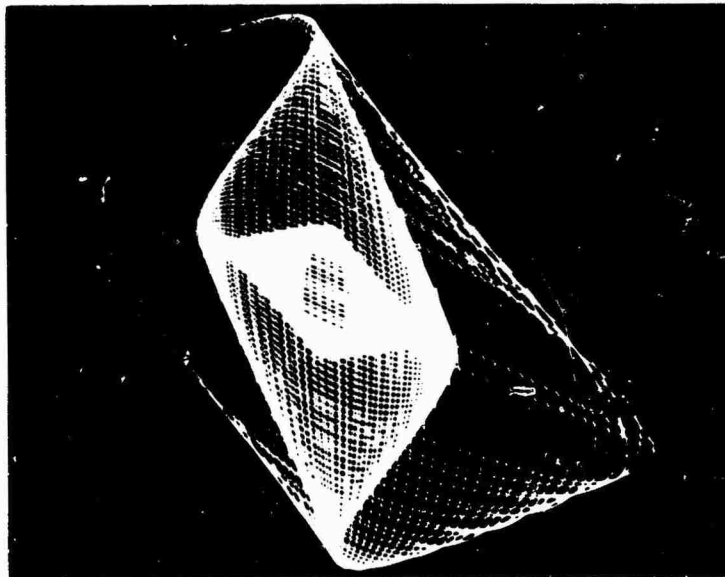

Fig. 9 - Photographic time exposure of boom tip motion after initial displacement in 45-deg direction

200

Fig. 10 - Photographic time exposure of boom tip motion after initial
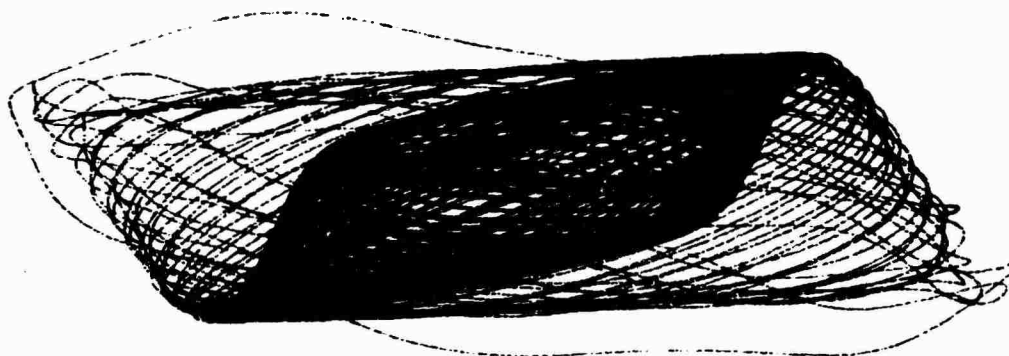displacement in 90-deg direction

Fig. 11 - X-Y plot of bending moments after initial displacement
in 0-deg direction

as X and Y coordinates on an X-Y plotter. Obviously, the boom tip motion illustrated in the previous set of figures has been fairly well reproduced by these bending strains as expected in theory.

By measuring bending moments in the principal planes of bending of the boom, it is possible to analyze the normal mode frequencies and damping characteristics in these planes. A preliminary analysis of these data has verified a difference in the fundamental mode frequencies in the principal planes, which is attributed to a difference in the bending rigidity in these planes.

CONCLUSION

Two unique experimental techniques for measuring the motions of extendible antenna booms have been described and typical test data

obtained by these techniques have been presented. The interesting, somewhat esthetic, patterns of motion generated by the boom motion, which have been illustrated, have been explained in terms of the normal bending modes in the two principal planes of the boom. It has been shown that it is both theoretically possible and practicable to reproduce the motion of the tip of the boom by measuring the bending moments at the root of the boom. It is hoped that the presentation of these techniques may serve to stimulate ideas for other applications of these techniques in the solution of similar experimental problems.

ACKNOWLEDGMENTS

The author wishes to acknowledge the valuable contributions of John Bauernschub and Keith Walters of Goddard Space Flight Center
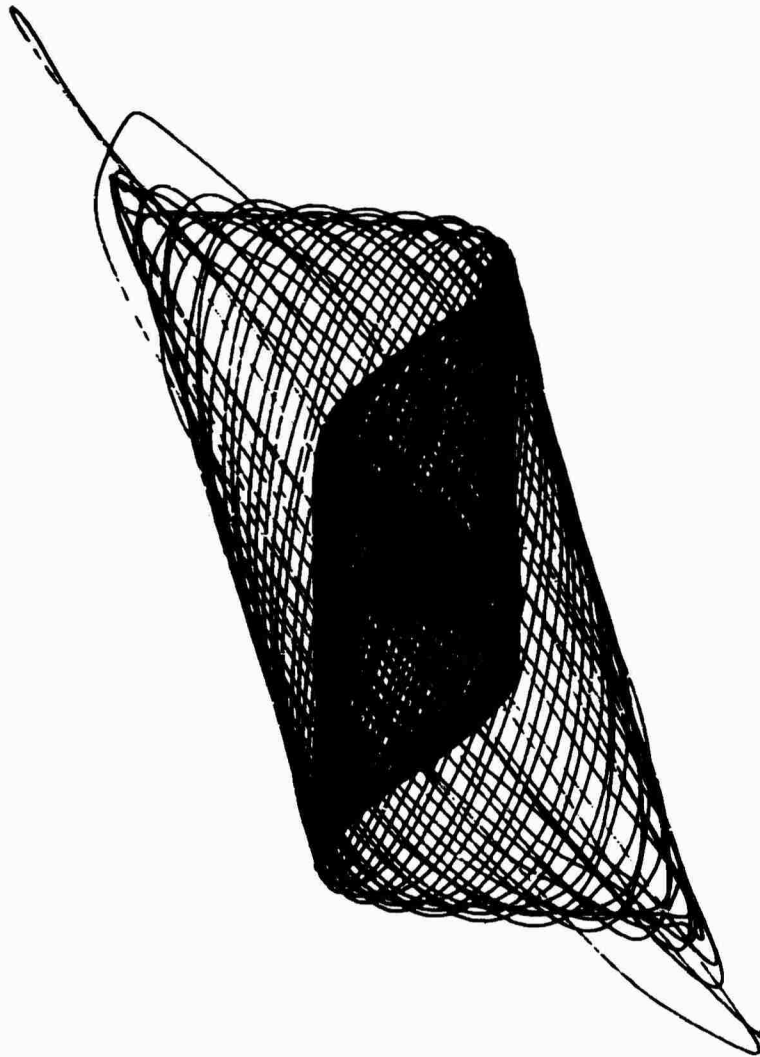
201

Fig. 12 - X-Y plot of bending moments after initial
displacement in 45-deg direction

Fig. 13 - X-Y plot of bending moments after initial displacement in 90-deg direction

who initially conceived and developed the photo-
graphic technique for recording boom tip motion,
and Meredith Wilson, also of Goddard Space
Flight Center, who suggested the application of
the strain gage technique.

REFERENCE

1. S. Timoshenko and D. H. Young, Advanced
   Dynamics, pp. 82-87. McGraw-Hill, New
   York, 1948

DEVELOPMENT OF LOW-COST FORCE TRANSDUCER*

Marlyn W. Sterk
Sandia Corporation
Albuquerque, New Mexico

and

James A. Ellison
California Institute of Technology
Pasadena, California

The Vibration Division of Sandia Corporation has developed
a low-cost force transducer from a commercially supplied
ceramic material. This transducer, as compared to com-
mercial types, is about 6 percent as expensive, 7 to 40 times
as sensitive, and comparable in all other aspects.

M. W. Sterk

INTRODUCTION

The need for a low-cost force transducer
is indicated by the increased emphasis on force
control vibration testing, the large number
needed to test large items, and the number of
replacements needed for those that become
damaged. In an attempt to satisfy this need, a
force transducer was constructed from a polar-
ized ferroelectric ceramic (PFC) material.
The following transducer properties were in-
vestigated: cost, sensitivity, frequency re-
sponse, preload effects, temperature effects,
stiffness, and age effects.

PFC TRANSDUCER

The PFC transducer is constructed from
two PFC disks (Figs. 1-3), thereby eliminating

the need for electrical isolation of the trans-
ducer. The two disks are placed, one on top of
the other, with their axes of polarization in op-
posite directions. A piece of copper placed be-
tween the two disks acts as a common lead, and
the insulation is used to prevent the bolt from
grounding the inside edge of the transducer.

The PFC transducer has an outside diameter
of 1.5 in., an inside diameter of 0.5+ in., and a
thickness of 0.4 in. However, the PFC material
can be purchased from the Electra Scientific
Corporation in many sizes and shapes.

TRANSDUCER PROPERTIES

Cost

The PFC transducer costs about $20, which
is 6 percent of the cost of some commercial
transducers. Of the total cost, $10 is for ma-
terials and $10 for modifications.

Sensitivity

Open-circuit nominal sensitivity is 420
mv/lb. This is at least 7 times the sensitivity
of the commercial transducers Sandia has
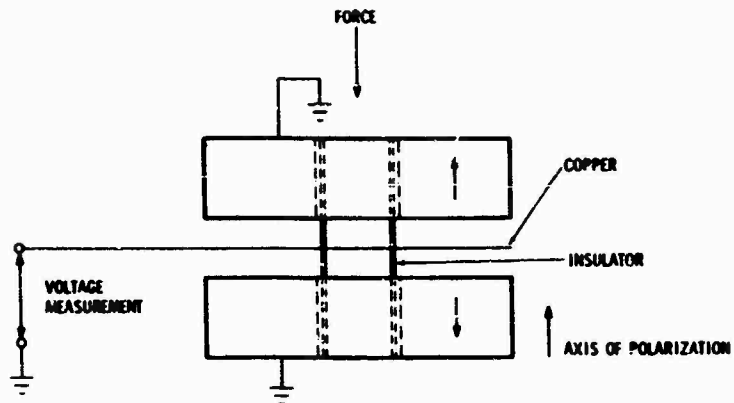evaluated.

203

Fig. 1 - Schematic of PFC transducer
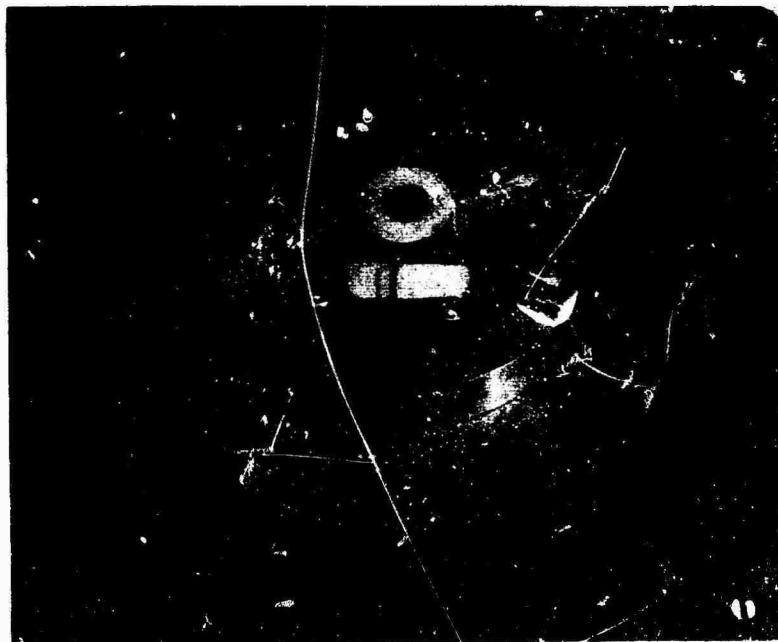

Fig. 2 - Disassembled PFC transducer

Fig. 3 - Assembled PFC transducer mounted on MB C-10 shaker

204

Frequency Response

The frequency response was checked between 20 and 2500 Hz and varied less than 2 percent.

Preload Effects

If the mating surfaces are clean, properly lubricated, parallel faced and smooth, there is little variation in sensitivity due to torque.

Temperature Effects

Between -65°F and 175°F, the PFC's sensitivity varies less than 10 percent.

Rigidity

The transducer showed nominal rigidity of 3.25×10^{-8} in./lb.

Aging

There may be a question about the variation of the transducer's properties with time.

This is no problem at Sandia, since system calibration is a part of each test procedure.

The voltage-dependent properties were measured by an experimental setup identical with that used at Sandia for force transducer calibration. The reliability of the experimental results is, therefore, the same as that of the force transducer results, which must be high. The experimental setup and method is detailed in the Sandia Corporation Development Report SC-DR-65-664.

Other properties are determined from information given by the manufacturer and from experience obtained during design and development of the transducer.

CONCLUSIONS

The investigation reveals the possibilities of a low-cost transducer. The PFC transducer is comparable to commercial transducers in frequency response, preload effect, temperature effects, stiffness, and aging. It is superior to commercial transducers in sensitivity and low cost.

*   *   *

AUTOMATIC CALIBRATION AND ENVIRONMENTAL
MEASUREMENT SYSTEM FOR LAUNCH PHASE SIMULATOR*

Harry D. Cyphers and Frank J. Holley
NASA Goddard Space Flight Center
Greenbelt, Maryland

A new environmental testing facility, the Launch Phase Simulator
(LPS), is presently undergoing acceptance testing at the Goddard Space
Flight Center. This facility will completely cover in a single exposure
the launch environmental condition; i.e., it will incorporate the latest
vibration, acoustic, and vacuum developments with the static (or
steady-state) loads generated during launch.

The LPS requires supporting instrumentation to monitor a large number
of parameters which vary considerably in amplitude severity and fre-
quency. Since this complex instrumentation involves many subsystems,
the checkout and calibration procedure must be properly sequenced to
minimize test preparation time. Therefore, the LPS data collection
system was designed to permit both automatic calibration and operation
from a master control panel. The control panel functions as a complete
status display of all data collection subsystems. The system can be
completely calibrated and checked in less than 15 min and produce a
digital printout to indicate system status.

The data collection facility is designed around a 98-channel constant
bandwidth frequency multiplex recording system which uses acceler-
ometer and bridge-type signal conditioners as inputs. Specific re-
quirements are frequency response 0 to 10,000 Hz, signal-to-noise
ratio of 45 db, and interchannel phase correlation of 5 degrees from 0
to 4,000 Hz. A unique feature of this complex system is the complete
integration of the many specialized calibrators by several automatic
calibrators, a digital voltmeter, a scanner, and a master control panel.
Several alternate methods of calibration, including some design con-
siderations for equipment setup and flexibility are briefly discussed.

INTRODUCTION

The complexity and quantity of data gener-
ated by advanced environmental testing facili-
ties have necessitated increasingly sophisticated
calibration techniques.

The system described here was designed
with maximum emphasis on operational sim-
plicity, accuracy, and rapid pretest and post-
test calibration. The system is presently being
installed at the Goddard Space Flight Center
and will be used to collect all the data generated
on the Launch Phase Simulator (LPS).

LPS INSTRUMENTATION
REQUIREMENTS

This simulator was designed to subject
spacecraft to the environments experienced
during the powered phase of launch. It is bas-
ically a 60-ft radius centrifuge with a vacuum
chamber located at its outer end. This chamber
houses a 3-degree-of-freedom vibration system
in a removable end cap and an acoustic noise
source (Fig. 1).

The centrifuge can produce up to 30 g of
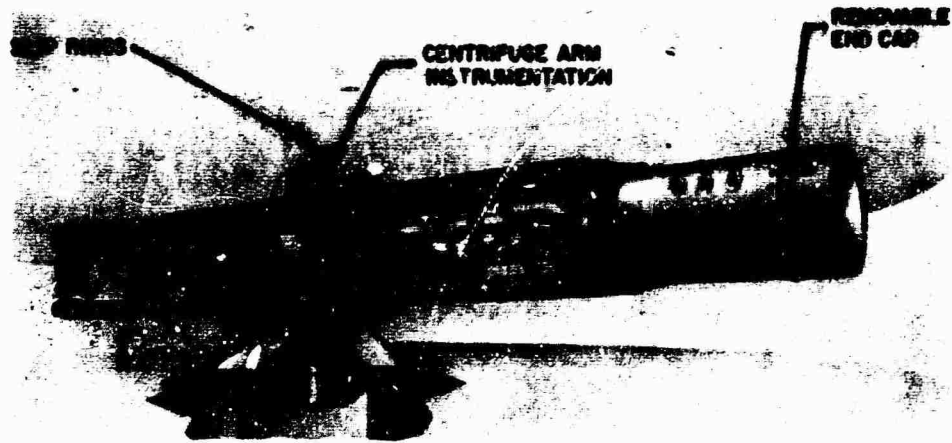steady-state acceleration. The vibration system

---

Fig. 1 - Launch phase simulator

is capable of operation in the thrust (radial) direction; producing yaw about a vertical axis, and transverse motion in a plane tangential to the arm rotation. Vibration can be sine or random from 1/2 to 200 Hz. The acoustic system can produce a sound pressure level of 145 db rms and has a frequency range of 100 to 10,000 Hz. The vacuum system can operate to 0.3 mm Hg (approximately 190,000 ft altitude). All environments can be simulated in real time.
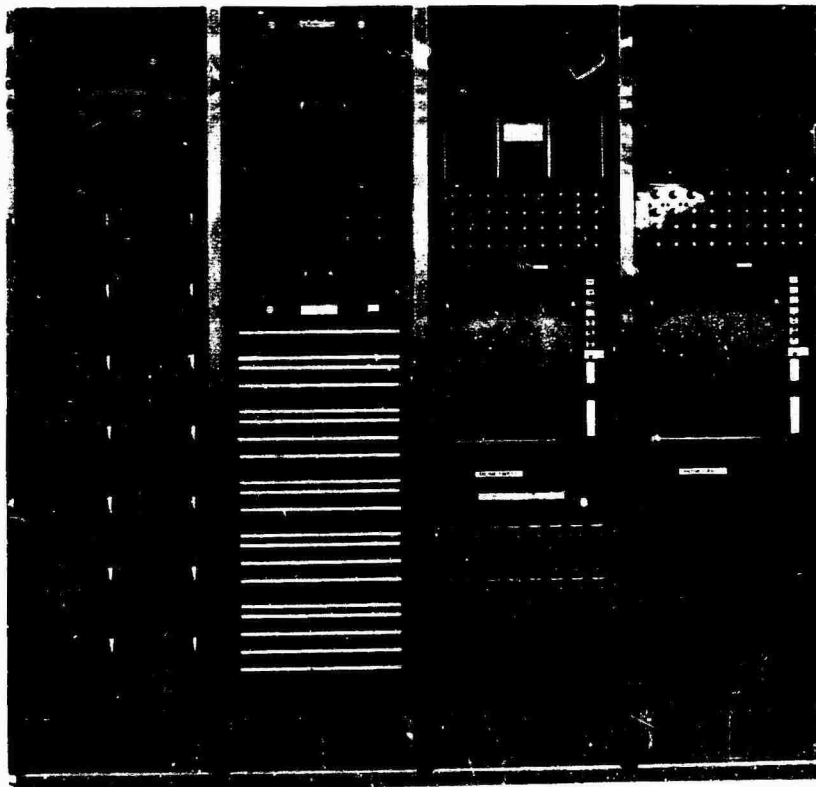

Fig. 2 - FM recording and display center

208

DESCRIPTION OF INSTRUMEN-
   TATION SYSTEM

This system is physically separated into
two parts: (a) the centrifuge arm instrumenta-
tion and its associated on-board calibrators
(Fig. 1) providing impedance matching and am-
plification of data signals prior to transmission
off-board via slip rings, and (b) the control
room instrumentation which displays and re-
cords on magnetic tape the data signals re-
ceived from the centrifuge arm (Fig. 2). This
second portion contains the calibration control
center which enables automatic checkout and
calibration of the entire system from the off-
board location (Fig. 3). The system require-
ments are frequency response of 0 to 10,000
Hz, 45-db signal-to-noise ratio, and interchan-
nel phase correlation of 5 degrees from 0 to
4,000 Hz with the tape recorder. Because of
the wide bandwidth, the great number of chan-
nels, and the phase correlation requirements,
the recording medium chosen is considered the
best. An analog-to-digital (A/D) conversion
system could also be used if the number of
channels and bandwidth requirements were
within the speed of presently available A/D
converters.

The significant difference between this and
other systems is the integration of the many
calibrators into a coordinated system with a
central control panel.

SYSTEM CALIBRATION

With the master program and calibrate
control (Fig. 4), the system may be calibrated
completely by one operator from the central
control area. Under system control, all cali-
bration equipment functions, such as the data
channel sequencing, measuring, calibrator
stepping, and limit testing, operate simultane-
ously.

Calibration of the system consists of the
application of voltages or frequencies to the
system or subsystem to determine system op-
erational capability. Under operator control,
discriminators, voltage control oscillators
(VCO) and discriminators, differential amplifi-
ers, charge amplifiers, and strain gages are
calibrated independently and automatically.
The outputs are tested against predetermined
limits. Digital printout accompanies calibra-
tion to identify subsystem and channel. Quanti-
tative information is printed only for out-of-
limit parameters. For a rapid pretest and
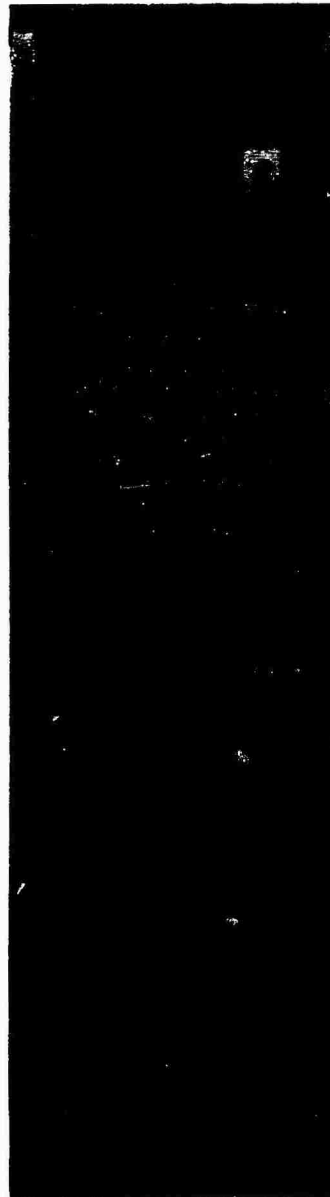posttest calibration, a 3-point calibrate mode

Fig. 3 - Master calibra-
tion and control center

records all channels simultaneously on mag-
netic tape.

In the calibration of the system, limit test-
ing is performed on the system employing fixed
parameters. These test results indicate under
static conditions, such as the application of a
constant band edge frequency to a discrimina-
tor, whether it is in or out of set limits. Simi-
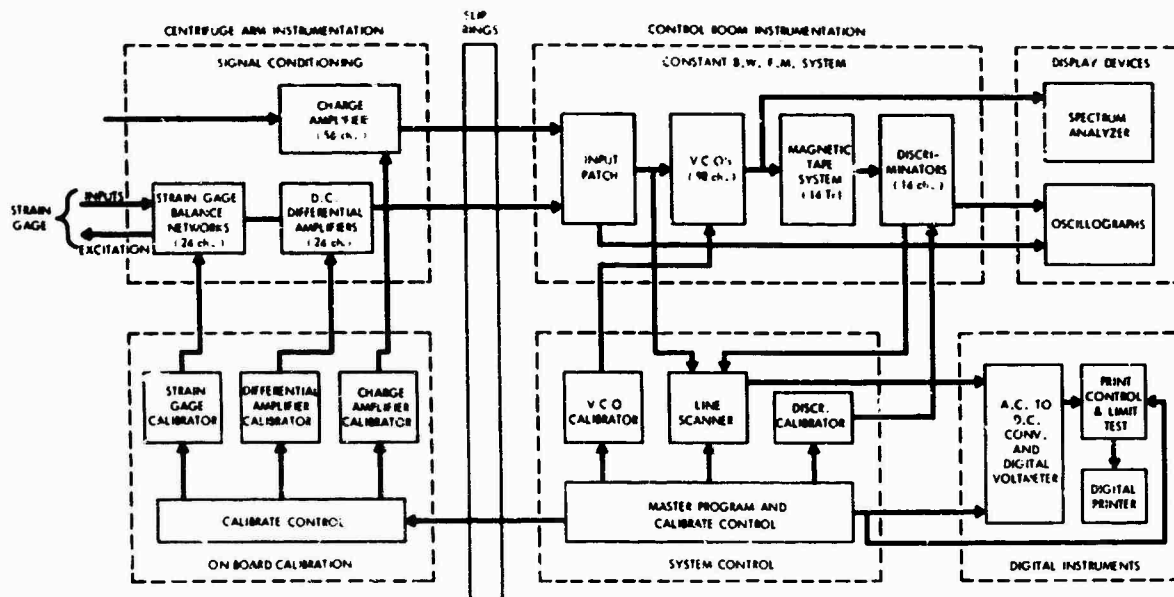lar static deviations are checked throughout the
system.

Fig. 4 - Block diagram of system

After static testing, sinusoidal signals of sequential amplitudes and frequencies are applied to charge amplifiers and differential amplifiers to determine whether rms deviation of amplitude linearity and frequency response of the system as a whole (exclusive of transducers) is within preset limits. An oscillographic recording of the sinusoidal response can also be made as the system is sequenced through selected frequencies. Flexibility in the selection of frequencies, levels, and dwell times is an inherent part of system design.

In addition to control functions required for calibration sequencing, the following specific calibrators are used: discriminator calibrator, VCO calibrator, charge amplifier calibrator, differential amplifier calibrator, and strain gage calibrator. Typically, calibration of the system will proceed when in AUTO-CAL as: (a) calibrate discriminators, (b) calibrate VCO/discriminators, (c) calibrate charge amplifiers, (d) calibrate differential amplifiers, and (e) calibrate strain gage. Results are recorded as digital printout and as an oscillographic record. The calibration time required depends only on the ac conversion rate of the digital voltmeter and the printer speed. The time saved in setup and checkout of the above system is illustrated by comparing it to another similar system in the Structural Dynamics Laboratory which contains no automatic features (Table 1).

SYSTEM DESIGN

The overall system is divided into three major subsystems: (a) the FM multiplex, (b) charge amplifier, and (c) strain gage conditioning and dc amplifier subsystem. The calibration system, which unifies these subsystems, consists of the individual remotely controlled calibrators to provide programmed calibration inputs, a 100-point scanner which scans all subsystem outputs, and an ac-dc digital voltmeter (DVM) and printer to record the outputs.

FM Multiplex System

The constant bandwidth FM multiplex system consists of 98 VCO's, associated summing amplifiers, a 14-track wideband tape recorder (7 VCO's per track), and two sets of 7 discriminators (Fig. 2) [1].

In addition to the completely manual method of setup and calibration, there are two concepts of FM system semiautomatic calibration, both using servo loops wherein the VCO frequency error voltage is used to drive a screwdriver which readjusts the VCO. One method uses voltage comparison and the other frequency comparison.

In the voltage comparison technique (Fig. 5), the discriminator is first calibrated using

210

TABLE 1
Comparison of Test Preparation Times for Manual and Automatic Calibration Systems

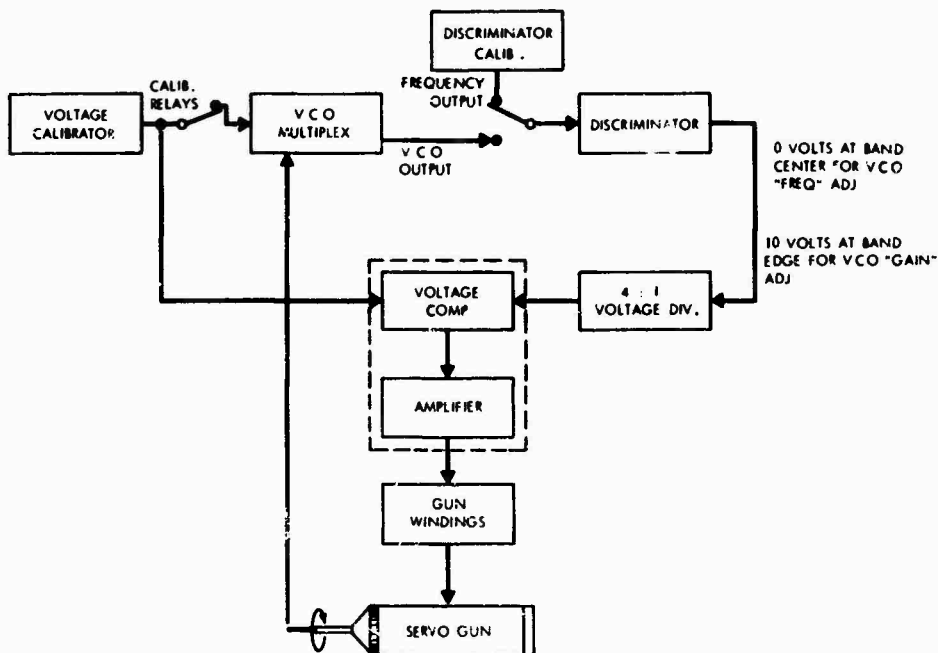| Subsystem	Operation	No. of Channels	Time Required (hr)	
			Automatic	Manual
FM system	Setup	98	0.50	5.00
	Check	98	0.10	2.00
Charge amplifier	Setup	56	1.00	2.00
	Check	56	0.05	1.00
Differential amplifiers	Setup	24	0.50	1.00
	Check	24	0.02	1.00
Signal conditioning	Setup	24	1.00	1.00
	Check	24	0.02	1.00
Total system time	Setup	-	3.00	9.00
	Check	-	0.19	5.00

Fig. 5 - Servo calibrator diagram (voltage comparison method)

crystal oscillators and a digital voltmeter for accuracy. Then upper band edge, lower band edge, and center frequency voltages from the VCO calibrator are inserted in the VCO input. These voltages are then compared with the output of the discriminator and the VCO frequency error voltage. This method is subject to discriminator drift (usually small) and limits the

discriminator output versatility because it is used as part of the comparison circuits. This limitation can be overcome by using the auxiliary output voltage tap (usually 1 v for full-scale deviation) available on several discriminators. This voltage is available before the adjustable output, thus allowing full use of the discriminator for playback purposes.
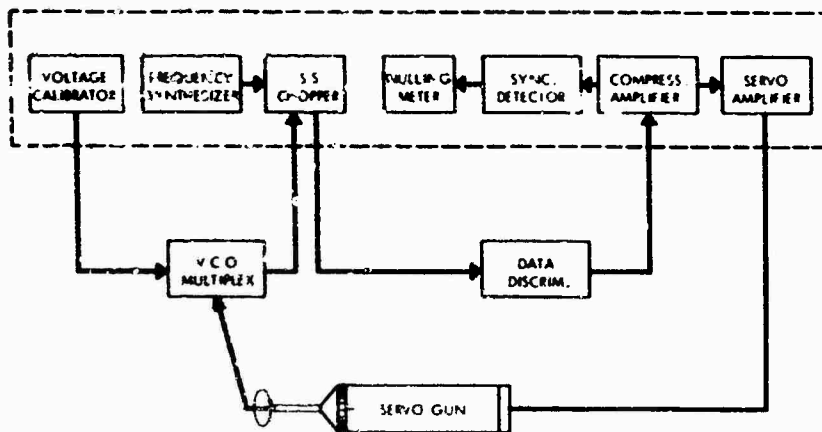
Fig. 6 - Servo calibrator diagram (frequency comparison method)

The frequency comparison method (Fig. 6) differs in that the VCO output is compared to crystal oscillators and the discriminator now serves as the comparison device.

The VCO and crystal oscillators are connected alternately to the discriminator. The difference between the two is the error voltage used to position the VCO zero and gain adjustments until the VCO output is the same as that of the appropriate crystal oscillator. The discriminator does not need to be accurately calibrated for this method, and the same crystal oscillators can be used to set up the discriminators. Both techniques are incorporated into systems which will automatically insert calibration signals and scan the discriminator and VCO/discriminator outputs. An accuracy of 0.1 percent of full bandwidth can be obtained with either system.

In the acoustic calibrate sequence, signals derived from the master calibrate control cause the discriminator calibrator to apply appropriate signal frequencies to discriminator banks and to sequence automatically through upper band edge, center frequency, and lower band edge. When operating with output scan and limit testing, the calibrator will apply seven frequencies corresponding to upper band edge for the seven oscillators in a discriminator bank. The line scanner then scans the output lines, connecting the DVM to each in sequence. Associated limit testing is accomplished on each output during the scan. As the calibrate sequence progresses, the digital printer produces a record of channel identification. In the event that an output falls outside set limits, the limit test will cause an appropriate control function to be generated so that binary coded

decimal (BCD) data are transferred from the DVM under print control for subsequent printout. Identification and quantity is printed for out-of-limit data. In the VCO/discriminator calibrate mode, VCO's will be automatically connected to discriminators, thus bypassing the tape recorder; the VCO calibrator is then programmed for a 3-point calibration and limit tests are run on discriminator outputs.

Charge Amplifier System

This subsystem uses a set of relays in the front end of the charge amplifier which permits series or shunt insertion of signals and a calibrator which controls these relays for its calibration system. This calibrator also has provisions for amplitude calibration from 0 to 100 percent of full scale in 3 or 9 steps in a manual or automatic mode of operation and manual selection of sinusoidal frequencies from 2 to 20 kHz.

Calibration of the charge amplifiers may be accomplished by local control or by automatic control of the charge amplifier calibrator as an integral part of system calibration. The actual calibration of the charge amplifiers consists of inserting sinusoidal signals for rms limit excursion and checking limits off-arm at the input to VCO's. During this phase of calibration, the signals at the input of the VCO's are converted from rms to parallel BCD by the ac to dc converter and DVM combination. A scan of all lines derived from charge amplifiers proceeds under system control with associated limit testing against preset limits. Printout with identification as to subsystem and channel accompanies calibration in the usual manner.

212

The relays enabling series insertion of signals to the input line are used to check the input lines to the charge amplifiers. Since the transducer used is a capacitive device, the line and the transducer serve as a capacitive divider. A meter can be used to determine whether the input line is open, shorted or normal [2,3]. The line test mode can be automated if desired. Gain normalization is obtained in the charge amplifiers by attenuators ganged to the input level selector. The proper level calibration voltage is automatically selected when the gain is determined for the transducer to be used.

Signal Conditioning System

The bridge completion and conditioning subsystem consists of the universal signal conditioning modules and the dc differential amplifiers. These modules will accommodate either bridge- or potentiometer-type transducers merely by changing printed circuit cards. The output of the module is fed to dc differential amplifiers and then to the recording system.

The calibrator used with the bridge completion networks provides simultaneous and/or sequential calibration in a manual or automatic mode and two levels of calibration: ±4 steps plus zero and ±1 step plus zero. Control functions, channel identification and calibration step identification are available both visually and in digital logic form for system integration.

This subsystem is calibrated by connecting the scanner to the dc differential amplifier outputs and the dc amplifier calibrator to the dc amplifier inputs. Since the differential amplifiers will have different settings, it is necessary to normalize the calibration input to the respective channel being calibrated. This can be done by a divider network on the calibrate input to the differential amplifier or by switching different resistors into the feedback circuit of the differential amplifiers. The latter method is more convenient in a system application but requires modification of the amplifier and, thereby, limits interchangeability.

Once the differential amplifiers have been set up and calibrated in a manner similar to that for the charge amplifiers, the bridge conditioning calibrator is programmed to step automatically through each channel applying shunting resistors to one or more arms of the bridge transducers. The differential amplifier output is fed to the scanner and then to the digital voltmeter where it is compared with the predetermined limits and flagged on the printer if it is out of tolerance.

Once the above subsystems have been set up and checked, it is possible to calibrate all channels simultaneously and record this on magnetic tape prior to and just after a test run.

Patching and Grounding System Design

The operational capability of a complex data acquisition and recording system hinges on the patching system which unifies its many components. Where possible, a one-for-one patching relationship should be maintained with functional grouping of inputs. An example of one-for-one patching would be charge amplifier 1 connected to VCO 1. Self-normalizing jacks which require no patching in a one-to-one or normal setup were used on this system. For other test configurations, it is only necessary to insert a patch cord to break the normal connection and patch the input where desired.

In any low-level data collection system a good grounding system is mandatory. In the LPS facility this consists of one central ground block tied to the main water line. Tied to this central block by individual connections are several satellite blocks. In addition, the separate building or earth ground is utilized for any circuits requiring ground returns. This prevents the instrumentation ground from becoming a current carrying ground. The equipment was selected with high common mode rejection ratios, ac and dc, and full differential isolated inputs and outputs where practicable. Proper procedures for termination of shields, selection of grounding points for various transducer configurations, etc., are available in the literature [4-6].

CONCLUSIONS

Test preparation time can be reduced to 1/5 of the time required for a manual system by using automatic calibration features. The automatic method is more comprehensive, less subject to operator error, and produces a printout verifying complete system status. Detailed dynamic analysis indicates that, exclusive of the transducers, an overall system error of less than 1 percent will be obtainable.

Despite the number of calibrators involved in a system of this size, they all operate in very similar ways. More effort should be exerted by industry to develop a universal modular ac-, dc-, and frequency-calibrator which could be easily adapted to various calibration requirements. Thus, one calibrator with some

213

programming could accommodate any portion of a complex system. Low-level (millivolts) voltage-controlled oscillators are now becoming available. These can in many instances obviate the need for signal amplification between transducer and recording medium. Also units have recently become available which combine signal conditioning, amplification, and VCO into one compact unit. These units have high- and low-voltage outputs plus the VCO frequency output. Other desirable features would include internal gain normalization capability and differential inputs and outputs.

REFERENCES

1. E. J. Kirchman and F. J. Holley, "A Telemetry Standard for Vibration and Acoustic Measurements," Shock and Vibration Bull. No. 34, Part 4, pp. 63-72, Feb. 1965

2. "Piezoelectric Transducer Calibration Simulation Method Using Series Voltage Insertion," Endevco Tech. Paper No. 216

3. "In Place Calibration of Piezoelectric Crystal Accelerometer Amplifier Systems," Endevco Tech. Paper No. 211

4. R. Morrison, "Shielding and Grounding for Instrumentation Systems," Dynamic Instrument Co. Tech. Paper No. 755-1

5. R. Morrison, "Isolation Considerations in Systems Design." Dynamic Instrument Co., Monterey Park, Calif.

6. D. Nalle, "Elimination of Noise in Low Level Circuits," ISA J., Aug. 1965

* * *

214

MICROMINIATURE INSTRUMENTATION AMPLIFIERS*

W. V. Bratkowski and P. F. Pittman
Westinghouse Research and Development Center
Pittsburgh, Pennsylvania

The measurement of physical variables such as strain, displacement, velocity, acceleration, and temperature has become increasingly important to both government and industry engineers and scientists. Associated with these measurements are serious problems of instrumentation size, cost, and number of data points required. The transducer amplifier used for these measurements plays a major role in attaining performance goals. In many areas, and particularly in the aerospace field, the number of measurements is dictated by the size, weight, and performance of the instrumentation. Many sensors and amplifiers are needed to insure a satisfactory number of measurements, but the vehicle cannot be overloaded. This paper describes the development of two families of microminiature amplifiers small enough that with existing technology they can be made an integral part of most transducers.

INTRODUCTION

Instrumentation amplifiers have played prominent roles in the field of experimental mechanics. Early amplifiers made from vacuum tubes were large, bulky, and expensive, but the introduction of the transistor made possible a considerable reduction in amplifier size and cost. Research and development in the field of solid-state devices during the past ten years has resulted in a new technique for the next generation of instrumentation amplifiers—molecular electronics. The active portion of each of these amplifiers is a monolithic linear integrated circuit which in its entirety is no larger than a single transistor of the type now used. Research and development work performed during the past year has resulted in the development of two families of instrumentation amplifiers suitable for use with conventional low- and high-impedance transducers.

The use of integrated circuit linear differential amplifiers not only reduces size and weight but improves circuit performance in certain areas owing to the unique features of monolithic silicon construction. Linear amplifiers made from integrated circuits have the following advantages over their counterparts made from discrete solid state components:

(a) small size and low weight, (b) well-matched device characteristics, (c) excellent device thermal tracking, (d) low noise, (e) high reliability, and (f) low cost.

MICROMINIATURE AMPLIFIER DEVELOPMENT

Generally speaking, the users of transducer amplifiers incorporate them into instrumentation systems such as those shown in Fig. 1. Although many different system applications are possible, several are worthy of note. In Fig. 1a, the present system connection is shown where the transducer is remotely connected, and all data processing and signal conditioning equipment including power supplies is centrally located. Owing to the small size and weight of the integrated circuit (I.C.) amplifiers, additional flexibility is available to the user either to locate amplifiers where he would have been unable to before, or to locate many more amplifiers in a given place. In Figs. 1b and 1c, system connections where transducer amplifiers are remotely located adjacent to the transducers are shown. Owing to the extremely small size of integrated circuit instrumentation amplifiers, they may easily be incorporated into the same case as the transducers with a negligible increase
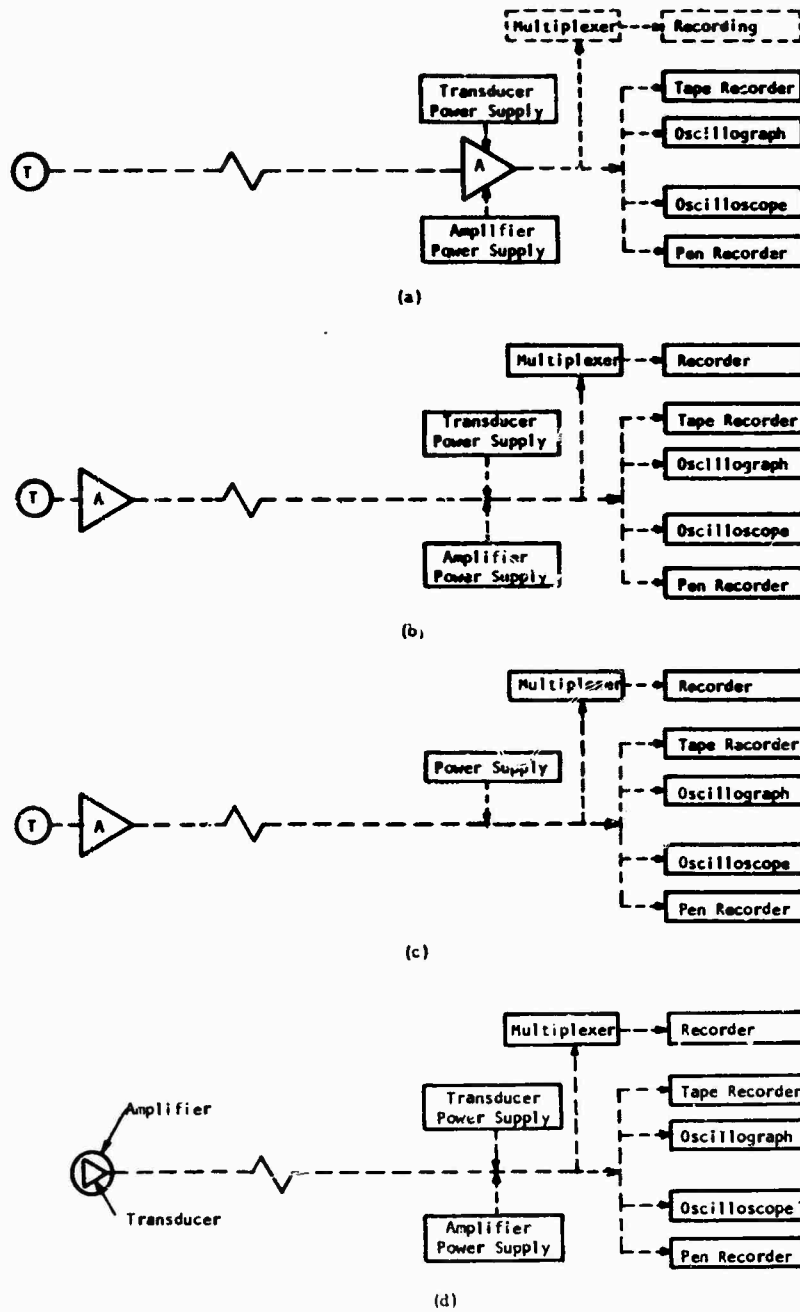
(a)

(b)

(c)

(d)

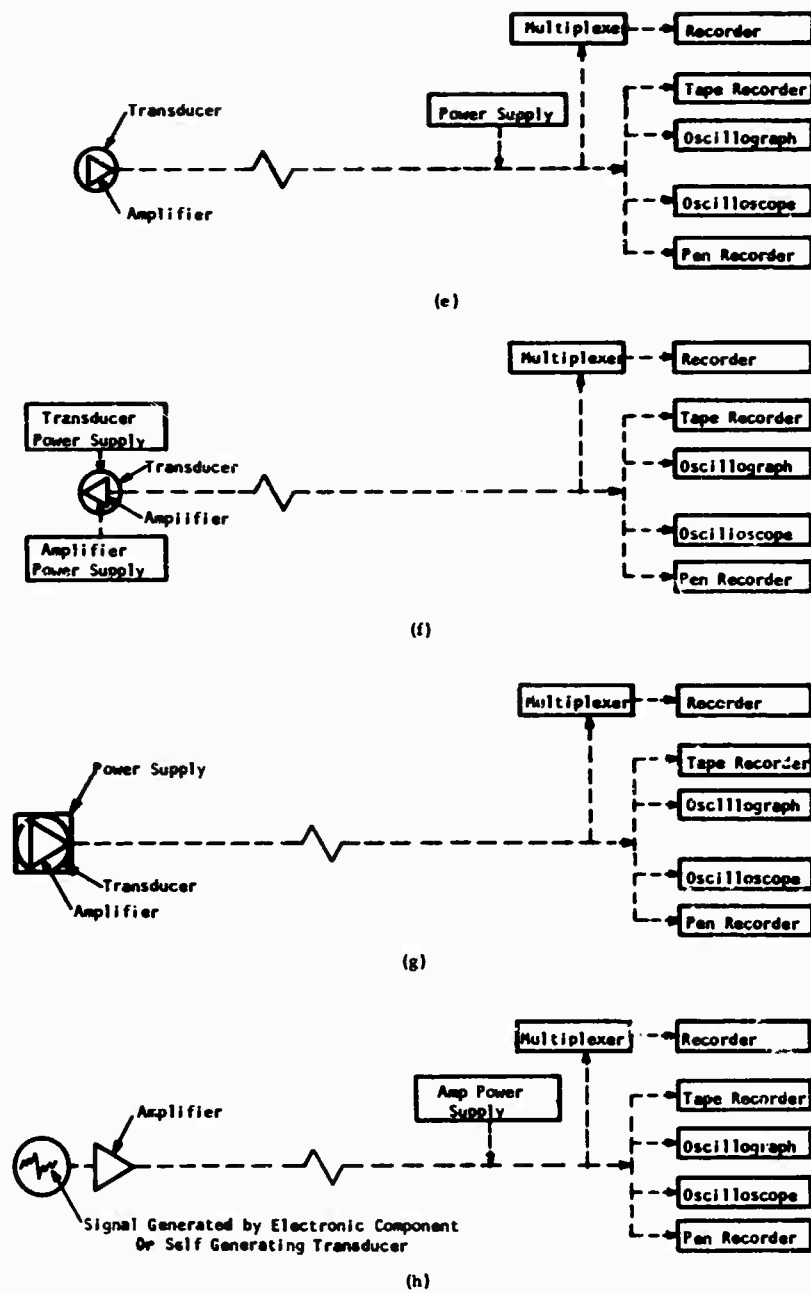Fig. 1 - Schematic diagrams of various measurement and recording systems

216

Fig. 1 (continued) - Schematic diagrams of various measurement and recording systems

217

in size and weight. Systems of this type are shown in Figs. 1d through 1h for various power supply locations. Although the system configurations shown in Fig. 1 are merely typical and quite general in nature, they effectively demonstrate the new freedom available to the instrumentation system designer as a result of removing constraints regarding amplifier location.

The microminiature amplifier was designed using a monolithic integrated circuit together with the smallest resistors, plugs, and capacitors commercially available. Examples of the types of resistors, capacitors, and integrated circuits used to develop the low-impedance strain gage amplifier are shown in Fig. 2. To illustrate the size reduction possible if further development work is done, a silicon die which could be designed to perform all functions now performed in hybrid fashion by the combination of an integrated circuit and discrete components has been placed in the upper edge by the foil strain gage and may be located beneath the point of the pencil at the upper right side of Fig. 2. Where sensors such as strain gages and thermocouples which have no case in which to house both transducer and amplifier are used, the amplifier may be separately encapsulated, but will be small enough to be mounted adjacent to the sensor and will be capable of operation in most environments suitable for the sensor. This amplifier is unusual because it uses the same 12-v dc power supply for the amplifier as well as the bridge circuit, and as a result, only one power supply is needed for such a system. A schematic diagram of a 120-ohm strain gage bridge and molecular amplifier is shown in Fig. 3.

In all, three types of microminiature amplifiers were designed, built, and evaluated, of which two were low-impedance or strain gage amplifiers. The first, shown in Fig. 4, has fixed gain of 250, and the other, shown in Fig. 5, has

a gain variable up to 500. Although incorporating the dual trimpot for gain adjustment increased amplifier size considerably, NASA, the customer, felt that the improved system flexibility provided by the variable gain feature outweighed the undesirable effect of increased size. The third amplifier, shown in Fig. 6, has high impedance and has a fixed gain of 15. A typical frequency-response curve for the low-impedance amplifier operating with a gain of 500 is shown in Fig. 7. The frequency-response curve for the high-impedance amplifier is shown in Fig. 8. The amplifiers investigated are only a few of the many which can be developed. Ranges of values for performance parameters of interest in instrumentation system design when integrated circuit amplifiers are used are given in Table 1. Because the design of a given amplifier always involves certain tradeoffs, arbitrarily chosen sets of parameter values may not necessarily be realizable. It is difficult to specify a value for the minimum physical size attainable because as the amplifier becomes small, other things such as connector size become determining factors instead of the amplifier active elements. Eventually, however, the size will approach that of the silicon chip shown in Fig. 2.

GENERAL SYSTEM CONFIGURATION

In most systems where amplifiers of the type developed are used, the basic function performed is a physical parameter measurement resulting in either a record or a display. In general, many parameters are sensed simultaneously, requiring a multiplicity of sensors.

A general system configuration is shown in Fig. 9. Many types of sensors which provide electrical signals in correspondence with some physical variable are available. Parameters which may be sensed include strain, acceleration, velocity, displacement, force, pressure, and temperature.
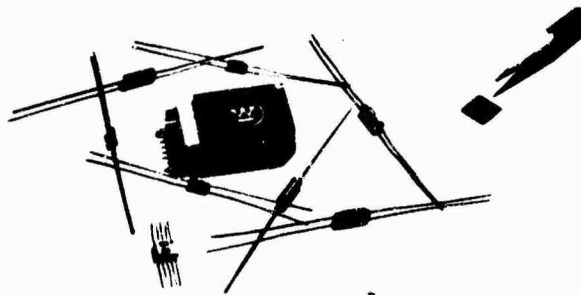

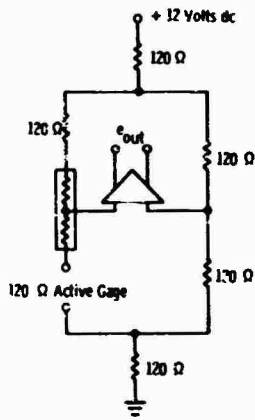Fig. 2 - Low-impedance strain gage amplifier
and its components

Fig. 3 - Schematic diagram of 120-ohm strain gage integrated circuit amplifier

Fig. 5 - Variable gain low-impedance strain gage amplifier

Fig. 4 - Fixed gain low-impedance strain gage amplifier

Fig. 6 - High-impedance fixed gain transducer amplifier

Because of the low signal levels produced by available sensors, an amplifier usually follows each transducer. The outputs of the amplifiers may go to a multiplexer—if needed—where the signals are combined, either by pulse duration or subcarrier multiplexing techniques, into a single signal capable of transmission over a single wire. As shown, signal paths may include telemetry loops where necessary.

The output of the multiplexer may then go to a tape or oscillograph recorder for permanent record or to an oscilloscope for instantaneous display. Where multiple-head tape recorders are available, multiplexer requirements may be reduced, or the multiplexer may even be eliminated if the number of sensors is small enough.

Certain systems may also include some circuitry for the purpose of trend or out-of-limit signal condition sensing. The outputs of such circuits may also be recorded or displayed as required.
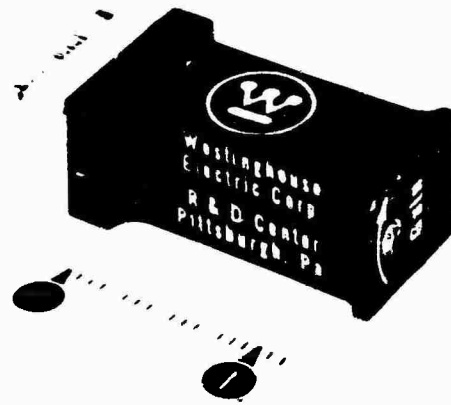
Electromechanical measurement systems and system performance monitors, two specific arrangements of the general system configuration using microminiature instrumentation, will be discussed in greater detail because of their many possible applications.

Electromechanical Measurement
System

The primary function of the electromechanical measurement system is collection of data concerning parameters of physical systems excited in certain ways. The embodiment of this system is quite similar to that of the general system configuration shown in Fig. 9. A multiplexer may or may not be used depending on the number of sensors and the number of simultaneous recording channels available.
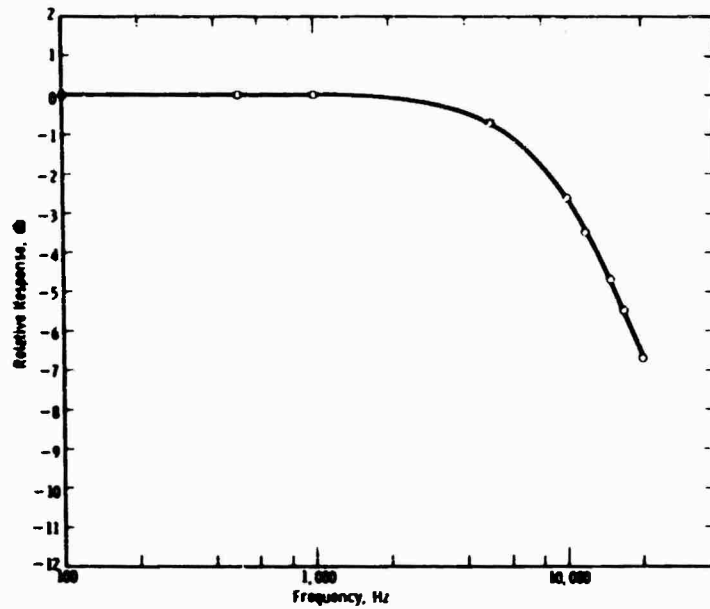
219

Fig. 7 - Frequency response of low-impedance amplifier
at maximum gain setting of 500

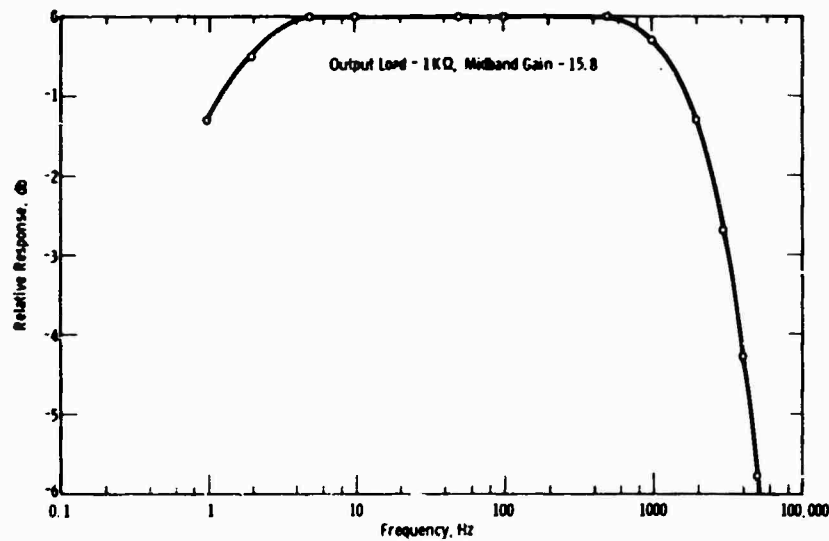Output Load - 1 KΩ, Midband Gain - 15.8

Fig. 8 - Frequency-response curve for Westinghouse high-
impedance molecular electronic amplifier with 1000-ohm load

The complete system is of interest for the following reasons. Amplifier size is decreasing rapidly and in many cases begins to approximate the size of the transducer used with it. From considerations of noise and calibration, it is advantageous from the point of view of system performance to locate the amplifier next to the transducer. The next most obvious step is to integrate sensor and amplifier into a single unit which would be lower in price than the combined prices of the amplifier and transducer.

In some situations, hard wiring between sensor and multiplexer is impossible, and in others, hard wiring between multiplexer and recording or display equipment is impossible.

220

TABLE 1
Typical Specification Ranges for Present R&D Microminiature Amplifiers

| Performance Parameter	Low-Impedance Model[a]			High-Impedance Model[a]		
	Minimum	Typical	Maximum	Minimum	Typical	Maximum
Input impedance (kilohms)	2	10	300	10^6		10^9
Output impedance (kilohms)	50	2.7	3	50	50	100
Output voltage swing (v)	--	--	±5	--	--	±5
Transfer Characteristics:						
Gain, continuously variable	10	--	1000	10	100	200
Common mode rejection (db)	60	70	90	--	--	--
Noise, referred to input (μv)	5	6	10	20	50	60
Frequency response, 3 db down (Hz)	DC	--	10^5	0.8	--	2×10^4
Gain stability (%/°C)	--	--	0.1	--	--	.1
DC offset stability (μv/°C)	3	5	7	--	--	--
Linearity (% of full scale)	0.1	--	1	0.1	--	1
Operating Temp. Range (°C)	-55	--	+125	-55	--	+125
Voltage requirement (v)	1.5	12 DC	15	1.5	12 DC	15

[a]Volume may range from 1/2 to 1/300 cu in.
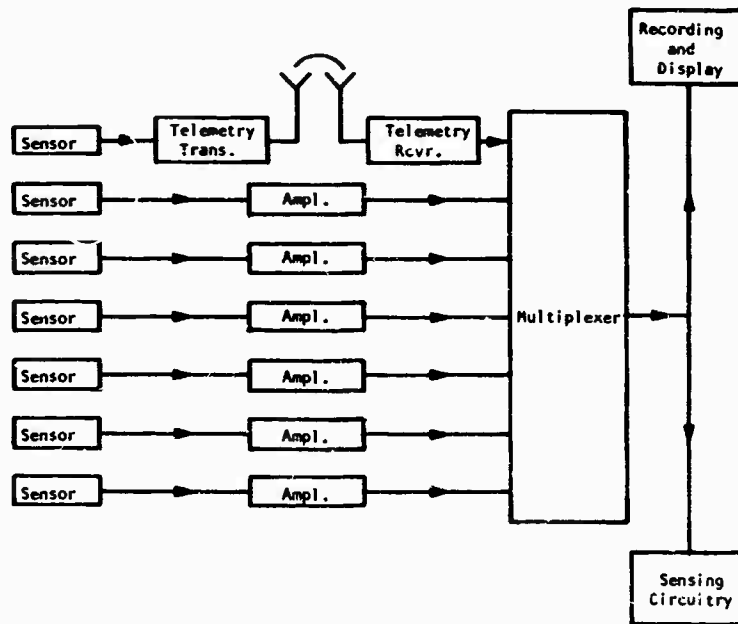
Fig. 9 - General instrumentation system block diagram

For these situations, telemetry lii s are required where signals are converted to FM by voltage-controlled oscillators and transmitted at some high carrier frequency. Telemetry links of the type needed may be constructed from combinations of integrated circuits and discrete components. Integrated circuit broadband amplifiers may easily be obtained, but where frequency selectivity is needed, discrete components must be used.

Except for the recording device — usually a tape recorder or oscillograph — the remainder of the system, which includes all display amplifiers as well as all fault-sensing circuits, can easily be made from microminiature instrumentation.

The type of system described can be used in physical test laboratories and for structure prototype tests on aircraft, spacecraft, rockets, mass transit vehicles, automobiles and trucks, ships, motors, turbines, generators, and fans. In many of these applications, measurements of physical parameters must be made at many different locations on the structures. Because of the present large size and high cost of the required instrumentation, general practice has been to use a small number of instruments and to take a few readings at several locations. As the size and price of the required instrumentation decreases, simultaneous measurement at more and more places will become more attractive, requiring the use of more amplifiers and more sophisticated time-sharing and multiplexing systems.

System Performance Monitor

The system performance monitor is most easily differentiated from the electromechanical measurement system by the fact that the performance monitor operates continuously as the monitored system is used. The previously described system, however, is used merely to evaluate a prototype structure or to make a one-time qualification evaluation of a finished structure.

The basic building blocks of the system performance monitor are the same as those shown in Fig. 9, and all considerations concerning their development and construction described in the previous section apply here as well. In general, the same types of parameters must be sensed using the same types of transducers or combined transducer-amplifiers as described previously. In some cases, the parameters to be sensed will be electrical signals taken from

a functioning system eliminating entirely the need for any transducer.

Although a common set of building blocks can be used, systems of this sort may take many different forms depending on the application. A partial but by far not all-inclusive list of some of the types of systems is given in the following paragraphs.

Simple Monitoring of Critical Parameter — In many instances, much money or the safety of people may be jeopardized if a system functions improperly. A fairly simple monitoring system can be used to sense and warn of either existing or impending trouble. An example of such a system would be an aircraft turbine vibration sensor which has been shown to be invaluable in sensing impending turbine failure.

Fault Detection — Some systems function properly only when a number of independently operating subsystems each operates properly. If any one of the subsystems malfunctions, the total system will not work, and when failure does occur, the indicators of failure may be such that it is difficult to quickly isolate the failed part. Most transportation systems including aircraft, automobiles, and ships are examples of such systems. In almost every case, the performance of the total system must be monitored by personnel, and when failure occurs, they must diagnose the indicators of failure to locate the failed part or subassembly as quickly as possible.

In general, the more diagnostic data available, the shorter is the time required to locate and replace the failed part or assembly. If the total system is an automobile, the amount of time required to diagnose and repair the failure is usually of little consequence. But, if the system is a warship or an aircraft, obviously time can be critical.

Data Logging — Many systems operate with no control, with inadequate control, or with unreliable or antiquated control. For any one of a number of reasons, it may be of interest to generate a continuous record of a critical parameter in such a system for future use. If the process or system considered is large and enough parameters are to be recorded, a process control or data logging computer is required. Such a system is not considered here. Under consideration are small systems where only a few parameters of interest are needed and where the cost of a computer would be out of the question.

222

Monitoring systems of the type suggested already exist, but they are mainly of old design, large, electromechanical in nature, and expensive. By using microminiature instrumentation and utilizing fully the new and unique features available in system design which arise from the use of integrated circuits, many applications today considered to be out of the question will be feasible.

Areas of applications of all three types of system performance monitoring systems include aircraft, mass transit vehicles, computer systems, power generation equipment, machine tools, water pollution control systems, and fabrication processes. In all of these cases, of course, the sale price of the system must be consistent with the economics of the market considered.

*   *   *

INVESTIGATION OF PULSE X-RAY TECHNIQUES FOR STUDY OF SHOCK-WAVE INDUCED EFFECTS IN SOIL*

Warren J. Baker and Frank J. Janza
Eric H. Wang Civil Engineering Research Facility
University of New Mexico
Albuquerque, New Mexico

The recent development of pulse x-ray systems provides an important new instrument with capabilities not previously available for testing in study of shock-wave phenomena. Technological advances in x-ray systems have resulted in pulse powers of 50 kv to over 2 mv and pulse widths of 20 to 30 nanoseconds. Such extremely narrow x-ray pulses and high-accelerating potentials now provide a means of radiographing the interaction effects of a shock wave with test models embedded in various homogeneous media. Soil can be penetrated to a depth of 12 in., and the interaction effects can be radiographed at repetition rates (or framing rates) from 10^3 to 10^5/sec. The feasibility of a pulse x-ray system in the study of shock-wave-induced motion of modeled structures buried in soil was investigated. The results from about 20 tests on models buried in soils are presented by radiographs and 35-mm photographs. Initial tests determined the techniques, model size, and density of soil which would yield optimum pictures. The use of gamma-ray sources and other x-ray phenomena for shock-wave measurements was also investigated.

INTRODUCTION

X-Rays Applied to Soil Research

With the recent advances in flash x-ray systems, the possibility of obtaining useful information of shock-wave-induced motion of objects buried in soils by the application of these systems was investigated. The prospects of being able to radiograph the shock wave as it interacted with a buried model warranted the initiation of a series of tests with a flash x-ray system which generated a group of eight 150-kev 1-μsec pulses space 1 msec apart.

Tests were conducted to determine: the capabilities of the pulse x-ray system to resolve density variations in soil, edge detail of the buried models, and the maximum soil sample that could be penetrated and still produce usable radiographs.

Previous radiography served as a basis for this study; unfortunately, most of this work had been done with static x-ray systems.

Role of X-Rays in Soil Studies

X-rays have been used occasionally in soil mechanics to monitor soil-density changes under load or as a result of various placement techniques [1,2]. Tracking the motion of small, x-ray-opaque pellets in the soil has also been an important application [2,3,4,5].

Three unique features of the x-ray technique make it a desirable method of measurement in soil. First, it is a whole-field technique which gives a full picture of the events in an area that can be photographed. In comparison, gages placed in soil to measure soil or structure motion can give, essentially, only point information. X-rays may be used to define the progression and shapes of failure planes, a decided advantage over other instrumentation techniques. Second, the penetration of x-rays through a soil sample, resulting in the exposure on recording film, is a direct function of the soil density and a convenient way to record density changes as stresses are developed in a soil

---

mass. Third, very small, opaque pellets (slightly larger than soil grains) embedded in a soil mass can be tracked when subjected to stress changes. Thus, many displacement measurements of soil can be taken in the field of view by setting up an array of pellets. The measurements may be taken without disturbance of the soil by internal instrumentation since the x-ray source and recording medium are outside of the soil sample. Generally, soil-placed gages will affect the surrounding soil motions which occur when stress is applied to the soil [6,7,8]. Factors such as modulus mismatch, acoustic impedance mismatch, and arching will influence the readings from an embedded gage.

The x-ray technique used in the study of soil dynamics has not yet produced the expected results [9]. Repetition rate, duration, and intensity of x-rays have not been developed to a point where the information on a dynamic record is adequate for analysis of the changes in the soil as a stress wave passes through it. The minimization of the scattering of x-rays in soil also requires extensive investigation.

Review of Static Work

In 1929 Gerber [3] used x-rays to determine the overall displacements in a soil sample when a failure load was applied. He was able to track 3-mm lead pellets in sand loaded by a 3-in. steel plate. The thickness of the sample was 8 in., the maximum thickness that could be effectively penetrated. The photographs were not clear enough to be reproduced, and some of the pellets did not show on the radiographs.

The next major step in the use of the x-ray technique, with a continuous source system, did not occur until 1949 when David and Woodward [2] investigated a two-dimensional, footing-failure problem. Their results were very encouraging: density changes and incipient failure planes and patterns were easily seen beneath the footing. Lead bird shot was placed in a mesh below the footing. Displacements of the bird shot were measurable at depths of three footing widths. A dense wedge which developed directly beneath the footing was also easily detected. Their study employed direct exposure of 11- by 17-in. x-ray film, as well as a fluorescent screen placed behind the soil sample and photographed with a 35-mm camera. The soil samples were moderately well-compacted sands, 3.0 to 4.5 in. thick. The latter dimension was the maximum thickness that could be penetrated by their x-ray systems.

In 1951 Berdan and Bernhard [1] performed pilot studies on density measurements by x-ray. In essence they took pictures before and after compaction of a soil sample. A granular beach sand and a cohesive silt were used; the samples were 3.11 in. thick. The x-ray equipment was a Westinghouse Industrial Unit with a 150-kv rating. The x-ray exposure – at 60 kv, 30 ma, and a 48-in. focal length – was 9 min and produced a readable x-ray film placed behind the soil sample. Large density changes (10 to 15 percent) did occur. However, the minimum density change that could be detected was not determined. The authors also embedded a pressure cell in the soil which was then compacted. The decreased density in the area below the cell was obvious from the radiographs.

More recently Roscoe et al. [4] used a continuous x-ray technique to determine strains in sand. This study was conducted in a model earth-pressure apparatus [5] to determine the state of stress and strain behind a vertical wall structure as the structure was rotated from the surface into the soil mass. The apparatus had glass walls 6 in. apart, and x-ray film was placed in a cassette directly behind the sample. The equipment was a continuous industrial-type Müller M. G. 150 x-ray machine with a maximum rating of 8 ma at 150 kv with a 1.5-mm focal spot. The sand was used in a dense state (void ratio, e = 0.55), and adequate pictures were obtained with a source current of 8 ma at 130 kv and an exposure time of 4 min. Displacements of lead shot, 2.5 mm in diameter and placed in a fine mesh behind the wall structure, were tracked with satisfactory results. Shear planes and planes of incipient failure could be detected from the dilatancy which took place on these planes.

Arthur et al. [5] were interested in studying plane-strain problems which required that the apparatus walls be rigid, have a low coefficient of friction, and be transparent to x-rays. Designing walls with these characteristics is difficult when the x-ray flux and exposure time are limited as in a dynamic situation. However, the information presented in Refs. 4 and 5 prove rather convincingly that for static work in soil the x-ray technique is a very useful means of instrumentation.

TECHNIQUES FOR USE OF X-RAYS IN DYNAMIC SOIL TESTS

The major difference between x-ray studies in static and dynamic soil tests is the amount of

226

time available during the test to pass sufficient x-rays through the sample to expose the recording film adequately.

When the tests are dynamic, two types of available x-ray machines may be used. The first has a multiple-flash x-ray source with a pulse width about 1 μsec. The duration of the pulse is short enough essentially to stop the motion in a soil sample loaded dynamically. The number of pictures per second (or frame rate, fr/sec) and the time lapse between pictures depend on the number of voltage pulses applied to the x-ray tube, or the pulse-repetition frequency (prf). The pictures are recorded with a high-speed motion picture camera after the shadowgraphs resulting from the transmitted x-rays have been transformed and converted to visible light through an x-ray image intensifier. The transmitted x-rays can be used to expose x-ray film directly without image intensifier and high-speed motion picture camera. If the film is held stationary, the record is in the form of a series of multiple exposures on one frame. The film on a drum can be rotated at a convenient rate to provide multiple frames with single exposure. The time history in all cases is provided by the pulse-repetition frequency.

The second machine has a constant-potential x-ray source which produces a continuous flow of x-rays through the soil sample. By rotating a drum with the film on it, a streak photograph of buried objects may be obtained. The deviation of this streak from its original path is directly related to the displacement of the object in the soil. Since the drum velocity provides the time base for this record, the slope of the streak is directly related to the object velocity.

The use of radioactive pellets (gamma-ray emitters) embedded in soil has also been given some attention [9,10]. In most cases detection of the motion of the radioactive pellet is the means of obtaining information. Since very little research on radioactive pellets has been done for applications to soil measurements, new designs and techniques will have to be tested. It is likely that such a measurement system would require from two to three years for development.

Some priorities based on penetrability, practicability, and availability have developed in the designation of x-ray (gamma-ray) systems for dynamic soil measurements. After research into the application of x-rays to nondestructive testing and fields closely associated with soil dynamics, priorities in the following order are suggested:

1. Multiple-flash x-ray system (field-emission type).

2. Multiple-flash x-ray system (hot-cathode type).

3. Embedded radioactive isotopes used with scintillating crystal detectors. (Considerable developmental work and experimentation are required before a usable system would be available for dynamic soil measurements; however, the feasibility of such a system has been demonstrated for other applications with similar stringent requirements.)

4. Embedded radioactive isotopes in an arrangement to maintain the whole-field characteristics of x-rays, or the application of the Mossbauer effect. (Both techniques require extensive development before a workable system would be avilable.)

Certain areas of research in soil dynamics are particularly suited to experiment with x-ray techniques, because displacements, density charges, and formation of shear or rupture planes as a function of time are important characteristics; and the formation of shear or rupture planes usually cannot be obtained conveniently with other techniques.

The changes in the free field as a stress wave passes through a soil sample may be studied with x-rays. The motion of small lead pellets which appear opaque to x-rays when embedded in soil samples 3 to 8 in. thick may be tracked on film with an appropriate time marker. However, information derived from x-ray records is limited by the effects of boundaries on samples only 3 to 8 in. thick, and boundary effects are serious when simulation of one-dimensional behavior at great depths is attempted. Displacement gages have been developed recently [6] which are reliable for free-field measurements. By using gages in progressively larger samples, the effects of sample thickness may be detected. Consequently, free-field information derived from x-ray records is expected to be somewhat limited; it probably can be outlined more easily and reliably by other means.

Laboratory experiments on direct explosion coupling, cratering, and underground explosion cavities [11] can be monitored using high-speed x-ray techniques. The x-ray records will provide information on the development of cavities, propagation of fractures in brittle materials, and the mechanism associated with cratering. The experiments are restricted by boundary

227

conditions imposed by sample thickness limited to 3 to 8 in. The type of information obtained in experiments with x-rays, however, cannot be as complete as with other techniques.

The greatest advantage of the x-ray technique is found in experiments where interaction between the soil and a structure takes place. It is nearly impossible to instrument such experiments adequately with gages on the structure and in the soil to define the interaction.

Buried models taken to failure or subjected to large deformation are well suited to the x-ray technique. Some success has already been achieved in monitoring with x-rays with collapse and deformation mechanisms of lined and unlined tunnels of various shapes and the resulting soil deformation. Model footings taken to failure dynamically develop displacements and failures in the soil that are easily detectable by x-ray.

An important feature in any laboratory test on large samples of soil is the effect of soil-container boundary conditions. Recording by x-ray the motions near boundaries can be particularly effective since most soil-placed gages are unreliable near boundaries.

Great effort has been expended recently to develop soil-placed gages for dynamic use. Berdan and Bernhard [1] showed that placement problems of buried pressure cells could be studied with x-rays. The placement and response of gages used in soil dynamics are particularly important, and the development of an evaluation technique using x-rays would be very worthwhile. The evaluation technique should be designed to assess the influence of the gage on the surrounding soil and to distinguish between the motions of the gage and the soil if the gage were not there.

FLASH X-RAY TECHNIQUES IN SOIL DYNAMICS

When flash x-ray studies in soil dynamics were first considered in 1963, it was difficult to provide comprehensive specifications for the test apparatus. The difficulty arose because great penetrating power was needed in very short time to record information. Proved flash x-ray equipment to provide this penetrating power in short bursts was not available, and some development was needed. Technology in flash x-rays has advanced rapidly in the past two years, and tests indicate that specially prepared soil samples and buried test objects can be studied under dynamic conditions with flash x-ray equipment.

Time

In dynamic events the time factor associated with sensing instruments means several things. Specifically, with a multiple-flash x-ray system, one is concerned with the x-ray-pulse duration, the pulse-repetition rate, and the total time span over which x-ray pulses can be produced. The pulse duration must be short enough so that a still picture of the soil sample can be taken (without objectionable blurring) while a shock wave is traveling through the soil at high velocities, i.e., 800 to 2,500 fps. Today x-ray technology can easily produce pulse widths from 18-nanosec to 2 μsec.

X-Ray Intensity

The most important requirement of a flash x-ray system in dynamic soil tests is the generation of flash x-rays of high intensity. This radiation intensity or flux emanating from nearly a point source is subject to geometric attenuation as the x-rays diverge from the source. In addition to geometric attenuation, the x-rays are also subject to severe attenuation from mass absorption of radiation as they penetrate the soil sample.

To obtain a shadowgraph of that portion of the soil bin (approximately a 9-in diameter field of view) containing the embedded pellets, the x-ray source was placed about 18 in. from the front of the soil bin. The intensity was thus limited by the requirement for the field of view.

The mass absorption was severe since it is an exponential decay function which depends on the mass-absorption coefficient and thickness of the material. The following example of the mass absorption of a 6-in. dense sample of 20-30 Ottawa sand (standard testing material) will delineate the problems in producing sufficiently intense x-rays of short-pulse widths.

In Ottawa sand a unit weight of 111 pcf — 1.775 gm/cc — represents a void ratio of 0.5. Ottawa sand is nearly 100 percent silica (a form of silicon dioxide, SiO_2) in the form of quartz, and a 6-in.-thick sample represents 4 in. of solid quartz which must be penetrated.

Mass-absorption coefficients for particular bodies can be calculated by weighting the mass-absorption coefficients of the elements in the body. In this example it is convenient to calculate an x-ray intensity-reduction factor as

$$\frac{I_t}{I_o} = e^{-(\mu/\rho)(\rho)t} \qquad (1)$$

228

where

I_t = radiation intensity after beam has passed through body,

I_o = radiation intensity incident to body,

μ = mass-absorption coefficient of body,

ρ = mass density of body, and

t = thickness of body to be penetrated.

The value of μ for SiO_2 at 150 kev is nearly 0.14 sq cm/gm given by Bloedow [9]. The density of quartz is 2.65 gm/cc. Thus I_t/I_o is computed to be 0.023, or the x-ray flux incident on a 6-in. sample of dense Ottawa sand suffers an attenuation of nearly 98 percent because of mass absorption of the sand. An 8-in. sample would absorb about 99.7 percent of the x-rays.

Resolution

Poor resolution in x-ray records limits the quantitative information which can be gathered. By using specially prepared soil samples and test objects, valuable information about dynamic behavior can be collected even if investigation is limited to large displacements. The displacements that might be effectively studied with x-rays are peak particle displacements of 150 to 250 mils. To determine the minimum detectable displacement, it will be assumed for purposes of calculation that the peak particle displacement decays linearly in 10 msec. It seems valid to require that a measurable change in displacement be recorded at least every 1 msec. This means that particle displacements between pulses should be resolvable to at least 33 percent in the interval (about 5 to 8 mils) so that the 15- to 25-mil change in displacement can be readily measured.

Field of View

The size of the field of view is dictated by the particular experiment. It is important to keep the field of view to a minimum to control better the various kinds of geometric distortion and scatter for higher radiographic sensitivity. In the experiments with model footings, lined and unlined cavities, explosion cratering, and instrumentation evaluation, the field of view cannot be reduced below certain minimums. The area of interest above model structures for which arching studies have been made is nearly 8 sq in. Consequently, a very large field of view is desirable; anything smaller than 8 in.

in diameter could seriously hamper the scope of studies in soil dynamics and soil-structure interaction.

The field of view must not be distorted dimensionally beyond correction. In particular tests where density changes and failure planes are of primary interest, the field of view should maintain a nearly uniform intensity (brightness or film density). In cases where image intensifiers are used, the inherent vignetting is very noticeable; however, the vignetting on recently developed image intensifiers has been greatly improved.

Material Properties

It is desirable to study various soils from dry sand to wet clay, with grain sizes from 0.6 to 1.2 mm and 0.0002 to 0.002 mm, respectively, and with mineral contents from SiO_2 (quartz) to $2H_2O \cdot Al_2O_3 \cdot SiO_2$ (kaolinite clay). The dynamic response of soil is generally attributed to the constitutive relationships exhibited by a particular soil. A dense, uniformly graded sand may exhibit a one-dimensional secant modulus of 40,000 psi at a stress level of 100 psi, while a soft clay could easily have a modulus of 4,000 psi. The density of the sand may be as high as 120 pcf, and that of the clay as low as 80 pcf. In a dynamic soil test on a column of soil 3 ft high, the surface will displace 0.1 in. if the material is the dense sand, and 1 in. if the material is the soft clay. The stress wave velocities at 100 psi in dense sand and soft clay will be about 1,300 fps for the sand, and 500 fps for the clay; and typical peak particle velocities will range from 2.5 fps for the sand to 12.5 fps for the clay. Thus, depending on the capabilities of the x-ray equipment, a wide variety of soil types can be studied. If the resolution and penetration factors of the x-ray system are low, the selected soil must be softer (less dense material) if adequate x-ray penetration is to occur.

Boundary Conditions

The boundary conditions of concern are those at the soil-container walls. The walls create a friction effect in the soil which carries shear stresses normally carried by the soil. The stresses developed at the wall are transmitted to the soil and influence the soil response. The walls must be nearly rigid (and maintain a high transparency to x-rays) to minimize the influence of three-dimensional deformations occurring in tests to simulate one-dimensional and two-dimensional behavior.

RESULTS OF EXPERIMENTS WITH FLASH X-RAY SYSTEM

Multiple-Flash X-Ray System

The pilot tests with the multiple-flash x-ray system were concerned with how well particular areas of soil dynamics and soil-structure inter-action could be studied by multiple-flash x-rays. The particular multiple-flash x-ray system which was used for tests was developed for specific soil experiments and has been used statically (for calibration purposes) and dynamically with sand and silt in rectangular cross-sectional containers. The dynamic inputs were developed with shock waves from a 45-ft vertical shock tube and with hydraulic rams. Figure 1 shows a typical test arrangement.

Figure 2 is a schematic of the multiple-flash x-ray system in a typical test arrangement. The system generates a series of eight 1-μsec pulses with a pulse-to-pulse time separation of $1,000$ μsec. As the pulse-repetition frequency is lowered, the number of pulses per sequence increases. The high pulse-repetition frequency is possible for only a limited number of x-ray pulses because of the low rate of heat dissipation by the anode of the x-ray tube.

The advantages of the multiple-flash x-ray system over conventional x-ray systems in medical and industrial laboratories are as follows:

1. The system has stop-motion capability for transient events. For example, a radiograph of a shock wave front having a velocity of $3,000$ fps is smeared out 36 mils by a 1-μsec x-ray pulse. A soil set in motion with a velocity of 100 fps by the shock wave has the radiograph of the motion smeared 1.2 mils by the 1-μsec x-ray pulse.

2. The system provides a sequence of 8 pulses at a pulse-repetition frequency (prf) of $1,000$ pulses per second (pps) which makes it possible to get sequential sets of data of the shock wave as it propagates through the sample.

3. The system has an 8-in. image-intensifier tube which converts x-rays to electrons at the input screen and then converts the electrons to visible light at the output screen. The tube provides a nominal gain of 3,000, thus the x-ray dosage can be lowered considerably. The information transformed to visible light can then be coupled to a motion picture camera by optical methods. The image intensifier permits use of longer x-ray wavelengths with consequent re-duction of the accelerating voltage, and allows improving the contrast, particularly when the x-ray wavelength can be set at the radiation absorption edge of a material. The image
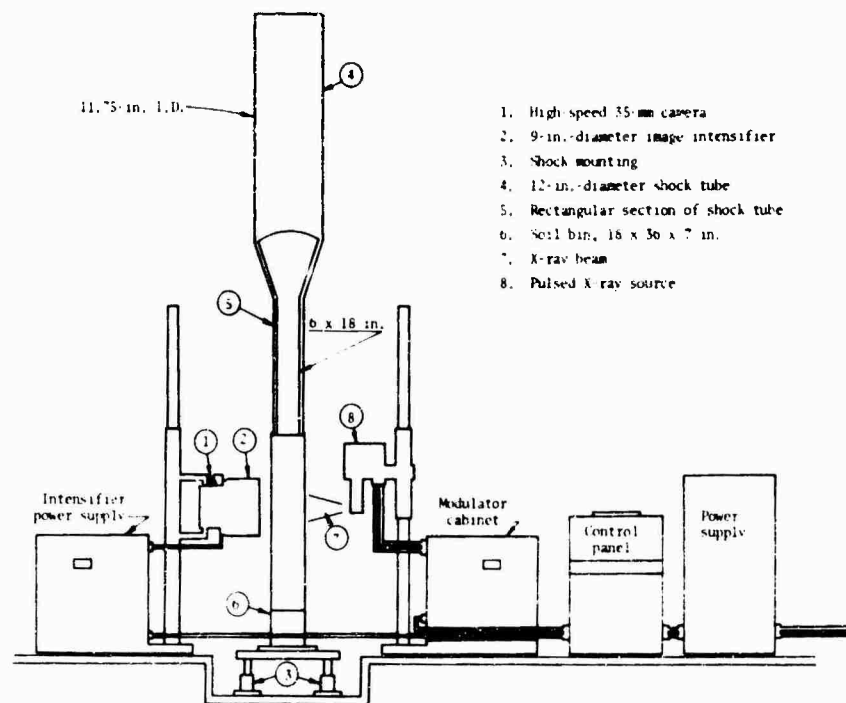

11.75-in. I.D.

6 x 18 in.

1. High speed 35-mm camera
2. 9-in.-diameter image intensifier
3. Shock mounting
4. 12-in.-diameter shock tube
5. Rectangular section of shock tube
6. Soil bin, 18 x 36 x 7 in.
7. X-ray beam
8. Pulsed X-ray source

Intensifier power supply

Modulator cabinet

Control panel

Power supply

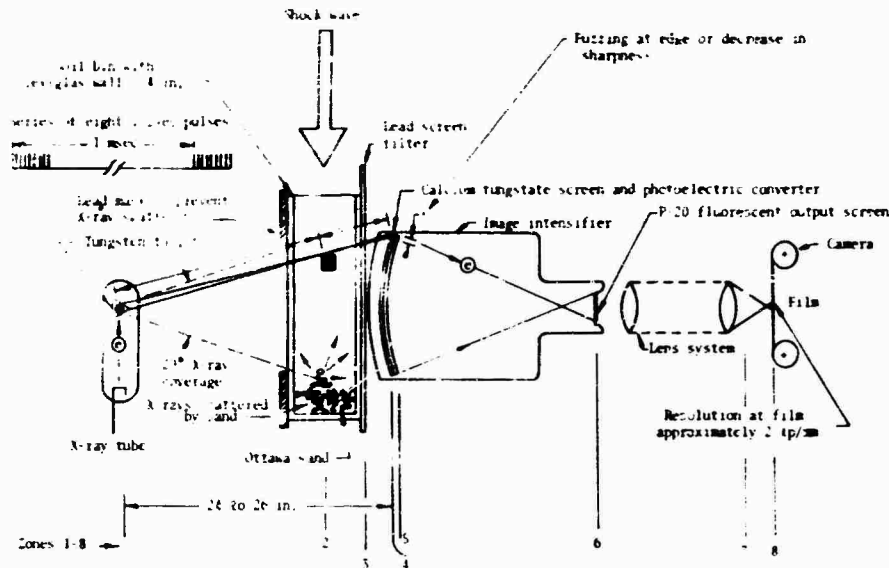Fig. 1 - Flash x-ray test setup for soil dynamics studies

230

Fig. 2 - Multiple-flash x-ray system used to analyze shock-
wave-induced pellet motion in Ottawa sand

intensifier allows the use of high-speed cameras
for photographing pulse-by-pulse information
over the same, or a fixed, field of view on 16-
or 35-mm high-speed high-contrast film.

For the desired dynamic soil measure-
ments, the multiple-pulse x-ray system has
certain limitations:

1. The upper pulse-repetition frequency of
1,000 pps is inadequate for recording the inter-
action of the leading edge of a fast-rising stress
wave with a small pellet (4-mm diameter); how-
ever, it is adequate for recording the slow decay
phenomena. For example, an x-ray system gen-
erating 10^5 pps could provide two radiographs
as the shock wave passes over the pellet.

2. Even with the image intensifier the in-
tensity developed with 150 kv is inadequate to
expose the film sufficiently when 4 in. of sand
has to be penetrated; 300 to 600 kv is required.

3. The resolution is limited by the image
intensifier and the optical system. The resolu-
tion at the output of the calcium tungstate sur-
face (Fig. 2) is about 2 line pairs per millimeter
(fp/mm); at the output of the lens system it is
about 1.5 fp/mm. (Exposing the film directly
with x-rays increases the resolution where the
extent of this increase is a function of the dis-
tance of the object from the film, the granular-
ity of the film, the x-ray target size, and the
density and scattering of the free-field medium.)

Test Procedure

Experimentation with the multiple-flash
x-ray equipment was necessary to determine
the most efficient procedure to get the best
data from rectangular soil samples loaded dy-
namically. Positioning the x-ray source at 24
to 28 in. from the image intensifier proved a
good compromise and yielded a reasonably
sharp final image, provided the maximum field
of view, and kept the spatial attenuation of in-
tensity to a minimum.

Clear Plexiglas supported by steel braces
was used for the soil-container walls. Other
materials tested were laminated wood and
aluminum. Wood was eliminated after a few
tests because of the large lateral deflections
experienced at high pressures (100 psi), its
nonuniform density, and its low strength. Alu-
minum was eliminated because aluminum walls,
as thin as 1/4 in., scattered and attenuated the
x-ray beam quite severely. Plexiglas offered
the advantages of low x-ray absorption, trans-
parency to light, uniform density, a relatively
high modulus of deformation, and adequate
strength when supported by steel braces spaced
sufficiently far apart to maintain a maximum
field of view.

The scattering of x-rays in soil and by the
side walls of the container was quite high. This
produced a foggy background on the film, caus-
ing decreased contrast between the soil and the

231

lead pellets. Scattered x-rays behave as numerous x-ray sources which cast shadows of the sand and the pellets from numerous directions on the x-ray film. By placing a lead sheet in front of the soil sample with a window cut to the size of the field of view, the scatter was greatly reduced (Fig. 2). The scatter was reduced further by using microline x-ray grids of lead (60 to 150 strips per inch) to clean the scattered x-rays out of the flux which has penetrated a test specimen.

The definition of the edges of the lead pellets was very poor due to their spherical geometry. Lead cubes (3/16 in.) were used in place of spherical pellets with much more success. Rectangular bars (3/16 in. square, 1/2 in. long) were also used with the long dimension placed along the path of the x-rays. These bars, as expected, were better defined than the cubes; however, it is difficult to place lead cubes and rectangular bars so that the edges are parallel to the x-ray beam. Any rotation of the pellets will distort the shadowgraph and could easily be interpreted as translation.

Pilot Tests

Pilot tests were performed to assess the utility of the multiple-flash x-ray system in tracking the motions of lead pellets and buried objects, and in detecting density changes in the soil. The first tests determined the quality of pictures that could be obtained through various thicknesses of soil. The x-rays were so attenuated by a 6-in. sample of dense Ottawa sand that no pictures could be obtained. Hence, a theoretical attenuation of 98 percent of the maximum x-ray intensity from the flash x-ray system is severe enough to prevent any data acquisition with present techniques. In 6 in. of loose Ottawa sand sufficient x-rays passed through the sample to actuate the image intensifier. Although film exposure was evident, little information was obtainable from the radiograph.

The photographs improved rapidly as sample density and thickness were decreased since the intensity on the film was raised to the required level. Tests were also conducted to show the improvements in film contrast using as models 5-mm lead cubes buried in the center of a 5-in. thick sample of medium-dense Ottawa sand and of a 4-in. thick sample of loose silt. The detail is more evident in the medium-dense Ottawa sand because of less x-ray scatter. Data-reduction techniques consisted of enlarging the frame size on an optical comparator and using x-y cross-hairs to measure changes in distance between the pellets and a fixed

reference frame. Considerably more detail was lost when these records were magnified, and the technique gave results only to the nearest 30 to 50 mils. In samples of loose silt the displacements expected under high-explosive loads will be quite large, and the detection of small movements will not be as important as in dense samples.

Another test was performed using 4-in. thick samples of loose soil; however, recording was limited to 1 pulse (from the multiple-flash x-ray system) directly on x-ray film in a cassette placed behind the back wall of the soil container. The inclusions were a 1/8-in. lead bar in Ottawa sand and a 1/8-in. thick lead T-section in silt. The results of the test show that the image is approximately 15 percent larger than actual size due to the shadowgraph effect. From these data it is evident that resolution, detail, and field of view can all be improved by direct recording on x-ray film. For dynamic studies there are problems in film transport and sensitivity. In this particular test the film was pre-exposed for 1 pulse to place the film higher on the gamma curve (density versus log-exposure) to obtain greater sensitivity.

Three types of cylindrical shells buried in soil were photographed using the multiple-flash x-ray system. The cylinders were 4, 2, and 5/8 in. in diameter and all had nearly the same wall thickness of 0.040 in. Pellets were placed around the 5/8- and 2-in. diameter cylinders and were loaded with a hydraulic-ram piston hitting the surface of the soil. A sequence of eight 35-mm photographs was taken which shows the time history of the 5/8-in. cylinder loaded with a pulse that had a rise time of nearly 60 msec and a long dwell at peak stress. The cylinder was in a layer of loose silt about 1-1/4 in. deep with medium-dense silt above and below. It is evident after close examination of the 35-mm films that some deformation occurred in the cylinder and that the soil density increased from the time of incident load, resulting in less exposure of the film. The progressive deformation of the cylinder from frame to frame was readily discernible; however, the density variations were barely perceptible.

Where the buried object is larger and edge detail is not of significance, the radiographs provide valuable information not obtainable by other methods. The deformations were clearly evident in the 2-in. cylinder. From these data it is reasonable to assume that by using this technique qualitative information can be collected when the deformations are large enough to change the shape of a buried object. The
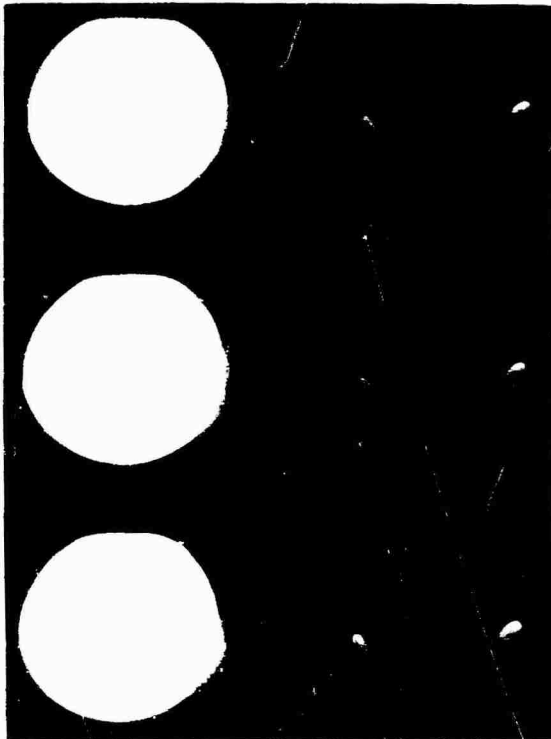
Fig. 3 - X-ray record of 4-in.-diameter
cylinder buried in Ottawa sand

4-in. cylinder was loaded to failure and is
shown in Fig. 3.

Field-Emission-Type X-Ray

Field-emission-type x-ray systems have
been recently developed which have a number of
desirable features for dynamic soil measure-
ments. The most significant are a very high
repetition rate of 10^6 pps for a multiple x-ray
source system, 10^5 pps with a single x-ray tube
and multiple pulsers, and a means of increasing
the time interval between pulses (from 1- and
10-μsec minimum for the multiple and single
x-ray source systems, respectively, to much
longer time intervals). This allows adjusting
the pulse-repetition rate to fit a pulse pressure-
time record as shown in Fig. 4.

Dynamic tests in soil show that a 600-kv
x-ray system is required to penetrate 8 to 10 in.
of Ottawa sand which provides the free-field in
the test soil bin. A 300-kv system has provided
useful results through 8 in. of sand but is expected

to be marginal under more limited conditions.
It is informative to review the specifications
of a 600-kv field emission flash x-ray system
now available (Field Emission Corporation,
McMinnville, Oregon, single or multiple x-ray
tube), since they can be used as a basis for
projecting the improvements over the radio-
graphs taken with a 150- or 300-kv system:

1. X-ray tube performance:

   X-ray pulse width at half intensity
   points, 18 nanosec;

   X-ray dose per pulse on axis 1 meter
   from tube face, 0.03 r;

   Total x-ray energy per pulse, 1.6 j;

   Peak x-ray power, 70 m;

   Effective x-ray source size, 5 mm
   (200 mils).

2. Absorber penetration:

   2.5 ft FTSD, 6 in.;

   Shadowgraph, 22 ft.

3. Angular distribution, cone half angle,
   18 deg.

A field-emission-type system has some
rather significant advantages particularly when
making dynamic soil measurements:

1. The field-emission-type system has
very high stop-motion capability on transient
events. For example, a radiograph of a shock-
wave front having a velocity of 3,000 fps is
smeared out 0.65 mil by the 18-nanosec pulse
and 1.08 mils by the 30-nanosec pulse. A soil
set into motion with a velocity of 100 fps by the
shock wave has that motion smeared 0.02 mil
by the 18-nanosec pulse and 0.036 mil by the
30-nanosec pulse.

2. A 300-kv field-emission-type single
x-ray tube system has the capability of gen-
erating x-ray pulses 18-nanosec wide with any
pulse separation from 10 to 100 msec. This
permits radiographing the interaction of the
leading edge of the shock wave with the buried
structure.

3. For a field-emission-type system the
number of pulses in a pulse sequence can be
increased by adding pulser units. Different
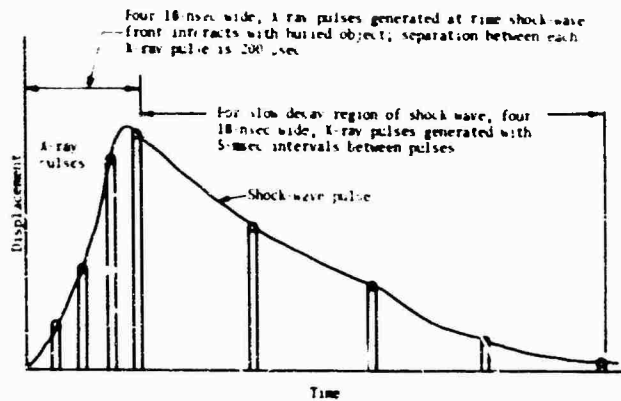time intervals between the pulses can be
programmed.

233

For slow decay region of shock wave, four
10-nsec wide, x-ray pulses generated with
5-msec intervals between pulses

Shock-wave pulse

X-ray
pulses

Displacement

Time

Fig. 4 – Application of x-ray system with
variable pulse-repetition frequency

4. A field emission multi-channel system incorporating more than one x-ray tube and pulser provides a very high framing rate. For example, a four-tube x-ray system can provide 4 pulses with a megacycle framing rate. This requires arranging the x-ray tubes around the object to be radiographed or along the path of stress wave propagation.

5. A 300-kv system has adequate output to penetrate 6 to 8 inches of sand allowing the recording of soil movements (Fig. 5) directly on Kodak Royal Blue film. This simplifies the entire system considerably since the image intensifier and lens-coupling systems are not required. In addition, for the tests to be conducted, the application of a higher voltage 600-kv system to soil experiments would remove the system from marginal operation.

6. A field-emission-type x-ray tube provides a decided advantage in soil experiments since it can be operated remotely up to 60 feet from the pulser and control panels by a coaxial transmission line.

There are a number of limitations for a field-emission-type system when applied to dynamic soil measurements:

1. Without an image-intensifier tube, the field-emission-type system requires special equipment to move large sheet film rapidly past the object being radiographed if a large field of view is required.

2. At present multiple x-ray heads are required to generate a string of pulses at the 600-kv level.

Experimental Results with Field
Emission X-Ray System

In one of the tests a 300-kv x-ray tube was placed 2 ft from Kodak Royal Blue film (with industrial screens containing calcium tungstate). An 8-in.-thick soil bin half filled with dry Ottawa sand and half filled with wet Ottawa sand (20 percent water by weight) was placed directly in front of the film. In the sand in each half of the bin three lead cubes were positioned: one about 1 in. from the front of the bin, one in the middle, and one about 1 in. in front of the film.

Figure 5 shows the results. The edge sharpness is quite pronounced for the cubes nearest the film since there is very little x-ray spot-size or scattering distortion. This contrasts with the detail associated with the cubes nearest the x-ray source.

The ability of the x-ray system to look through 8 in. of Ottawa sand and to expose the film directly without image intensification is of major importance. Close scrutiny of the original film shows a definite difference in exposure due to the slight difference in densities between the dry and wet sand.

CONCLUSIONS

From the pilot tests it can be concluded that soil is a severe x-ray-scattering medium. However, there is ample indication that this can be reduced to a tolerable level by the use of masks, filters, and lead screens. The maximum thickness of Ottawa sand of density of 112 pcf that can be penetrated with a 150-kv flash

234

Fig. 5 - Direct exposure x-ray record of six 3/16-in. lead
cubes buried in 8 in. of medium-dense Ottawa sand at var-
ious locations along the thickness (1 pulse, 300-kv Field
Emission Model 735-3-C-235)

x-ray system is 5 in. With a 300-kv system, the
maximum thickness is 8 in.; with a 600-kv sys-
tem, penetration of from 8 to 12 in. is expected.

The average range of density changes that
might be expected in soil columns confined in
test containers is 0.5 percent for dense sands
to 5 percent for loose clays.

Where soil movement or particle velocities
are under 100 fps, the shadow edge smearing is
about 1.2 mils. In comparison, this decreases
the resolution far less than the loss of edge
sharpness due to scattering.

Frame rates as high as 100,000/sec are
desirable to resolve the interaction effects
caused by the leading edge of a stress wave
with an object embedded in soils.

The incorporation of an image intensifier
makes it possible to photograph the object
x-rayed on 16- or 35-mm film, thereby elimi-
nating difficult transport problems. Because of
the transport problems, one cannot take advantage

of the resolution obtainable by placing the film
directly behind the soil bin if more than one
frame is required.

A field-emission-type x-ray system shows
promise of providing the required data for dy-
namic soil measurements since sufficient in-
tensity, short pulse width, and capability of
high-pulse-repetition rates can be obtained.

ACKNOWLEDGMENTS

235

REFERENCES

1. D. Berdan and R. R. Bernhard, "Pilot Studies of Soil Density Measurements by Means of X-Rays," Trans. ASTM, pp. 1328-1342, 1951

2. H. E. Davis and R. J. Woodward, "Some Laboratory Studies of Factors Pertaining to the Bearing Capacity of Soils," Proc. Highway Research Board, pp. 467-476, 1949

3. E. Gerber, "Untersuchungen ueber die Druckoerteilung Oertlich Belasteten Sand, Dissertation, Technische Hochschule, Zurich, 1929

4. K. H. Roscoe, J. R. F. Arthur, and R. G. James, "The Determination of Strains in Soils by an X-Ray Method," Civil Engineering and Public Works Review, pp. 873-876, July 1963

5. J. R. F. Arthur, R. G. James, and K. H. Roscoe, "The Determination of Stress Fields During Plane Strain of a Sand Mass," Geotechnique, Vol. 14, No. 4, pp. 283-308, Dec. 1963

6. W. J. Baker and R. E. Lynch, "A Study of the Parameters Involved in Displacement Measurements in Soil," AFWL TR-65-75, June 1965

7. E. T. Selig and R. Rusin, "Gage Placement Study D-TDR-63-3024, Aug. 1963

8. E. T. S. ig, "Detection of Transient Stresses and Strains in Soil," Proc., Symposium on Detection of Underground Objects, Materials, and Properties, Ft. Belvoir, Va., pp. 163-190, 1962

9. Fred H. Bloedow, "Radiographic Instrumentation Study," AFSWC-TDR-62-44, April 1962

10. Jerome Kohl, Rene D. Zentner, and Herbert E. Luckens, Radioisotope Applications Engineering, p. 351. D. Van Nostrand, New York, 1961

11. Kenneth Kaplan, "Experimental Study of the Effect of Material Properties on Coupling of Explosion Energy," AFSWC-TDR-63-47, May 1963

*   *   *

DISTRIBUTION

Aberdeen Proving Ground, Md.
Att: Ballistic Research Lab. — 1
Att: Development & Proof Services — 1
Att: Physical Test Lab. — 1

Air Defense Command, Ent AFB
Att: ADIRP — 1

Air Force Academy, Colo.
Att: Dept. Mech. DFME (U) — 1

Air Force Headquarters, DC
Att: Operations Analysis Off.,
Off. Vice Chief of Staff, Library — 2
Att: AFDRD-GW — 1

Air Force Missile Development Center,
Holloman AFB
Att: RRRT/Miss R. Porter — 1
Att: MDS/Dr. M. G. Jaenke — 1
Att: MDSSS/Mr. G. R. Moser — 1

Air Force Missile Test Center, Patrick AFB
Att: MT LLL-3 (Classified Material) — 2
Att: MU-135, Technical Library (U) — 1

Air Force Office of Scientific Research, DC
Att: Library (U) — 1

Air Force Packaging Evaluation Agency,
Brookley AFB
Att: MOSPR — 1
Att: MONE — 1

Air Force Regional Civil Engineer
Att: North Atlantic Region,
AFRCE-NA-A — 1

Air Force Rocket Propulsion Lab., Calif.
Att: Mr. A. J. Davies (RPFDE) — 1

Air Force Systems Command, Andrews AFB
Att: Technical Library — 2

Air Force Weapons Laboratory, Kirtland AFB
Att: Development Test Division — 1
Att: Dr. W. E. Fisher, WLRS — 1
Att: SWOI 631-276 — 1

Air Proving Ground Center, Eglin AFB
Att: PGTRI, Technical Library — 1

Army Edgewood Arsenal, Maryland
Att: Library — 1

Army Electronics Command, Phila. — 1

Army Electronics Command, Ft. Monmouth
Att: Mr. J. J. Oliveri — 1

Army Engineer R&D Laboratories, Ft. Belvoir
Att: Package Development Branch — 1
Att: Director of Research — 1
Att: Chief, Spec. Proj. Branch — 4

Army Engineer Waterways Experiment
Station, Vicksburg
Att: Library — 1

Army Frankford Arsenal, Phila.
Att: Library Branch, CC 0270/40 — 1
Att: Mr. David Askir, Q6200 — 1

Army Materials Research Agency, Watertown
Att: Dr. Reinier Beeuwkes, Jr. — 2

Army Materiel Command, DC
Att: AMCRD-R — 1

Army Missile Command, Redstone Arsenal
Att: AMSMI-RB — 1
Att: AMSMI-RG — 1
Att: AMSMI-RL — 1
Att: AMSMI-RS — 1
Att: AMSMI-RT — 1
Att: AMSMI-RTR, Mr. J. M. Taylor — 1
Att: AMSMI-RSM, Mr. E. J. Wheelahan — 1

Army Mobility Command, Centerline
Att: Mr. Otto Renius — 1

Army Natick Laboratories, Mass.
Att: Technical Library — 2
Att: Mr. W. B. Brierly — 1
Att: Chief, Container Div. — 1

Army, Office Chief of Engineers, DC
Att: ENGMC-EM — 2

Army, Office Chief of R&D, DC
Att: Scientific & Tech. Information Div. — 1

Army, Office Chief of Staff, Logistics
Att: Director of Transportation Engrg. — 1

Army Tank-Automotive Center, Warren
Att: SMOTA-RRS, Tech. Library — 1
Att: SMOTA-RCE, Mr. D. J. Hackenbruch — 1
Att: SMOTA-RRC — 1

Army Transportation Engineering Agency,
Ft. Eustis
Att: Library — 1
Att: Mr. L. J. Pursifull — 1

Army Transportation Research Command,
Ft. Eustis
Att: Dr. R. L. Echols,
Physical Sci. Res. Group — 1

237

Naval Ammunition Depot, Crane
    Att: Code 3540   1
    Att: Code 3400   1

Naval Ammunition Depot, Portsmouth
    Att: Mr. Jerome Smith, Code QALE   1

Naval Ammunition Depot, Red Bank
    Att: Chief Engineer   1

Naval Ammunition Depot (Oahu)
    Att: Weapons Technical Library   1

Naval Applied Sci. Lab., Brooklyn
    Att: Library   3

Naval Attache & Naval Attache for Air,
Navy No. 100, NY
    Att: Logistics Division   1

Naval Avionics Facility, Indianapolis
    Att: MAL Library   1

Naval Civil Engineering Lab., Pt. Hueneme
    Att: Library   2

Naval Medical Field Res. Lab., Camp Lejeune   1

Naval Mine Engrg. Facility, Yorktown
    Att: Library   1

Naval Missile Center, Pt. Mugu
    Att: Library, N-03022   1
    Att: Env. Div., N314   2

Naval Operations, Office of Chief, DC
    Att: Op 31   1
    Att: Op 34   1
    Att: Op 75   1
    Att: Op 07T6, Mr. T. Soo-Hoo   1
    Att: Op 725   1

Naval Ordnance Laboratory, Corona
    Att: Code 234, Technical Library   1
    Att: Code 56, Sys. Eval. Division   1

Naval Ordnance Lab., Silver Spring
    Att: Technical Director   1
    Att: Library   3
    Att: Environmental Simulation Div.   6
    Att: Mr. G. Stathopoulos   1

Naval Ordnance Plant, Forest Park
    Att: Mr. R. E. Seely, Div. 5500   1

Naval Ordnance Test Station, China Lake
    Att: Technical Library   1
    Att: Code 3073   1
    Att: Code 4062   2
    Att: Code 4533   1
    Att: Code 5516   1

Naval Ordnance Test Station, Pasadena
    Att: P8087   3
    Att: P8092   1
    Att: P8073   1
    Att: P80962   1

Naval Plant Representative Office, Pomona
    Att: Chief Engineer   1
    Att: Metrology Engrg. Ctr.   1

Naval Plant Representative Office, Sunnyvale   1

Naval Postgraduate School, Monterey
    Att: Library   1

Naval Propellant Plant, Indian Head
    Att: Library   1

Naval Radiological Def. Lab., San Francisco
    Att: Library   3

Naval Research Lab., USRL Div., Orlando
    Att: Library   1

Naval Research Lab., DC
    Att: Code 6250   1
    Att: Code 6260   1
    Att: Code 6201   1
    Att: Code 6020   2
    Att: Code 2027   2

Naval Security Engineering Facility, DC
    Att: R&D Branch   1

Naval Ship Systems Command Hdqs., DC
    Att: Code 052, Mr. J. R. Sullivan   10

Naval Supply Systems Command Hdqs., DC
    Att: Library   1

Naval Torpedo Station, Keyport
    Att: QEL, Technical Library   1

Naval Training Device Center, Orlando
    Att: Technical Library   1

Naval Underwater Weapons Station, Newport
    Att: Technical Documents Library   1

Naval Weapons Eval. Facility, Albuquerque
    Att: Library, Code 42   1

Naval Weapons Laboratory, Dahlgren
    Att: Technical Library   1

Navy Electronics Lab., San Diego
    Att: Library   1
    Att: Code 3360   1

Navy Electronics Supply Office, Great Lakes   1

Navy Marine Engrg. Lab., Annapolis
    Att: Library   1
    Att: Code 512, Dr. M. Solow (U)   1

Navy Mine Defense Lab., Panama City
    Att: Library   1

Navy ROTC and Admin. Unit, MIT,
Cambridge (U)   1

Navy Underwater Sound Lab., New London
    Att: Technical Director   1

Norfolk Naval Shipyard, Portsmouth
    Att: Design Superintendent   1

Office Director of Defense R&E, DC
    Att: Technical Library   2
    Att: Mr. W. M. Carlson   1

Office of Naval Research, DC   7

Office of Naval Res. Branch Office, Boston   1

Office of Naval Res. Branch Office, Pasadena   1

Ogden Air Materiel Area, Hill AFB
    Att: Service Engrg, Dept., OONEOO   1

Pearl Harbor Naval Shipyard
    Att: Shipyard Tech. Library, Code 246P   1

Philadelphia Naval Shipyard, Pa.
    Att: Ship Design Section   1
    Att: Naval Boiler & Turbine Lab.   1

Picatinny Arsenal, Dover
    Att: Library SMUPA-VA6   1
    Att: SMUPA-VP7, Mr.R.G. Leonardi   1
    Att: SMUPA-T, Mr. R. J. Klem   1
    Att: SMUPA-D, Mr. E. Newstead   1
    Att: Mr. A. H. Landrock
        PLASTEC, Bldg. 3401   1

Portsmouth Naval Shipyard, NH
    Att: Code 246   1
    Att: Mr. E. C. Taylor   1

Puget Sound Naval Shipyard, Bremerton
    Att: Code 275   1
    Att: Code 242, Mr. K. G. Johnson   1
    Att: Code 281   1
    Att: Material Laboratories   1

Rome Air Development Center, Griffiss AFB
    Att: Mr. Dana Benson, RASSM   1

6511th Test Group (Parachute), USAF, El Centro
    Att: Mr. E. C. Myers. Tech. Director   1

6570th Aerospace Medical Res. Labs., W-PAFB
    Att: MRMAE   1
    Att: Mr. R. G. Powell, MRBAE   1

San Francisco Bay Naval Shipyard, Calif.
    Att: Shipyard Tech. Library,
        Code M303L1   1

Strategic Air Command, Offutt AFB
    Att: Operations Analysis Office   1

Supervisor of Shipbuilding, USN, Brooklyn
    Att: Mr. M. J. Macy   1

Supervisor of Shipbuilding, USN, Camden
    Att: Code 299   2

Technical Training Center, Sheppard AFB
    Att: Capt. C. B. Coy,
        Dept. of Missile Training   1

Tobyhanna Army Depot, Pa.
    Att: SMC Packaging & Storage Center   1
    Att: Metrology Division   1

Watervliet Arsenal, New York
    Att: ORDBF-RR   2

White Sands Missile Range, Las Cruces
    Att: STEWS-AMTED-E   2

Wright-Patterson AFB, Ohio
    Att: AFFDL (FDFE, E. H. Schell)   1
    Att: AFFDL (FDFE, C. W.Gerhardt)   1
    Att: AFFDL (FDD, H. A. Magrath)   1
    Att: AFFDL (FDDS, C. A. Golueke)   1
    Att: AFML (MAMD, J. P. Henderson)   1
    Att: SEG (SEFSD, R. F. Wilkus)   1

Yuma Proving Ground, Arizona
    Att: Library   1